An absence of dystrophin in cerebellar Purkinje cells impairs inhibitory synaptic function in mature dystrophic mice

Chek Ying Tan (BMedSc Honours)

A thesis submitted in fulfilment of the requirements for the degree of

Doctor of Philosophy

School of Medicine

March 2021

Statement of Authentication

The work presented in this thesis is, to the best of my knowledge and belief, original except as acknowledged in the text. I hereby declare that I have not submitted this material, either in full or in part, for a degree at this or any other institution.

Chek Ying Tan
March 2021

Acknowledgment

First and foremost, I would like to express my most profound gratitude to my three supervisors Professor John William Morley, Professor Stewart Ian Head, and Dr Sindy Lyn Ling Kueh for their expertise, supervision, and support. Thank you John for giving me an opportunity to be one of your PhD students and thank you for providing the professional guidance and patience throughout my candidature. Thank you Stewart for your critical and inspiring comments for my experimental work and thesis writing throughout my candidature. And finally, thank you Sindy for your encouragement and for providing me with the freedom to pursue different ideas, which has given me the confidence to carry out my project independently.

I would also like to thank Dr Yossi Buskila and Dr Morven Cameron for their insightful knowledge and for helping with my electrophysiology recording. As well, thank you Ashleigh Deschamps, Nikola Mills, and Lauren Hughes from the Animal Facility for their expertise and care for my experimental animals. I would also like to thank the administrative staff, Sue Nile, for her wonderful assistance with the complex paperwork associated with my PhD.

I would like to thank my best e-phys buddy Dr Orsolya Kekesi for her encouragement, guidance and support while overcoming the greatest technical challenge of my PhD being electrophysiological recording. I am grateful for all new friendships formed and support of my fellow peers: Dr Alba Bellot Saez, Dr Victor Perez-Fernandez, Winston Sei, Leon Kiriaev, Joan Nguyen, Dr Afia Akhtar, Dr Monokesh Sen, Rebecca Stevenson, Sush Raja, Evgeniia Samokhina, Elif Sakiz, and Asma Redwan.

Thank you to all my oldest friends from UNSW who have always supported and helped me through the important milestones in my life. In particular, I would like to thank Dr Dennis Lawrence Cheung, Dr Laurence Don Wai Luu, Yeojoon (April) Cha, Dr Colin Kong, Kristy Wang, Stephanie Halena, Naomi Wu, William Fu, Joanna Wong, Dr Budi Tan, Dr Joshua Yap, Dr Louis Yeung, Stephen Zhang, and Laura Hung.

Most importantly, I would like to thank my parents, my sister Check Ling, and my family in law for their unconditional love and constant support. I am also especially thankful to my husband, Joe, without whom I would not have been able to get this far. I am indebted to you for your love, understanding and continued support.

Lastly, to my late grandma, I acknowledge the sacrifices made and thank you immensely for the love and inspiration you have provided to shape me into the person I am today. This thesis is dedicated to you.

Contents

List of Figures

List of Tables

List of Abbreviations

aCSF	Artificial cerebrospinal fluid
ADP	Adenosine diphosphate
AHP	Afterhyperpolarisation
AM	Acetoxymethyl
AMPA	α-amino-3-hydroxy-5-methyl-4-isoxazole propionic acid
AMO	Antisense morpholino oligonucleotide
AOs	Antisense oligonucleotides
AP	Action potential
APs	Action potentials
APV	2- amino-5-phosphonovalerate
ARC	Animal Resource Centre
ATP	Adenosine triphosphate
BBB	Blood brain barrier
BDNF	Brain-derived neurotrophic factor
BK channels	Large conductance calcium-activated potassium channels
$[Ca^{2+}]_i$	Intracellular calcium concentration
C. elegans	*Caenorhabditis elegans*
CF	Climbing fibres
CI	Confidence interval
CNQX	6-cyano-7-nitroquinoxaline-2,3-dione
CNS	Central nervous system
CPP	Cell-penetrating peptides
CT	Computerised tomography
C-terminal	Carboxyl-terminal
DAPC	Dystrophin-associated protein complex

DGC	Dystrophin-glycoprotein complex
DIV	Day *in vitro*
DMD	Duchenne muscular dystrophy
DMD	Dystrophin gene
Dp 427	Full-length dystrophin
DPBS	Dulbecco's phosphate-buffered saline
DPH	Diphenylhydantoin
EMCCD	Electron multiplying charge coupled device
EPSP	Excitatory postsynaptic potential
FDB	Flexor digitorum brevis
FLSMN2	Full-length *SMN2*
FSIQ	Full scale intelligence quotient
Fura-2 AM	Fura-2 acetoxymethyl ester
GABA	Gamma-aminobutyric acid
$GABA_A$	Gamma-aminobutyric acid type A
$GABA_AR$	Gamma-aminobutyric acid type A receptors
I_A	A-type K^+ currents
$InsP_3$	Inositol 1,4,5-trisphosphate
IPSCs	Inhibitory postsynaptic currents
IPSP	Inhibitory postsynaptic potentials
IQ	Intelligence quotient
kD	Kilodaltons
LC	Littermate control
LTD	Long-term depression
LTP	Long-term potentiation
mdx	X-chromosome-linked muscular dystrophy

mEPSCs	miniature excitatory postsynaptic currents
mGluR1	Metabotropic glutamate receptor 1
mGluRs	Metabotropic glutamate receptors
mIPSCs	Miniature inhibitory postsynaptic currents
MRI	Magnetic resonance imaging
MRS	Magnetic resonance spectroscopy
NMDA	N-methyl-D-aspartate
NMDAR	N-methyl-D-aspartate receptors
N-terminal	Amino-terminal
PET	Position emission tomography
PF	Parallel fibres
P_i	Inorganic phosphate
Pips	PMO internalisation peptides
PIQ	Performance intelligence quotient
PMO	Phosphorodiamidate morpholino oligomer
PPF	Paired-pulse facilitation
PTP	Post-tetanic potentiation
RyR	Ryanodine receptor
RyRs	Ryanodine receptors
SEM	Standard error of the mean
SK channels	Small conductance calcium-activated potassium channels
SMA	Spinal muscular atrophy
SMN	Survival motor neuron
SR	Sarcoplasmic reticulum
STD	Short-term depression
STP	Short-term potentiation

TBS	Tris buffered saline
TBST	Tris buffered saline with Tween 20
TTX	Tetrodotoxin
VGCCs	Voltage-gated calcium channels
VIQ	Verbal intelligence quotient
WT	Wild type

List of Abstracts

Tan, C.Y., Kueh, S.L.L., Head, S.I., Morley, J.W. (2019). Miniature inhibitory postsynaptic current in cerebellar Purkinje cells of old dystrophic *mdx* mice in 9th Federation of the Asian and Oceanian Physiological Societies Congress, Kobe, Japan.

Tan, C.Y., Kueh, S.L.L., Head, S.I., Morley, J.W. (2018). Miniature inhibitory postsynaptic current in cerebellar Purkinje cells of old dystrophic *mdx* mice. *Proceedings of the Australian Physiological Society*, 49, pp 40, Sydney Australia.

Tan, C.Y., Kueh, S.L.L., Head, S.I., Morley, J.W. (2018). Duchenne muscular dystrophy: the role of abnormal calcium handling in brain and muscle in Health Beyond Research & Innovative Showcase, Sydney, Australia.

Tan, C.Y., Kueh, S.L.L., Head, S.I., Morley, J.W. (2018). Duchenne muscular dystrophy: the role of abnormal calcium handling in brain and muscle in Neuroscience Colloquium, Newcastle, Australia.

Abstract

Duchenne muscular dystrophy (DMD) is a rapidly progressive X-linked recessive disease affecting about 1 in 3500 live male births. It is caused by mutations in the dystrophin gene, which result in the loss of dystrophin or expression of a non-functional truncated protein product. Full-length dystrophin is mainly expressed in muscles and the central nervous system. The absence of dystrophin results in irreversible progressive motor dysfunction, leading to muscle wasting, respiratory insufficiency, cardiac failure and eventually premature death. In addition to the degeneration of skeletal musculature, about one-third of patients with DMD display various degrees of intellectual impairment, commonly found with intelligence quotient (IQ) scores of one standard deviation below (IQ of 85) the normal population mean (IQ of 100). However, the mechanism underlying the cognitive deficits in DMD remains unclear and no effective treatment is available to reverse this condition in the affected individual.

To date, the life-threatening muscular aspects of DMD have received significant attention. Effective treatment and care which focuses on the management of respiratory failure and other disease complication have significantly improved the life expectancy of DMD patients. Recent studies showed that the life span of DMD patients today has increased from teens to their fourth decades. With longer survival, the quality of life becomes increasing important. Therefore, research on the cognitive aspect of DMD is as important as research on the muscular aspects because improvements in cognitive function will enhance the quality of life for the growing population of adult DMD patients.

The aim of this thesis was to investigate the role of dystrophin in the central nervous system of the *mdx* mouse, a widely accepted murine model for DMD. This study employed the use of

animal with different age groups, corresponding to young (3-4 months), adult (11-12 months), and aged (23-26 months). Adult and aged *mdx* mice are the focus in this study with findings from the older mouse especially valuable as, disease progression in aged mice closely resembling that of DMD. As numerous evidence has shown a high similarity between the specific cognitive dysfunctions seen in DMD (i.e. impaired verbal intelligence) and in patients with cerebellar lesions (i.e. language disorders), this study examined the function of cerebellar Purkinje cells in *mdx* mice using electrophysiological recording and calcium imaging.

The first experimental chapter (Chapter 3) focused on the impact of aging on the miniature inhibitory postsynaptic currents (mIPSCs) mediated by the $GABA_A$ receptors in Purkinje cell of *mdx* mice. Whole-cell patch clamp recordings showed that the frequency and amplitude of mIPSCs were significantly reduced in the aged *mdx* mice compared to the age-matched littermate controls, consistent with the findings shown in young *mdx* mice. In addition, when comparing the results from the aged *mdx* to the young *mdx* cohort, it was found that both the frequency and amplitude of mIPSCs remained similar between the two age groups, suggesting that the changes in mIPSCs in the *mdx* mice are independent of aging.

In the second experimental chapter (Chapter 4), the possibility of rescuing dystrophin expression using an exon skipping strategy with an antisense oligonucleotide, Pip6f-PMO, in organotypic cerebellar cultures developed from young *mdx* mice (P8-P11) was explored. Using immunofluorescence staining with a dystrophin antibody, rescued dystrophin was shown as the strong punctate staining along the somatic membrane and in the proximal dendritic layer of the Purkinje cell. More importantly, these results showed that the rescued dystrophin was functional as improved $GABA_A$ receptor clustering was found in Purkinje cells of *mdx*-Pip6f-

PMO culture. Electrophysiological recording on Pip6f-PMO treated Purkinje cells also showed an increased peak amplitude of mIPSCs when compared to untreated *mdx* Purkinje cells.

In the third experimental chapter (Chapter 6), using whole-cell patch clamp recording combined with calcium imaging, an investigation into the impact of dystrophin deficiency on the electrophysiological properties of the cell membrane and intracellular calcium dynamics of adult Purkinje cells was performed. The optimisation of calcium dye loading into Purkinje neuron is described in Chapter 5. The key findings in Chapter 6 include altered active membrane properties (i.e. reduced amplitude, increased 10-90% rise time, and reduced 10-90% rise slope of action potential) and a significant increase in baseline intracellular calcium concentration ($[Ca^{2+}]_i$) in the *mdx* Purkinje cell soma. Although the $[Ca^{2+}]_i$ in the distal dendritic regions were also increased in the *mdx* neurons, they were not significantly different from the littermate controls. Similarly, no significant difference was found for the calcium handling properties of the distal dendritic region of *mdx* Purkinje cells when it was electrically stimulated with a stimulating theta electrode.

Overall, the data presented in this thesis provides new insights into the role of dystrophin in cerebellar Purkinje neurons. The findings suggest that dystrophin is important for normal inhibitory synaptic function, intrinsic electrophysiological properties, and calcium handling of the mature cerebellar Purkinje cells. The consequences of the absence of dystrophin including the altered $GABA_A$ receptor clustering and reduced peak amplitude of mIPSCs could be ameliorated when dystrophin was successfully rescued with Pip6f-PMO in an organotypic *mdx* cerebellar culture. If *mdx* mice and DMD patients share similar neuropathogenesis, the development of drugs targeting the altered functions in *mdx* Purkinje cells may serve as a potential therapy in alleviating the cognitive impairments seen in DMD.

Chapter 1. General Introduction

1.1 Discovery of Duchenne Muscular Dystrophy

Duchenne muscular dystrophy (DMD) was named after the French neurologist, Guillaume-Benjamin-Amand Duchenne (1806-1875). In 1861 and 1868, Duchenne described this childhood myopathy as "*paralysie musculaire pseudohypertrophique"*, characterised with a higher incident rate in boys and disease progression in three stages: feeble movement, apparent hypertrophy, and finally paralysis (Jay & Vajsar, 2001; Plotogea *et al.*, 2009). The first stage of symptoms was believed to be caused by wasting of muscles involved in movement, which started initially in the lower limbs and lumbar region, progressing to the upper limbs (Jay & Vajsar, 2001). Enlargement of calf muscles is seen in the second stage, and is due to hyperplasia of interstitial connective tissue and over supply of fibroses and adipose tissue which replaces muscle (Jay & Vajsar, 2001; Plotogea *et al.*, 2009). Finally, a loss of locomotion renders the boys wheelchair-bound by 11 years of age (Hoffman & Gorospe, 1991). This occurs when all the healthy muscles are wasted and can no longer regenerate.

Although this disorder had been described by numerous investigators such as Charles Bell (1774-1842), Edward Meryon (1809-1880), and William Richard Gower (1845-1915), it now bears Duchenne's name (Emery & Emery, 1993; Jay & Vajsar, 2001).

1.2 Early descriptions on the intellectual impairment in DMD patients

In his original report, Duchenne noted a cognitive involvement in his DMD patients. He found that 40% of his cases present with mental deficits (Duchenne, 1868). Other investigators also reported a reduction in intelligence quotient (IQ) in DMD patients (Del Carlo Giannini & Marcheschi, 1959; Erb, 1891; Gowers, 1879). Wardon and Vignos argued that while these boys

have specific difficulties in reading and mathematics, the degree of intellectual impairment is independent of the severity of this disease (i.e. no progressive mental deterioration with advancement of the disease) and is not associated with DMD pathology (Worden & Vignos, 1962). Additionally, some authors suggested that the lower IQ scores in some DMD patients could be due to the social and educational outcomes (Walton & Nattrass, 1954). Nevertheless, Dubowitz argued that the intellectual impairment in DMD boys is actually pathologically related (Dubowitz, 1965). He proposed that the impaired cognitive function in DMD patients was potentially due to the abnormality of a common biochemical substance found in brain and muscle. Indeed, Dubowitz's hypothesis was correct. The primary defective biochemical substance was eventually discovered by Kunkel and their team in 1987 (Kunkel *et al.*, 1987). Today, this biochemical substance is widely known as dystrophin, which is a cytoskeletal protein found in various tissues including skeletal muscles, smooth muscles, and the central nervous system (CNS) (Hoffman, Brown, *et al.*, 1987; Mandel, 1989).

1.3 DMD and dystrophin gene (*DMD*), protein

Duchenne muscular dystrophy is a fatal, X-linked recessive progressive muscle disorder caused by inherent biochemical deformity of muscle tissue. The defective biochemical compound remained a mystery until the late 20th century (Koenig *et al.*, 1987; Monaco *et al.*, 1986; Murray *et al.*, 1982). In 1982, the dystrophin gene or *DMD* locus that encodes for dystrophin protein was identified by positional cloning (Murray *et al.*, 1982). This gene is localised on the short arm of the X chromosome in the Xp 21 region (Figure 1.1 A) (Hoffman, Knudson, *et al.*, 1987; Murray *et al.*, 1982; Puliti *et al.*, 2007). This locus also accounts for the milder and less prevalent Becker muscular dystrophy (Kingston *et al.*, 1983). To date, *DMD* is the second largest gene described in humans, spanning more than 2 million base pairs of genomic sequence. It corresponds to nearly 0.1% of the whole human genome or about 1.5% of the X

chromosome (Koenig *et al.*, 1987; Kunkel *et al.*, 1989; Mandel, 1989; Manole, 1995; van Ommen *et al.*, 1987). Only 1% of *DMD* is made up of exons, which comprises 79 exons and 7 promoters (Muntoni *et al.*, 2003). These exons form the 14kb messenger RNA which encodes for dystrophin, a 427 kilodaltons (kD) or 3685 amino acid protein.

The dystrophin gene gives rise to numerous transcripts of the full-length, 427 kD and several shorter isoforms (Figure 1.1 B) (Torelli *et al.*, 1999). These isoforms are generated from different tissue specific promoters, and as a consequence of alternative splicing of the dystrophin exons (Mehler, 2000). The full-length dystrophin (Dp 427), is generated from three different tissue specific promoters; namely muscle type (M), brain type (B), and Purkinje cell type (P) (Bies, Phelps, *et al.*, 1992; Gorecki *et al.*, 1992; Nudel *et al.*, 1989). The M-promoter drives expression predominantly in the skeletal muscle and cardiomyocytes but minor expression is found in CNS glial cells (Chelly *et al.*, 1990; Torelli *et al.*, 1999). The B-promoter, also known as cerebral promoter, drives expression mainly in cortical and hippocampal (CA1-3 region) pyramidal neurons whereas the P-promoter drives expression in mature cerebellar Purkinje cells and in the foetal cerebral cortex (Bies, Phelps, *et al.*, 1992; Gorecki *et al.*, 1992; Nudel *et al.*, 1989). In the CNS, Dp 427 is primarily expressed along plasma membranes in the soma and in the postsynaptic densities, specialised regions of the synaptic submembraneous cytoskeleton of principal neurons, specifically in the hippocampus, cerebral cortex and in the cerebellum (Lidov *et al.*, 1990; Perronnet & Vaillend, 2010). Several studies have provided evidence that these brain dystrophins are involved in higher order functions, in learning and memory (Snow *et al.*, 2013).

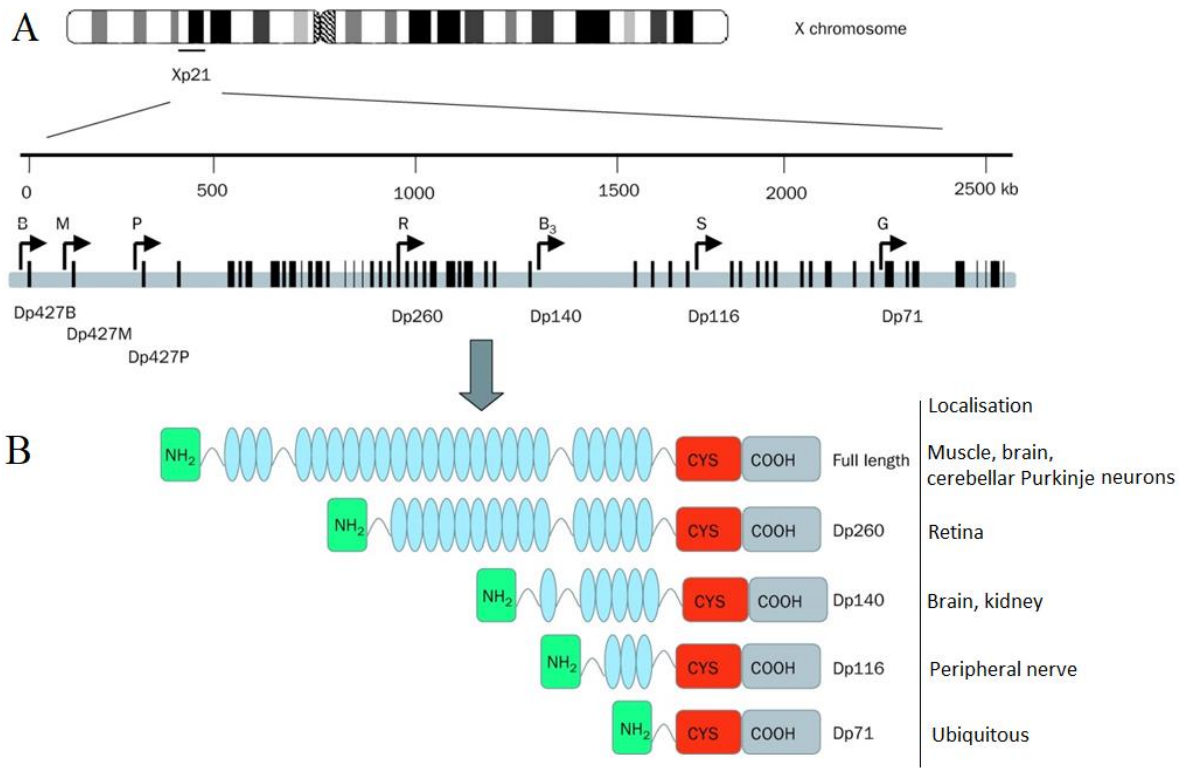

Figure 1.1 Dystrophin gene and isoforms.

(A) Genomic organisation of the dystrophin gene, located in Xp21. The black horizontal lines represent the 79 exons of the dystrophin gene distributed over about 2.5 million bases. Arrows depict the positions of the seven promoters in the dystrophin gene. In particular, brain (B), muscle (M), and Purkinje (P) promoters drive the expression of 'full-length' dystrophin, Dp 427. R, B_3, S and G represent the Dp 260 (retinal), Dp 140 (brain), Dp 116 (Schwann cells), and Dp 71 (general) promoters that drive the short isoform dystrophins. (B) The domain composition and localisation of the various dystrophin isoforms are indicated. The amino-terminal domain is followed by the spectrin-like domain, the cysteine rich, and the carboxyl-terminal domain. Adapted and modified from Blake and Kroger (2000) and Muntoni *et al.* (2003).

Dystrophin, a rod-shaped protein, is primarily expressed in skeletal muscle, smooth and cardiac muscle, and the CNS (Bies, Friedman, *et al.*, 1992; Bies, Phelps, *et al.*, 1992; Feener *et al.*, 1989; Lambert *et al.*, 1993; Mandel, 1989; Sironi *et al.*, 2001; Torelli *et al.*, 1999). It consists of four different domains: an amino-terminal (N-terminal) with an actin-binding site, a large spectrin-like central domain, a cysteine-rich domain and a unique carboxyl-terminal (C-terminal) domain. The N-terminal contains the actin-binding site which links the macromolecule to the underlying actin-based cytoskeleton. The C-terminal of dystrophin interacts with several membrane-bound proteins such as dystrobrevin and other dystrophin associate proteins to form the dystrophin-associated protein complex (DAPC) (or dystrophin-glycoprotein complex: DGC) (Figure 1.2) (Koenig *et al.*, 1988; Sadoulet-Puccio & Kunkel, 1996). In muscle, the DGC stabilises the plasma membrane by forming a critical bridge between the actin cytoskeleton and the extracellular matrix (Ervasti & Campbell, 1993). At the neuromuscular junction, the DGC is involved in the stabilisation of acetylcholine receptors and acetylcholinesterase (Kong & Anderson, 1999; Peng *et al.*, 1999). The absence of dystrophin in DMD results in the collapse of the DGC, thereby rendering the sarcolemma susceptible to mechanical damage during contraction, altered calcium homeostasis, and consequently muscle degeneration (Carlson, 1998; Hendriksen *et al.*, 2015; Pilgram *et al.*, 2010). To date, the role of dystrophin/DGC in the brain is far less known. In CNS, the brain-specific DGC is expressed at the postsynaptic site of neurons, consists mainly of dystrophin, dystroglycan, dystrobrevin and syntrophin (Figure 1.3) (Pilgram *et al.*, 2010). It colocalises with gamma-aminobutyric acid type A ($GABA_A$) receptors ($GABA_AR$) and plays an important role in the membrane stabilisation of $GABA_AR$ clustering (Figure 1.4 A) (Brunig, Suter, *et al.*, 2002). In a mouse model of DMD, the absence of dystrophin results in the reduction of $GABA_AR$ cluster size and number (Figure 1.4 B) (Fuenzalida *et al.*, 2016; Knuesel *et al.*, 1999; Kueh *et al.*, 2008).

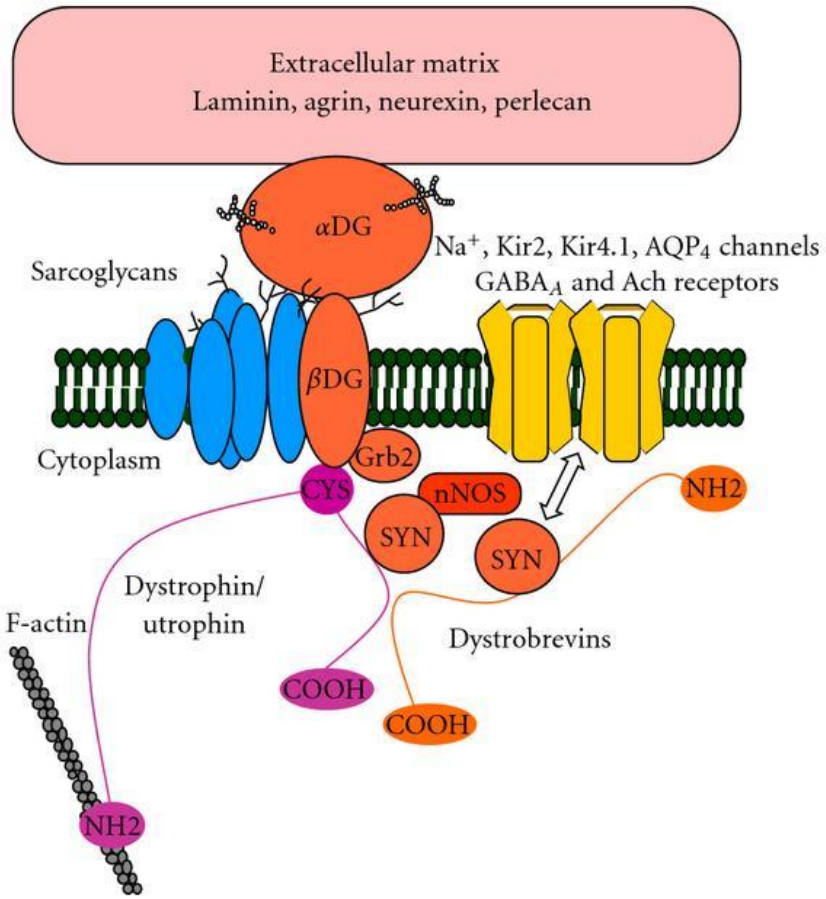

Figure 1.2 Organisation and composition of the DGC.

The NH_2-terminus of dystrophin (purple) binds to cytoskeleton actin while the cysteine-rich and COOH domain interacts with the DGC components. The cysteine-rich domain binds the dystroglycan subcomplex composed of transmembrane β-dystroglycan (β-DG) and extracellular α-dystroglycan (α-DG). The β-DG may interact with the sarcoglycan-sarcospan subcomplex (blue) and with signalling protein such as Grb2. The α-DG is a glycosylated receptor for extracellular matrix proteins, such as laminin, agrin, perlecan, and neuroxin depending on tissue- and cell-specific expression. The COOH-terminus of dystrophin binds the cytosolic syntrophins and dystrobrevins. Dystrobrevins associate with syncoilin, dysbindin, and syntrophins (SYN). Syntrophins contain a PDZ domain enabling associations of the DGCs with a variety of proteins including signalling and synaptic proteins, such as neuronal nitric oxide synthase (nNOS) or neuroligins, as well as several transmembrane channels (AQP-4, potassium Kir2 and Kir4.1, and voltage-gated sodium channels) and receptors (AchR, $GABA_AR$). Adapted and modified from Perronnet and Vaillend (2010).

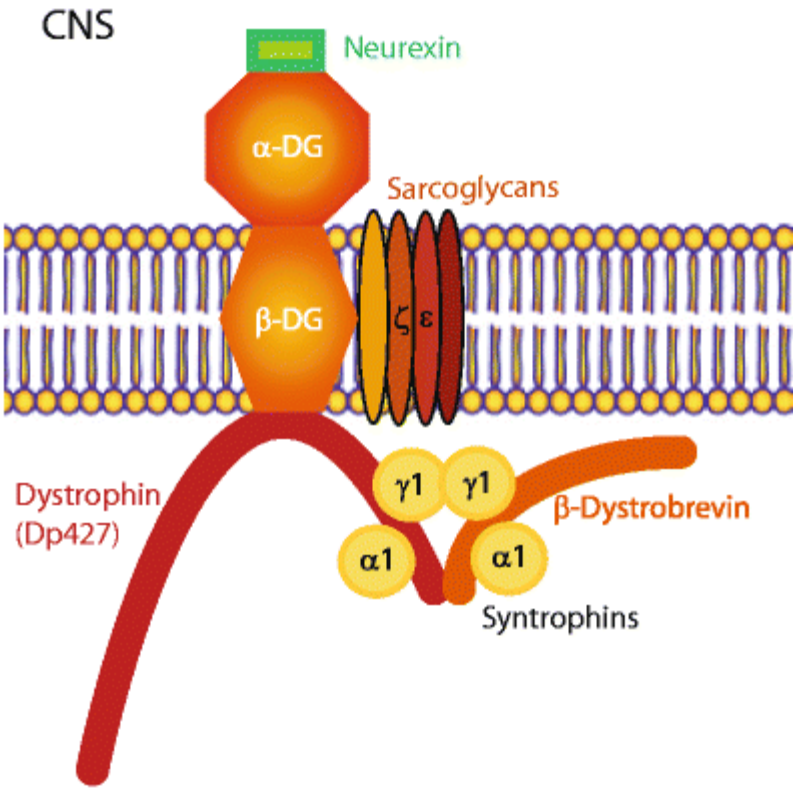

Figure 1.3 DGC complex composition in mammalian CNS.

The neuronal DGC consists of a Dp 427 bound to β-dystrobrevin and dystroglycan, which in turn associates with presynaptic neurexin-α. The complex also contains α1- and γ1- syntrophin as well as ζ- and ε-sarcoglycan. Adapted and modified from Pilgram *et al.* (2010).

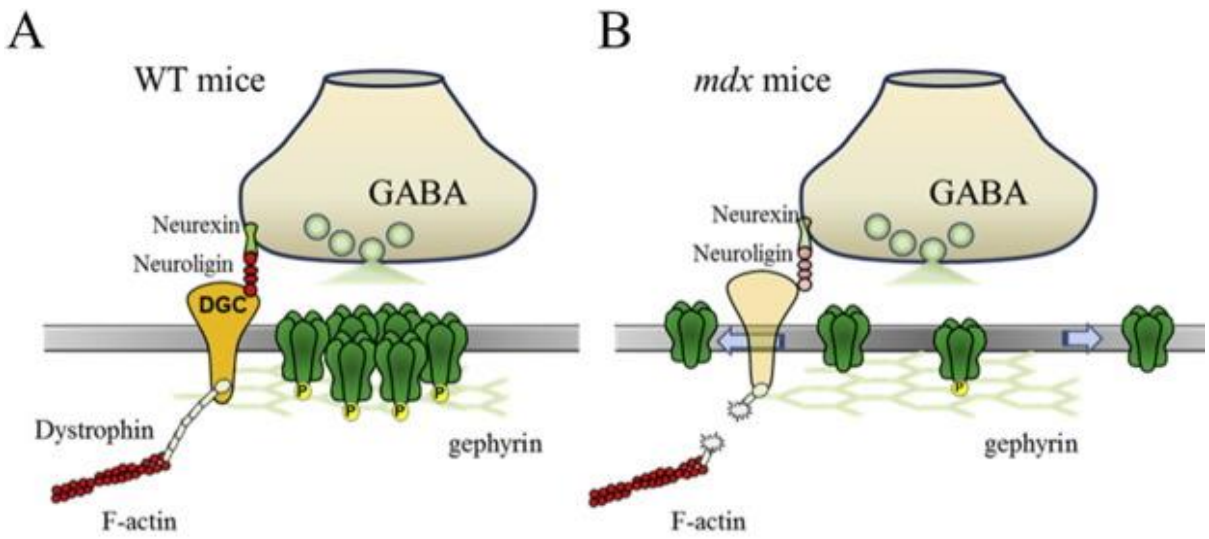

Figure 1.4 The involvement of dystrophin in the stabilisation of $GABA_AR$ clustering.

A schematic drawing depicting the role that dystrophin plays in $GABA_AR$ clustering. (A) In the wild type (WT) mice, the synaptic $GABA_AR$ are stabilised by scaffold protein gephyrin. The presence of dystrophin helps to stabilise the $GABA_AR$ clustering at the postsynaptic site and neuroligin links synaptic cleft by interaction with presynaptic neurexin. (B) The *mdx* mice, a murine model of DMD lacking all Dp 427, showed a marked reduction in the number and size of $GARA_AR$ cluster in the hippocampus and cerebellum. Adapted and modified from Fuenzalida *et al.* (2016) and Knuesel *et al.* (1999).

In addition to full-length dystrophin, several shorter isoforms of dystrophins including Dp 260, Dp 140, Dp 116, and Dp 71 are derived from four internal promoters as a result of splicing between promoter-specific first exons and exons 30, 45, 56, 63 respectively (Desguerre *et al.*, 2009). These isoforms are expressed in the CNS and in various tissues (Knuesel *et al.*, 1999; Perronnet & Vaillend, 2010). The distinct dystrophin isoform expression in various part of the CNS indicates that these proteins play a role in normal brain function in which its deficiency may be related to the cognitive impairment seen in DMD patients. In fact, several genetic studies have suggested a possible association between the type and location of mutations in the DMD gene with mental retardation (Rapaport *et al.*, 1991; Rapaport *et al.*, 1992). In particular, mutations in the C-terminal regions of *DMD* which leads to the disruption of the shorter C-terminal isoforms (Dp 71, Dp 116 and Dp 140) have been shown to result in a more severe intellectual disability in DMD (Lenk *et al.*, 1993; Robert *et al.*, 1992). A deletion extending to the 3' end of exon 63 will affect all dystrophin isoforms (Moizard *et al.*, 1998; Moizard *et al.*, 2000). Dp 71, the short isoform that harbours only the cysteine-rich and C-terminal region of dystrophin, is affected by this distal mutation and the deficiency of this additional isoform is linked to severe mental deficits (mean full-scale IQ of <50.0) (Banihani *et al.*, 2015). However, studies using mice models lacking these short CNS dystrophin isoforms failed to reveal any specific contribution of Dp71 to cognitive dysfunction (Vaillend *et al.*, 1998; Vaillend & Ungerer, 1999). It is likely that the Dp71 is not directly linked to severe cognitive dysfunction. Rather, mutations occurring in the distal region of the DMD gene disrupt expression of all brain dystrophin isoforms hence, resulting in a cumulative deleterious effect and a more severe intellectual disability.

1.4 Evidence for impaired cognitive function in DMD

Since Duchenne's original report of a cognitive involvement in DMD, substantial evidences now exists to support his observation of a CNS component in DMD (Dubowitz, 1965; Duchenne, 1868). However, Gowers did not agree that mental retardation is a feature of DMD (Dubowitz, 1965; Gowers, 1879). Walton and Nattress and Truitt also argued that the majority of their DMD patients were not mentally defective and that the previously observed deficits may be due to poor living or environmental conditions such as the loss of education and low socio-economic ability (Dubowitz, 1965; Truitt, 1955; Walton & Nattrass, 1954). After many years of debate, it is now well established that Duchenne's observation is true. A meta-analysis by Cotton *et al.* (2001) documented the mean IQ of 1146 DMD patients, collected from 32 studies is on average, one standard deviation below the population mean, strongly supporting Duchenne's findings. Furthermore, the uncertainty of whether the reduction in IQ levels are associated with social and educational backgrounds such as family income and parent's education levels was ruled out by Prosser *et al.* (1969). In this study, the DMD patients' Full Scale Intelligence Quotient (FSIQ) scores, which measures the verbal and performance intelligence, were significantly lower than those of their normal siblings who shared similar background when growing up (Prosser *et al.*, 1969). This reinforces the idea that the intellectual deficit in DMD patients is not impacted by socioeconomic factors but is of CNS origin. To further elucidate if cognitive impairment in DMD is a consequence of living with a chronic and progressive disease with limited physical capability, Ogasawara (1989) examined the memory and IQ of two groups of young patients with DMD and another with spinal muscular atrophy (SMA) from the same residential school (Ogasawara, 1989). The authors found that boys from the DMD group performed worse than SMA boys in memory tests and scored poorer for FSIQ. Taken together, these findings demonstrated that lower IQ is one of the

manifestations of DMD and not a sequela from musculoskeletal dysfunction and motor impairment.

1.4.1 Selective cognitive function: Verbal IQ

While numerous investigators suggested that the cognitive impairment of DMD is global in nature, some authors have argued that only selective cognitive functions are affected in these children (Dubowitz, 1965; Prosser *et al.*, 1969; Smith *et al.*, 1990). It was reported that verbal intelligence and verbal skills are more affected in this population than non-verbal or performance intelligence (Cotton *et al.*, 2001). Indeed, DMD children tend to have a delay in speech or specific language impairment (Essex & Roper, 2001; Kaplan *et al.*, 1986). Supporting this notion is a study by Hinton *et al.* (2004), who argued that the "limited verbal span" is the principal cognitive deficit in DMD as their Verbal IQ (VIQ) scores were significantly lower than their Performance IQ (PIQ) scores. The VIQ and PIQ scores of the Wechsler Intelligence Scales are widely utilised for the assessment in language functions and visuospatial abilities in children with DMD (Billard *et al.*, 1992; Cotton *et al.*, 2001). Several studies using different approaches such as sentence repetition (Billard *et al.*, 1992; Hinton *et al.*, 2007), tests of story recall (Hinton *et al.*, 2004; Hinton *et al.*, 2001; Wicksell *et al.*, 2004), and digits recall (Billard *et al.*, 1998; Ogasawara, 1989) have shown that DMD patients present with difficulties during tests that require attention to and repetition of verbal material.

Deficiencies in verbal span are associated with deficits in the acquirement of phonological knowledge and single word vocabulary (Adams & Gathercole, 2000). The acquirement of phonological skill is disrupted when a person fails to detect individual speech sounds, or phonemes. Dorman *et al.* (1988) demonstrated that boys with DMD performed poorly on the sound deletion test when they were required to pronounce some target word with a single

phoneme left out. For example, DMD boys were unable to pronounce “sand” when the phoneme “t” was deleted from “stand”, instead, they pronounced it as “stib”. Moreover, Hendriksen and Vles (2006), from a neuropsychological angle, proposed that reading skills and language are strongly associated with each other and should be treated as a continuum. Children with a delay in language development have also been shown to have increased risk for reading deficit at a later age (Bishop, 2002; Bishop & Snowling, 2004). A study on 25 Dutch DMD boys, aged 8 to 12 years, found that 40% of the subjects were reading disabled and impaired with a significantly reduced reading quotient percentage when compared to the normal population (Billard *et al.*, 1998; Hendriksen & Vles, 2006). Interestingly, a recent study showed that the distinct language-based learning deficits in DMD is similar to that demonstrated in developmental dysphonetic (auditory) and dyseidesia (visual) dyslexia, language disorders that are associated with the cerebellum (Anderson *et al.*, 2012; Bishop, 2002; Hinton *et al.*, 2004; Yang *et al.*, 2016). These cerebellar disorders refer to the difficulties in reading or interpreting words due to deficiency with phonic analysis and synthesis of words as well as perception of the visual words (Anderson *et al.*, 2012; Billard *et al.*, 1998; Bishop & Snowling, 2004; Cotton *et al.*, 2001). Taken together with the expression of Dp 427 in normal cerebellar Purkinje cells but absence in patients with DMD, Lidov *et al.* (1993) emphasised that there may be an involvement of cerebellar non-motor dysfunction in DMD’s cognitive impairment. In summary, this evidence strongly emphasised a cognitive involvement (language delay, phonological production, poor verbal fluency and reading) in DMD boys, which may be due to cerebellar dysfunction.

1.4.2 Histological/Biochemical evidence for a CNS deformity in DMD patients

As shown in section 1.4 and 1.4.1, neurophysiological tests strongly suggest an involvement of brain dysfunction in DMD. However, findings from brain autopsy and brain imaging are

inconsistent, ranging from grossly normal to significantly abnormal neuroanatomy and biochemistry. Post-mortem analyses showed normal weight with no gross abnormalities in the brains of DMD patient, with the exception of only one patient who showed striking histological abnormalities (Dubowitz & Crome, 1969; Jagadha & Becker, 1988). Magnetic resonance imaging (MRI) studies did not reveal any significant anatomical brain modification in DMD patients compared to healthy controls, and no positive association between ventricle dilation and verbal intelligence (al-Qudah *et al.*, 1990; Bresolin *et al.*, 1994). Using another approach, Rae *et al.* (1998) studied the possible involvement of cerebral atrophy in young DMD patients, aged below 13 years old, using magnetic resonance spectroscopy (MRS). They found both the ventricular sizes in DMD patients and control brains to be comparable (Rae *et al.*, 1998). However, this finding is in contrast to previous computerised tomography (CT) scans which showed clear signs of cortical atrophy and ventricular dilations in the older patients and patients with severe physical disability (Yoshioka *et al.*, 1980).

Although the gross brain structure in DMD is normal, many studies have found anatomical and metabolic abnormalities in DMD patients. In contrast to Dubowitz and Crome (1969) and Jagadha and Becker (1988), numerous reports have shown several post-mortem brain abnormalities including reduced brain weight, ventricle dilation, cortical atrophy, heteropias, pachygyria, dendritic abnormalities (i.e. reduction in cortical dendritic length and arborisation), extensive Purkinje cell loss, and gliosis in DMD patients (Anderson *et al.*, 2002; Jagadha & Becker, 1988; Rosman, 1970; Rosman & Kakulas, 1966). In addition, a recent quantitative MRI study on the microstructure of DMD patients showed a smaller total brain and gray matter volume, lower white matter fractional anisotropy, and higher white matter mean and radial diffusivity than healthy controls (Doorenweerd *et al.*, 2014). Doorenweerd and colleagues suggested that the reduced fractional anisotropy and higher mean diffusivity implied a

compromised structural complexity, and proposed a reduced fiber density, increased membrane permeability, and/or decreased structural organisation (Assaf & Pasternak, 2008). The higher radial diffusivity indicates increase fibre branching and demyelination which can result in increased membrane permeability (Song *et al.*, 2005; Vandermosten *et al.*, 2012). In addition, they revealed that a subgroup of DMD patients who lack Dp 140 had the smallest gray matter, total brain, and intracranial volumes. Furthermore, a structural and functional MRI study in ten DMD patients (6.4-14.0 years of age) demonstrated a neuronal circuitry alteration in DMD showing decrease gray matter concentration and decrease local synchronization of spontaneous activity in the motor cortex when compared to healthy controls (Lv *et al.*, 2011). Other CNS alteration such as reduced excitability in the left motor cortex was also demonstrated in four DMD patients (11-15 years of age) in a transcranial magnetic stimulation study (Di Lazzaro *et al.*, 1998). Taken together, these studies showed that the subtle alterations in cortical circuitry are found in patient with dystrophin deficiency.

In addition to the possible anatomical compensation associated with DMD, several metabolic abnormalities have also been demonstrated in DMD brains. A phosphorous-31 MRS study revealed a significant increase brain ratios of inorganic phosphate (P_i) to adenosine triphosphate (ATP), to phosphomonoesters, and to phosphocreatine, implying potential mitochondrial dysfunction leading to bioenergetic changes (Barbiroli *et al.*, 1993; Tracey *et al.*, 1995). Similarly, a hydrogen MRS study showed an increase in the ratio of cerebellar choline-containing compound to *N*-acetylaspartate in patients with DMD, suggesting developmental abnormalities (Rae *et al.*, 1998). In addition, positron emission tomography (PET) imaging studies revealed a reduction in glucose metabolism in the cerebellum, temporal cortical areas, and the right sensorimotor cortex in DMD patients compared to healthy controls (Bresolin *et al.*, 1994; Lee *et al.*, 2002). Lee *et al.* (2002) suggests that this regional glucose

hypometabolism may indicate an association between dysfunction of cerebellum and intellectual deficits, temporal cortical areas and cognitive and behavioural impairment, as well as sensorimotor cortex and reduced manual dexterity (Darian-Smith *et al.*, 1996; Devinsky & Bear, 1984; Eichenbaum, 2000; Fiez *et al.*, 1992; Lee *et al.*, 2002; Liu & Rouiller, 1999; Schmahmann, 1991). In short, these functional studies suggest an alteration in brain metabolism or biochemistry in brains lacking dystrophin.

1.5 Murine model of DMD: the *mdx* mouse

It is evident from the above literature (Sections 1.4 Evidence for impaired cognitive function in DMD), that there is indeed a CNS component in DMD. This evidence was generated from the cross sectional, longitudinal, and retrospective studies, which employed non-invasive approaches. Nevertheless, findings acquired from human subjects are very scarce and limited, especially in studying the mechanism for cognitive dysfunction as a result of dystrophin deficiency, due to the inaccessibility of more invasive measurement on human subjects. As an alternative, over the last decade, animal models which allow for more intrusive studies in DMD have been described. Several animal models for DMD studies have been proposed, which include zebrafish, mouse, *Caenorhabditis elegans* (*C. elegans*), dog, and chicken (Bassett & Currie, 2004; Bulfield *et al.*, 1984; Collins & Morgan, 2003; Kornegay *et al.*, 2012; Lemaire *et al.*, 1988). Despite the great variety of choices in animal models, there is no single agreement on which animal model best represents DMD. In addition, while these animal models share a similar defective gene, there is considerable variability in their phenotypic expression across and within a species. This could in part be due to the ability of different species to adapt to a defective gene product. Thus, the selection of a model is often experimental and reliant upon which animal is well-matched for the tests to be investigated.

Currently, the most extensively used animal model to study the effect of the lack of dystrophin on CNS function is the dystrophin-deficient *mdx* (X-chromosome-linked muscular dystrophy) mouse. This is due to its short breeding time, genetic uniformity, budget, and handiness for laboratory experiments (Grounds *et al.*, 2008). The discovery of the naturally occurring *mdx* mouse (C57BL/10ScSn-*Dmd*^{mdx}) was first reported by Bulfield *et al.* (1984). Together with other authors, he described this mutant as an X-linked recessive model with elevated serum pyruvate kinase and creatine kinase levels as well as the initial development of some similar features of muscle histopathology to DMD, such as degeneration of the limb musculature (Bulfield *et al.*, 1984; Dangain & Vrbova, 1984; Torres & Duchen, 1987). Despite sharing parallel histopathological features, this mouse has milder clinical presentation which is in contrast to DMD patients (Hoffman, Brown, *et al.*, 1987). The muscle pathology in *mdx* mice is different from DMD patients in some important aspects, such as the successful muscle fibre regeneration and reduced endomysial fibrosis (Torres & Duchen, 1987). As a consequence of its successful regeneration process, the fibrosis and fat tissue replacement, commonly seen in DMD muscles, are not prominent in young adult *mdx* mice(Araki *et al.*, 1997; Torres & Duchen, 1987). These findings are in marked contrast to the manifestation observed in DMD, questioning its genetic homology (Avner *et al.*, 1987).

However, several studies have shown that the *mdx* mouse may be more representative of the disease pathology in DMD than has been appreciated. Histopathological studies showed that after the age of 16 weeks, there is a steady increase in the number of malformed (branched) myofibres in the aging *mdx* mouse (Chan *et al.*, 2007a; Head *et al.*, 1992; Pastoret & Sebille, 1995). In addition, the aged *mdx* mouse was also more susceptible to injury from lengthening-contraction protocols. While the absolute force (not corrected for cross-sectional area) generated by the *mdx* mouse muscle was not significantly different from that of age-matched

littermate control (LC), the specific force (corrected for cross-sectional area) produced by *mdx* mice was significantly reduced when compared to LC. This indicated that as the *mdx* mouse ages, muscle weakness becomes more apparent in that the force generation is markedly reduced (Chan *et al.*, 2007a). The aged *mdx* mouse is able to compensate for this weakness by muscle hypertrophy, a likely explanation for the milder phenotype in comparison to DMD patients. Furthermore, the diaphragm of the *mdx* mouse also showed progressive replacement with fibrous connective tissue, demonstrating the severe pathology seen in DMD where loss of diaphragmatic function is a main concern (Lynch *et al.*, 1997; Stedman *et al.*, 1991). Additionally, it was found that fibrosis and fatty deposits appear in the limb muscles of old *mdx* mice (Lefaucheur *et al.*, 1995; Pastoret & Sebille, 1995). Mapping studies demonstrated that the *mdx* mutation is indeed located within the mouse dystrophin gene, which is equivalent to the mutation in the DMD gene in the human X chromosome (Ryder-Cook *et al.*, 1988). Sicinski *et al.* (1989) also showed that a point mutation in exon 23 induced a premature stop codon, preventing the synthesis of Dp 427 further confirming that the *mdx* mouse is a valid genetic model for DMD and us especially useful for studying the effect of dystrophin in the CNS (Sicinski *et al.*, 1989; Willmann *et al.*, 2009).

To date, the *mdx* mouse model has been widely adopted for muscular dystrophy studies. Since a single dystrophin gene can give rise to different dystrophin products, genetically engineered and chemically induced *mdx* variants with an absence of different dystrophin isoforms have been generated, as summarised below (Table 1.1) (Araki *et al.*, 1997; Bulfield *et al.*, 1984; Chapman *et al.*, 1989; Cox *et al.*, 1993; Wertz & Fuchtbauer, 1998).

Table 1.1 Mouse models of DMD, relative to its absence of dystrophin isoforms.

Mouse model of DMD	Absence of dystrophin isoforms	Mutation	Authors and published year
mdx	Dp 427	Exon 23 point mutation	Bulfield *et al.* (1984)
mdx^{5cv}	Dp 427	Exon 10 point mutation	Cox *et al.* (1993)
mdx^{2cv}	Dp 427 and Dp260	Intron 42 point mutation	Chapman *et al.* (1989)
mdx^{4cv}	Dp 427, Dp260, and Dp140	Exon 53 point mutation	Chapman *et al.* (1989)
mdx^{3cv}	Dp 427, Dp260, Dp140, Dp116, and Dp71	Intron 65 point mutation	Chapman *et al.* (1989)
mdx52	Dp 427, Dp140 and Dp260	Exon 52 deletion	Araki *et al.* (1997)
mdx-βgeo	All dystrophin gene product	Insertion of β-geo trap cassette in Exon 63	Wertz and Fuchtbauer (1998)

1.6 Evidence for CNS involvement in the *mdx* mice

1.6.1 Histological evidence for a CNS deformity

The *mdx* mouse shows no gross structural abnormalities in the brain or spinal cord (Bulfield *et al.*, 1984; Dunn & Zaim-Wadghiri, 1999; Miranda *et al.*, 2009; Torres & Duchen, 1987; Yoshihara *et al.*, 2003). Nevertheless, alteration in cell number, size and/shape have been demonstrated in areas of the cerebral cortex and brain stem of *mdx* mice (Carretta *et al.*, 2004; Carretta *et al.*, 2001; Carretta *et al.*, 2003; Minciacchi *et al.*, 2010; Sbriccoli *et al.*, 1995). Using a tract tracing approach, Sbriccoli *et al*. 1995 reported a lower absolute number (reduced of about one half) and cell packing density of the cortico-spinal neurons in *mdx* mice compared to controls. Despite the normal perikaryal sizes, these neurons were smaller on average and round in shape, whereas the control neurons displayed bigger cell sizes and were pyramidal in shape. Moreover, this group also reported a significant reduction of rubro-spinal neurons in *mdx* mice and postulated that it might be due to the reduced cortico-rubral or cortico-spinal collateral input. (Carretta *et al.*, 2001).

As the involvement of altered calcium metabolism in neurons was reported in *mdx* mice, Carretta and co-workers investigated the expression of the calcium-binding proteins parvalbumin, calbindin, and calretinin in the cerebral cortex of *mdx* mice (Carretta *et al.*, 2003; Hopf & Steinhardt, 1992). In somatosensory and motor cortices, it was reported that the parvalbumin-positive and calbindin-positive interneurons were significantly more numerous (increase by 16-39%) in *mdx* mutant than wild type (WT) mice. The laminar distributions of parvalbumin-positive interneurons in both brain regions were altered, displaying less defined laminar segregations. This group speculated that the increased number of these interneurons possibly contributed by the perturbed calcium metabolism during development, as a compensatory mechanism to counteract for the increased intracellular calcium concentration ($[Ca^{2+}]_i$) and subsequent calcium-driven excitotoxicity and cell death (Carretta *et al.*, 2003). Next, Carretta *et al*. (2004) concluded three different modalities of cortical remodelling for calcium-binding protein populations in the *mdx* mouse. This group reported that the changes of spatial distributions were parallel to the increased number of parvalbumin-positive neurons in the motor cortex, whereas in the anterior cingulate cortex, it was paired with unchanged cell numbers (parvalbumin- and calbindin-positive neurons). In the somatosensory cortex, there was no change in the spatial distribution despite the increase numbers of parvalbumin- and calbindin- positive neurons. Consistently, Del Tongo *et al.* (2009) also showed that there is an increase in parvalbumin interneuron density across the CA1-CA3 and dentate gyrus subfields and of inhibitory synapses in CA1 proximal radiatum in *mdx* mice. Taken together, these findings indicate that the loss of dystrophin has resulted in cytoarchitectural rearrangement of calcium-binding protein cells in *mdx* mice. These changes may reflect a distinctive involvement in the damage and/or a differential structural and functional ability in response to dystrophin deficiency (Carretta *et al.*, 2004; Del Tongo *et al.*, 2009).

As the cytoarchitectural rearrangement has been noted in the cortex of *mdx* mice, the same group went on to clarify the fine anatomical organization of associative cortico-cortical neurons on the primary motor and somatosensory cortices in the *mdx* mice (Minciacchi *et al.,* 2010). They reported that the absolute number of associative pyramidal neurons was significantly greater in *mdx* than in control animals. The terminal branches of the basal dendrites of layer 2/3 pyramidal neurons were significantly longer in *mdx* compared to control mice, whereas the density of dendritic spines was significantly lower in *mdx* animals. Collectively, the anomalies of associative cortico-cortical projection in *mdx* mice suggest that the impaired neurobiology potentially underlies the cognitive dysfunction in DMD (Minciacchi *et al.,* 2010).

Currently, the investigation of the structural abnormalities in CNS has been extended to the ultrastructural levels. A marked reduction in the number and size of $GABA_AR$ clusters in the hippocampal region CA1 and cerebellum in dystrophin deficient *mdx* mice was first reported by Knuessel *et al*. (1999). Subsequently, the malformed synapses in the dendritic and pyramidal layers of *mdx* hippocampus were reported by several other investigators (Knuesel *et al.,* 2001; Miranda *et al.,* 2011; Miranda *et al.,* 2009). By using a quantitative electron microscopy, Miranda *et al.* (2009) evaluated the density and ultrastructure of CA1 hippocampal synapses in *mdx* mice. Miranda and colleagues found that *mdx* mice have significantly increased density of axodendritic symmetric inhibitory synapses and larger postsynaptic densities in perforated asymmetric excitatory synapses in the proximal, CA1 apical dendrites which normally express dystrophin. The increased inhibitory synapse density may reflect a partial compensation of reduced dendritic inhibition mediated by GABAergic transmission, in response to an altered clustering of α2 subunit-containing $GABA_AR$ in CA1 dendrites. The increased postsynaptic density length in perforated synapses may suggest alterations in glutamatergic synapse organization that is associated with an enhanced synaptic excitation.

Next, Miranda and co-workers went on to examine the integrity of the presynaptic ultrastructure, especially on the distribution of the synaptic vesicles in axospinous non-perforated-excitatory synapses of the CA1 hippocampal dendritic field in *mdx* mice. Using the same technique, they reported an increased number of docked vesicles, that were characterised by an abnormal shift of the vesicle distribution from the reserve pools, and a marked reduction of vesicles size as the major alterations of presynaptic ultrastructure in the *mdx* mouse (Miranda *et al.*, 2011). The increase of this specific vesicle pool may result in an enhanced release probability in excitatory synapses of dystrophin-deficient neurons. This is consistent with their previous finding that showed an increased length of the postsynaptic densities in the perforated subtype of excitatory synapses, as both factors can be viewed as the hallmarks of enhanced activity and/or plasticity at glutamatergic synapses in dystrophin deficient mice (Miranda *et al.*, 2009).

The macro-level modification in *mdx* brain was revealed in an MRI study (Xu *et al.*, 2015). Xu and colleagues reported enlarged lateral ventricles despite no differences in total brain volume, indicating possible gray matter atrophy in *mdx* mice (Xu *et al.*, 2015). Furthermore, using an unbiased stereological estimation technique, a globally reduced neuron density in the hippocampus of *mdx* mice was reported in a later study (Miranda *et al.*, 2016). Miranda and co-workers found a significant reduction (~34%) in the number of CA1 pyramidal neurons in the anterodorsal hippocampus. However, the quantitative decrease varies along the hippocampal antero-posterior axis. This finding contradicts their previous reports that failed to demonstrate any significant modification in the *mdx* hippocampal neuron density, possibly due to the different methods used in prior studies (Miranda *et al.*, 2011; Miranda *et al.*, 2009). In summary, these findings have extended knowledge of the brain morphofunctional alterations

induced by dystrophin deficiency and that the perturbation of neurogenesis and/or neuron survival is potentially contributing to cognitive deficits in DMD (Miranda *et al.*, 2016).

Although there are numerous studies investigating brain morphology or histopathological changes due to dystrophin loss in cerebral cortex and hippocampus, only limited reports have documented the effect of dystrophin deficiency on cerebellar histopathology. A pilot immunohistochemistry study by Sim and Rae (2011) suggests a trend towards a decrease in cerebellar Purkinje cell populations in *mdx* mutant. Perhaps due to the small mouse number (n=4 for each group), the authors did not show any significant differences in *mdx* mice when compared to the control group. Consistently, a recent haematoxylin and eosin staining study also showed no significant histopathological changes or neuronal loss in the cerebellum of *mdx* mice at different stages of age, including 24-day, 12-week, and 9-month compared with age-matched controls (Tuckett *et al.*, 2015). Nevertheless, when these neurons were stained with Alizarin red, a water-soluble sodium salt of Alizarin sulfonic acid that is used to stain calcium deposits in tissues, an increased percentage of calcium-positive neurons were observed in the *mdx* cerebellum. Taken together, these studies suggest possible morphological changes and altered number of cerebellar neurons in *mdx* cerebellum which needs to be further characterised.

1.6.2 Behavioural studies

1.6.2.1 *mdx* mice

A pioneering study addressing the involvement of cognitive deficits in the *mdx* mouse was first reported by Muntoni and co-workers in 1991 (Muntoni *et al.*, 1991). These investigators suggested that the passive avoidance learning in *mdx* mice was significantly impaired when

compared to control mice, as indicated by the difference in the retention of passive avoidance responses (Vaillend *et al.*, 1995). Additionally, the long-term recognition memories of these mice were also compromised. Vaillend and co-workers further characterised this cognitive deficit with a follow up water maze study in 2004. In this study, they revealed that dystrophin deficiency had disrupted the long term object recognition and spatial memory in *mdx* mice (Vaillend *et al.*, 2004). These mice also displayed a severe deficit in spatial memory, indicated by their failure to look for the hidden platform in the water maze. Interestingly, additional behavioural studies reported that the ability to learn and consolidate short term memory, procedural memory and spatial discrimination tasks, novelty-seeking behaviour and exploration in an elevated plus maze were all unaffected in this animal model (Sesay *et al.*, 1996; Vaillend *et al.*, 1998; Vaillend *et al.*, 1995).

More interestingly, in addition to hippocampus, an immunostaining study in WT mice demonstrated the expression of Dp 427 in the amygdala, which is a brain region associated with contextual fear (Maren & Fanselow, 1995; Sekiguchi *et al.*, 2009). In the *mdx* mouse which lacks Dp 427, the authors found an enhanced defensive freezing behaviour to aversive stimuli (restraint and foot shock) when compared to WT control. Furthermore, these fear responses were ameliorated after the intracerebroventricularly administration of an antisense morpholino oligonucleotide. This treatment induces skipping of the premature stop codon located at exon 23 in the *mdx* mouse and produces a truncated dystrophin that retains the physiological function of full-length dystrophin (Alter *et al.*, 2006).

Taken together, these behavioral studies showed that the loss of Dp 427 is implicated in the cognitive dysfunction of *mdx* mice. The absence of Dp 427 expression in different brain regions (hippocampus and amygdala) contributes to distinct cognitive deficit profiles. These

studies also suggest that Dp 427 deficiency alone is sufficient to impact cognitive functions and that this deficiency may underlie the poor reading, learning and memory in children with DMD.

1.6.2.2 *mdx*^{3cv} mice

To date, overwhelming evidence suggests that the diverse severity of cognitive dysfunction in DMD patients is likely due to the cumulative effects of inactivation of Dp 427 and other *DMD* expressed short isoforms products (Dp 260, Dp 140, Dp 116, Dp 71) (Daoud *et al.*, 2009; Desguerre *et al.*, 2009; Taylor *et al.*, 2010). Thus, the study of DMD using the *mdx* mice model which only lacks the full length Dp 427, yet retains other short dystrophin isoforms, is not inclusive enough to address the distinct cognitive deficits associated with this disorder. Since *mdx* mice display limited and task-specific impairments in learning and memory, research on the behavioural and physiological aspect of the disease would benefit from a mouse model that lacks other short dystrophin isoforms in the CNS.

To overcome these concerns, Vaillend *et al.* (1998) employed the *mdx*^{3cv} mouse model, which was generated by *N*-ethylnitrosourea chemical mutagenesis with a point mutation in intron 65 in their study (Chapman *et al.*, 1989). In this mouse model, all dystrophin gene products that are normally expressed in mouse brain are absent, including both Dp140 and Dp 71 (Cox *et al.*, 1993; Vaillend *et al.*, 1998). Given this advantage, the *mdx*^{3cv} mutant appears to be a suitable model for Vaillend *et al.* to study the effects of C-terminal dystrophins (Dp 140 and Dp 71) deficiency on the hippocampal cognitive functions. This specific cognitive function was of particular interest due to its essential role in learning and memory, which are profoundly disturbed in DMD patients with severe cognitive deficits. Previous studies have linked hippocampal injury to impaired spatial memory which is important in various tasks, such as

spatial discrimination learning in a radial maze (Jarrard, 1995; O'Keefe & Conway, 1978; Olton *et al.*, 1979). However, spatial learning in the *mdx*^{3cv} mice was unaltered. The authors postulated that this unexpected finding could possibly be due to the implementation of a high degree of training in these mice, which is known to strengthen performance.

Additional behavioural characterisation of *mdx*^{3cv} mice had been done by Vaillend and Ungerer in 1999. They tested the mice's learning skills, emotional reactivity, and motor capabilities using the operant learning task and delayed spontaneous alternation task in a T-maze, light-dark choice situation, and spontaneous locomotor activity test (Vaillend & Ungerer, 1999). Through these extensive experimental tests, this group reported that the learning abilities of this mutant were mild delays (or moderate) but not impaired. The learning capabilities of *mdx*^{3cv} mice were comparable to the original *mdx* mouse and they did not have noticeable learning deficits. However, the anxiety-related behaviours of *mdx*^{3cv} mice were enhanced when they were submitted to a bright light environment, an anxiogenic situation for animals (Belzung, 1992). The hesitation and anxiousness of *mdx*^{3cv} mice were shown by the longer latencies to enter the lit box and a shorter time spent within it. In addition to this, the *mdx*^{3cv} mice showed a reduced locomotion contrary to the earlier findings of the original *mdx* mice (Vaillend *et al.*, 1998; Vaillend *et al.*, 1995). Vaillend and colleagues concluded that the lack of C-terminal dystrophins may not have a big impact on the hippocampal associated learning and memory function and suggested a masking effect by some unknown compensatory mechanisms in *mdx*^{3cv} mice. In addition, the potential impact of C-terminal dystrophin deficiency on other brain functions that are independent from hippocampus function, such as cerebellar-associated verbal function, remains an open question.

1.6.3 Electrophysiological studies

Although behavioural studies have shed some light on the involvement of dystrophin in CNS function, these types of studies do not provide insights into the electrical properties or activities of neuronal cells. Moreover, the findings of these studies are vulnerable to experimenter effects such as different judgments or rating of behaviours, differences in body odours and handling methods; methodological and environmental effects such as habituation of the animals to the apparatus, time of day for testing, traffic and noise in the colony, which may affect the results (Wahlsten *et al.*, 2003). In contrast, electrophysiological studies provide more conclusive evidences on the mechanisms of system interactions. These studies allow the direct correlation between neuronal lesions and its unique physiological consequences in regard to higher-order cognitive processing. Electrophysiological studies of dystrophin-deficient mouse models are very important for the appreciation of the cognitive consequences of DMD, as invasive measurements are highly unlikely to be carried out on human patients.

1.6.3.1 Hippocampus (Schaffer-commissural projections to pyramidal cells of CA1)

The role of dystrophin in synaptic function was revealed by an electrophysiological study that showed altered synaptic transmission in *mdx* hippocampal brain slices (Mehler *et al.*, 1992). Mehler and colleagues reported that synaptic transmissions in hippocampal pyramidal neurons were significantly more vulnerable to hypoxia-induced damage in *mdx* mice. The authors explained that the enhanced sensitivity of *mdx* neurons to hypoxic insults may be due to the increased calcium influx, triggering the neuronal excitotoxicity cascade, as a result of plasmalemmal instability caused by dystrophin deficiency (Haws & Lansman, 1991; Menke & Jockusch, 1991). Interestingly, this altered synaptic transmission was reversed when the neurons were pre-treated with an anticonvulsant compound diphenylhydantoin (DPH) prior to the 5-minute hypoxic insult. The authors proposed that DPH recovered this synaptic

transmission potentially by its ability to work against neuronal excitotoxicity such as dampening neuronal excitability, obstructing several calcium-dependent neuronal functions, inhibiting both the high-frequency sodium-dependent action potentials (APs), and low-threshold, transient calcium channel conductance (Stanton & Moskal, 1991). This finding is very valuable as it indicates that the disrupted synaptic transmission in *mdx* mutant may be related to an altered $[Ca^{2+}]_i$ levels, although it is not well established yet.

To gain further insight into the synaptic function of *mdx* mutant, several groups have investigated the long-term potentiation (LTP) in hippocampus, using both *in vivo* and *ex vivo* approaches (Sesay *et al.*, 1996; Vaillend *et al.*, 1998). LTP is a form of synaptic transmission with an increased synaptic strength that lasts for many hours, as a result of the brief repetitive activation of excitatory synapses (Malenka *et al.*, 1988). LTP is of particular interest because it is assumed to have important roles in cellular mechanisms that may underlie some forms of information processing, in which its subtle alteration might underlie the cognitive dysfunction in DMD (Bliss & Collingridge, 1993; Silva *et al.*, 1996; Vaillend *et al.*, 1998). Although both authors used different experimental setups, they reported a similar finding, that the *mdx* evoked synaptic responses were unchanged, after the induction of tetanic stimulations (i.e. constant current stimuli delivered at various time) in two hippocampal pathways (the performant and the Schaffer-commissural projection). Additionally, Vaillend *et al.* (1998) reported that the hippocampal LTP in the more severely dystrophic *mdx*^{3cv}mice was also unchanged. Strikingly, sustained enhancement of hippocampal LTP in *mdx* mice was found in a latter study by the same authors (Vaillend *et al.*, 2004). Vaillend and co-authors explained that the conflicting findings were due to differences in the experimental design: the use of extended and distributed training paradigms in the previous studies were known to improve long-term memory (i.e. which led to the failure in reporting the alteration of this synaptic transmission in the previous

studies) versus the masses training paradigm in the 2004 study. More importantly, as enhancement of hippocampal LTP had been reported to be involved in other memory-impaired genetic mouse models. The authors concluded that this abnormally enhanced hippocampal synaptic plasticity or LTP may be involved in the cognitive dysfunction in *mdx* mice and perhaps explain the cognitive deficits seen in boys with DMD (Vaillend *et al.*, 2004).

On the other hand, when investigating short-term synaptic plasticity, another form of hippocampal-dependent learning, Vaillend *et al.* (1998) found an increase of post-tetanic potentiation (PTP) but not paired-pulse facilitation (PPF) in *mdx* mutants, suggesting that the facilitated expression of short-term plasticity occurs postsynaptically instead of presynaptically. PPF is a potentiation of the second of two responses at intervals of ten milliseconds, and is frequently assumed to occur as a consequence from a transient presynaptic calcium discharge triggered by the first stimulation (Creager *et al.*, 1980). Unchanged PPF indicates that the presynaptic mechanism involved in the calcium-dependent release of glutamate was normal in the *mdx* mouse model. Conversely, an increase of PTP is an enhanced postsynaptic response to presynaptic release of neurotransmitter following a high frequency stimulation, which last at most a few minutes (Binder *et al.*, 2009; Vaillend *et al.*, 1998). More importantly, the authors argued that an alteration of postsynaptic modulation of free Ca^{2+} that resulted from tetanic stimulation might also contribute to PTP enhancement, which may potentially underlie the enhanced short-term plasticity in the *mdx* mouse (Malenka *et al.*, 1988).

Facilitated synaptic potentiation by high frequency stimulation is regulated by both the pre-and postsynaptic mechanisms, which involve the simultaneous presynaptic release of neurotransmitter and adequate depolarization to cause activation of the N-methyl-D-Aspartate (NMDA) subtype of glutamate receptor channel complex, which results in an increase of

calcium influx into the postsynaptic cell (Bliss & Collingridge, 1993; Fisher *et al.*, 1997; Hanse & Gustafsson, 1994; Malenka & Nicoll, 1993). In line with the findings in Vaillend *et al.* (1998), instead of presynaptic contribution, a follow-up study by Vaillend *et al.* (1999) suggests that the enhanced short-term synaptic plasticity was due to a facilitated NMDA receptor (NMDAR) activation at the postsynaptic density as a result of reduced sensitivity to magnesium block. Other postsynaptic input such as calcium-permeable ion channels (i.e. voltage-gated calcium channels (VGCCs) were tested using antagonists nifedipine or $NiCl_2$) was reported not to play any significant role in this synaptic transmission. Taken together, these findings indicate that the enhanced short-term synaptic potentiation in *mdx* mice is due to a facilitated NMDAR activation at the postsynaptic membrane, further supporting the important role dystrophin plays in postsynaptic transmission (Lidov, 1996).

Under normal physiological conditions, it was suggested that the excitability of the synapse is modulated by the balance between synaptic excitation mediated by NMDAR and synaptic inhibition that is mediated by GABA receptors (Dingledine *et al.*, 1986). Interestingly, a decreased number of postsynaptic $GABA_AR$ clusters were found in the hippocampus and cerebellum of the *mdx* mouse (Knuesel *et al.*, 1999). This indicates that there is a possibility where dystrophin deficiency may reduce GABAergic neurotransmission, and that subsequently leads to neuronal disinhibition, increased NMDAR activation, and eventually resulting in an enhanced NMDAR-mediated short-term potentiation (STP) (Vaillend & Billard, 2002). In addition to STP, the induction and/or expression of CA1 hippocampal short-term depression (STD), which is triggered by the prolonged episodes of low-frequency stimulation, may also be mediated by the enhanced NMDAR activity in the *mdx* mouse (Malenka & Nicoll, 1993; Vaillend & Billard, 2002). In the presence of $GABA_AR$ antagonist, bicuculline (10μM), both abnormally enhanced STP and STD mediated by NMDAR were abolished, indicating that an

altered $GABA_A$ transmission was responsible for the neuronal disinhibition which potentially further contributes to the facilitated NMDAR activity, and thus enhanced synaptic potentiation, as a result of dystrophin loss (Vaillend & Billard, 2002).

Since deficiency of GABAergic transmission in *mdx* mice has been proposed by Vaillend's group, Graciotti *et al.* (2008) went on to further characterise the functional aspects of this synaptic transmission in dystrophic hippocampus. Using whole-cell patch clamp technique, they reported that there was no gross postsynaptic alteration in response to GABA released onto CA1 pyramidal neurons of *mdx* mice, as indicated by the unchanged amplitudes of both the evoked and miniature inhibitory postsynaptic currents (mIPSCs). Inhibitory postsynaptic current (IPSCs) is an induced electrical event, occurring in a postsynaptic cell, as a result of neurotransmitters release by the presynaptic terminal. This subsequently leads to the opening of chloride channels, allowing the cell to hyperpolarise (Binder *et al.,* 2009). When tetrodotoxin (TTX), a naturally occurring sodium channel blocker, is added to the recording bath, the TTX-resistance IPSCs mediated by $GABA_AR$ are named mIPSCs (Graciotti *et al.,* 2008). Although the amplitudes of mIPSCs remained unaltered, the frequency of mIPSCs (i.e. the number of events by time unit) which is an indicator of release probability, was significantly higher in *mdx* mice when compare to control mice (Graciotti *et al.*, 2008). The possibility of an increased release probability of inhibitory synapses in the hippocampus of *mdx* mice was tested using PPF analysis. The PPF index is the ratio of the amplitude of the second vs the first response (Vaillend *et al.,* 1998). It is worthwhile to note that GABAergic synapses undergo PPF when their release probability is low (Ouardouz & Lacaille, 1997). Graciotti *et al.* (2008) reported that the release probability at GABAergic synapses in the hippocampus of *mdx* mice was higher than the controls, as demonstrated by the marginally facilitated second IPSCs. This facilitation was consistently present in wildtype mice, indicating a low release probability. This

study concluded that the altered presynaptic release probability of GABAergic synapse may contribute to alterations of inhibitory synaptic transmission in the brain of dystrophic mice.

1.6.3.2 Cerebellum

In addition to hippocampal function, recently there is increased interest in studying the impact of cerebellar dystrophin (P-dystrophin) deficiency on cognitive function. As detailed in section 1.4.1, the lack of full-length dystrophin may be involved in the cerebellar-associated cognitive dysfunction in DMD boys. Previous studies on synaptic function in *mdx* hippocampus have been detailed by Vaillend and other groups. They revealed that the dystrophin deficiency has detrimental effects on synaptic efficacy. These alterations include the abnormally enhanced short-term and long-term potentiation, and short-term depression in the *mdx* hippocampus. These altered hippocampal synaptic functions were believed to be caused by the imbalance between synaptic excitation and inhibition, as demonstrated by the facilitated NMDAR activation and higher release probability of GABAergic synapses. It is now well established that cerebellar Purkinje cells have a major role in the inhibitory (GABAergic) synaptic transmission in the CNS. Since full-length dystrophin is also expressed abundantly in the cerebellar Purkinje cells, any alteration of synaptic transmission in this brain region as a results of dystrophin loss may impose a devastating influence on normal brain function, that may be correlated with the intellectual deficits demonstrated in patients with DMD.

There are three distinct neuronal layers in the cerebellum, the outermost molecular layer, the middle Purkinje cell layer, and the innermost granular layer (Figure 1.5). The cerebellar Purkinje cells receive both the inhibitory and excitatory inputs from the molecular and granular layers. Purkinje cell axons make inhibitory synapses (by releasing GABA) with neurons in the vestibular and cerebellar nuclei, this constitutes the only output from the cerebellar cortex (Ito

& Yoshida, 1964, 1966; Ito *et al.*, 1964; Voogd & Glickstein, 1998). The parallel fibres (PF) (i.e. the axonal extensions of granule cells) at molecular layer and the climbing fibres (CF) (i.e. the terminals of the axons from interior olive neurons) at Purkinje cell layer are the excitatory inputs to Purkinje cells (Kandel, Schwartz, & Jessell, 2012). Stimulation of PF results in a simple spike action potential (AP) with a firing rate of about 50-100 Hz (Eccles *et al.*, 1966b) (Figure 1.6 A), whereas the excitation of CF evokes a complex spike consisting of a large excitatory postsynaptic potential (EPSP). The complex spike is the summed electric responses of many cells evoked by short electrical stimulation of Purkinje dendrites or synaptic inputs (Binder *et al.*, 2009; Eccles *et al.*, 1966a), superimposed with calcium spikes, with a discharge rate of about 1 Hz (Llinas & Sugimori, 1980a, 1980b) (Figure 1.6 B). On the other hand, the inhibitory inputs (i.e. GABAergic) onto the Purkinje cells are transmitted by the molecular layer interneurons, the basket cells and stellate cells. The excitation of these interneurons leads to a hyperpolarising inhibitory postsynaptic potential (IPSP) (Eccles *et al.*, 1967; Vincent & Marty, 1996).

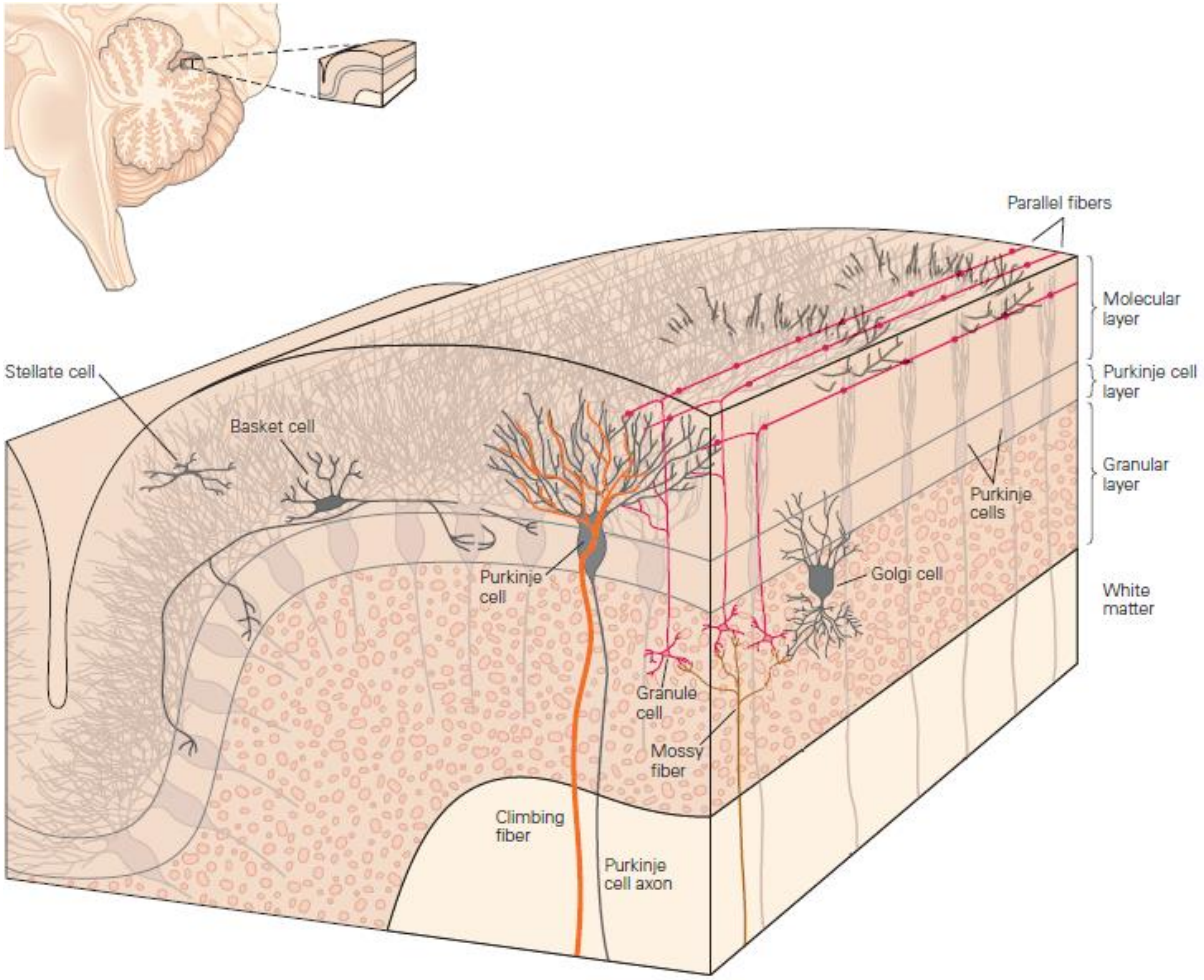

Figure 1.5 The cerebellar cortex contains three layers and five types of neurons.

A schematic drawing shows the general organisation of the cerebellar cortex from the vertical section of a single cerebellar folium. The three neuronal layers include the outermost molecular layer, the middle Purkinje cell layer, and the innermost granular layer. The granular layer is the input layer and contains a vast number of granule cells and a few larger Golgi interneurons. The Purkinje cell layer is the only output layer from the cerebellar cortex. It receives excitatory inputs from the CF (originate from the inferior olivary nucleus) and PF (axons of the granule cells) and inhibitory inputs from the interneurons. The molecular layer is the processing layer and it contains the two inhibitory neurons, the stellate and basket cells, the dendrites of Purkinje cells, and the PF. Adapted and modified from Kandel, Schwartz, Jessell, *et al.* (2012).

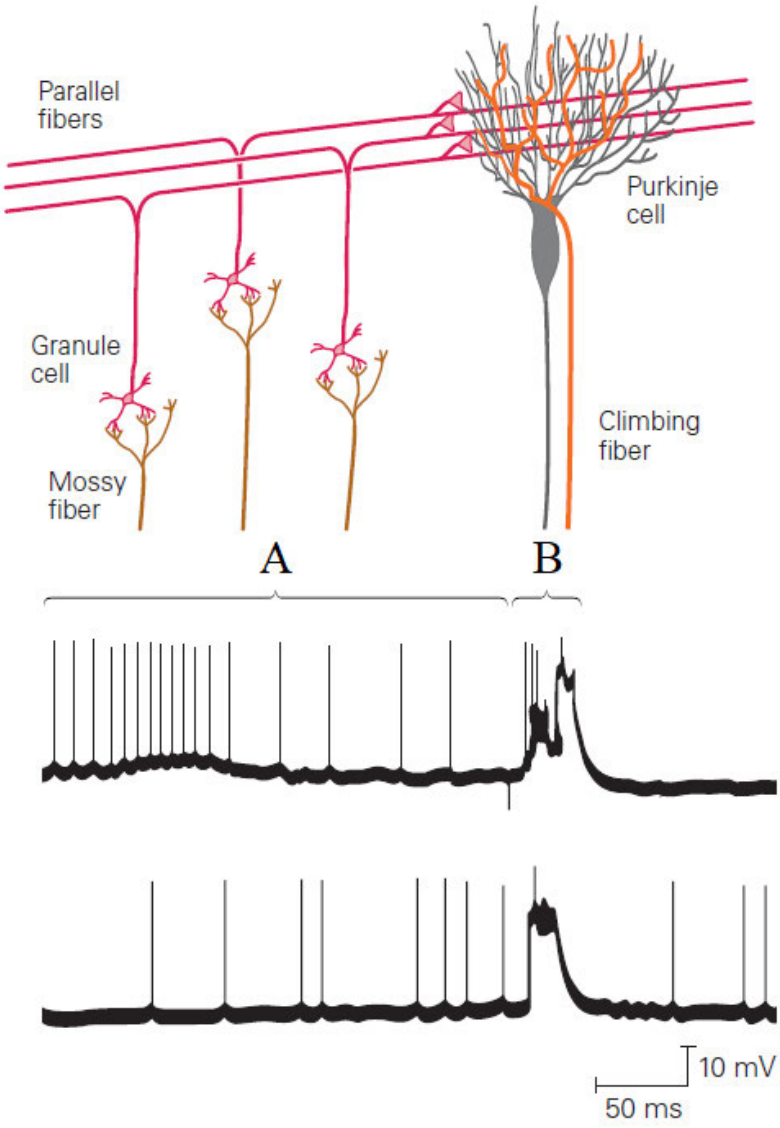

Figure 1.6 Simple and complex spikes recorded intracellularly from a cerebellar Purkinje cell.

Granule cell receives excitatory inputs from mossy fibres that originate from cell bodies in the spinal cord and brain stem. During excitation, PF, the axons of granule cells, produce brief and small excitatory potentials called (A) simple spikes (~100 Hz) in Purkinje neurons. In contrast, (B) complex spike (~1-3 Hz) is a prolonged depolarisation that is characterised by an initial large-amplitude AP followed by a high-frequency burst of smaller-amplitude APs. Complex spikes in Purkinje cells are evoked by CF synapses. Each Purkinje cell body and proximate dendrites are enwrapped by a single CF that originates from the inferior olivary nucleus. Adapted and modified from Kandel, Schwartz, Jessell, *et al.* (2012).

The fast inhibitory GABAergic synaptic transmission in CNS is involved in the regulation of normal neuronal excitability (Jacob *et al.*, 2008). This central synaptic inhibition is facilitated by the activation of $GABA_AR$, which is predominantly comprised of various α and β subunits together with the γ2 subunit that allows the rapid influx of Cl^- into the cell (Belelli & Lambert, 2005; Essrich *et al.*, 1998). Molecular studies have shown that $GABA_AR$ belong to the ligand-gated ion-channel superfamily, which are expressed throughout the brain and targeted to different subcellular regions. These regions include the postsynaptic and extra- or perisynaptic sites where they mediate the transient (phasic) and tonic inhibitions (Baer *et al.*, 1999; Brunig, Scotti, *et al.*, 2002; Draguhn *et al.*, 2008; Essrich *et al.*, 1998; Fritschy *et al.*, 1998; Lidov *et al.*, 1990). In addition to this, some $GABA_AR$ are also found at presynaptic sites (Draguhn *et al.*, 2008). The stability of $GABA_AR$ cluster localisation in different CNS sites is predominantly determined by the complex trafficking mechanisms and interactions with the intracellular proteins. These proteins are expressed at the postsynaptic density and they serve as a connection to cytoskeleton (Essrich *et al.*, 1998). Dystrophin is a good example as it is found abundantly at the postsynaptic density of neurons in the cerebral cortex, hippocampus, and most importantly in the cerebellum (Lidov *et al.*, 1990). Cerebellar dystrophin is co-localised with $GABA_AR$ subunits (α1 or γ2 subunit) at the postsynaptic regions of axondendritic and axonsomatic synapses of Purkinje cells (Knuesel *et al.*, 1999; Lidov *et al.*, 1990).

The important role dystrophin plays in postsynaptic $GABA_AR$ clustering was first addressed by Knuesel *et al.* (1999). The authors reported that the lack of dystrophin caused a marked reduction in the number of $GABA_AR$ clusters in cerebellar Purkinje cells of *mdx* mice. In addition, a recent finding from a whole-cell patch clamping study by Kueh *et al.* (2011) in the same animal model further support the finding from Knuesel *et al.* (1999). A variation in the amplitude of mIPSCs occurs when there is a change in the number of channels at the

postsynaptic membrane (Nusser *et al.*, 1997). Although the postsynaptic $GABA_A$ channels function normally in the Purkinje cells of *mdx* mice, Kueh *et al.* (2011) reported that both the average amplitude of mIPSCs as well as the average number of functional receptors localised at GABAergic synapses was significantly reduced when compared to LC. Moreover, they showed that the reduction of this postsynaptic $GABA_AR$ numbers had resulted in an increased number of extrasynaptic $GABA_AR$, possibly due to the impaired anchoring of $GABA_AR$ at the postsynaptic membrane as a consequence of dystrophin loss. More importantly, the studies on both the gene and protein expression levels of cerebellar $GABA_AR$ demonstrated that there were no significant differences in expressions levels between *mdx* and control mice (Kueh *et al.*, 2008; Wallis *et al.*, 2004). Taken together, these findings indicate that, the loss of dystrophin has led to a reduced number of functional $GABA_AR$ clusters at the postsynaptic domain and resulted in an increased number of extrasynaptic $GABA_AR$. This alteration is independent of $GABA_AR$ gene and protein expressions levels. The authors further concluded that the changes of receptor localisation are likely to influence the inhibitory input to Purkinje cells in *mdx* mice.

As a reduction in the number and size of postsynaptic $GABA_AR$ clusters in *mdx* mice were reported, Anderson and colleagues investigated the extent to which inhibitory input was affected by the altered $GABA_AR$ clustering in the dystrophic Purkinje cells using standard sharp electrode and whole cell patch-clamp techniques (Anderson *et al.*, 2003). Anderson *et al.* (2003) recorded evoked EPSPs and mIPSCs from *mdx* Purkinje cells. Evoked EPSPs were generated by stimulating the molecular layer within 250 µM of the Purkinje cells. The amplitude of evoked EPSPs in control Purkinje cells was increased upon the removal of the $GABA_A$ mediated inhibitory input using bicuculline whereas this increase in EPSP amplitude was relatively less in *mdx* Purkinje cells, suggesting that the reduction in size and number of

$GABA_AR$ clusters of *mdx* mice has resulted in a reduction of the inhibitory drive to Purkinje cells. Further supporting this view, the authors also reported a significant reduction in the mean amplitude of mIPSCs in *mdx* mice compared to control mice. As a previous study had emphasised that the amplitude of mIPSCs is predominantly determined by the number of postsynaptic receptors (Nusser *et al.*, 1997), the result from this study support the suggestion that the reduced GABA mediated activity is due to the decrease in postsynaptic $GABA_AR$ clusters size and number. Therefore, the loss of postsynaptic dystrophin is associated with a dampened inhibitory input to Purkinje cells as a result of reduced $GABA_AR$ cluster number in the *mdx* mouse.

Anderson and co-workers further investigated the impact of dystrophin deficiency on both the cerebellar short-term and long-term plasticity by examining the presynaptically mediated PPF and postsynaptically mediated heterosynaptic long-term depression (LTD) in the presence of bicuculline (Anderson *et al.*, 2004). Heterosynaptic LTD occurs when two excitatory synaptic inputs to Purkinje cells, induced by PF and CF, are activated repetitively and conjunctively (Ito, 2001). Anderson *et al.* (2004) reported that the presynaptically mediated PPF recordings were not significantly different between *mdx* and wildtype mice at all interstimulus intervals tested, suggesting that the short-term plasticity of *mdx* mice is normal and unaffected. In contrast, the postsynaptically mediated LTD was reduced in *mdx* Purkinje cells compared to wildtype, as indicated by the significant reduction in evoked EPSP slopes at 10 minutes and 35 minutes following LTD induction. Since these examinations were conducted in the absence of GABAergic transmission ($GABA_AR$ were blocked by $GABA_A$ antagonist bicuculline), the authors concluded that the functional consequences of an absence of dystrophin was not restricted to the reduced number and size of $GABA_AR$ clusters that have been reported in their earlier study (Anderson *et al.*, 2003). Instead, the absence of dystrophin at the Purkinje cell

postsynaptic density was responsible for the observed deficit in LTD, perhaps via its direct interaction with LTD induction.

Heterosynaptic LTD is one of the main forms of synaptic plasticity in the cerebellum and has been considered a critical cellular mechanism for learning and memory (Collingridge *et al.*, 2010; Hirano, 2013; Ito, 2001). It occurs at excitatory synapses between a Purkinje cell and both the parallel and climbing fibres in the cerebellar cortex, and is expressed as a reduced sensitivity to neurotransmitter glutamate (Hirano, 2013). The induction of cerebellar LTD requires several molecular cascades in Purkinje cells. One of the most important signalling is the postsynaptic calcium signalling. An increase in $[Ca^{2+}]_i$ is critical for LTD induction (Kimura *et al.*, 2005). This increase in cytoplasmic Ca^{2+} level is regulated by various signalling pathways. The activation of CF results in calcium influx to the Purkinje cell via VGCCs on the plasma membrane whereas the activation of a PF triggers the release of $Ca^{2+}$from intracellular endoplasmic reticulum through inositol 1,4,5-trisphosphate ($InsP_3$) receptor downstream of metabotropic glutamate receptor 1 (mGluR1) (Aiba *et al.*, 1994; Berridge, 2009; Llinas & Sugimori, 1980b; Miyakawa *et al.*, 1992; Shigemoto *et al.*, 1994). Metabotropic glutamate receptor 1 is also responsible for the opening of transient receptor potential canonical 3 channel that are permeable to calcium (Chae *et al.*, 2012). Interestingly, some studies have shown that the large $[Ca^{2+}]_i$ increase by itself was sufficient to induce LTD (Hartell, 1996; Tanaka *et al.*, 2007), therefore, any disturbances in this calcium signalling and/or homeostasis will have an impact on LTD induction.

Previous studies have shown that dystrophin deficiency impairs the inhibitory inputs to *mdx* Purkinje cells through the reduced number and size of functional postsynaptic $GABA_AR$ clusters as well as directly blunting the induction of LTD without the need for GABAergic

input. This is not surprising as the induction of LTD is determined by a series of signal transduction cascades that involve various types of receptors, ions concentrations, second messengers, protein kinases and other factors (Ito, 2001). An impaired calcium homeostasis has been a compelling candidate for the disruption of cerebellar LTD in *mdx* mice (Blake & Kroger, 2000; Carlson, 1998; O'Brien & Kunkel, 2001). Evidence showed that the excessive increase in $[Ca^{2+}]_i$ leads to dendritic damage in Purkinje neurons due to over excitation (Llinas & Sugimori, 1990). In normal circumstances, when the increase of $[Ca^{2+}]_i$ reaches the threshold level, LTD is triggered. This in turn stimulates a reduction in ionotropic glutamate receptor sensitivity and a reduction in calcium influx via voltage-dependent channels (Ito, 2001). The requirement for increased $[Ca^{2+}]_i$ level for LTD induction was further demonstrated by Kimura *et al.* (2005), where Purkinje cell LTD is prevented by T-588, (1R)-1-benzothiophen-5-yl-2[2-(diethylamino)ethoxy]-ethanol hydrochloride, a neuroprotective drug that functions to reduce cytosolic calcium release from intracellular stores. This implied that LTD is no longer required to desensitise the glutamate receptor for reducing the influx of calcium from extracellular source, since $[Ca^{2+}]_i$ level has been regulated by the action of T-588 intracellularly. In summary, LTD induction is very sensitive to and dependent on $[Ca^{2+}]_i$ level. This may be a protective mechanism for Purkinje cells as they regulate $[Ca^{2+}]_i$ within a narrow range, below the threshold for triggering cell damage, through decreasing the sensitivity of metabotropic glutamate receptors (mGluRs) in the spines of Purkinje cells' dendrites. In view of the stringent requirement of $[Ca^{2+}]_i$ level in LTD induction, there is a possibility that the impaired LTD in *mdx* mice was due to dysregulated $[Ca^{2+}]_i$ levels in Purkinje cells, however, no data is available to date.

Although the $[Ca^{2+}]_i$ level in dystrophic Purkinje cells remains unknown, Hopf and Steinhardt (1992) demonstrated that the resting level of free $[Ca^{2+}]_i$ in cultured *mdx* granule cells was 24%

higher than normal neurons. Interestingly, when the *mdx* granule cells were challenged with a high extracellular calcium load, they showed significantly elevated $[Ca^{2+}]_i$ levels, indicating that this $[Ca^{2+}]_i$ dyshomeostasis may be due to an increased permeability to calcium as a result of enhanced Ca^{2+}-permeable ion channel activity (Haws & Lansman, 1991). Despite the calcium dyshomeostasis reported in *mdx* granule cells, it is important to note that dystrophin is not normally expressed in the granule cell and that the mechanism that underlies this altered $[Ca^{2+}]_i$ in *mdx* granule cells remains unclear. On the other hand, when other dystrophin-expressed brain regions were examined, Lopez and colleagues showed a significant increase in resting $[Ca^{2+}]_i$ levels, which is contributed by both the extracellular and intracellular sources, in the pyramidal cortical and hippocampal neurons from 3 and 6 months *mdx* mice (Lopez *et al.*, 2016). These dysregulated $[Ca^{2+}]_i$ levels were reversed when the mutants were treated with blockers of stretch-activated cations channels (GsMTx-4), ryanodine receptors (RyRs), and inositol triphosphate receptors indicating that all these pathways contribute to the increase of $[Ca^{2+}]_i$ level. Remarkably, the cognitive functions of these mice improved after the reduction of the abnormally elevated $[Ca^{2+}]_i$ levels. The authors also reported that there is an association between $[Ca^{2+}]_i$ dyshomeostasis and elevated levels of reactive oxygen species that contributes to neuronal damage in *mdx* mice. In view of this, there is a high possibility that the calcium homeostasis in dystrophic Purkinje neurons might have also been disturbed since dystrophin is highly expressed in normal Purkinje cells but absent in dystrophic neurons. Whether this impaired calcium regulation occurs in *mdx* Purkinje cells is still unclear as the level of resting $[Ca^{2+}]_i$ in this neuron has never been investigated.

Researching the resting $[Ca^{2+}]_i$ level in Purkinje neuron is very important as it could provide a better understanding of its role in cerebellar LTD induction in *mdx* mice. This in turn may reveal the role of dystrophin in Purkinje cells' $[Ca^{2+}]_i$ levels and subsequently its relationship to

cerebellar LTD. If impaired cerebellar LTD is the underlying cause for the cognitive deficits in boys with DMD, the development of an effective therapeutic strategy that targets the molecules that are involved in this LTD induction mechanism, such as $[Ca^{2+}]_i$ levels, would be beneficial in ameliorating the intellectual deficits that consistently challenge these patients.

1.7 Potential therapeutic approach: rescue of a dystrophin-like protein by exon skipping

Currently, various nonpharmacological and pharmacological treatments options have been introduced to alleviate the symptoms of DMD and to slow down the disease progression. These efforts have successfully increased the life expectancy of DMD patients from less than 20 years of age to their late 20s (Eagle *et al.*, 2002; Passamano *et al.*, 2012). Due to the limited benefits from symptomatic management, other therapeutic approaches including stem-cell therapy, gene replacement, aminoglycoside antibiotics and proteasome inhibitors have been introduced in an attempt to restore dystrophin expression (Sun *et al.*, 2020; Wurster & Ludolph, 2018).

DMD contains 79 exons encoding a 14 kb mRNA transcript and is considered one of the largest genes (2.5 Mb) in the human genome. It is located in a genomic region with high rates of recombination (Buzin *et al.*, 2005; Nachman & Crowell, 2000; Takeshima *et al.*, 2010). Owing to its length and location, *DMD* is vulnerable to mutation. Many DMD cases (~60%) are caused by spontaneous insertions or deletions of one or more exons, whereas approximately 40% of cases are due to point mutations (Hoffman & Dressman, 2001; Manzur *et al.*, 2008; Nowak & Davies, 2004; van Deutekom & van Ommen, 2003; White *et al.*, 2002; Yokota *et al.*, 2007). These alterations interrupt the reading frame or result in a premature stop codon, both of which resulting in an out-of-frame transcript or absence of the protein dystrophin.

Exon skipping using antisense oligonucleotides (AOs) is one of the most promising approaches to restore dystrophin expression in muscle (Dickson *et al.*, 2002; Dunckley *et al.*, 1998; Wilton *et al.*, 1999; Wurster & Ludolph, 2018). As implied by its name, AOs are short, synthetic single-stranded nucleic acid that made up of 8-50 bases which bind to complementary target mRNA sequences (Lee & Yokota, 2013; Wu *et al.*, 2004). AO-mediated exon-skipping strategies are used to restore the reading frame by removing the exons that carries the mutation from the *DMD* pre-mRNA, thereby enabling the translation of truncated proteins that retain some or most of the function of dystrophin as opposed to no dystrophin (Aartsma-Rus *et al.*, 2003; Alter *et al.*, 2006; Bennett *et al.*, 2017). Eteplirsen, an AO of the phosphorodiamidate morpholino oligomer (PMO) subclass targeting *DMD* exon 51, was approved by the United States US Food and Drug Administration for the treatment of DMD in 2016 (US Food and Drug Administration. 2016). This PMO or chemically modified AO have the deoxyribose/ribose moiety and the charged phosphodiester inter-subunit linkage replaced by a morpholine ring and uncharged phosphorodiamidate linkages, respectively, making it nuclease-resistance and charge-neutral (Hudziak *et al.*, 1996; Summerton *et al.*, 1997). As stability and potential toxicity in cells are the main concerns when using nucleic acid-based molecules for therapeutics, the charge-neutral PMO has overcome these difficulties. Being charge-neutral, PMO is more resistant to nucleases, which specifically target charged molecules. In addition, the lack of charge PMO is less harmful since it is not likely to activate the receptors responsible for innate responses against pathogenic material (Moulton, 2016).

The effectiveness of AO in rescuing dystrophin expression in skeletal muscle has been outlined in several reports (Cirak *et al.*, 2012; Kinali *et al.*, 2009; Mendell *et al.*, 2013). A 23% increase in dystrophin-positive fibres was found in the biopsies of DMD patients after they have been given weekly intravenous infusion of 30 mg/kg eteplirsen for 24 weeks when compared to

placebo-treated patients (Mendell *et al.*, 2013). The longer the patients received eteplirsen treatment the greater the increases in their dystrophin-positive fibre expression level. The increased dystrophin-positive fibres are functional as evident by the improved distance walked on the 6-minute walk test in these patients. Although PMO successfully rescued dystrophin expression in skeletal muscles, they are highly inefficient in cardiac muscles and in the CNS due to its internalisation in endomembrane compartments before reaching their intracellular targets and its inability to cross the blood brain barrier (BBB) (Bennett *et al.*, 2017; Khorkova & Wahlestedt, 2017; Maruyama *et al.*, 2017; Yokota *et al.*, 2009). Animal studies show that less than 1% of systemically administered oligonucleotides reached the brain (Banks *et al.*, 2001; Farr *et al.*, 2014; Khorkova & Wahlestedt, 2017).

Various strategies have been developed to improve the bioavailability of systemically delivered antisense therapeutics to overcome the challenges faced, including poor tissue penetration and cellular uptake, and difficult delivery to the intracellular targets in the CNS (Nguyen & Yokota, 2019). Among the various delivery systems studied, cell-penetrating peptides (CPPs) conjugated to charge neutral PMO have gained the most attention. Cell-penetrating peptides contain cationic and/or amphipathic amino acids, particularly multiple arginines, which are highly effective in enhancing delivery of nucleic acid-based molecules due to their exclusive ability to transport associated cargoes across the plasma and endosomal membranes (Mitchell *et al.*, 2000). The derivatives of the CPP Penetratin, PMO internalisation peptides (Pips) that have six arginine residues added to the N terminus, is one of the most promising class of CPPs for transporting the PMO to the tissues and leading to systemic dystrophin production (Betts *et al.*, 2012). Pip series are characterized by a central hydrophobic core anchored on each side by arginine-rich sequences and they are found to be more resistance to serum proteolysis (Betts *et al.*, 2012; Ivanova *et al.*, 2008). Pip6, one of the most efficient members in this series,

conjugated with PMO can successfully redirect the splicing of dystrophin pre-mRNA in dystrophic *mdx* mouse, omitting the mutation in exon 23, to restore the reading frame and rescue the expression of dystrophin in various muscles including the heart (Betts *et al.*, 2012; Yin *et al.*, 2011).

In addition to the successful systematic delivery of Pip6-PMO into the heart, the unique characteristics of Pips including their small size, targeting specificity, low toxicity, and ability for transcapillary delivery of associated large bio-cargos have allowed some of their members to reach the CNS (Farkhani *et al.*, 2014; Kang *et al.*, 2014; Pardridge, 2012). A study in the SMA mouse model showed that Pip6a-PMO demonstrates potent efficacy in the CNS as well as in the peripheral tissues in the severe SMA mouse model following systemic administration (Hammond *et al.*, 2016). Spinal muscular atrophy is characterised by a lower motor neuron degeneration and progressive muscle weakness as a result of mutations in the *SMN1* gene that codes for the ubiquitously expressed survival motor neuron (SMN) protein (Lefebvre *et al.*, 1995; Wirth, 2000). Gene-therapy based approach for SMA aims to enhance the expression levels of full-length *SMN2* (*FLSMN2*) to compensate for the loss of functional levels of full-length SMN protein (Hammond & Wood, 2011; Wirth, 2000). The authors showed that intravenous facial vein delivery of the Pip6a-PMO conjugate significantly enhanced the expressions of *FLSMN2* mRNA and SMN2 protein in both the peripheral (i.e. skeletal muscles, heart, liver) and central (i.e. brain and spinal cord) tissues in severe SMA pups (Hammond *et al.*, 2016). In addition, these authors also successfully demonstrated increased expression levels of *FLSMN2* transcript within the CNS of adult (i.e. 7.5 week of age) mice carrying SMN2 transgene after they were given two doses of Pip6a-PMO (18 mg/kg), delivered 2 days apart via tail vein administration.

In addition to the systemic delivery of Pip6a-PMO in the SMA mouse model, an earlier study by Du *et al.* (2011) also showed the capability of an arginine-rich CPP, $(RXRRBR)_2XB$, to deliver the antisense morpholino oligonucleotide (AMO) to the brain and cerebellum of the WT (C57BL/6) mice after a single tail vein injection (60 mg/kg). The intravenously injected $(RXRRBR)_2XB$-AMO was labelled with fluorescein isothiocyanate (FITC), which allowed tracking of the nucleic acid-based molecule after it was systemically delivered into the target cells. The authors demonstrated that the $(RXRRBR)_2XB$-AMO had successfully crossed the BBB as fluorescence was evident in many areas of the brain, notably in the cerebellum and Purkinje cells of the $(RXRRBR)_2XB$-AMO treated animals whereas no fluorescence was observed in the brains of control mice treated with PBS. The fluorescence intensity was also increased in mice that received multiple tail vein injections as compared to mice which received a single injection. No apparent signs of toxicity was found after the mice were treated with 60 mg/kg/day for four consecutive days at 24 hours intervals. Taken together, the arginine rich CPP is a promising peptide to aid the systemic delivery of PMO into the CNS, providing confidences that systemic administration of this conjugate could become a handy way to effectively target the CNS for treating the neurogenetic disorders in the future.

While the application of systemic administration of CPP-PMO conjugates to correct defects in the CNS of DMD is yet to be established, Vaillend *et al.* (2010) has shown the efficacy of exon skipping in the 8 weeks old *mdx* hippocampus via a single intrahippocampal injection of adenovirus associated vector (rAAV2/1 sterotype) expressing antisense sequences linked to a modified U7 small nuclear RNA. Several groups reported that the loss of brain dystrophins in the *mdx* mouse model of DMD has reduced the number and size of $GABA_AR$ clustering in the central inhibitory synapses in brain regions involved in cognitive functions including the hippocampus, cerebellum, and amygdala (Knuesel *et al.*, 1999; Sekiguchi *et al.*, 2009). This

suggests that the perturbations in $GABA_AR$ clustering can be a major molecular defect leading to brain and cognitive alterations in DMD. The dystrophin rescue in *mdx* hippocampus by the rAAV2/1-U7 systemic injection was positive as evident of the expression of dystrophin-like protein to 15-25% of normal dystrophin levels near the injection site as well as the complete restoration of $GABA_AR$ clustering in the pyramidal and dendritic layers of CA1-hippocampus. In addition, a follow up study by the same group showed that the abnormally enhanced LTP phenotype at CA3-CA1 synapses of *mdx* mice, which is believed to be due to the lack of $GABA_AR$ clustering, was also successfully reversed by the rAAV2/1-U7 injection (Dallerac *et al.*, 2011). Taken together, exon skipping is an effective and promising strategy for the re-expression of brain dystrophin and normalising the perturbed synaptic plasticity caused by the absence of dystrophin through the modulation of $GABA_AR$ clustering.

However, there are still some challenges to the development of AO-mediated exon skipping therapies (Koo & Wood, 2013). Firstly, the significant genetic heterogeneity of DMD makes it impossible to have a single exon-skipping therapy for all DMD patients since this therapy is only available for specific exons corresponding to certain mutations. The development of personalised AOs with different sequences targeting unique exons is currently challenging due to the high manufacturing cost. Another challenge is that the dystrophin restoration level is very inconsistent among different muscle groups even after repeated systemic administration of AOs. A study showed that without the correction of dystrophin expression in cardiac muscle, there was a five-fold increase in cardiac injury along with dilated cardiomyopathy in *mdx* mice when the expression of dystrophin in skeletal muscle was improved and resulted in an increased activity (Townsend *et al.*, 2008). Although a recent study showed the rescue of dystrophin in all tissues including the CNS using AOs improved the cognitive function in the *mdx* mouse, the risk of different tolerance between mouse and man still exists (Goyenvalle *et*

al., 2015). Since AOs have a short half-life in biological environments, repeated administration of therapeutic doses of AOs would likely be required for the lifetime of DMD patients to maintain adequate therapeutic effect. Therefore, the safety issue of this approach needs to be addressed for long-term administration.

In contrast to the personalised AOs-mediated exon skipping therapy, a generalised therapeutic strategy targeting the perturbed neurophysiology commonly seen in DMD patients will be more desirable. Therefore, the understanding of mechanisms that underlie the altered neurophysiology in dystrophin deficient models is very important for the development of an effective drug treatment in DMD.

1.8 Summary

Duchenne muscular dystrophy is a fatal X-linked progressive muscular dystrophy with mild to severe cognitive dysfunction that affects approximately 1 in 3500 live male birth. It is caused by a loss or expression of a truncated non-functional protein, dystrophin. The life-threatening muscular aspects of DMD have received much attention compared with the limited studies addressing CNS impairments. In the CNS, dystrophin is highly expressed in regions associated with higher cognitive functions such as cerebral cortex, hippocampus, amygdala, and cerebellum. To date, it is widely accepted that the general IQ score of DMD patients is on average one standard deviation below that of the normal population mean. Verbal impairments such as language delay, impair phonological production, poor verbal fluency and reading are more prevalent in DMD boys. Interestingly, these verbal dysfunctions share similarities to dyslexia, a language disorder that is associated with cerebellar dysfunction, implying a potential involvement of the cerebellar non-motor dysfunction in DMD's cognitive function.

The CNS deformity in DMD patients has been extensively described by various histological studies using different approaches. Post-mortem brain abnormalities include reduced brain weight, ventricle dilation, cortical atrophy, heteropias, pachygyria, dendritic abnormalities, extensive Purkinje cell loss, and gliosis were reported. Position emission tomography imaging studies found alterations in brain metabolism and biochemistry such as reduced glucose metabolism in the cerebellum, temporal cortical areas, and the right sensorimotor cortex. The *mdx* mouse model, a naturally occurring mutant has commonly been adopted for research. In *mdx* mice, cytoarchitectural rearrangement of calcium-binding protein cells has been noted in the cortex, suggesting a compensatory mechanism in response to calcium dyshomeostasis during development. When the ultrastructure of hippocampal CA1 region was examined, the altered inhibitory synapse density and number of docked vesicles were reported, implying that these factors may potentially contribute to the dysregulated synaptic plasticity in *mdx* mice. Although no significant finding was made, a pilot immunohistochemistry study with limited animal number showed a trend towards a decrease in cerebellar Purkinje cell populations in *mdx* mutant. Altered number of calcium-positive neurons was also reported in *mdx* cerebellum. However, the effect of dystrophin loss on neurogenesis, cellular organization, synaptic spine density and dendritic processes in the cerebellum remains unknown.

Electrophysiology studies in *mdx* hippocampus showed that the deficiency of dystrophin has detrimental effects on synaptic plasticity. These alterations include the abnormally enhanced hippocampal short-term and long-term potentiation, and STD potentially due to the imbalance between synaptic excitation and inhibition. On the other hand, studies in *mdx* cerebellum by our group revealed that the loss of dystrophin has led to a reduced number of functional $GABA_AR$ clusters at postsynaptic Purkinje cells, and an increased number of extrasynaptic $GABA_AR$, implicating a potential altered inhibitory input to Purkinje cells in *mdx* mice.

Interestingly, our group showed an impairment of LTD, a form of synaptic plasticity that plays a very important role in cerebellar learning and memory function, in the cerebellum of *mdx* mice. The LTD induction is closely related and dependent on $[Ca^{2+}]_i$ level. However, whether there is a perturbation of resting calcium level in Purkinje cells remains unclear. Interestingly, although cerebellar granule cell does not normally express dystrophin, an increased resting $[Ca^{2+}]_i$ was found in the *mdx* granule cells. While the underlying mechanism for this intracellular calcium dyshomeostasis remained unclear, this finding showed a possible altered Ca^{2+}-permeable ion channel activity in the *mdx* cerebellum. Remarkably, by using the calcium receptor blockers that target both the intracellular and extracellular calcium sources, the dysregulated $[Ca^{2+}]_i$ levels in pyramidal cortical and hippocampal neurons of *mdx* mice was partially restored with improved cognitive function.

Recent studies have shown that exon skipping which involves the binding of AOs to complementary sequences of the dystrophin pre-mRNA, was able to restore the open reading frame of *DMD* and produce partially functional dystrophin protein. This makes AOs, a promising approach to correct both brain and muscle alterations. However, the development of personalised AOs for DMD patients with different mutations, the biodistribution of AOs, and the safety issue for long-term use of AOs remain a big obstacle for exon skipping to become an effective therapeutic strategy in DMD. Therefore, a solid understanding of both the electrophysiological and morphological changes in dystrophic cerebellum may provide a better insight for the development of an effective and more generalised therapeutic approach to counteract or restore the perturbed neurophysiology shared among DMD patients and thereby ameliorate the cerebellar associated cognitive dysfunction.

1.9 Aims and Hypothesis

The previous electrophysiological data from our group showed a significant reduction in the inhibitory input to the cerebellar Purkinje neurons of dystrophin-deficient *mdx* mice compared to LC. Reduced mIPSCs amplitude and frequency were reported in the young *mdx* mice. As DMD is a progressive disease, further understanding in Purkinje cell functions in the aging *mdx* population is needed. The first aim of this study was to investigate the mIPSCs properties in the aged *mdx* mice (23-26 months old).

Exon skipping using AOs has shown promising results in restoring the expression of dystrophin in skeletal muscle. To date, there is limited studies showing the use of AOs in rescuing dystrophin expression in the CNS. Therefore, the second aim of this study was to investigate if Pip6f-PMO can rescue dystrophin expression in the cerebellum, using an organotypic brain slice method. In addition, whether the rescued dystrophin was functional and able to reverse the reported altered inhibitory input in cerebellar Purkinje cells were also examined.

As there are very limited studies examining the impact of dystrophin deficiency on the electrical properties of Purkinje cells in the mature *mdx* mouse, the third aim of this study was to investigate the passive and active membrane properties, and the firing patterns of mature *mdx* Purkinje cell (11-12 months old). The impairments of calcium homeostasis in *mdx* mice have been reported in different tissues including the skeletal muscles and the hippocampal neurons. As a reduction in postsynaptically mediated LTD in cerebellar Purkinje neurons in *mdx* mice was reported in our previous study, and the fact that the induction of LTD is strongly dependent on $[Ca^{2+}]_i$ level, the final aim of this study was to investigate the functional impact of the absence of dystrophin on $[Ca^{2+}]_i$ levels in Purkinje

cells when at rest and during the stimulation of PF in the mature *mdx* mice (11-12 months old).

With all the aims stated above, I hypothesised that:

1. **The alterations in the mIPSCs properties of the aged *mdx* mice is similar to that in the young *mdx* mice when compared to their age-matched LC.**

   The first hypothesis was tested on the Purkinje cells in *mdx* mice using whole-cell voltage clamp recording. The mIPSCs properties (i.e. amplitude and frequency) of young (3-4 months old) and aged (23-26 months old) *mdx* mice were compared.

2. **The loss of dystrophin in *mdx* Purkinje cells can be restored by exon skipping using Pip6f-PMO, and that the rescued dystrophin is functional.**

   The second hypothesis was tested on the organotypic cerebellar culture (8-12 DIV) developed from very young (P8-P11) *mdx* and WT mice using immunofluorescence staining and whole-cell voltage clamp recording. The mIPSCs properties of Purkinje cells from *mdx* culture that were treated with Pip6f-PMO was compared to the Purkinje cells from untreated *mdx* culture.

3. **The electrical properties of *mdx* Purkinje cell is altered compared to age-matched LC.**

   The third hypothesis was tested on the Purkinje cells in mature (11-12 months old) *mdx* mice and LC using whole-cell current clamp recording. Passive and active membrane properties were compared between *mdx* and LC.

4. The calcium homeostasis in *mdx* Purkinje cells is altered compared to age-matched LC.

The fourth hypothesis was tested on the Purkinje cells in mature (11-12 months old) *mdx* mice and LC using whole-cell current clamp recording combined with calcium imaging using calcium indicator Fura-FF. Resting $[Ca^{2+}]_i$ in cell soma and distal dendrites of Purkinje cells were examined. Calcium handing of *mdx* Purkinje dendrites were also examined by injecting electrical stimulation on the PF.

Chapter 2. Materials and Methods

2.1 Ethics

All experiments and breeding programs were conducted in accordance with the international guidelines on the care and use of experimental animals and approved by the Animal Care and Ethics Committee, Western Sydney University Animal Ethics Committee.

2.2 Animals (*mdx* mice)

Breeders (P_0) were originally purchased from the Animal Resource Centre (ARC), Perth Western Australia. Mice, male C57BL/10ScSn were bred with female C57BL/10ScSn-*Dmd*^{mdx}/Arc mice (*mdx*). The offspring of this mating (F1) were mated together to produce an F2 offspring with a genetic ratio of 25% WT male (X^+/ Y), 25% hemizygous male (X^{mdx}/ Y), 25% heterozygous female (X^+/ X^{mdx}), 25% hemizygous female (X^{mdx}/ X^{mdx}). Only F2 hemizygous male (X^{mdx}/ Y) and F2 WT male (X^+/ Y) (LC) were used in this study. Mice were divided into three different age groups corresponding to young (3-4 months old), adult (11-12 months old), and aged (23-26 months old) mice. Female and male mice were segregated after weaning. All mice were housed under 12-hour day/light cycles, in standardised Individually Ventilated Cages (IVC), with polysulfone solid floored base, lid and stainless steel feed hopper. Shredded paper, mouse igloo as well as plastic tubes were provided as environmental enrichments and were used for "nestlets". All mice were housed in groups of 3-4 for companionship.

2.3 Cerebellar brain slice preparation

2.3.1 Tissue harvest

Young mice (≤12 weeks) were anaesthetised with isoflurane and decapitated. The cerebellum was rapidly removed, and a parasagittal cut was made on the lateral part of both sides of the cerebellar cortex to assist in attaching the cerebellum on to a pedestal for slicing. Then the cerebellum was rapidly removed and transferred to ice-cold NMDG-HEPES recovery artificial cerebrospinal fluid (aCSF). In young mice, the cerebellum was incubated in ice-cold NMDG-HEPES recovery aCSF of composition (in mmol/L): NMDG 93, KCl 2.5, NaH_2PO_4 1.2, $NaHCO_3$ 30, HEPES 20, D-glucose 25, sodium ascorbate 5, thiourea 2, sodium pyruvate 3, $MgSO_4.7H_2O$ 10, $CaCl_2.2H_2O$ 0.5 (saturated with 95% O_2 and 5% CO_2 mixture; 300-310 mOsm; adjusted to pH 7.4 using 10 mol/L HCl) for approximately 2-3 minutes, however, a 5-6 minutes incubation was used if the mouse was more than 3 months old (Moyer & Brown, 1998). This step has been shown to improve slice viability.

2.3.2 Tissue slicing

A thin layer of cyanoacrylate glue was applied on the pedestal of the tissue slicer. The cerebellum was carefully removed from the ice-cold NMDG-HEPES recovery aCSF with a spatula, and excess aCSF was removed using Whatman filter paper (No. 1, Whatman, Maidstone, UK), before attaching onto the pedestal of a motorised vibroslicer (Leica VT1200S, Leica Microsystems). The above steps were done swiftly to ensure that the cerebellum remained cold. The pedestal was installed onto the cutting chamber and then, the cerebellum was rapidly resubmerged in ice-cold NMDG-HEPES recovery aCSF (saturated with 95% O_2 and 5% CO_2 mixture). For slicing, the dorsal part of the cerebellum was positioned closest to the blade with the spinal cord facing away from the blade. The cutting chamber was advanced

slowly towards the cold stainless-steel blade and was advanced at a speed of 0.18mm-0.20mm/sec and vibration was set at an amplitude of 1 mm. Parasagittal slices of 250 µm thick were made in the same plane as the dendritic trees of Purkinje cells to reduce damage to the extensive dendritic tree of these cells.

2.3.3 Tissue recovery and maintenance

Brain slices were removed from the cutting chamber using the wide end of a fire-polished Pasteur pipette, transferred into a holding chamber containing NMDG-HEPES recovery aCSF at 37°C. Slices were maintained in NMDG-HEPES recovery aCSF for 15 minutes. During incubation, the beaker was sealed with laboratory film (Parafilm™, America National Can, Chicago USA) to avoid evaporation. Slices were then transferred into HEPES holding aCSF of composition (in mmol/L): NaCl 92, KCl 2.5, NaH_2PO_4 1.2, $NaHCO_3$ 30, HEPES 20, D-glucose 25, sodium ascorbate 5, thiourea 2, sodium pyruvate 3, $MgSO_4.7H_2O$ 2, $CaCl_2.2H_2O$ 2 (saturated with 95% O_2 and 5% CO_2 mixture; 300-310 mOsm; pH 7.4) maintained at room temperature (22°C) for 1 hour, followed by 16°C in the Braincubator™ (Buskila *et al.*, 2014) until used for experiment (Figure 2.1).

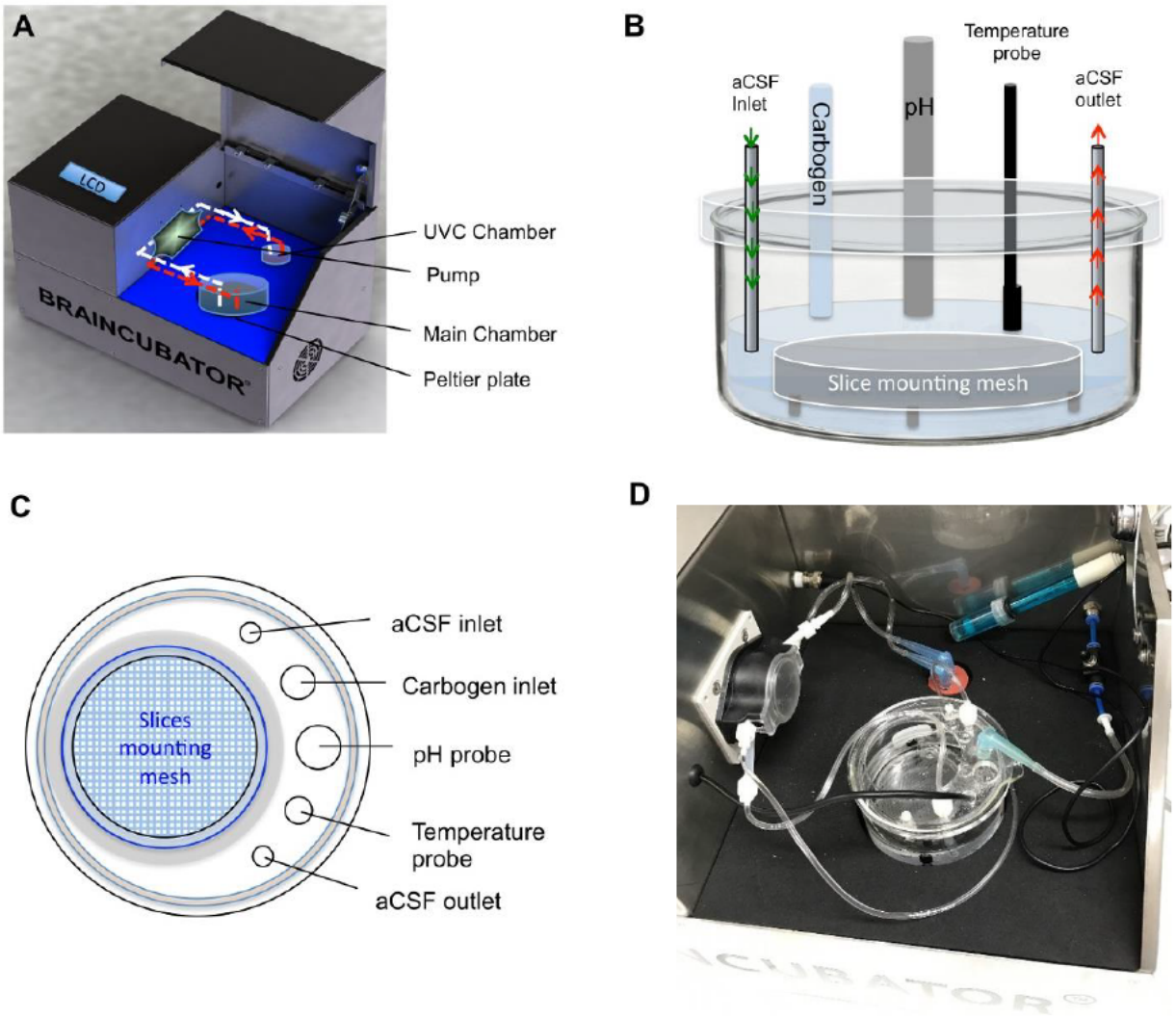

Figure 2.1 Braincubator™, an incubation system that maintaining tissue in a tightly regulated environment.

(A) Schematic drawing of the Braincubator™ consisting of a Peltier thermoelectric cold plate, main chamber, peristaltic pump and UVC chamber. (B) Brain slices are maintained inside the main chamber, placed on the slice mounting mesh, supplied with circulated aCSF (aCSF inlet), constantly being irradiated with UVC light (aCSF leaving via aCSF outlet), continuously bubbled with carbogen gas (95% O_2 and 5% CO_2) through the carbogen inlet. Temperature and pH probes allowed the temperature and pH of the aCSF to be monitored. (C) Top view of the main chamber depicting the slice mounting mesh, and the mounting holes for connecting the aCSF and carbogen inlets, and the measuring probes (pH, temperature). (D) An image of the Braincubator™. Adapted and modified from Cameron *et al.* (2017).

2.4 Electrophysiological recordings

2.4.1 Purkinje cell visualisation

A healthy cerebellar slice was transferred into the recording bath (22°C) containing aCSF of composition (in mmol/L): NaCl 124, KCl 3.2, $CaCl_2$ 2.5, $MgCl_2$ 1.3, $NaHCO_3$ 26, NaH_2PO_4 1.25, and D-glucose 25 (saturated with 95% O_2 and 5% CO_2 mixture; 324 mOsm; pH 7.4) with the wide end of a fire-polished glass Pasteur pipette. The cerebellar slice was held in place with a harp fabricated from a flatted U-shaped platinum wire and stringed with parallel nylon threads. The harp measured approximately 8 mm in diameter and the strings was stretched about 2 mm apart, held in place with cyanoacrylate glue. The cerebellar slice was equilibrated from 16°C (Braincubator^{TM}) to 22°C (recording bath) for 15 minutes prior the first recording on Purkinje cell.

Brain slice was continuously superfused with aCSF at a flow rate of 2-3 mL per minute. Silicon tubing (Masterflex® Tygon ® tubing, Cole Palmer Vernon Hills, Illinois USA) was used for delivery of physiological buffers by gravity feed. All experiments were conducted at room temperature. The Purkinje cell was visualised using a fixed stage upright microscope (Olympus BX51WI, Olympus Coporation, Tokyo, Japan) equipped with an infrared (IR) filter (λmax=780 nm) and a 100 W halogen white light source, used in conjunction with an electron multiplying charge coupled device (EMCCD) camera (ANDOR iXON, Oxford Instruments, Abingdon, UK). The Purkinje cell layer was first identified at low magnification, using a long working distance water immersion objective (10X UMPlan FL with numerical aperture of 0.30, working distance of 3.30 mm). At high magnification (40X LUMPlanFL numerical aperture of 0.80, working distance of 3.30 mm and a 60X LUMPlanFL with numerical aperture of 0.90 and a working distance of 2.00 mm) and in conjunction with, differential interference contrast optics,

a healthy Purkinje cell was identified. The microscope is secured on a Vibraplane (Kinetic systems, Boston, MA, USA), together with the micromanipulator and microelectrode headstages were mounted on a vibration isolation table and enclosed in a Faraday cage (Figure 2.2).

The Purkinje cell layer can be easily identified between the granule cell layer and molecular layer. The Purkinje cell body can be recognised by their big, pear-shaped somata as well as extensive branching dendrites extending into the molecular layer (Llinas & Sugimori, 1980a; Perkel *et al.*, 1990).

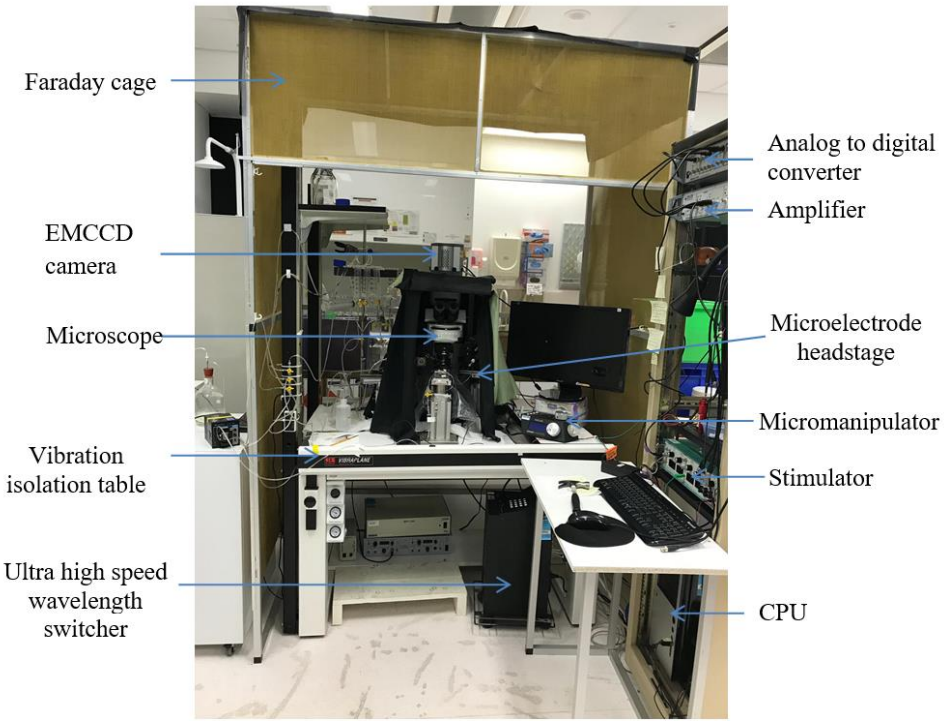

Figure 2.2 Electrophysiology recording rig.

Several instruments are enclosed in the Faraday cage. This includes the microscope, EMCCD camera, vibration isolation table, microelectrode headstages, micromanipulator, ultra high speed wavelength switcher. Other instruments include the analog to digital converter, amplifier, stimulator, and computer are placed inside the rack that next to the Faraday cage.

2.4.2 Recording electrode

For experiments, a sharp electrode or patch electrode was used. A sharp electrode was freshly fabricated from borosilicate glass of 1 mm outside diameter and 0.58 mm inside diameter, 10 mm long (Sutter Instrument Co., Novato USA) using a P-97 Flaming/Brown micropipette puller (Sutter Instrument Co., Novato USA) on the day of experiment. The electrode showed a resistance of 60-100 MΩ when filled with 2M potassium acetate. A thin silver wire coated with chloride (5% NaOCl) was introduced into contact with potassium acetate and secured in place by a polycarbonate electrode holder (Axon Instrument, Union City USA) in contact, via a gold-plated pin, with the headstage (CV-7B Current Clamp and Voltage Clamp Headstage, Axon Instruments, Union City USA).

A patch electrode was fabricated with a thin walled borosilicate glass of 1.5 mm outside diameter and 1.17 mm inside diameter, 10 mm long (Warner Instrument Co., Hamden, USA) using a P-97 Flaming/Brown micropipette puller. The tip of this glass electrode was fire-polished using a MF-830 Microforge (Narishige, Tokyo, Japan) to a resistance of 3-5 MΩ when filled with intracellular solution of composition (in mM) 130 K-gluconate, 10 Na-gluconate, 4 NaCl, 2 Mg-ATP, 0.3 Na-GTP, 0.3 Fura-FF using non-metalic syringe needles (MicroFil MF28g-5, World Precision Instruments Inc, Sarasota, USA) attached to a 0.22 µM filter (Millex GV filter unit, Millipore, Bedford, USA).

A computer-controlled microelectrode amplifier (Multiclamp-700B) and an analog to digital converter (Digidata 1440A) were used in conjunction with the MutiClamp 700B Commander software and pClamp 10.0 software (all from Axon Instruments, Inc., Union City, CA, USA) to perform current/voltage clamp protocols and data acquisition, that were stored for offline analysis.

All sharp electrode recordings were made in current clamp mode. A brief repetitive pulse of current (-100 pA) was applied to the electrode once it was in the bath. On the MutiClamp 700B Commander software, “pipette offset” or an opposing voltage was applied to reset the pipette potential to zero with respect to the bath (i.e. to correct the liquid junction potentials). Bridge was balanced to compensate the series resistance after the cell was impaled successfully. The electrode tip was advanced to the target cell, and in some instances the cell was impaled when the electrode was pressed against the cell membrane. However, in most cases when the microelectrode was pressed against a cell, the membrane dimpled but the microelectrode failed to penetrate. In this case, the cell can be impaled by applying a brief, high-frequency oscillatory current through the microelectrode. Alternatively, a large positive or negative current step can be used to penetrate the cell. If these failed, a gentle vibration can be introduced to the microelectrode by lightly tapping on the MPC-200 multi-micromanipulator (Sutter Instrument Co., Novato USA). A sudden change in the membrane potential traces indicates successful penetration. A negative current (500 pA) was then applied to help seal the membrane around the electrode and this was gradually removed.

For whole-cell patch clamping, under voltage clamp mode, the microelectrode was lowered into the recording bath. A positive pressure was applied by injecting approximately 0.6 ml of air using a 1 ml syringe. Tip potential was zeroed by “pipette offset”. A 10mV square-wave pulse of 20 ms duration was repetitively applied under the membrane test mode (bath mode) of the amplifier when the electrode was advanced towards the target cell. During this process, the positive pressure inside the microelectrode could be observed “cleaning” away any debris or tissue covering the target cell membrane. As the microelectrode approaches the cell soma, the positive pressure pushes on the membrane causing a dimple to form. At this stage, the positive pressure was slowly removed, and gentle suction was applied to allow a giga-ohm seal to be

formed. Once the seal resistance exceeded 1 GΩ, the voltage was set to -80 mV and large capacitance transient was compensated in the whole cell section. After the seal formation, gentle mouth suction was applied to break the patched membrane. When whole-cell configuration was established, an access resistance that is approximately less than 3 times the electrode resistance indicates a clean “break in”.

Whole-cell patch clamp recordings were also performed in current clamp mode. A repetitive pulse of -100 pA current of 100 ms duration was applied to the microelectrode once it was in the bath then the tip potentials was zeroed. The forming of giga seal and breaking into the cell were as described above. The bridge was balanced immediately when the whole-cell mode was achieved.

2.4.3 Stimulating electrode

Similar to the fabrication of the recording electrode, the stimulating electrode was fabricated using the P-97 microelectrode puller, from double barrel theta glass of 1.5 mm outside diameter and 1.0 mm inside diameter, 10 mm long, and 0.25 mm septum (Warner Instrument Co., Hamden, USA). The tip of the theta electrode was carefully broken to ~ 10 µm wide by inserting the tip gentle into a Kimwipe tissue (Kimberley-Clark, Texas, USA). The stimulating electrode was filled with the extracellular solution, aCSF, and two thin PFA-coated platinum wires (A-M Systems, Washington, USA) were introduced into contact with aCSF in separate barrel. The microelectrode was secured in place with a theta microelectrode holder connected to the 2100 isolated pulse stimulator (A-M Systems, Washington, USA) which controls the timing, duration, and strength of the stimulus.

2.4.4 Data acquisition

All recordings were done at room temperature (22°C). Whole-cell recordings were recorded using a MutiClamp 700B microelectrode amplifier (Molecular Devices, California, USA) and digitised using a Digidata 1440 (Molecular Devices, California, USA). All data were sampled at a frequency of 10 kHz and low pass filtered at 3 kHz using Clampex 10.6 software.

2.5 Calcium Imaging

2.5.1 Fura-2 AM loading (Bath loading)

Calcium dye (50 µg, Fura-2 acetoxymethyl ester (Fura-2 AM), Molecular Probes, Ore., USA) was dissolved in dimethyl sulfoxide to a final concentration of a 1mM solution and 2% pluronic acid-127 and sonicated for 5 minutes. Experiments were performed on acute cerebellar brain slices of mice at different ages [section 2.2 Animals (*mdx* mice)]. After incubation with NMDG-HEPES recovery aCSF (section 2.3.3 Tissue recovery and maintenance), the brain slices were transferred into a 6-well cell culture plate equipped with cell strainers and filled with aCSF of composition (in mmol/L): NaCl 124, KCl 3.2, $CaCl_2$ 2.5, $MgCl_2$ 1.3, $NaHCO_3$ 26, NaH_2PO_4 1.25, and D-glucose 25 (saturated with 95% O_2 and 5% CO_2 mixture; 324 mOsm; pH 7.4) (6 mL per well) supplemented with 0.5% kolliphor (16 µl) (Sigma Aldrich), at 37°C for 3 minutes. Then, the cerebellar slices were washed twice with aCSF to remove the kolliphor. For calcium indicator loading, Fura-2 AM (1mM) was applied directly to the brain slices in aCSF to a final bath concentration of 10 µM Fura-2 AM and 0.02% (w/v) pluronic F-127 (both from Molecular Probes, Ore., USA). The plate was sealed with parafilm, covered in aluminium foil, and incubated in a 37 C water bath for 1 hour. After incubation, the brain slices were washed 2-3 times with aCSF to remove the excess dye before imaging. To allow

sufficient time for the de-esterification, brain slices were kept in a beaker containing aCSF (saturated with 95% O_2 and 5% CO_2 mixture) for at least 20 minutes) prior the imaging.

2.5.2 Fura -2 free acid loading (Ionophoresis with sharp electrode)

Fura-2 pentapotassium salt (Cayman Chemical, Michigan, USA) (1 mM) in Milli Q water was introduced into the tip of the ionophoretic electrode and the shank was then filled with 2M potassium acetate. Dye was ionophoresed into the cell with a 250 ms pulse, of amplitude -1 nA for 1 minute (Purkinje cell) or -9 nA for 2 minutes (flexor digitorum brevis (FDB) fibre) at 1 Hz. As a negatively charge carboxylate group is present in Fura-2 free acid, negative current was applied to aid the delivery of the dye from the electrode into the cell (Ruggiu 2010). After filling with Fura-2, the cells were allowed to stabilize for 10 minutes to assist in the homogenous distribution of Fura-2 in the cytoplasm, before any readings were taken.

2.5.3 Fura-FF loading (Diffusion with patch electrode)

Fura-FF pentapotassium salt (AAT Bioquest, Carlifornia, USA), a difluorinated derivative of Fura-2, is a low affinity calcium indicator that has similar excitation/emission spectral properties to Fura-2 (Figure 2.3) (Ruggiu *et al.*, 2010). Due to its low affinity property, it is favoured for use in areas such as neuronal dendrites and spines with relatively low calcium buffering capacities or in mitochondria that have high calcium concentrations (Aponte *et al.*, 2008; Canepari *et al.*, 2008; Marcu *et al.*, 2012). Intracellular solution containing 0.3 mM Fura-FF was introduced into the Purkinje cell by free diffusion of the dyes from a patch-electrode into the cell body for 20-30 minutes. The calcium imaging commenced after the equilibration of dye over the entire dendritic field was achieved.

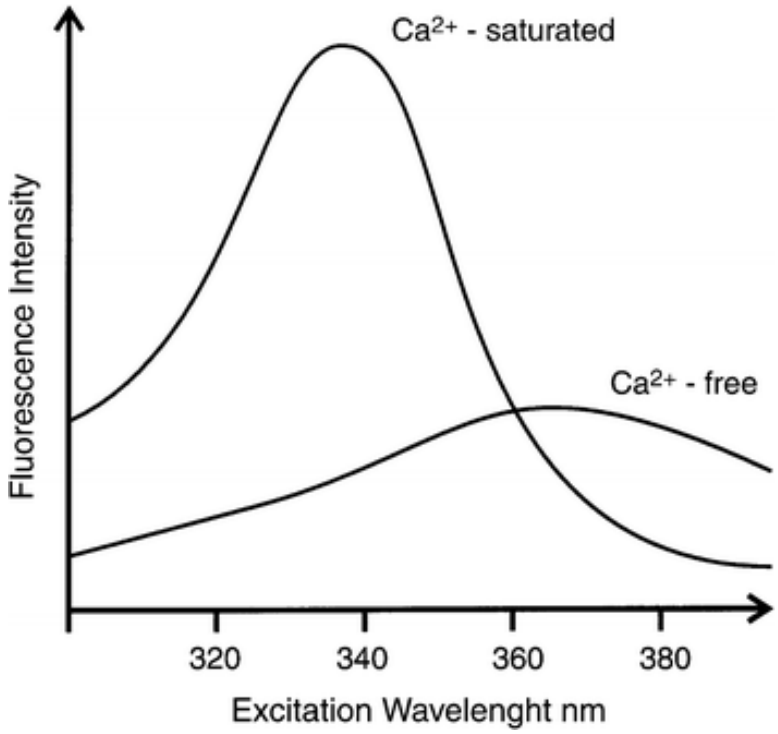

Figure 2.3 Fluorescence excitation spectra of Ca^{2+}-free and Ca^{2+}-saturated Fura-2.

The two spectra coincide at 360 nm results in $[Ca^{2+}]_i$-insensitive fluorescence emission, defining as the isosbestic (or isoemissive) point. Upon Ca^{2+} binding to Fura-2, the fluorescence intensity increases when the Fura-2 is excited at 340 nm relative to when it is excited at 380 nm. The peak emission intensity for Ca^{2+}-free Fura-2 is near 380 nm. The ratio of fluorescence intensity generated at 340 nm and 380 nm can be used to monitor $[Ca^{2+}]_i$ when Fura-2 is excited in quick succession at 340 and 380 nm. Ratiometric (340/380) measurement of Fura-2 is independent from dye concentration, illumination intensity, or optical path length. Adapted and modified from Simpson (2006).

2.5.4 Calcium imaging and fluorescence measurement

For calcium imaging, a brain slice was placed in a submerged recording chamber under a fixed stage upright Olympus BX51WI microscope (Olympus Coporation, Tokyo, Japan) fitted with a EMCCD camera (ANDOR iXON, Oxford Instrument, Abingdon, UK). The brain slice was held in place using a harp to prevent tissue movement during continuous aCSF superfusion. For ratiometric imaging of Fura-2, excitation at 340 and 380 nm (exposure time of 10 ms each, straight after another, with an interval of 80 ms between these pulses) was delivered using an Ultra High Speed Wavelength Switcher (xenon lamp, Lamda DG-4; Sutter instruments, Novato, CA). Emission light from individual cells was passed through an emission filter of 510 ± 20 nm, captured using an EMCCD camera. Image time series were acquired with 40X water-immersion objectives at 10 Hz (an interval of 100 ms). Acquisition protocols consisted of 2-60 seconds time-lapse sequence of Fura-2 fluorescence. Changes in fluorescence as a function of time were measured using the wavelength ratio method, as previously described (Barreto-Chang & Dolmetsch, 2009; Cameron *et al.*, 2016).

All analysis and processing, as well as playback of the image sequences for visual examination, were made using ImageJ /FIJI software (http://fiji.sc/Fiji) (Schindelin *et al.*, 2012). To visualize the spatial and temporal changes in calcium resulting from PF stimulation, region of changes in fluorescence intensity between frames were selected, and the mean pixel intensity at each frame was measured.

2.6 Data Analysis

Electrophysiology data were analysed off-line using pClamp software (Clampfit 10.6, Molecular device, California, USA). Statistical analysis on group data was performed with Prism 8 (GraphPad Software, SanDiego California USA). All data are listed as mean ±

standard error of the mean (SEM) unless otherwise stated. All statistical significance was set at $p<0.05$ for both two-tailed student unpaired *t*-test and Kolmogorov-Smirnov test.

Chapter 3. Miniature inhibitory postsynaptic current in cerebellar Purkinje cells of old dystrophic mice

3.1 Introduction

Modification of the trans-synaptic organisation between cells is an essential mechanism for plasticity in the brain. This synaptic plasticity allows the nervous system the ability to learn (or store) new information. However, if it is not tightly controlled, the alterations in the dynamics of neuronal networks may underlie brain dysfunction (Goddard *et al.*, 1969; Racine, 1972). In DMD, the absence of dystrophin at the postsynaptic density of cerebellar Purkinje cells has resulted in abnormal cerebellar synaptic transmission (Kueh *et al.*, 2011; Kueh *et al.*, 2008). This cerebellar abnormality supports the notion that DMD is a cerebellar disorder due to the similarity of specific cognitive deficits (e.g., restricted verbal span, struggle with phonological processing and reading) displayed between patients with DMD and cerebellar injury (Bishop, 2002; Cabeza & Nyberg, 2000; Eckert *et al.*, 2003; Nicolson *et al.*, 2001; Rae, Harasty, *et al.*, 2002; Ravizza *et al.*, 2006; van Dongen *et al.*, 1994).

At the ultrastructural level, dystrophin is an elongated molecule with a long central rod segment; its N-terminal region binds to cytoskeleton actin, while C-terminal region reacts with a complex of integral membrane glycoprotein (Perronnet & Vaillend, 2010). This dystrophin glycoprotein complex co-localised with $GABA_AR$ at Purkinje cells and the absence of dystrophin resulted in a 50% reduction in the $GABA_AR$ clustering in *mdx* mice (Knuesel *et al.*, 1999). In regard to this $GABA_AR$ clustering abnormality, our group has carried out several electrophysiological studies to examine the synaptic transmission at the cerebellar synapses of *mdx* mice. An alteration in the mIPSCs of Purkinje cells in *mdx* mice was first reported by Anderson *et al.* (2003). The mIPSCs are small currents that arise as a consequence of the

spontaneous release (without a presynaptic action potential) of one (or more) GABA containing transmitter vesicle(s) by presynaptic terminals (Wierenga & Wadman, 1999). The mIPSCs reflect properties of the underlying GABAergic synapses and alteration in synapse morphology inevitably leads to a modification in miniature amplitude distribution (Faber, 1998). Using whole-cell patch clamp recording, Anderson *et al.* (2003) showed a significant reduction in mIPSCs amplitude (~2- fold decrease) in 3 months old *mdx* Purkinje cells when compared to age-matched WT controls. These mIPSCs were mediated by GABA release because they were reversibly blocked by the application of 5 μM bicuculline (competitive antagonist of $GABA_AR$) to the recording solution. The authors suggested that this reduced mIPSCs amplitude pointed to a functional deficit in Purkinje cells for mediating GABAergic synaptic transmission in *mdx* mice. Similarly, other studies from our group also found parallel findings when comparing young *mdx* mice to LC mice that share a common genetic background (Kueh *et al.*, 2011; Kueh *et al.*, 2008). Using peak-scaled non-stationary noise analysis of mIPSCs, Kueh *et al.* (2011) showed a significant reduction in the number of functional $GABA_AR$ in the cerebellar Purkinje cells of dystrophin-deficient *mdx* mice. The author and colleagues concluded that the absence of dystrophin had resulted in the destabilisation of $GABA_AR$ at the postsynaptic membrane and led to an increase in the number of extrasynaptic $GABA_AR$ in Purkinje cells.

Interestingly, when examining the very young (30-45 days) hippocampus, another brain region in which dystrophin is usually expressed but also deficient in *mdx* mice, a different finding was found (Graciotti *et al.*, 2008; Knuesel *et al.*, 1999). Apart from a significant increase in mIPSCs frequency, Graciotti *et al.* (2008) reported no change in the mean mIPSCs amplitude of hippocampal CA1 pyramidal cells in these very young *mdx* mice when compared to B10 controls. The change in mIPSCs frequency may indicate an alteration in the number of

spontaneous active synapses (Wierenga & Wadman, 1999). The difference of these findings may be due to the distinct role that dystrophin plays in specific cell and brain regions or that the impact of dystrophin deficiency on mIPSCs could be age dependent. Taken together, the loss of dystrophin altered the normal GABAergic synaptic transmission at postsynaptic sites and the results seemed contrasting when the *mdx* mice grew older.

Different disease progression during aging in the *mdx* mouse has been reported by various groups. The findings in older *mdx* mice are highly relevant for the understanding of DMD development in humans due to several reasons. Firstly, the progression of muscle disease in *mdx* mice is very slow when they are younger whereas the muscle pathophysiology in the old mice (> 12 months old) is comparable to DMD development in human (Pastoret & Sebille, 1995). Secondly, the behavioural alteration and biochemical abnormalities in the brain are more evident in *mdx* mice that are older than 6 months old (Rae, Griffin, *et al.*, 2002). The finding of brain abnormality in older *mdx* mice may be relevant to human DMD disease progression as a recent study showed that the cognitive function of patients with DMD deteriorates with age (Suzuki *et al.*, 2017).

In view of the importance of dystrophin in the GABAergic synaptic transmission and the relevance of the findings in older *mdx* mice and human DMD disease development, I examined the mIPSCs of cerebellar Purkinje cells in old *mdx* mice. This chapter presents the mIPSCs results comparing the young (3-4 months old) and old (23-26 months old) *mdx* mice with age-matched LC using whole-cell patch clamp recording.

3.2 Method and materials

3.2.1 Animals and brain slice preparation

All experiments were conducted in accordance with the international guidelines on the care and use of experimental animals and approved by the Animal Care and Ethics Committee of Western Sydney University. Mice, 3-4 months old (*mdx*, *n*=3; LC, *n*=3) and 23-26 months old (*mdx*, *n*=3; LC, *n*=4) were anesthetized with isoflurane then decapitated for cerebellum collection.

3.2.1.1 Cerebellum brain slice preparation

The details of cerebellar brain slice preparation were reported in Chapter 2, section 2.3. Briefly, cerebellar section (250 µm) was cut parasagittally using a vibroslicer (Leica VT1200s, Leica Microsystems) and maintained in HEPES buffered aCSF (300-310 mOsm; pH 7.4), continuously bubbled with carbogen until used.

3.2.2 Electrophysiological recording

The details for whole-cell patch clamp recording of mIPSCs in Purkinje cells are reported in Chapter 2, section 2.4. Briefly, patch electrodes were fabricated from borosilicate glass (Warner's instrument, 1.5 mm outside diameter, 1.17 mm inside diameter) and fire polished to give a resistance between 2.9 and 5 MΩ when filled with internal solution containing in mM: CsCl 140, NaCl 4, $CaCl_2$ 0.5, HEPES 10, EGTA 5, Mg-ATP 2 (295-305 mOsm; pH 7.3). Recording was obtained by slowly advancing the electrode to the cell of interest while monitoring its resistance with repetitive small voltage pulses (10 mV). Slight positive pressure was maintained as the electrode approached the cell soma. The positive pressure was immediately released when a small "dimple" was observed. The dimple is an indication of the positive pressure pushing on the membrane of a neuron. During the giga-seal, the cell was held

at -80 mV before additional suction was used to obtain whole-cell configuration. During the whole-cell mode, cells that required input current greater than -300 pA to achieve a membrane potential of -80 mV were excluded for analysis. All recordings were made after the cell with whole-cell mode was rested for 10 minutes. A 10 mV pulse (100 ms duration) was applied and the resulting current response was recorded. An average of 20 initial responses was used to determine access resistance (Ra) and the steady state to determine membrane resistance (Rm). Cells with an access resistance of > 30 MΩ were excluded from analysis. Whole-cell recordings were made using a Multiclamp 700 B amplifier (Axons Instruments) and digitised using a Digidata 1440 (Axon Instruments). All data were sampled at 10 kHz and low pass filtered at 3 kHz. Cell capacitance and series resistance were compensated for all recordings.

3.2.2.1 mIPSCs

With a high internal Cl^- concentration and holding potential of -80 mV, $GABA_AR$ mediated mIPSCs of Purkinje cells were identified as spontaneous synaptic inward currents at room temperature, in the presence of TTX (0.4 µM) to prevent evoked events. The mIPSCs was confirmed by the reversibly blocking effect of the addition of bicuculline (5 µM), a competitive antagonist of $GABA_AR$, into the recording bath.

3.2.3 Data Analysis

A three-minute recording of mIPSC was analysed from each cell using Clampfit 10.6 (Axon Instrument). Using Clampfit 10.6, a template was created based on the average of all selected representative event traces. A template search function under the event detection menu was then applied to identify the individual event within the three minutes recording of mIPSCs. Every event was being examined carefully and it was excluded for analysis if any parameters (i.e., half- width time, 10-90% rise slope, time to rise half-amplitude, etc) of the event are not

available. A range of 12-250 and 100-400 events were recorded in Purkinje cells of young *mdx* and LC mice, whereas in aged animal groups, a range of 51-335 and 152-653 events were recorded in Purkinje cells of *mdx* and LC mice, respectively. Statistical analyses were performed using Prism 7.0 (GraphPad Software, San Diego California USA). Unless otherwise stated, all values are reported as mean ± SEM. Significance level was set at $p<0.05$ for both student unpaired *t*-test and Kolmogorov-Smirnov test.

3.3 Results

3.3.1 General results

Table 3.1 details the ages and average membrane resistance of LC and *mdx* cells. A one-way ANOVA was performed to compare the membrane resistance between groups. There was no significant difference in membrane resistance between all age groups ($p=0.1101$, $R^2=0.1743$, n= 35 cells) (Multiplicity adjusted *p* value: young animals $p=0.3073$; old animals $p>0.9999$, Bonferroni test).

Table 3.1 Ages and average membrane resistance of Purkinje cells.

Group	Young LC (3-4 months)	Young *mdx* (3-4 months)	Old LC (23-26 months)	Old *mdx* (23-26 months)
Number of animals	3	3	4	3
Number of cells	7	9	10	9
Age (days)	112 ± 6	108 ± 4	752 ± 28	725 +76
Average membrane resistance (R) (MΩ)	713.5	365.1	332.8	342.3
R min (MΩ)	267	199	159.5	138.7
R max (MΩ)	1815	725.5	986.2	1156
SEM	219.5	55.16	78.76	105.6

3.3.2 TTX and spontaneous synaptic currents in Purkinje neurons

In normal aCSF, when the cell was held at -80 mV under voltage clamp recording, spontaneous inward currents with a rapid rising phase and slower exponential decay phase were observed in young and old Purkinje neurons from both *mdx* and LC mice (Figure 3.1 A & B). The currents had variable amplitudes, ranging from less than 10 pA up to 4 nA. When TTX (0.4 µM) was added, the large amplitude spontaneous IPSCs mediated by sodium currents were gradually abolished, resulting in lower frequency and amplitude mIPSCs. As expected for $GABA_A$-mediated mIPSCs, these currents were reversibly blocked by the addition of bicuculline (5 µM), the competitive antagonist of $GABA_AR$, to the recording bath (Figure 3.1 C) (Llano & Gerschenfeld, 1993).

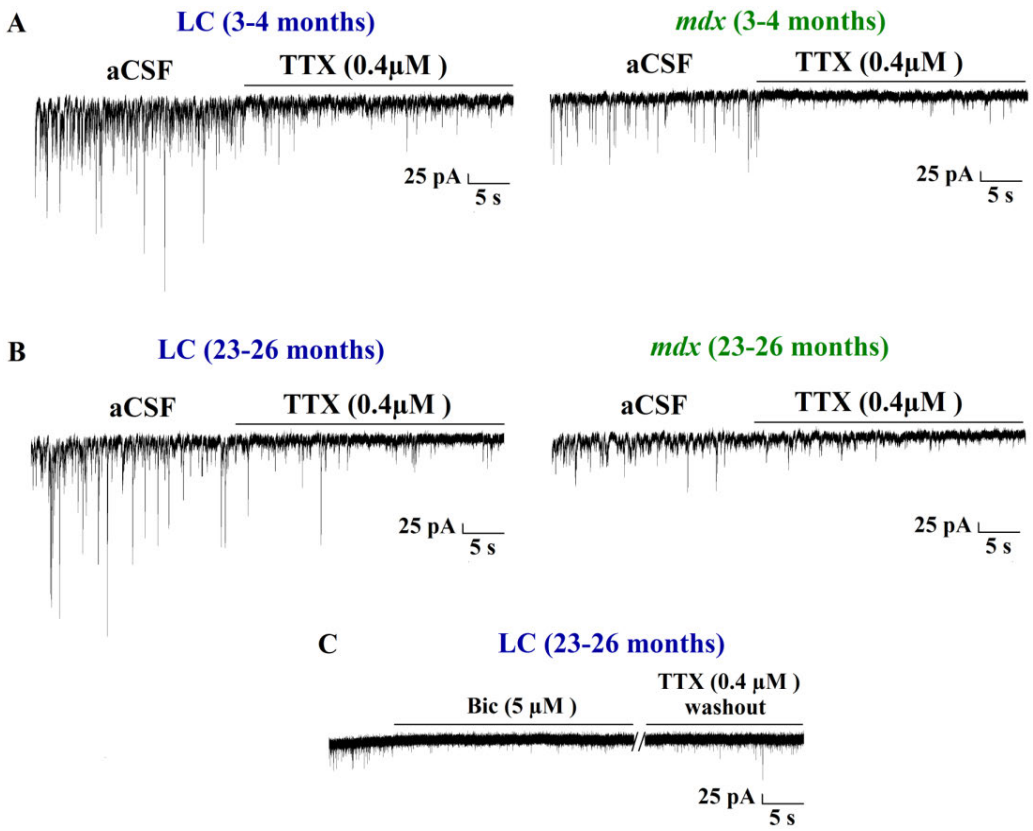

Figure 3.1 Impacts of TTX and bicuculline on inhibitory postsynaptic currents of a Purkinje cell.

Recordings showing TTX-resistant mIPSCs with reduced frequency and amplitude in a LC and an *mdx* mouse from (A) young (3-4 months old) and (B) old (23-26 months old) age groups. (C) Representative recording showing that bicuculline (5µM), $GABA_AR$ antagonist, reversibly blocked mIPSCs in GABAergic Purkinje cell of an old LC. These effects were consistent for all tested animals.

3.3.3 Reduced peak amplitude of mIPSCs in young and old *mdx* mice

The representative of one minute mIPSCs recordings in LC and *mdx* Purkinje cell from the young and old animals are shown in Figure 3.2 and Figure 3.3 respectively. These recordings show that the large amplitude mIPSCs were reduced in *mdx* mice compared to LC mice in both age groups. To compare the mIPSCs amplitude between different animal groups, a 3-minutes recording of mIPSCs from each cell was used for the analysis. A section of this recording is depicted in Figure 3.4 A. A representative Purkinje cell from young (3-4 months old) *mdx* mice showed reduced average amplitude of mIPSCs in comparison to LC (*mdx* 36.17 ± 1.08 pA; LC 52.52 ± 1.97 pA; Figure 3.4 B). In the old age group (23-26 months old), there was no significant difference in average mIPSCs amplitude between the representative *mdx* (41.36 ± 2.7 pA) and LC (45.42 ± 2.54 pA) cells (Figure 3.4 C).

When comparing the results from all animals, the average amplitudes of mIPSCs in *mdx* mice were reduced in both age groups in comparison to LC (Figure 3.5). However, it was only statistically significant in the young age group (young *mdx* 36.53 ± 2.16 pA (n=9 cells); young LC 55.5 ± 3.28 pA (n=7 cells), p= 0.0002, student unpaired *t*-test) but not in the old age group (old *mdx* 41.62 ± 2.84 pA (n=9 ells); old LC 47.17 ± 5.17 pA (n=10 cells), p= 0.3748, student unpaired *t*-test). The finding from the young age group was consistent with the earlier report from our group (Kueh *et al.*, 2011). The current results showed that aging has no obvious impact on the amplitude of mIPSCs of mice with the same genotype (LC groups, p=0.2392; *mdx* groups p=0.1735, student unpaired *t*-test).

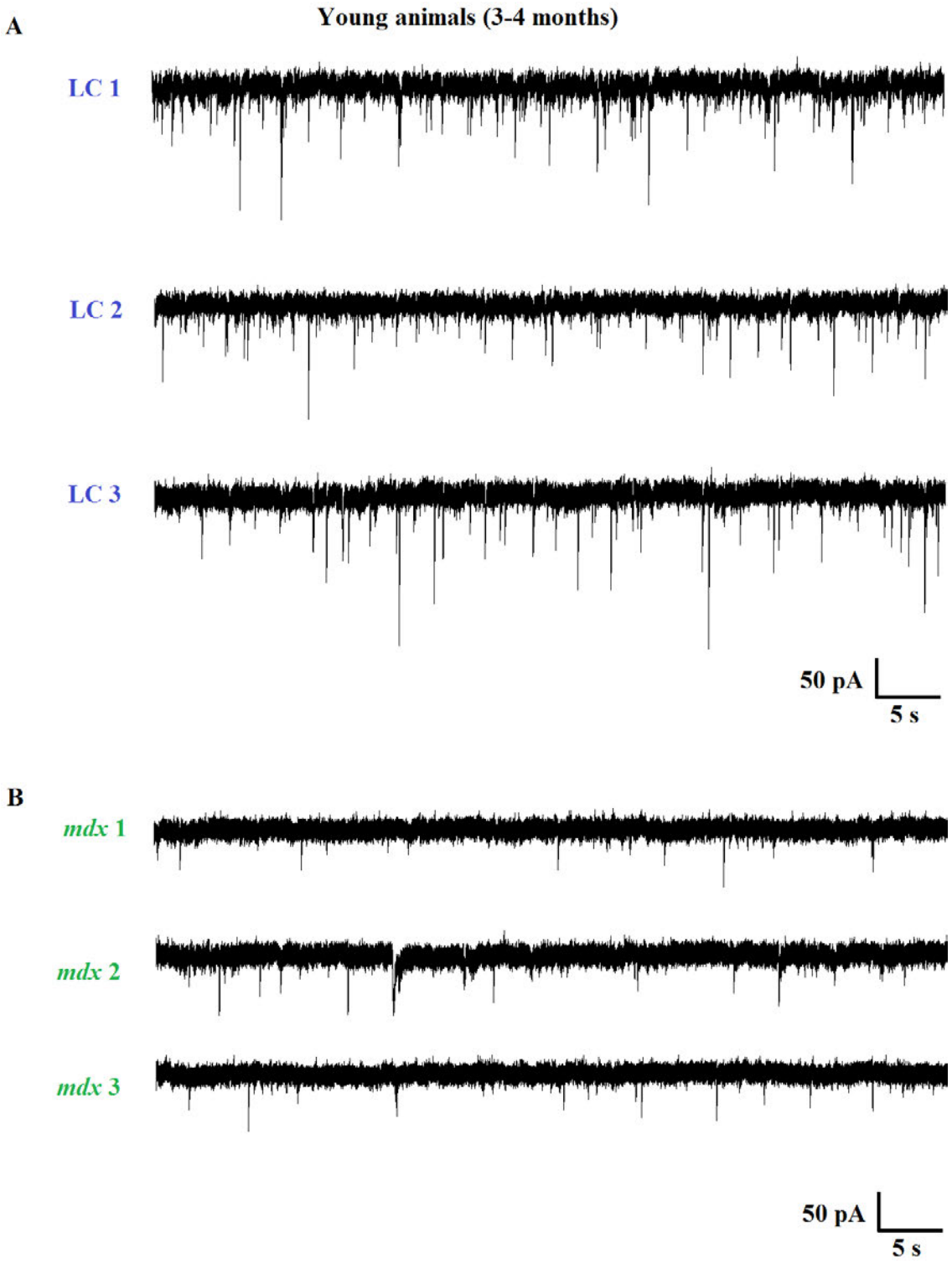

Figure 3.2 Miniature inhibitory postsynaptic current recordings in LC and *mdx* Purkinje cells from young (3-4 months) animal group.

(A) mIPSCs recordings in Purkinje cell from 3 LC and (B) 3 *mdx* mice. Large amplitude mIPSCs were reduced in *mdx* mice compared to LC mice.

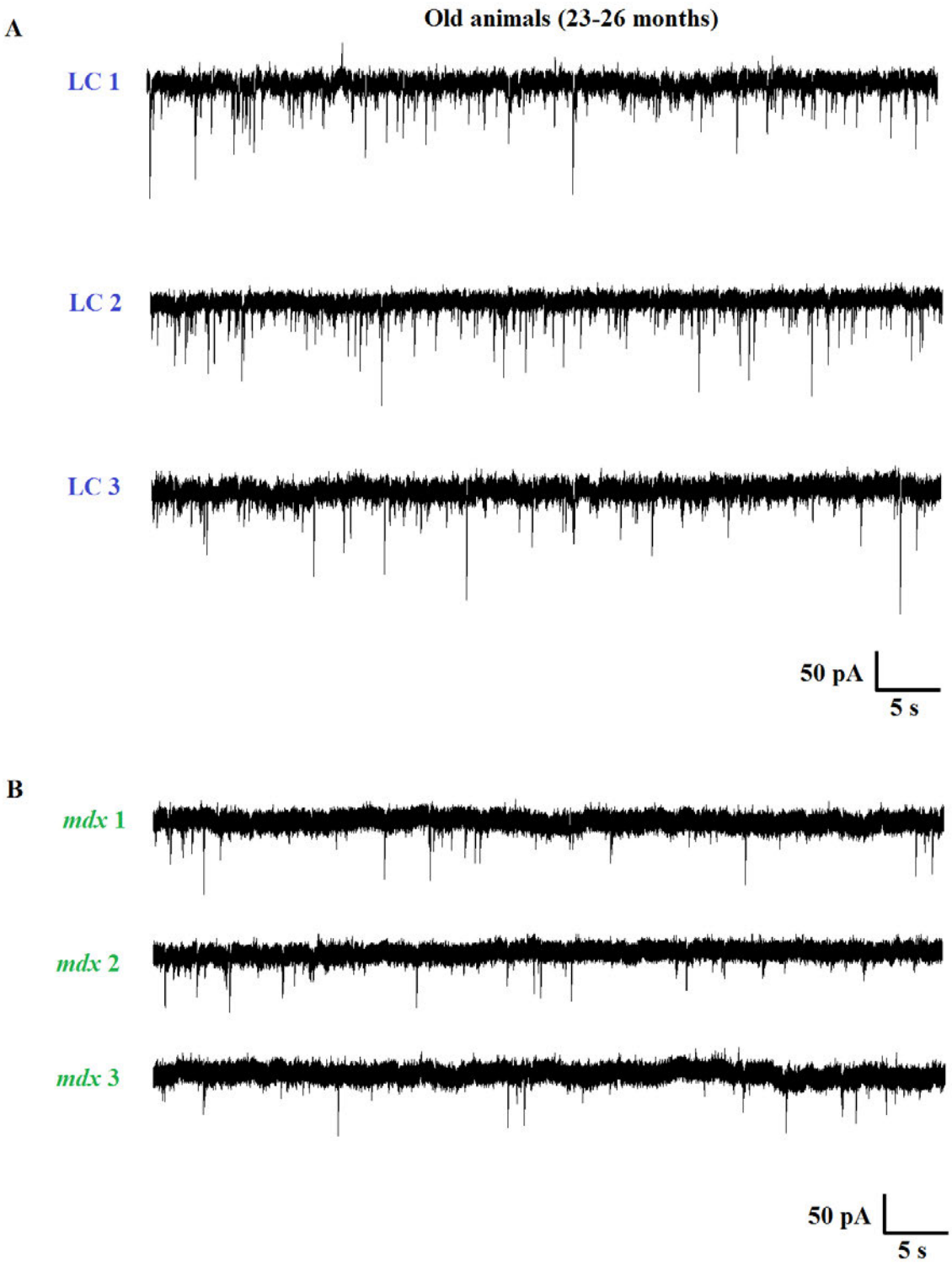

Figure 3.3 Miniature inhibitory postsynaptic current recordings in LC and *mdx* Purkinje cells from old (23-26 months) animal group.

(A) mIPSCs recordings in Purkinje cell from 3 LC and (B) 3 *mdx* mice. Large amplitude mIPSCs were reduced in *mdx* mice compared to LC mice.

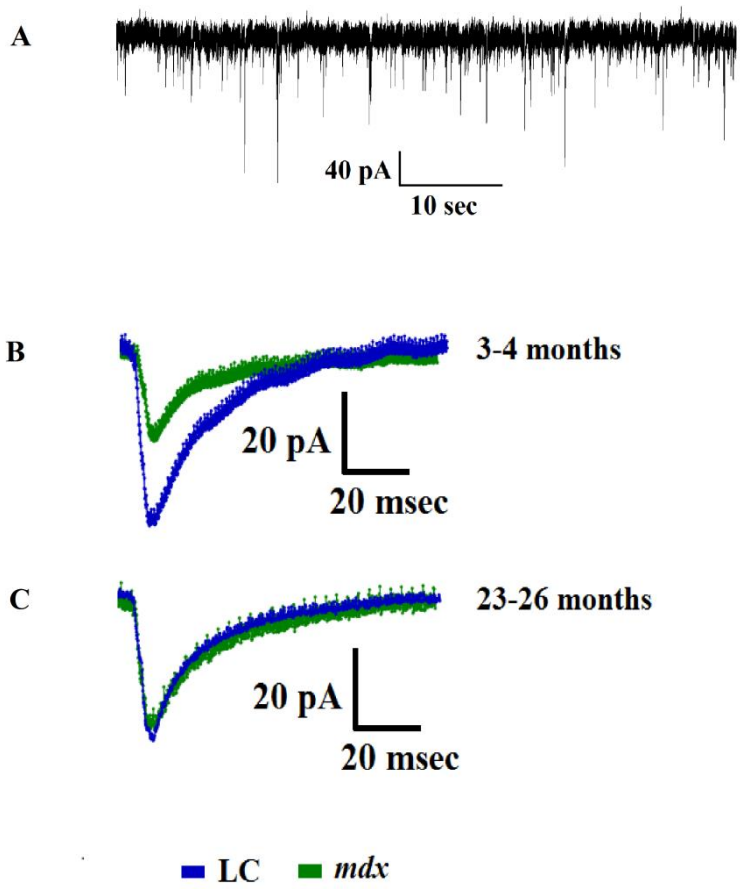

Figure 3.4 Miniature inhibitory postsynaptic current recordings and the average of mIPSCs from a representative Purkinje cell from different age groups.

(A) Representative trace of mIPSCs from a Purkinje cell recorded from young (3-4 months old) LC. Recording was done using whole-cell voltage clamp while the cell membrane potential was held at -80 mV. A total of 3 minutes mIPSCs recording from each cell was used to calculate the average amplitude. (B) Time course of a representative single peak event of mIPSCs from young *mdx* and LC. The average amplitude of mIPSCs was greatly reduced in *mdx* (36.17 ± 1.08 pA) cell in comparison to age-matched LC (52.52 ± 1.97 pA). (C) Time course of a representative single peak event of mIPSCs from old *mdx* and LC (23-26 months old). The average amplitude of mIPSCs in LC was 45.42 ± 2.54 pA while *mdx* was 41.36 ± 2.7 pA. All data are presented as mean ± SEM.

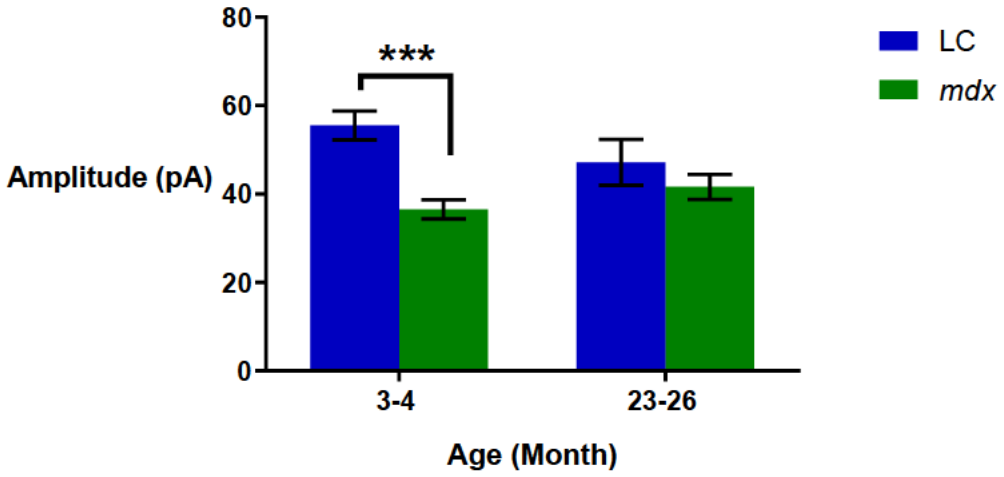

Figure 3.5 Summary data showing the average amplitude of mIPSCs in LC and *mdx* mice Purkinje cells from different age groups.

Average amplitude of mIPSCs in each group was calculated from an average of 3 minutes of recording from each cell. Mean amplitude of young *mdx* (n=9 cells; 36.53 ± 2.16 pA) was significantly reduced when compared to LC (n=7 cells; 55.5 ± 3.28 pA, p= 0.0002, student unpaired t-test). The mean amplitude of old *mdx* (n=9 cells) was 41.62 ± 2.84 pA while LC (n=10 cells) was 47.17 ± 5.17 pA (p= 0.3748, student unpaired t-test). All data are presented as mean ± SEM.

Although there was no significant difference in the average amplitude of mIPSCs between the old *mdx* and LC, the distribution of mIPSCs amplitudes of these two groups varied enormously, from tens of pA to several hundred pA (Figure 3.6 A & B). The amplitudes of the smallest and largest mIPSCs in old *mdx* were 13.75 pA and 290.75 pA while LC were 8.91 pA and 438.18 pA, respectively. In addition, the distribution of the larger current was less in old *mdx* than LC. The top quantile (75% percentile) in old *mdx* amplitude was 52.27 pA while in LC it was 62.82 pA. The median of the old *mdx* amplitude was 38.64 pA while in LC it was 42.68 pA. The cumulative probability plot of mIPSCs amplitude clearly indicated a significant shift to the left in the old *mdx* when compared to their LC, depicting a reduced peak amplitude in these mice (p<0.0001, Kolmogorov-Smirnov test) (Figure 3.6 C).

Similarly, the histograms of mIPSCs amplitude distributions in young animals also resembled those found in the old age groups (Figure 3.6 D & E). The amplitudes of the smallest and largest mIPSCs in young *mdx* were 10.49 pA and 144.33 pA while in LC, they were 9.19 pA and 2538.49 pA, respectively. These plots also showed a reduction of larger events in the young *mdx* when compared to young LC. The top quantile (75% percentile) in young *mdx* amplitude was 45.17 pA while in LC it was 66.61 pA. The median of young *mdx* amplitude was 33.81 pA while LC was 46.44 pA. Consistent with the results in the old age group, the cumulative probability plot of mIPSCs amplitude in young animals also showed a significant shift to the left in the *mdx* when compared to their LC, again indicating a reduced peak amplitude in the *mdx* population (p<0.0001, Kolmogorov-Smirnov test) (Figure 3.6 F).

3.3.4 Reduced average frequency of mIPSCs in young and old *mdx* mice

The average mIPSCs frequency of each group was calculated from a 3 minutes recording from all cells. Both age groups showed a significantly reduced mIPSCs frequency in *mdx* mice in

comparison to LC (Figure 3.7). In the 3-4 months old animal, the average frequency of mIPSCs in *mdx* was 0.73 ± 0.15 Hz while in LC, it was 1.507 ± 0.23 Hz (p=0.0106, student unpaired t-test). In the 23-26 months old group, the mean frequency of *mdx* was 0.68 ± 0.17 Hz while in LC, it was 1.61 ± 0.26 Hz (p=0.009, student unpaired t-test). Interestingly, for the same genotype, there was no difference in mIPSCs frequency between the young and old animals (*mdx* p=0.8409; LC, p=0.7762, student unpaired t-test).

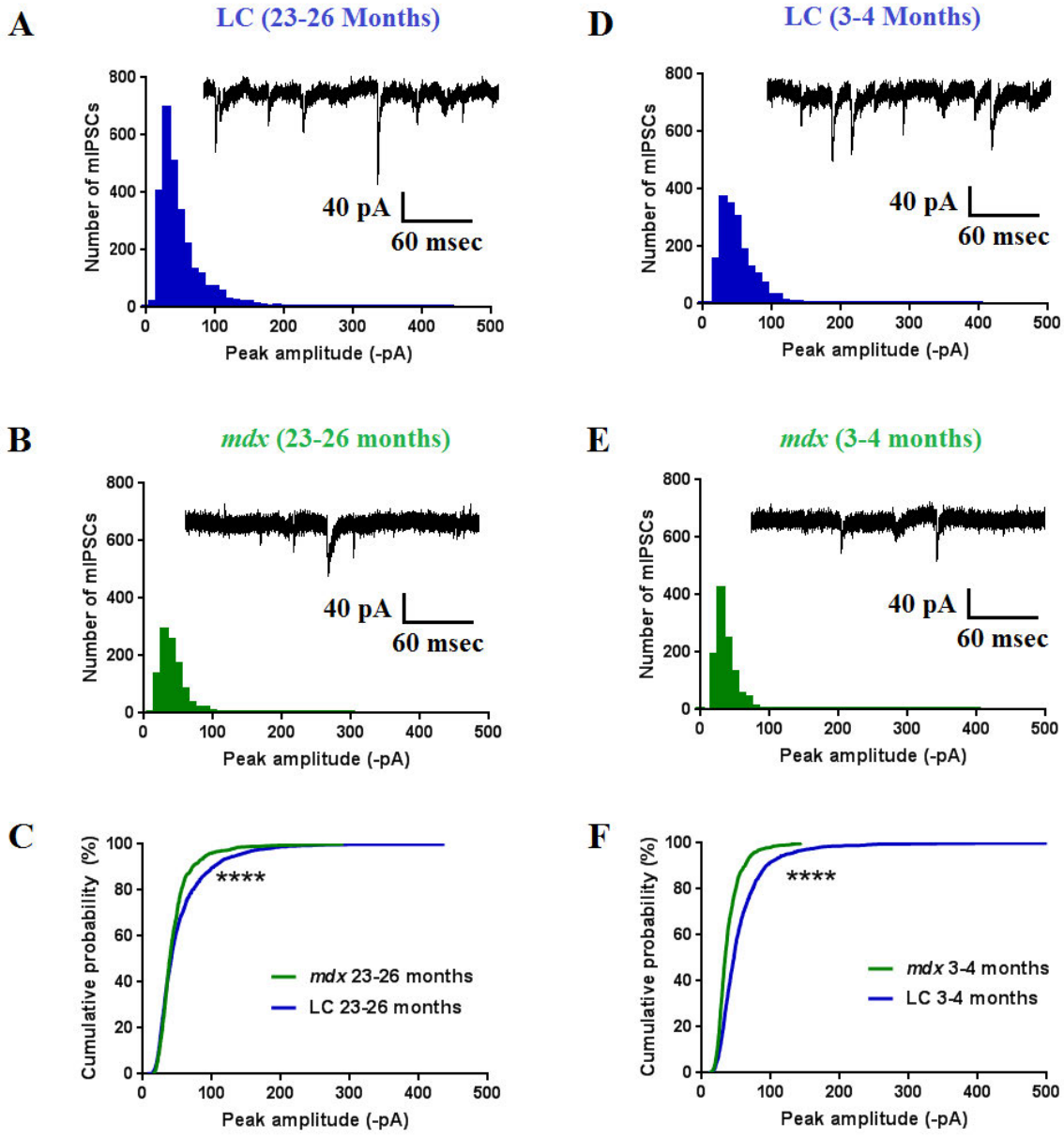

Figure 3.6 Summary histograms and cumulative plot of mIPSCs amplitude of LC and *mdx* mice from different age groups.

Amplitude histograms of mIPSCs of all cells from old (A) LC and (B) *mdx* mice. *Inset*: example of mIPSCs from individual Purkinje neuron. The distribution of larger currents in *mdx* mice was reduced drastically between old LC and *mdx* mice (75% percentile, *mdx*=52.27 pA, LC= 62.82 pA). (C) Cumulative plot summarising mIPSCs amplitude distribution for the old age groups. The two distributions overlapped for the smaller amplitudes but started to deviate from each other after -36 pA. The mean peak amplitude decreased from 53.73 ± 0.74 (-pA) LC to 45.75 ± 0.82 (-pA) *mdx*, $p<0.0001$, Kolmogorov-Smirnov test. Amplitude histograms of mIPSCs of all cells from young (D) LC and (E) *mdx* mice. Inset: example of mIPSCs from individual Purkinje neuron. When comparing LC and *mdx* amplitude histograms, the distribution of larger currents in *mdx* mice was reduced drastically (75% percentile, *mdx*=45.17 pA, LC=66.61 pA). (F) Cumulative plot summarising mIPSCs amplitude distribution for the young age groups. The two distributions overlapped for the smaller amplitudes but started to deviate from each other after -20 pA. The mean peak amplitude decreased from 57.52 ± 1.59 (-pA) LC to 38.77 ± 0.54 (-pA) *mdx*, $p<0.0001$, Kolmogorov-Smirnov test.

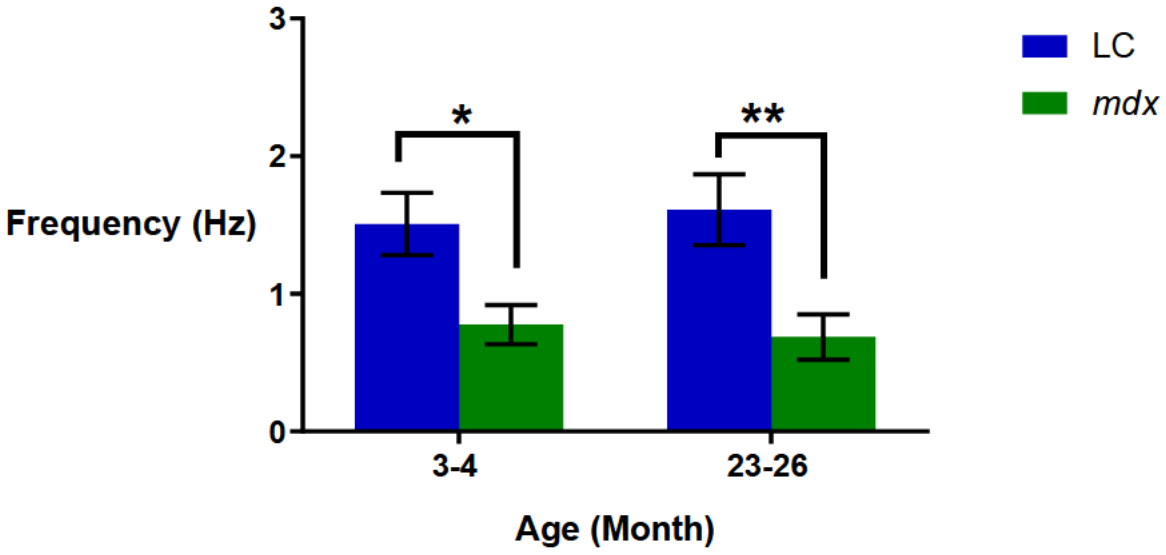

Figure 3.7 Summary data showing average frequency of mIPSCs in LC and *mdx* mice Purkinje cells from different age groups.

Average frequencies of mIPSCs in *mdx* mice were significantly reduced in both the young (3-4 months old) and old age groups (23-26 months old) when compared to age-matched LC. In the young age group, the mean frequency of *mdx* (n=9 cells) was 0.73 ± 0.15 Hz, compared to that in LC (n=7 cells) which was 1.507 ± 0.23 Hz, p=0.0106, student unpaired t-test. The mean frequency of old *mdx* (n=9 cells) was 0.68 ± 0.17 Hz while LC (n=10 cells) was 1.61 ± 0.26 Hz, p=0.009, student unpaired t-test. The data are presented as mean ± SEM.

3.4 Discussion

In this study, I was able to reproduce the results from our previous work demonstrating a reduction in the average frequency and amplitude of mIPSCs in young *mdx* mice (3-4 months), when compared to age-matched LC (Kueh *et al.*, 2011). In addition, the electrophysiological investigation compared mIPSCs of Purkinje cells between *mdx* and LC from young (3-4 months) and old (23-26 months) mice. Consistent with the results from the young animal, the changes in mIPSCs of old *mdx* resembled that found in young *mdx* mice, indicating that other than dystrophin deficiency, aging may not have an impact on postsynaptic current transmission.

Membrane resistance, a basic membrane property, was also measured in this study prior to the measurement of postsynaptic currents. It defines the conductance or resistance of the membrane upon current injection or membrane depolarisation, facilitated by ionic channels on cell membrane. It is influenced by the leakiness (i.e. the cell is "leaky" if many channels are open in a cell) of the membrane. When more channels are activated, the neuron has a high membrane conductance with a low membrane resistance. Conversely, a neuron with a high membrane resistance suggests that it has fewer channels that are in the active state and its conductance level is low. It was found that the average membrane resistance was not significantly different between *mdx* and LC in both the young and old animal groups. The average membrane resistance of Purkinje cells in both animal groups is around 350 MΩ (except for the young LC which had an average membrane resistance of 713.5 MΩ). The sum of membrane resistance and access resistance (access resistance was maintained below 30 MΩ in the current experiment setting) is equal to input resistance. Sharing a similar access resistance requirement, the membrane resistance results reported here are consistent with the findings in Snow *et al.* (2014), in which they reported a grand mean input resistance of 337.83 ± 24.65 MΩ (N=55) in dissociated Purkinje cells of both genotypes. Contradictory to the

findings in Purkinje neurons, the group of Conte-Camerino and collaborators showed a reduction of membrane resistance in *mdx* muscle fibres (between 8 and 13 weeks of age) when compared to control mice (De Luca *et al.*, 1999; De Luca *et al.*, 1995; De Luca *et al.*, 1997). This reduced membrane resistance was credited to an increase in resting chloride conductance. Similarly, alteration in other ion channel activity has also been reported by Denetclaw *et al.* (1994). The authors demonstrated a threefold increase in open probability of Ca^{2+} leak channels resulting from abnormally long open times in *mdx* primary myotube cultures, isolated from the hind-limb muscles of 10-week-old adult mice, when compared to normal control. Interestingly, opposing results were obtained in the *mdx* diaphragm. It was reported by De Luca *et al.* (1997) that a higher membrane resistance was associated with a lower value of resting chloride conductance in comparison to controls. Although findings from studies investigating dystrophin-deficient muscle fibres reported a change (decrease or increase) of membrane resistance, the current results showed that there was no significant difference between the membrane resistance of Purkinje cell from *mdx* and LC mice. This indicates that the consequences of the absence of dystrophin are quite diverse and conflicting in different cell types.

The current findings also showed that aging has no impact on the membrane resistance of old Purkinje cells in both groups of mice. This result is consistent with an earlier finding in the rat neostriatum, a major nucleus in the basal ganglia, which has been used extensively for studies in aging (Cepeda *et al.*, 1992). The authors reported that the membrane resistance in the aged neostriatal neurons (24-26 months) remains unchanged compared to the young (3-5 months) cells despite the decreases in cellular excitability in the aged neostriatal neurons. Furthermore, a recent mouse study in the aged (29-30 months) bed nucleus of the stria terminalis, a limbic forebrain structure involved in fear, stress, and anxiety, also showed no statistically significant

effect of age on input resistance when compared to the young (3-4 months) cells. Contradictory, age related input resistance alteration is reported in the layer 2/3 pyramidal neurons of the prefrontal cortex of rhesus monkeys (Chang *et al.*, 2005). The authors reported that there was a significant increase in the input resistance of pyramidal cells from aged monkeys (19.2–29 years) when compared to cells from young monkeys (6.0-10.2 years). It was suggested that the changes (i.e. increase) in input resistance with age could be due to the alterations in the size of cell soma (i.e. smaller) and dendrites (i.e. loss or regression), and the decrease in the density of ion channels in the aged cells (de Brabander *et al.*, 1998; Duan *et al.*, 2003; Page *et al.*, 2002; Wong *et al.*, 2000). Taken together, these findings and current findings supported the suggestion that dystrophin deficiency has no significant impact on the membrane resistance of *mdx* Purkinje cells from both young and aged animals.

Examining the synaptic current transmission, significant reductions in the average and peak amplitude of $GABA_AR$-mediated mIPSCs were found in young *mdx* mice when compared to age-matched controls. These mIPSCs were isolated using TTX and confirmed as $GABA_A$ conductance by bath application of bicuculline. The results from the 3-4 months old *mdx* again confirmed the findings from our previous study (Kueh *et al.*, 2011; Kueh *et al.*, 2008). On the other hand, at first glance the reduced average amplitude of old *mdx* mice was subtle and not significantly different to that of age-matched LC. However, the peak amplitude distribution of old *mdx* was significantly reduced, consistent with the finding in the younger population. The amplitude of recorded mIPSCs in this study varied, ranging between 10 pA and 2540 pA and showed a skewed distribution in all groups. When comparing between *mdx* and LC, the amplitude distribution in *mdx* populations were left-shifted, indicating a reduction in the larger events. The current amplitude is associated with postsynaptic neurotransmitter sensitivity, which is controlled by postsynaptic receptor number and conductance (Graziane & Dong,

2016; Nusser *et al.*, 1997). Wan *et al.* (1997) demonstrated an enhancement of mIPSCs amplitude when there was an increase in translocation of functional $GABA_AR$ from the intracellular compartment to the dendritic and postsynaptic membrane of CA1 hippocampal neurons as a result of insulin signalling (receptor translocation by activation of insulin-receptor tyrosine kinase). On the other hand, a quick decline in $GABA_AR$ number induced by brain-derived neurotrophic factor (BDNF) exposure has been shown to reduce GABAergic mIPSC amplitudes (Brunig *et al.*, 2001). Their finding was further supported by immunocytochemical results, demonstrating a decrease of punctate staining of $GABA_AR$ subunits after 15 minutes of BDNF treatment. They also reported that BDNF did not affect the shape or kinetics of mIPSC, indicating that the $GABA_AR$ channel properties, such as open probability, open time or ligand affinity remained the same, and concluded that the reduced number of synaptic $GABA_AR$ serves as the main contributor to the decrease in amplitude (Brunig *et al.*, 2001). To that regard, the wide variability in the mIPSCs amplitude in the current study can be explained by the difference in postsynaptic receptor numbers present, and that the reduced amplitude (i.e. reduce GABAergic synaptic transmission) in *mdx* mice in all age groups may be due to a reduction in the number of $GABA_AR$ at the postsynaptic membrane of the *mdx* Purkinje cell.

Dystrophin is detected in the postsynaptic densities of neurons at inhibitory synapses in several brain regions such as cerebellum, hippocampus, and amygdala (Knuesel *et al.*, 1999). This protein plays an important role in the clustering and fixation of $GABA_AR$ at postsynaptic sites of the cell membrane. A deficit of dystrophin has resulted in the destablisation of $GABA_AR$ at postsynaptic sites, which in turn led to a 40-70% reduction in the number of $GABA_AR$ clusters and subsequently the reduced amplitudes of mIPSCs (Anderson *et al.*, 2003; Knuesel *et al.*, 1999; Kueh *et al.*, 2011; Sekiguchi *et al.*, 2009; Vaillend *et al.*, 2010). Supported by an electrophysiological study, Kueh *et al.* (2011) shows that these defects in $GABA_AR$ clustering

had resulted in a 14% reduction in the amplitude of intermediate to large mIPSCs (>45 pA) at the post-synaptic membrane of cerebellar Purkinje cells in 2-4-month-old *mdx* mice when compared to age-matched LC mice. Interestingly, the destabilisation of $GABA_AR$ at postsynaptic sites had resulted in an increase in the number of extrasynaptic $GABA_AR$ in Purkinje cells of *mdx* mice. An enhanced sensitivity to gaboxadol, a selective pharmacological activator of extrasynaptic $GABA_AR$, was displayed in *mdx* mice (Kueh *et al.*, 2011; Vaillend & Chaussenot, 2017). Therefore, current findings of reduced amplitude of mIPSCs in all *mdx* age groups, along with those of Kueh and colleagues, provide evidence that the dystrophin is required for the maintenance and stabilisation of postsynaptic $GABA_AR$ clusters throughout the animal's lifespan, perhaps by limiting the lateral diffusion of unstable $GABA_AR$ to extrasynaptic sites.

In addition to mIPSCs amplitude, this study also found a significant reduction (~2-fold reduction) in mIPSCs frequency in *mdx* compared to LC for both age groups. This result is similar to the finding in our earlier study (Kueh *et al.*, 2011; Kueh *et al.*, 2008). On the other hand, when comparing the same dystrophic mouse model with $C57/BL10^{sc/sn}$ (BL10) control, Graciotti *et al.* (2008) reported an increase in mIPSCs frequency in CA1 hippocampal neuron. They confirmed this increase in frequency was due to the altered presynaptic release probability, as examined by PPF analysis. Since the mIPSCs frequency can be regulated by the presynaptic release mechanism, the reduced mIPSCs frequency in the current study may be associated with an alteration at the presynaptic site. Purkinje cells receive two main inhibitory inputs from the inhibitory interneurons: basket and stellate cells. These presynaptic inhibitory neurons release GABA that activates the $GABA_AR$ located at the postsynaptic density of Purkinje cells. It has been reported that spontaneous GABA release is dependent on the increase of $[Ca^{2+}]_i$ level and its probability of release can determine the frequency of mIPSCs

(Fatt & Katz, 1952; Ke *et al.*, 2010; Llano *et al.*, 2000; Poisbeau *et al.*, 1996; Warrier *et al.*, 2005). Increase $[Ca^{2+}]_i$ levels at presynaptic cells can be achieved by Ca^{2+} release from intracellular stores and extracellular Ca^{2+} influx. Llano and colleagues reported that Ca^{2+} release through the ryanodine receptor (RyR)-sensitive presynaptic stores plays a role in regulating the frequency of mIPSCs of rat cerebellar Purkinje cells (Llano *et al.*, 2000). In a separate study, Kelm *et al.* (2007) showed that calcium release from presynaptic internal stores plays an important role in the ethanol-enhanced spontaneous GABA release at the interneuron-Purkinje cell synapse. Additionally, Ke *et al.* (2010) demonstrated that the reduction or blockade of $[Ca^{2+}]_i$ release mediated by $InsP_3$-induced Ca^{2+} release from intracellular stores as well as extracellular calcium influx through presynaptic calcium channels significantly reduced the frequency of GABAergic mIPSCs. These studies suggested that changes in presynaptic $[Ca^{2+}]_i$ levels can alter the frequency of GABAergic mIPSCs at the postsynaptic site. Interestingly, $[Ca^{2+}]_i$ in granule cells (where fibres form excitatory synapses with Purkinje cells) of *mdx* mice was significantly elevated (Hopf & Steinhardt, 1992). With regard to the alteration in presynaptic $[Ca^{2+}]_i$ level at the granule-Purkinje cell excitatory synapse of *mdx* mice, it is conceivable that the presynaptic $[Ca^{2+}]_i$ level at the interneuron-Purkinje cell inhibitory synapse may be affected by the absence of dystrophin. Further study looking for possible dysregulated presynaptic/neuronal $[Ca^{2+}]_i$ levels in *mdx* cerebellum may be interesting.

DMD is a progressive disease involving gradual breakdown of muscle fibre with non-progressive cognitive impairments involving reduced IQ scores (i.e. a reduction of one standard deviation below the normal range) (Felisari *et al.*, 2000). However, it was recently reported that the executive functions (i.e. strategic planning, organised searching, utilisation of environmental feedback to shift cognitive sets, behavioural direction toward achieving goal,

and modulation of impulsive responses) of older DMD patients (30-37 years old) were worse than younger DMD patients (18-25 years old) when assessed with the Wisconsin Card Sorting Test, indicating a progressive cognitive decline with age in DMD (Suzuki *et al.*, 2017). While many studies have focused on the muscle pathophysiology of the *mdx* mice, little is known about the cognitive progression during aging in these mice. Behavioural studies show that there are impairments in the passive avoidance learning and long term spatial and recognition memory of these mice (Muntoni *et al.*, 1991; Vaillend *et al.*, 2004). Although the cognitive dysfunctions in *mdx* mice have been reported by various groups, there has been no study to date addressing if this cognitive impairment is exacerbated with age. Understanding the neuropathophyisology of DMD is very important for the development of early interventions to improve or preserve normal intellectual function especially with the current improved palliative care, including prednisone for prolonged muscle ambulation, and mechanical ventilation for respiratory care of DMD patients who are surviving into their 30s-40s (Rae & O'Malley, 2016; Saito *et al.*, 2017).

Interestingly, when I studied the $GABA_AR$ mediated mIPSCs in Purkinje cells, I found that the frequency and amplitude of these currents remained similar in both young and aged *mdx* mice. These results are important, and it may indicate that the impaired GABAergic synaptic transmission in cerebellar Purkinje cells does not improve or worsen with age (i.e. non-progressing) and that the function of these cells remained similar throughout the lifespan of *mdx* mice. As the verbal impairment in DMD patients is thought to be non-progressive (Leibowitz & Dubowitz, 1981; Marsh & Munsat, 1974), and may be regulated by the cerebellum (Cyrulnik & Hinton, 2008), the findings of non-progressive GABAergic perturbations in *mdx* cerebellum supports the notion that the verbal intelligence in DMD is non-progressive. Furthermore, the current finding also parallels the findings in DMD patients, in

which it shows no significant decline in cerebellar $GABA_AR$, except in the prefrontal cortex of older patients (30-37 years old), when compared to younger DMD patients (18-25 years old) (Suzuki *et al.*, 2017). Taken together, if the decline in cognitive function (i.e. executive function) is progressive in DMD patients or in *mdx* mice, current findings would also imply that instead of cerebellum and cerebellar Purkinje cells, other brain regions may be involved and affected by dystrophin deficiency. Whether or not the cognitive deficits are progressing in *mdx* mice remains to be determined. Behavioural, neuroanatomy, and electrophysiology studies throughout the lifespan of the *mdx* mouse may be beneficial for providing further insights on the mechanisms which are responsible for CNS dysfunctions in DMD.

3.5 Conclusion

This study has shown no change in membrane resistance of Purkinje cells in *mdx* mice. I also re-confirmed the results from our previous studies that both mIPSCs amplitude and frequency were significantly reduced in 3-4 months old dystrophic mice in comparison to LC. More importantly, this is the first report showing a significant reduction in mIPSCs amplitude and frequency in the old *mdx* mice when compared to age-matched LC. The current finding is valuable since old *mdx* mice are very scarce due to their shorter lifespan compared to LC, as well as the disease progression closely resembles the DMD pathophysiology in human. Together with the results from young mice, this study showed that the lack of dystrophin disrupts the normal synaptic transmission at GABAergic synapses. This perturbed synaptic transmission may underlie the behavioural deficits and cognitive impairments seen in the *mdx* mice. If similar disruptions are found in human brains with dystrophin deficiency, this may explain the intellectual deficits reported in patients with DMD. Furthermore, the similar frequency and amplitude of mIPSCs between young and old *mdx* mice indicate that the GABAergic transmission in dystrophin deficient cerebellum was not altered during aging. As

cerebellar involvement was suggested for the non-progressive cognitive deficits (i.e. impairments in verbal working memory and reading) displayed in DMD boys (Cyrulnik & Hinton, 2008), the similar findings in mIPSCs quantal analyses (i.e. amplitude and frequency) in both young and old *mdx* mice supports the notion that the verbal impairment in DMD is non-progressive.

Chapter 4. Rescue of a dystrophin-like-protein by exon skipping normalises $GABA_AR$ clustering and mIPSCs in the cerebellar Purkinje cells of the *mdx* organotypic culture

4.1 Introduction

Although the mutation in *DMD* gene has been identified as the cause of DMD since late in the 20th century, to date there is still no effective cure for this fatal disease. *DMD* gene is the second largest gene described in humans with approximately 2.5 million base pairs, encoding 79 exons (Koenig *et al.*, 1987; Muntoni *et al.*, 2003; Roberts *et al.*, 1993). These exons form the 14kb messenger RNA which encodes the protein dystrophin, containing 3685 amino acids and is 427 kD in size. Owing to the large size of the *DMD* gene, dystrophin expression is highly vulnerable to different forms of genetic mutations including deletion, duplication, insertion, nonsense, and missense mutations (Taylor *et al.*, 2010). As consequence of the many different types of mutations, the development of a universal pharmacological intervention that provides effective dystrophin restoration in DMD is deemed impossible. Despite this, approaches including stem-cell therapy, gene replacement, aminoglycoside antibiotics and proteasome inhibitors have been introduced in an attempt to restore dystrophin expression (Wurster & Ludolph, 2018). Importantly, as described in Chapter 1 section 1.7, exon skipping using AOs has emerged as a promising therapeutic approach in DMD. Successful dystrophin restoration has been reported using animal models of DMD both *in vitro* (Dunckley *et al.*, 1998; Graham *et al.*, 2004; Iversen *et al.*, 2009) and *in vivo* (Goyenvalle *et al.*, 2015; Vaillend *et al.*, 2010), in cultured cells from DMD (Aartsma-Rus *et al.*, 2004; van Deutekom *et al.*, 2001) and in muscles of DMD patient (Koo & Wood, 2013; Scaglioni *et al.*, 2021; van Deutekom *et al.*, 2007).

Currently, the use of AOs in DMD is mainly focused on rescuing dystrophin expression in skeletal muscles and cardiac muscles to delay the progressive muscle degeneration that ultimately leads to premature death. Research investigating the rescue of dystrophin in the brain has been impeded by the difficulty in successfully delivering potential therapeutic agents across the BBB to the CNS. Nevertheless, some pioneer work has been done in *mdx* mice to demonstrate the potential use of AOs in restoring brain dystrophin. Using intrahippocampal injection of a recombinant adeno-associated viral vector expressing AOs, Vaillend *et al.* (2010) was able to redirect splicing of the dystrophin pre-mRNA and induced skipping of the mutated exon 23 which contains a stop codon in *mdx* mice, thus rescuing expression of brain dystrophin (15-25%) in these mice for months. The authors reported a complete recovery of $GABA_AR$ clustering in *mdx* hippocampus, indicating that the synaptic molecular alteration associated with dystrophin loss is reversible. In addition to local administration of AOs, a study also showed a systemic delivery of AOs through intravenous administration, was able to rescue dystrophin in all tissues affected by the lack of dystrophin (including skeletal muscles, heart and the CNS) with improved cardio-respiratory function and a correction in behavioural features in *mdx* mice (Goyenvalle *et al.*, 2015). Taken together, exon skipping-mediated dystrophin recovery is a promising therapeutic strategy in restoring dystrophin expression and function.

Although exon skipping provides promising results in the *mdx* hippocampus, no study to-date has addressed the efficacy of dystrophin rescue by AOs in the *mdx* cerebellar Purkinje cells, which are large GABAergic neurons that serve as the sole output from the cerebellar cortex. Findings from earlier studies and Chapter 3 of this thesis have shown that the normal GABAergic function of Purkinje cells are also severely impacted by the absence of dystrophin (Anderson *et al.*, 2003; Knuesel *et al.*, 1999; Kueh *et al.*, 2011; Kueh *et al.*, 2008). In view of

the positive effects of exon skipping in rescuing dystrophin expression in the CNS, the aim of this study is to investigate if the dystrophin expression in cerebellar Purkinje cells can be restored by the AOs, Pip6f-PMO *in vitro* using organotypic cerebellar cultures prepared from postnatal day 8-11 (P8-P11) *mdx* and WT mice. The organotypic culture model was chosen because it is a powerful *in vitro* system that preserves in part the complex three-dimensional structures that are found in an *in vivo* environment (Humpel, 2015). This model permits easy drug testing and also allows the study of cellular and molecular activity of the treated brain *in vitro* without the impediment of the BBB. Pip6f-PMO is a phosphorodiamidate morpholino oligonucleotide conjugated to an arginine-rich cell-penetrating peptide to improve the AOs tissue penetration abilities (Betts *et al.*, 2012). In this chapter, the efficacy of Pip6f-PMO was examined, specifically on the dystrophin re-expression levels and its impact on $GABA_AR$ clustering using immunofluorescence staining. Since the mIPSCs in Purkinje cells are altered in *mdx* mice (see Chapter 3), electrophysiological recording of mIPSCs on Purkinje cells was also performed to examine whether the rescued dystrophin is sufficient for functional recovery.

4.2 Method and Materials

4.2.1 Homozygous WT and *mdx* mice

Breeders (P_0) were originally purchased from the ARC, Perth Western Australia. Wild type (WT) homozygous male mice (C57BL/10J) were obtained by mating male C57BL/10 with female C57BL/10. Dystrophin deficient *mdx* homozygous male mice were obtained by mating male C57BL/10ScSn-*Dmd*^{mdx}/Arc with female C57BL/10ScSn-*Dmd*^{mdx}/Arc mice. All mice were housed under 12-hour day/light cycles, in standardised Individually Ventilated Cages (IVC), with polysulfone solid floored base, lid and stainless steel feed hopper. Food and water were available *ad libitum*.

4.2.2 Organotypic cerebellar cell cultures

Organotypic cerebellar slice cultures were prepared from P8-P11 *mdx* and WT mice. Mice were anesthetised with isoflurane then decapitated. The cerebellum was removed under aseptic conditions. Parasagittal slices (350 µm thick) were cut using a motorised vibroslicer (Leica VT1200S, Leica Microsystems) in ice cold Dulbecco's phosphate-buffered saline (DPBS) (Cat #: D8537, Gibco). Using a sterile pasture pipette with fire-polished edges, individual slices were gently transferred and cultured on a 30-mm diameter, porous (0.4 µm), hydrophilic PTFE cell culture insert (PICM03050, Millicell, Millipore). Culture inserts were placed in a 6-well plate containing 1 ml culture medium consisting of 50% vol/vol minimum essential media-no glutamine (Cat #: 11090-081, Gibco), 25% vol/vol basal medium eagle low glucose-no glutamine (Cat #: 21010-046, Gibco), 25% vol/vol horse serum (Cat #: 26050-070, Gibco), 0.65% wt/vol glucose supplied with 0.5 mM glutamax (Cat #: 35050061, Gibco), 100 units/ml of penicillin, 100 µg/mL of streptomycin, and 0.25 µg/mL of amphotericin B (Cat #: 15240096, Gibco). Culture media were replaced every other day and maintained in a 37°C incubator with 95% O_2 and 5% CO_2. On the 8th day *in vitro* (DIV), the cultured media was replaced in the treated *mdx* group with culture medium supplemented with 1 µM of Pip6f-PMO (gift from Professor Matthew Wood and Dr Susan Hammond, Oxford, UK). This concentration was selected based on previous findings in Betts *et al.* (2012), in which the authors reported that 1 µM of Pip6f-PMO resulted in the highest (80%) exon 23 skipping activity in differentiated H2K *mdx* myotubes when concentrations of 0.125, 0.25, 0.5, and 1 µM were tested.

To prepare the Pip6f-PMO solution, stocked Pip6f-PMO was thawed in a 37^{o}C water bath sonicated for 5 minutes then diluted with culture medium. The *mdx* cultures were treated with 1 µM of Pip6f-PMO for 24 hours. Half of the media was replaced using fresh culture medium

and this concentration was maintained until the cultures were harvested on day 12. Following harvesting, electrophysiological recordings and immunohistochemistry were performed. For immunohistochemistry, the organotypic cerebellar cultures were briefly rinsed with DPBS and fixed in 4% paraformaldehyde for 45 minutes at room temperature then stored in antifreeze solution (Polyethylene glycol, PBS) at -20°C until used.

4.2.3 Antibodies and Immunohistochemistry

Double labelling immunofluorescence assays were performed. Dystrophin was detected with a monoclonal antibody raised in mouse recognising an epitope at the C-terminus of dystrophin (1:10; Cat#: NCL-DYS2, Novocastra, Newcastle Upon Tyne NE12 8EW UK). $GABA_AR$s were detected with a rabbit polyclonal anti-$GABA_AR$ α1 subunit (1:100; Cat#: 06-868, Chemicon, Temecula CA 92950 USA). Negative control rabbit IgG (Cat#: X0936, Agilent DAKO, Santa Clara CA 95051 USA) and mouse IgG1 (Cat#: X0931, Agilent DAKO, Santa Clara CA 95051 USA) are used in place of the primary antibodies with cultures of WT and *mdx* mice to evaluate nonspecific staining.

For immunohistochemistry, sections were removed from antifreeze solution and were washed briefly in DPBS followed by antigen retrieval process. The use of paraformaldehyde covalently cross-linked proteins thus masking the epitope of interest and resulting in a reduction of the available epitopes for primary antibody binding (Shi *et al.*, 2001; Shi *et al.*, 1991). To eliminate the chemical modification and to restore the binding of epitope-antibody, antigen retrieval using high heat was performed to break the formalin-induced cross-linkages thereby restoring the protein structure that resembles its native structure. For antigen retrieval, the sections were placed in a glass tube filled with 0.01M Tris-EDTA-Tween 20, pH 9.0 antigen retrieval buffer (0.01M Tris Base, 1mM EDTA, 0.05% (v/v) Tween 20) and heated in a water bath at 95 °C for

1.5 hours. After 1.5 hours incubation, the glass bottles containing samples were placed in the sink with running water to allow the sections to cool to room temperature. After cooling for 20-30 minutes, the sections were briefly rinsed with 0.1M Tris buffered saline with Tween 20 (TBST), pH 7.4. To avoid nonspecific binding of the antibodies, the sections were first blocked with serum-free protein block (Cat#: X0909, Agilent DAKO, Santa Clara CA 95051 USA) for 40 minutes at room temperature. The sections were then washed three times, 10 minutes each in TBST. The sections were then incubated overnight (16-20 hours), on a rocker, at room temperature with primary antibodies diluted in 0.1M TBS containing 1% bovine serum albumin, 0.2% TX-100. After three washes with TBST, the sections were incubated for 2 hours at room temperature with Alexa Fluor 594 conjugated goat anti-mouse IgG secondary antibody (1: 500; Invitrogen) and Alexa Fluor 488 conjugated goat anti-rabbit IgG secondary antibody (1: 500; Invitrogen). Finally, the sections were washed three times in TBST, mounted and coversliped in fluorescence mounting medium (Dako, Denmark, S302380).

4.2.4 Electrophysiology recording

The details for whole-cell patch clamp recording and analysis of mIPSCs in Purkinje cells are described in Chapter 2, section 2.4 and Chapter 3, section 3.2.2 & 3.2.3.

4.2.5 Confocal imaging and data analysis

The sections were imaged using the LSM 800 Airyscan Confocal Microscope equipped with Axio Observer 7 inverted optical microscope and ZEN 2.6 software (Carl Zeiss MicroImaging, Jena, Germany). Images were collected by dual-channel recording of simultaneous excitations at 488 and 561 nm. Typically, stacks of 6-7 images (1024 X 1024 pixels) spaced by 230 nm were recorded at a planar resolution of 99 nm/pixel. All images were captured using the optimised acquisition settings. The laser power, master gain, and digital offset for each channel

was adjusted until there were few red pixels (overexposure) and blue pixels (underexposure visible) were shown on the section when the range indicator in ZEN 2.6 was selected. For semiquantitative analysis of $GABA_AR$ α1 subunit and dystrophin clusters, digital images from confocal microscopy were processed with Image J Fiji. The punctate immunoreactivity for dystrophin was analysed along the Purkinje somatic membrane while the punctate immunoreactivity for $GABA_AR$ α1 subunit was analysed at the molecular layer where the proximal dendrites of Purkinje cells are localised (40 X 40 µm, magnification: 63X, 99 nm/pixel). A threshold segmentation algorithm was applied for automatic detection of individual clusters (minimal size, 0.03 μm^2, corresponding to three pixels). A total tissue surface area of 8000 μm^2 derived from five measurements (each with 1600 μm^2) in cerebellar brain sections per animal (n=4 per animal group) were analysed for dystrophin clusters, and the number and size of $GABA_AR$ α1 subunit clusters. Unless otherwise stated, all values are reported as mean ± SEM. Error bars were ± SEM, which estimated the data variability between different animals. Significance level was set at $p<0.05$ for student unpaired t-test, Kolmogorov-Smirnov test, and Mann-Whitney U test.

4.3 Results

4.3.1 Pip6f-PMO rescued dystrophin expression in *mdx* cerebellar Purkinje cell organotypic culture

In organotypic cerebellar sections, immunofluorescence staining using the DYS2 antibody showed strong punctate staining along the somatic membrane and in the proximal dendritic layer of the WT Purkinje cell (Figure 4.1 A). This dystrophin immunoreactivity pattern parallels that of previous reports in the cerebellum (Knuesel *et al.*, 1999). As expected, this typical presentation of dystrophin-immunoreactivity in Purkinje cells was not found in the

untreated *mdx* cultures (Figure 4.1 B). In contrast, *mdx* cultures treated with Pip6f-PMO showed positive immunoreactivity for dystrophin in the Purkinje cells (Figure 4.1 C). While DYS2 immunoreactivities were found in WT and *mdx*-Pip6f-PMO cultures, they were absent in the isotype controls of WT and *mdx* organotypic cultures. The expression of dystrophin in *mdx*-Pip6f-PMO culture is specific to the Purkinje cells only, resembling dystrophin expression pattern in WT mice. This indicates that the rescued dystrophin induced by the exon skipping process is cell specific. To estimate the extent to which dystrophin is being rescued in *mdx*-Pip6f-PMO mice, dystrophin-immunoreactivity in large perisomatic and dendritic clusters along the Purkinje cells (WT, n=4; *mdx*, n=4; *mdx*-Pip6f-PMO, n=4) were quantified. While examining a total tissue surface of 8000 μm^2 in the Purkinje cell layer, the *mdx*-Pip6f-PMO culture demonstrated a significant increase in area covered by dystrophin-immunoreactivity (52.1 ± 10.17% of WT levels, range 22.20-67.30%, p= 0.0033, Figure 4.1D) while untreated *mdx* mice revealed a complete absence of dystrophin-immunoreactivity except for the minimal background staining (< 5% of WT levels).

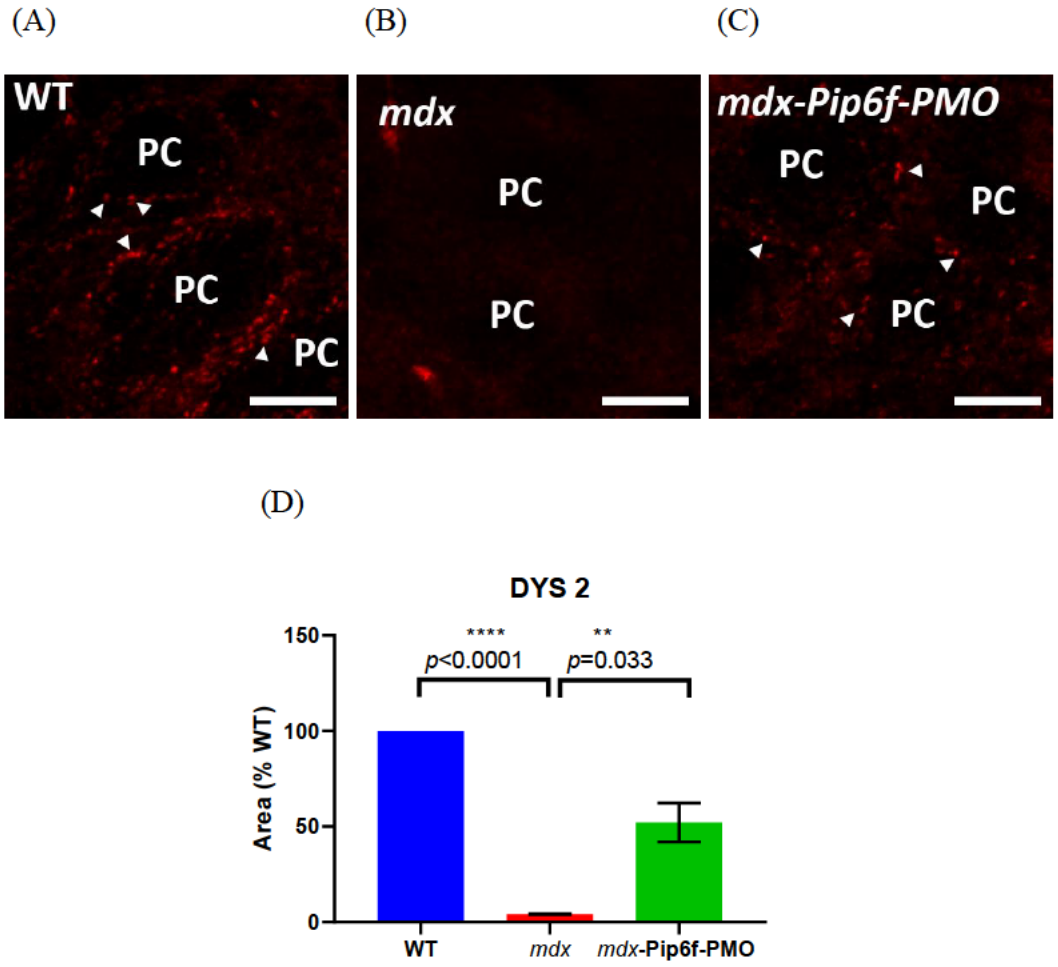

Figure 4.1 Immunoreactivity of rescued dystrophin in cerebellar Purkinje cells.

Dystrophin-immunoreactivity was visualized in sections processed for immunofluorescence staining with the monoclonal antibody Dys-2. Each panel represents projections of six-seven image stacks spaced by 230 nm. Note the clusters of dystrophin-immunoreactivity along the somatic membrane in (A) WT cultures, but were absent in the (B) *mdx* culture. A partial re-expression of dystrophin-stained puncta were seen in the (C) Pip6f-PMO treated *mdx* cultures. Scale bars, 10 µm, 63X magnification. (D) Area covered by dystrophin-immunoreactivity in Purkinje cell layer as a % of WT. The untreated *mdx* cultures were absent for dystrophin immunoreactivity (< 5% of WT level). In contrast, Pip6f-PMO treated *mdx* cultures showed significant expression of dystrophin in Purkinje cells (52.1 ± 10.17% of WT levels, range 22.20-67.30%, p= 0.0033, student unpaired t-test. All data were collected and analysed from a total tissue surface area of 8000 µm^2 derived from five measurements (each with 1600 µm^2) in cerebellar sections per animal (n=4 per group). All data are presented as mean ± SEM.

4.3.2 Co-localisation of dystrophin and GABA$_A$R α1 subunit in *mdx*-Pip6f-PMO culture

In the cerebellum, dystrophin is partially co-localised with a subset of GABA synapses around the soma and proximal dendritic layer of Purkinje cells (Knuesel *et al.*, 1999). In the organotypic cultures, the single labelling imaging revealed that the immunoreactivity of α1 subunit-containing GABA$_A$R clusters presented as distinct and intense labelled clusters around the somata and proximal dendrites of cerebellar Purkinje cells (Figure 4.2), a pattern similar to dystrophin-immunoreactivity in cerebellum. As predicted, the double immunofluorescence labelled slices showed some juxtaposition and co-localisation of dystrophin clusters with α1 subunit containing GABA$_A$R clusters (Figure 4.3).

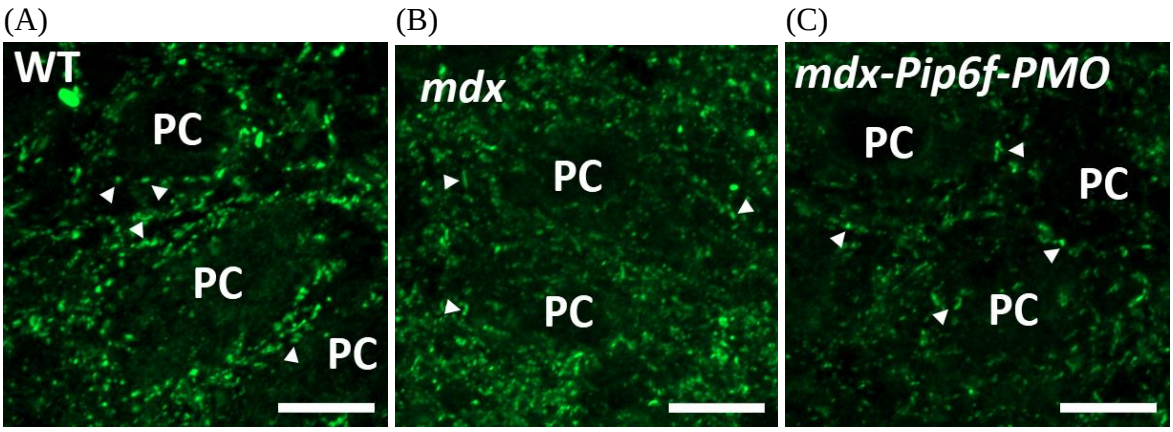

Figure 4.2 Immunoreactivity of GABA$_A$R α1 subunit in cerebellar Purkinje cells.

GABA$_A$R α1 subunit immunoreactivity was visualized in sections processed for immunofluorescence staining with the polyclonal anti-GABA$_A$R α1 subunit. Each panel represents orthogonal projections of six-seven image stacks (interval of 230 nm). Note that the clusters of GABA$_A$R α1 subunit-immunoreactivity (arrowhead) along the somatic membrane of Purkinje cells in (A) WT cultures, (B) *mdx* culture, and (C) *mdx*-Pip6f-PMO. Scale bars, 10 µm, 63X magnification.

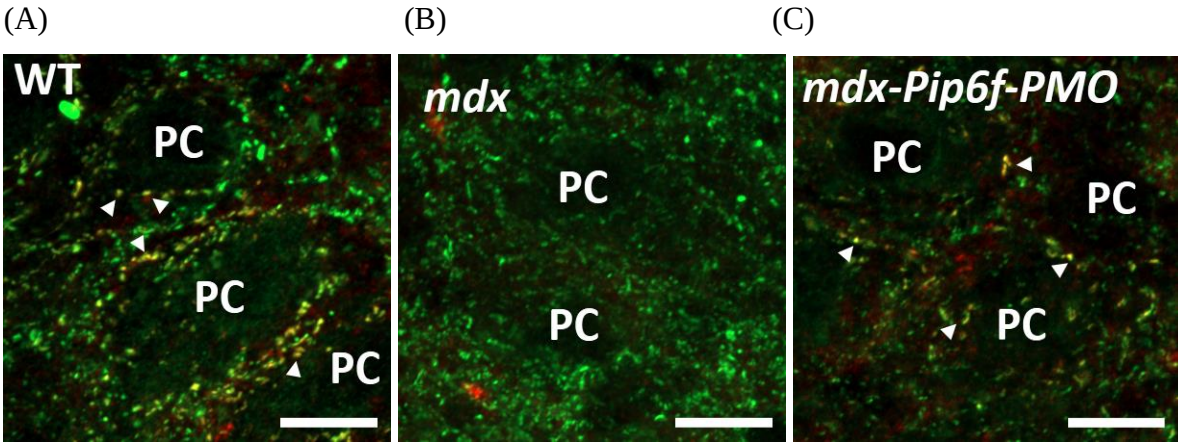

Figure 4.3 Co-localisation of dystrophin and GABA$_A$R α1 subunit immunoreactivity in cerebellar Purkinje cells.

Co-localisation of dystrophin (red) and GABA$_A$R α1 subunit immunoreactivity (green) were depicted in yellow in (A) WT culture (arrowhead). Note that the co-localisation of these two proteins were absent in (B) *mdx* cultures but were recovered in (C) *mdx*-Pip6f-PMO cultures (arrowhead). Scale bars, 10 µm, 63X magnification.

4.3.3 Pip6f-PMO treatment reverses the reduced $GABA_AR$ α1 subunit clusters size in *mdx* cultures

The co-localisation of dystrophin and $GABA_AR$ suggest that there is a functional relevance between these two proteins in a subset of inhibitory synapses. In fact, the reduction of $GABA_AR$ clustering has been reported in the cerebellum, hippocampus, and amygdala of *mdx* mice, regions where dystrophin is absent in the *mdx* mouse (Knuesel *et al.*, 1999; Sekiguchi *et al.*, 2009; Vaillend *et al.*, 2010). The number and size of α1 subunit-immunoreactive clusters in the *mdx*-Pip6f-PMO treated cultures were examined to investigate the extent to which the rescued dystrophin impacts on GABAergic function in the *mdx* culture. The number of α1 subunit-immunoreactivity clusters in *mdx* cultures was not significantly different to WT cultures (92.78 ± 6.72% of WT levels, range 74.90-106.90%, p=0.6042, Figure 4.4 A, Table 4.1). Similarly, there was no significant difference in α1 subunit cluster number when comparing the *mdx* to *mdx*-Pip6f-PMO cultures, although there was an increase in the Pip6f-PMO treated *mdx* cultures (116.60 ± 14.38% of WT levels, range 80.60-146.60%, p=0.1837, Figure 4.4 A, Table 4.1). Conversely, while the number of α1 subunit clusters was not significantly different between WT and *mdx* cultures, the clusters size of $GABA_AR$ containing α1 subunit was significantly reduced in the *mdx* cultures when compared to WT cultures (76.76 ± 3.472% of WT levels, range 69.40-84.50%, p=0.0080, Figure 4.4 B, Table 4.1). Interestingly, the reduced $GABA_AR$ α1 subunit cluster size was significantly reversed in the *mdx*-Pip6f-PMO cultures (96.25 ± 25.50% of WT levels, range 90.20-102.30%, p=0.0038, Figure 4.4 B, Table 4.1) with similar expression level to that in WT cultures (100.00 ± 4.86%, range 89.40-110.60%, p=0.5178, Figure 4.4 B, Table 4.1). Thus, these organotypic culture results showed that it is the *mdx* $GABA_AR$ α1 subunit cluster size but not the cluster number that was impacted by the absence of dystrophin and that the reduction in cluster size could be corrected by Pip6f-PMO mediated dystrophin rescue in organotypic *mdx* culture.

(A) (B)

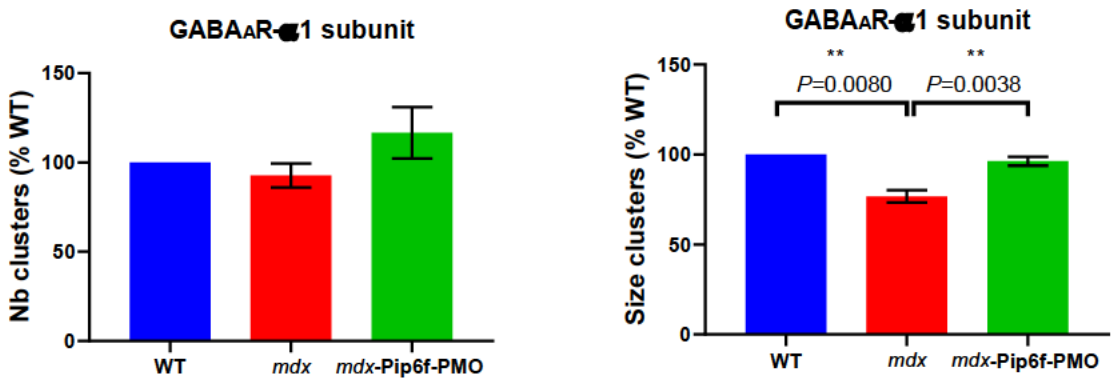

Figure 4.4 Average number and size of GABAAR α1 subunit clusters in cerebellum (molecular layer) as a % of WT.

(A) The average number of GABA$_A$R α1 subunit clusters in *mdx* cultures (n=4) (92.78 ± 6.72% of WT levels, range 74.90-106.90%, p=0.6042) was not significantly different to WT cultures (n=4). The cluster number of *mdx*-Pip6f-PMO cultures (n=4) (116.60 ± 14.38% of WT levels, range 80.60-146.60%, p=0.1837) was also not significantly different from the *mdx* cultures. (B) The average size of clusters in *mdx* cultures (76.76 ± 3.472% of WT levels, range 69.40-84.50%, p=0.0080) was significantly reduced in comparison to WT cultures. *mdx* cultures with Pip6f-PMO (96.25 ± 25.50% of WT levels, range 90.20-102.30%, p=0.0038) treatment showed a significant recovery in cluster size to the extent that it was comparable to WT control (100 ± 4.86%, range 89.40-110.60%, p=0.5178). All data were collected and analysed from a total sample area of 8000 µm^2 derived from five randomly selected areas in each cerebellar section, per animal. All data are presented as mean ± SEM. Significance level was set at p <0.05, student unpaired *t*-test.

Table 4.1 The absolute number and size of $GABA_AR$ α1 subunit clusters in Purkinje cells of WT, *mdx*, *mdx*-Pip6f-PMO organotypic cultures.

	Number of clusters			Size of clusters (μm^2)		
	WT	*mdx*	*mdx*-Pip6f-PMO	WT	*mdx*	*mdx*-Pip6f-PMO
$GABA_AR$ α1 subunit	2344 ± 266	2175 ± 157	2734 ± 337	0.22 ± 0.011	0.174 ± 0.008	0.218 ± 0.006

Data are shown as mean ± SEM.

4.3.4 Pip6f-PMO treatment reverses the reduced peak amplitude of mIPSCs in *mdx* cultures

To examine the inhibitory synaptic activity of Purkinje cell activity in the organotypic cultures, whole-cell patch clamp recording was performed on cerebellar Purkinje cells on 12-15 DIV from all organotypic culture groups. Action potential evoked IPSCs in WT, *mdx*, and *mdx*-Pip6f-PMO Purkinje cells were all inhibited by the addition of TTX (0.4µM) to the recording bath (Figure 4.5 A). The TTX-resistant mIPSCs were abolished by bicuculline (5 µM), a $GABA_AR$ antagonist, proving that they were mediated by $GABA_AR$ (Figure 4.5 B). The recording traces of mIPSCs from representative cells from all groups are shown in Figure 4.6.

These recordings together with the histogram of amplitude distribution of mIPSCs in Figure 4.7 showed that dystrophin loss in Purkinje cells led to a reduction of large amplitude mIPSCs in *mdx* cultures (n=4 cells) compared to its age matched WT cultures (n=3 cells), leading to a left skewed peak amplitude distribution trace in the *mdx* cultures ($p<0.0001$, Mann-Whitney test). Supporting this is the cumulative probability curve shown in Figure 4.8 A, in which the mean peak amplitude in *mdx* (68.13 ± 1.40 pA) was significantly reduced compared to the WT cultures (83.40 ± 1.33 pA, $p<0.0001$, Kolmogorov-Smirnov test). Remarkably, the treatment with Pip6f-PMO resulted in a significant increase of large amplitude mIPSCs in the treated *mdx* cultures, leading to a right skewed peak amplitude distribution ($p<0.0001$, Mann-Whitney test), in the *mdx*-Pip6f-PMO culture (n=3 cells) when compared to the untreated *mdx* cultures (Figure 4.7). The mean peak amplitude in *mdx*-Pip6f-PMO was also significantly increased (85.22 ± 1.30 pA, $p<0.0001$, Kolmogorov-Smirnov test, Figure 4.8 B).

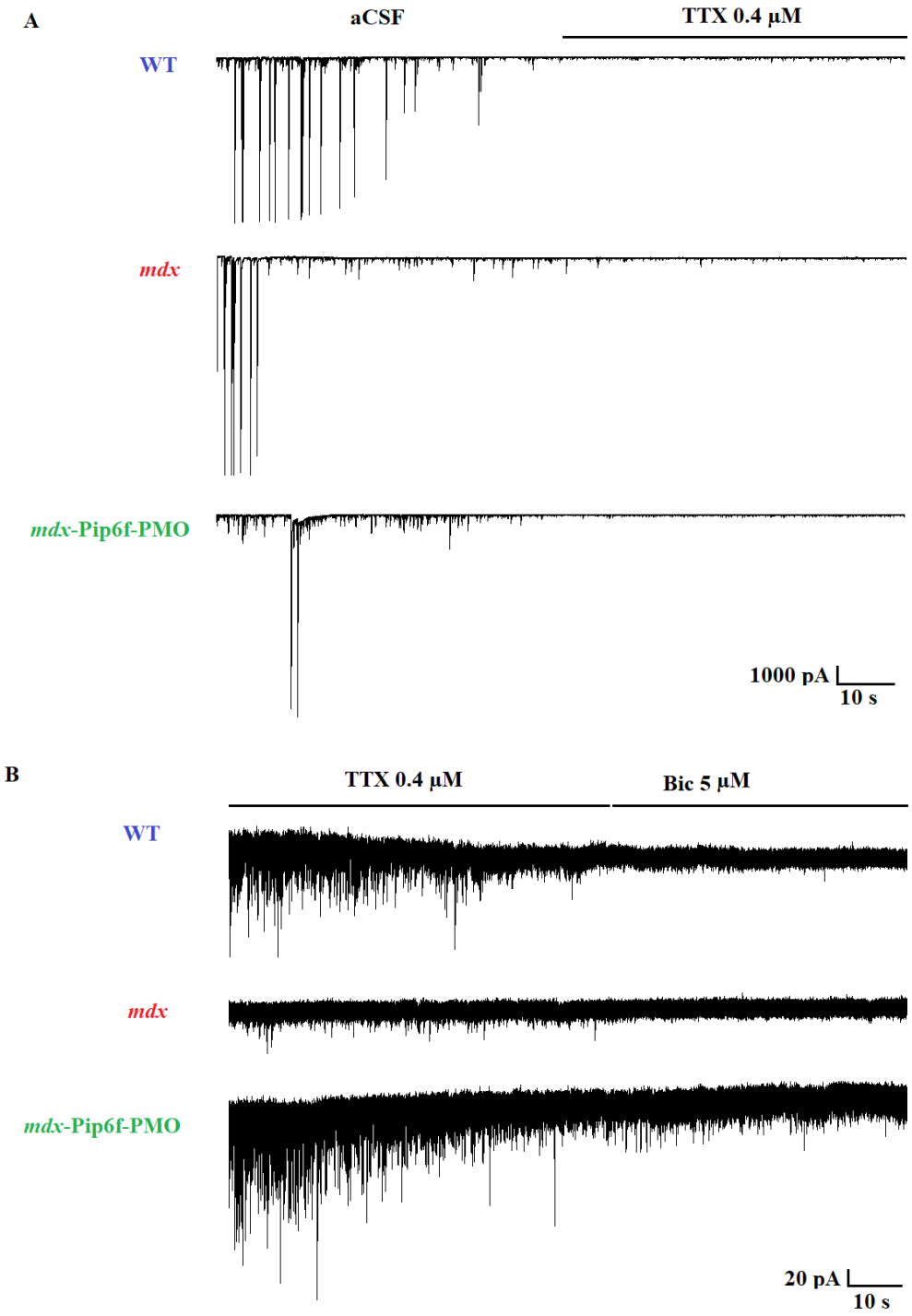

Figure 4.5 Impacts of TTX and bicuculline on miniature inhibitory postsynaptic currents in representative Purkinje cell from different organotypic cultures.

(A) Recordings showing TTX-resistant mIPSCs with reduced frequency and amplitude in the WT, *mdx*, and *mdx*-Pip6f-PMO organotypic Purkinje cell cultures. (B) Recordings showing that TTX-resistant mIPSCs were blocked by the $GABA_AR$ antagonist bicuculline (5µM).

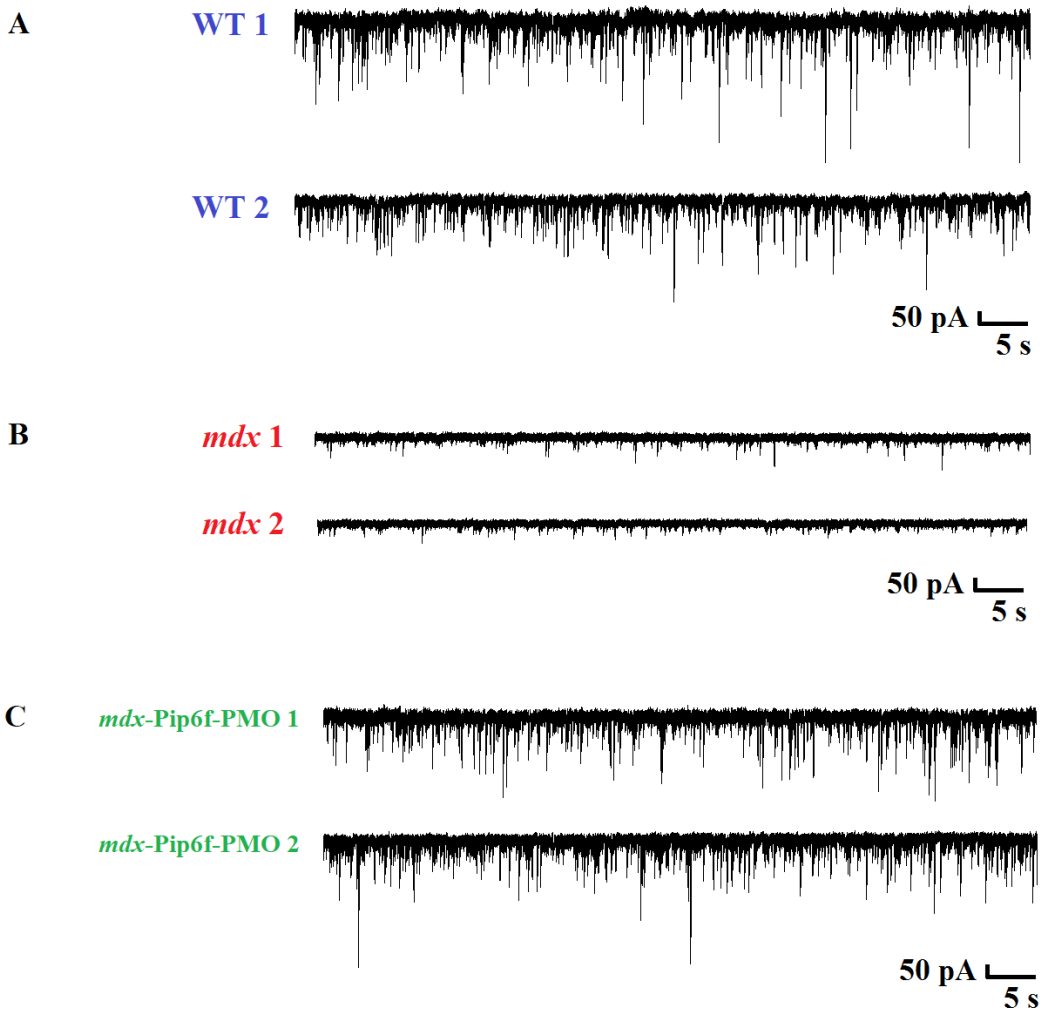

Figure 4.6 Representative miniature inhibitory postsynaptic current recordings in WT, *mdx*, and *mdx*-Pip6f-PMO organotypic cultures.

Sample traces of mIPSCs recorded from (A) WT, (B) *mdx*, (C) *mdx*-Pip6f-PMO Purkinje cells. Note that the traces in the *mdx* culture showed a reduction in mIPSCs amplitudes which is not seen in the *mdx*-Pip6f-PMO cultures.

A

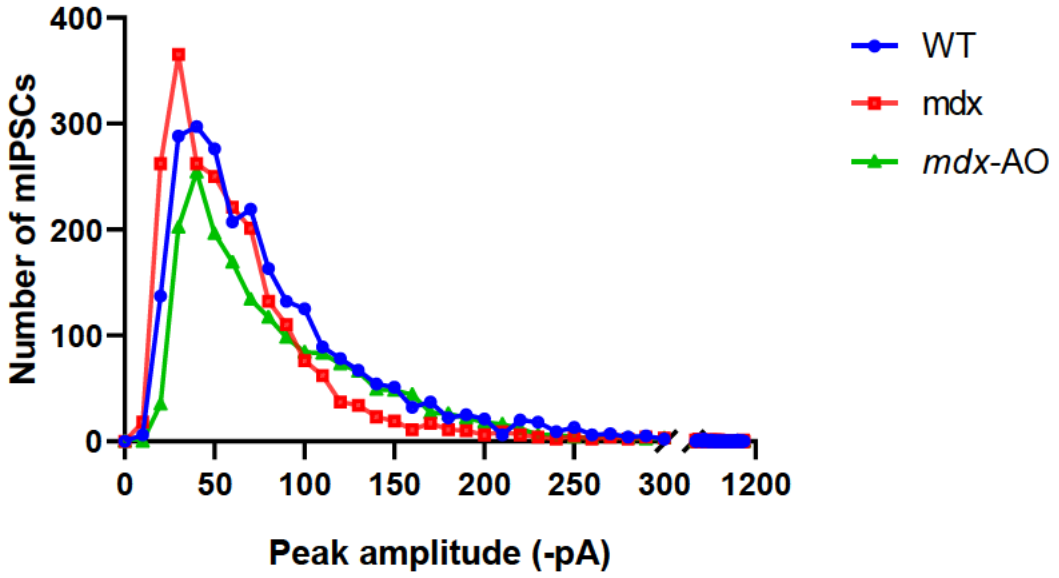
Number of mIPSCs
400
300
200
100
0
0
50
100
150
200
250
300
1200
Peak amplitude (-pA)
WT
mdx
mdx-AO

B

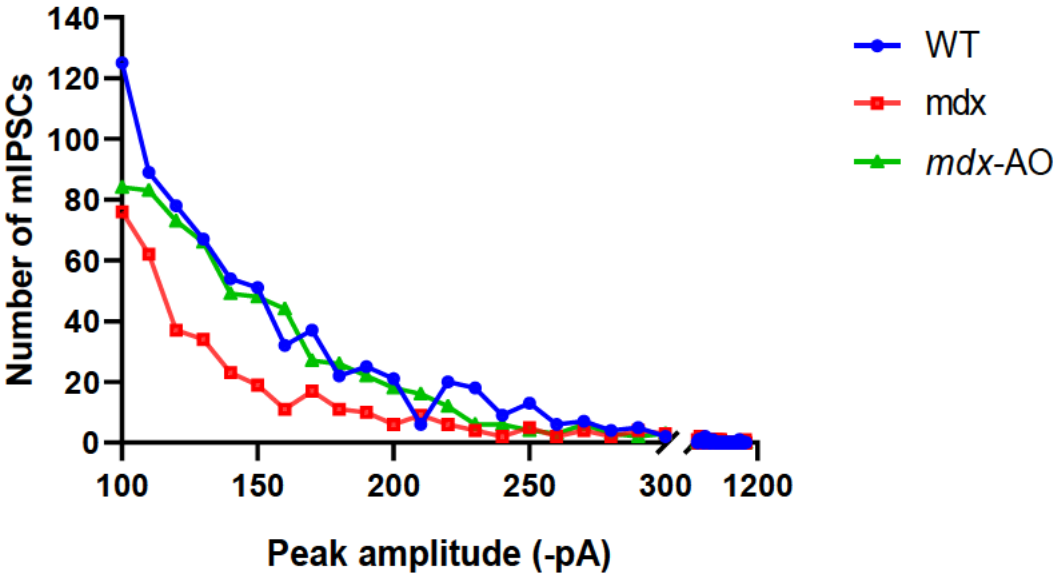
Number of mIPSCs
140
120
100
80
60
40
20
0
100
150
200
250
300
1200
Peak amplitude (-pA)
WT
mdx
mdx-AO

Figure 4.7 Distribution of mIPSCs amplitude for Purkinje cells of WT, *mdx*, and *mdx*-Pip6f-PMO cultures (12-15 DIV).

(A) Distribution of mIPSCs amplitudes were recorded in Purkinje cells of WT (*n*=3 cells), *mdx* (*n*=4 cells), and *mdx*-Pip6f-PMO (*n*=3 cells) in the presence of TTX. When comparing WT (blue trace) and *mdx* (red trace) amplitudes, the distribution of larger currents in *mdx* Purkinje cells was significantly reduced, as depicted by the left shifted histogram (median amplitude, WT: 65.55 pA, *mdx*: 52.18 pA, $p<0.0001$, Mann-Whitney U test). This shift was not seen in the *mdx*-Pip6f-PMO cultures (green trace). Following the treatment with Pip6f-PMO, the distribution of larger amplitudes was significantly increased in the *mdx*-Pip6f-PMO Purkinje cells (median amplitude: *mdx*-Pip6f-PMO: 68.84 pA) as compared to untreated *mdx* Purkinje cells ($p<0.0001$, Mann-Whitney U test). (B) Distribution of large mIPSCs amplitudes (>100 pA). The top quantile of all mIPSCs amplitudes in *mdx* and *mdx*-Pip6f-PMO Purkinje cells were 79.88 pA and 113 pA, respectively. Note that the top quantile mIPSCs amplitude in *mdx*-Pip6f-PMO Purkinje cells was closely resembled those in WT cultures which is 103.50 pA.

(A)

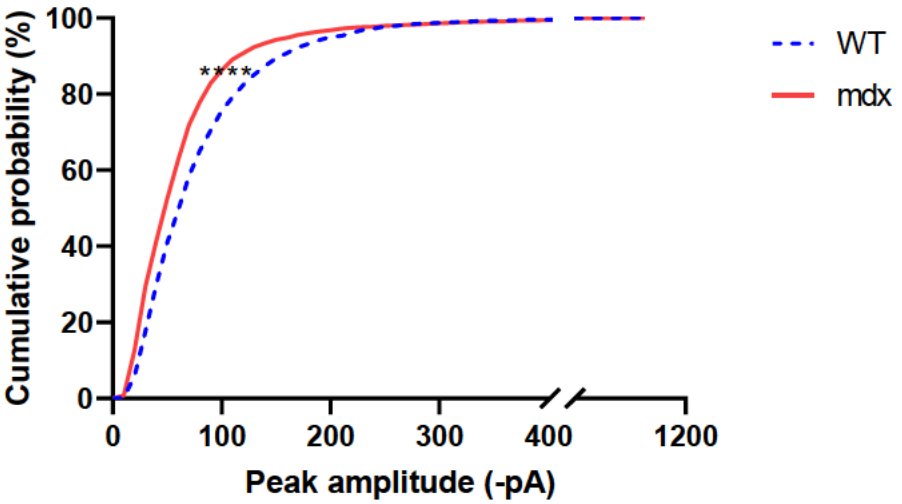

(B)

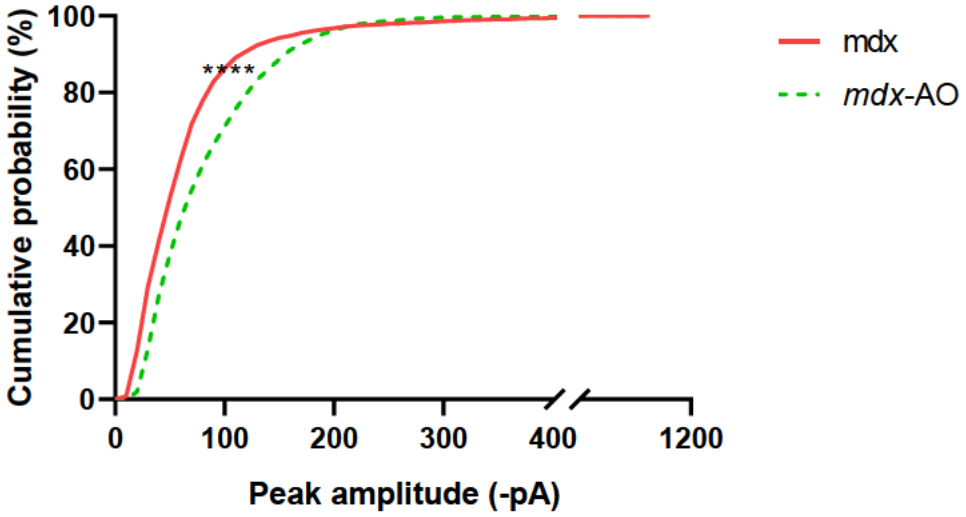

Figure 4.8 Cumulative plot of mIPSCs peak amplitude of WT, *mdx*, *mdx*-Pip6f-PMO cultures (12-15 DIV).

(A) The cumulative distributions of mIPSCs from the WT and *mdx* cultures were significantly different. The mean peak amplitude decreased from 83.40 ± 1.33 (-pA) WT to 68.13 ± 1.40 (-pA) *mdx*, $p<0.0001$, Kolmogorov-Smirnov test. (B) The cumulative distributions of mIPSCs from the *mdx* and *mdx*-Pip6f-PMO cultures were significantly different. The treatment with Pip6f-PMO resulted in an increase in the mean peak amplitude from 68.13 ± 1.40 (-pA) *mdx* to 85.22 ± 1.30 (-pA) *mdx*-Pip6f-PMO, $p<0.0001$, Kolmogorov-Smirnov test.

Furthermore, the average amplitude of mIPSCs from all groups were compared in Figure 4.9. The average amplitude of *mdx* cells was 58.80 pA (with a 95% confidence interval (CI) of 10.78; 106.8), which was not significantly different to the WT cells, 83.08 pA (with a 95% CI of 19.38; 146.4, p=0.4000, Mann-Whitney U test). When comparing *mdx* and *mdx*-Pip6f-PMO cultures, the average amplitude in the *mdx*-Pip6f-PMO cells increased to 74.01pA (with a 95% CI of -7.29; 155.3), however this increase was not significantly different to *mdx* (p=0.6286, Mann-Whitney U test). Similarly, the average frequency of mIPSCs showed no statistically significant differences between *mdx* and WT cultures nor the *mdx* and *mdx*-Pip6f-PMO (Figure 4.10). The average frequency of mIPSCs in the *mdx*, WT, and *mdx*-Pip6f-PMO cultures were 3.058 Hz (with a 95% CI of 0.88; 5.23), 4.643 Hz (with a 95% CI of 3.97; 5.32), and 3.363 Hz (with a 95% CI of -1.318; 8.044), respectively.

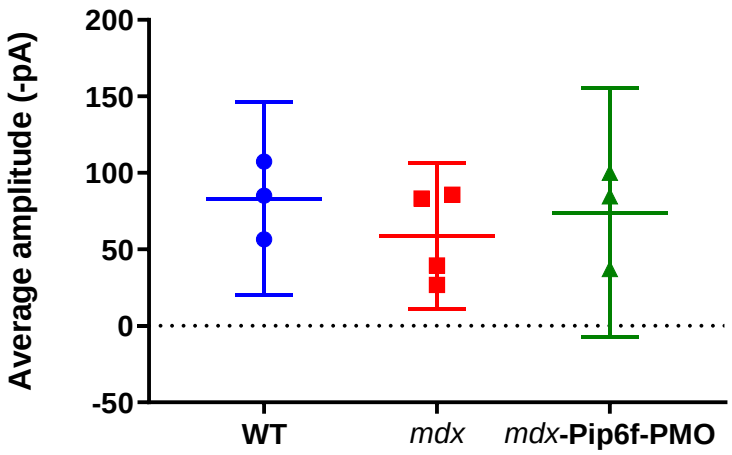

Figure 4.9 Summary data showing average amplitude of mIPSCs in WT, *mdx*, and *mdx*-Pip6f-PMO cultures.

Scatterplot showing the average amplitude and 95% CI of mIPSCs in *mdx* Purkinje cells (58.80 pA, 95% CI [10.78; 106.8]) was reduced when compared to WT (83.08 pA, 95% CI [19.38; 146.4]), but this reduction was not statistically significant (p=0.4000, Mann-Whitney U test). Similarly, no significant difference (p=0.6286, Mann-Whitney U test) was found between *mdx* and *mdx*-Pip6f-PMO groups, although the treatment of Pip6f-PMO did result in a slight increase in the average amplitude of mIPSCs in treated Purkinje cells (74.01 pA, 95% CI [-7.29; 155.3]) when compared to untreated *mdx*. Data are presented as mean with 95% CI.

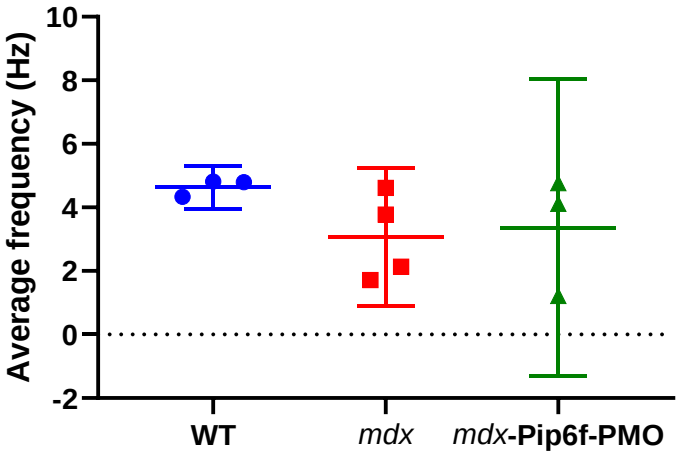

Figure 4.10 Summary data showing average frequency of mIPSCs in WT, *mdx*, and *mdx*-Pip6f-PMO cultures.

Scatterplot showing the average frequency and 95% CI of mIPSCs in *mdx* Purkinje cell (3.058 Hz, 95% CI [0.88; 5.23]) was reduced when compared to WT (4.643 Hz, 95% CI [3.97; 5.32]), but this reduction was not statistically significant (p=0.1143, Mann-Whitney U test). Similarly, no significant difference (p=0.8571, Mann-Whitney U test) was found between *mdx* and *mdx*-Pip6f-PMO groups, as the treatment of Pip6f-PMO only resulted in a very small increase in the average frequency of mIPSCs in treated Purkinje cells (3.363 Hz, 95% CI [-1.318; 8.044]) when compared to untreated *mdx*. Data are presented as mean with 95% CI.

4.4 Discussion

Exon skipping has recently emerged as a promising therapeutic approach to rescue the expression of dystrophin in animal models of DMD, leading to improved motor and cognitive functions (Dallerac *et al.*, 2011; Komaki *et al.*, 2020). Skipping of the mutated exon to restore the reading frame in dystrophin pre-mRNA and generating a truncated but semi-functional dystrophin can be achieved through the successful delivery of AOs into the target tissues (Aartsma-Rus *et al.*, 2009). While systemic delivery of AOs to restore dystrophin in muscle tissue has been proven to be possible, investigation into dystrophin rescue in regions of the brain has received less attention for a number of reasons, including the relative increased importance of rescuing muscle function to increase the life span of those with DMD, and the technical limitations associated with AOs crossing the BBB (Perronnet & Vaillend, 2010). To avoid the hurdles created by the BBB, the organotypic culture of cerebellar slices developed from P8-P11 *mdx* mice was used in the current study. This tissue-based system is a good model because it provides a complex multi-cellular *in vitro* environment and allows quick drug testing and subsequent investigation into the function of target cells in response to drug treatment (Sundstrom *et al.*, 2005). In this chapter, I showed that the efficacy of Pip6f-PMO, which is one of the potential AOs used for DMD treatments, can be successfully examined in the organotypic cerebellar cultures of *mdx* mice.

The results showed that the loss of dystrophin in *mdx* Purkinje cell cultures was rescued by the application of 1 µM of Pip6f-PMO, evident by the presence of DYS2- immunoreactivity in the *mdx*-Pip6f-PMO cultures. This result showed that the loss of dystrophin in cerebellar Purkinje cells can be reversed by AOs-mediated exon skipping. While Pip6f-PMO has been shown to restore dystrophin in cardiac as well as in skeletal muscles (Betts *et al.*, 2012), the current finding provides further proof of concept for using Pip6f-PMO to restore dystrophin in brain

tissue, specifically in the cerebellar Purkinje cells. It has been reported in several animal studies that dystrophin deficiency is associated with significant ultrastructural modifications of GABAergic synapses. A reduction of $GABA_AR$ clustering was reported in the brain regions of *mdx* mice that lack dystrophin such as in the hippocampus, cerebellum, and amygdala (Knuesel *et al.*, 1999; Sekiguchi *et al.*, 2009; Vaillend *et al.*, 2010). In line with the findings of previous studies, the reduction of $GABA_AR$ cluster size in *mdx* Purkinje cells was also observed in the organotypic cultures, confirming that dystrophin is essential for the maintenance and stabilisation of postsynaptic of $GABA_AR$ clusters. This ultrastructural modification was corrected in the *mdx*-Pip6f-PMO cultures, suggesting that partial expression of rescued dystrophin is sufficient to normalise the size of $GABA_AR$ clustering at GABAergic synapses of Purkinje cells.

The restoration of abnormal $GABA_AR$ clustering associated with dystrophin loss using AOs was also reported in earlier studies. Vaillend and colleagues reported a 15-25% restoration of the dystrophin-like protein in 8 week old *mdx* mice after intra-hippocampus injection of the adenovirus-associated vector expressing antisense sequences linked to a modified u7 small nuclear RNA (rAAV2/1-U7 system) was sufficient to completely restore both the number and size of $GABA_AR$ clusters to a level comparable to WT control (Vaillend *et al.*, 2010). While Vaillend's study shows both the number and size of $GABA_AR$ clusters were restored by rAAV2/1-U7 system, the current results show only the size but not the number of $GABA_AR$ clusters was significantly increased in *mdx*-Pip6f-PMO culture in comparison to *mdx* culture. The difference in these findings may be due to the use of different experiment models, animal age, and type of AOs used between the two studies.

The unaltered number of $GABA_AR$ clusters after Pip6f-PMO treatment in the current study was not unanticipated as there was no difference in the number of $GABA_AR$ clusters between the *mdx* and WT organotypic cultures from the beginning. The similar number of $GABA_AR$ clusters between young *mdx* and WT cultures indicates that dystrophin may not be essential for $GABA_AR$ synaptogenesis (Fritschy *et al.*, 2003). Indeed, the current finding is in line with the previous findings of Levi *et al.* (2002). The authors showed that neither dystroglycan nor dystrophin were involved in the initial clustering (i.e. synaptogenesis) of $GABA_AR$, since the formation of GABAergic synapses and clustering of $GABA_AR$ were not altered in embryonic hippocampal cultures lacking these two proteins when compared to its control culture. Moreover, a recent study by Briatore *et al.* (2020) which used a similar sensitivity confocal imaging setting of 0.008 μm^2/pixel (the current setting used in this study was 0.010 μm^2/pixel), also reported a similar density of $GABA_AR$ clusters in the molecular layer of adult (aged 3 months) *mdx* and WT control. Taken together, the results using the organotypic model used here indicate, and confirm, that dystrophin has a strong involvement in the maintenance and stabilisation of the postsynaptic $GABA_AR$ clusters.

Despite the inconsistent findings on the impacts of dystrophin deficits on the number and size of $GABA_AR$ clustering in this study, it is important to note that dystrophin is necessary for normal GABAergic function in cerebellar Purkinje cells and amygdala neurons (Anderson *et al.*, 2003; Kueh *et al.*, 2008; Sekiguchi *et al.*, 2009). In the dystrophin deficit *mdx* mice, significant reductions in both the frequency and amplitude of GABA-mediated mIPSCs were reported in cerebellar Purkinje cells while in the basolateral amygdala nucleus the frequency of norepinephrine-induced GABAergic inhibitory synaptic currents was significantly reduced. It is also important to note that dystrophin deficiency had resulted in the enhancement of fear-motivated defensive behaviours in *mdx* mice and that these abnormal behaviours were

successfully ameliorated by exon skipping via microinjection of AOs (Sekiguchi *et al.*, 2009). Using the same AOs administration technique, Dallerac *et al.* (2011) also showed a complete reversal of the abnormal enhancement of hippocampal LTP in *mdx* mice with the rescued dystrophin.

In the current study, to assess if the recovery of $GABA_AR$ clustering is also followed by a functional recovery following the Pip6f-PO treatment in cerebellar Purkinje cells, both the frequency and amplitude of mIPSCs were measured in all organotypic cultures. The findings showed that the peak amplitude of mIPSCs was significantly reduced in *mdx* cultures (*n*=4 cells) when compared to its WT control (*n*=3 cells). This present finding also supports the earlier findings in Chapter 3 as well as in Anderson *et al.* (2003), in which dystrophin loss is linked to a reduced mIPSCs peak amplitude in the *mdx* mice. Following the Pip6f-PMO treatment, the reduction in peak amplitude of mIPSCs in *mdx* Purkinje cells was significantly rescued in the treated cultures, indicating that the rescued dystrophin by Pip6f-PMO also resulted in a functional recovery of GABAergic transmission.

When measuring both the average amplitude and frequency of mIPSCs in Purkinje cells, no significant differences were found across the WT, *mdx,* and *mdx*-Pip6f-PMO cultures. Nevertheless, it should be noted that the average amplitude in *mdx* cultures increased by 25.86% from 58.80 pA (with a 95% CI of 10.78; 106.8) to 74.01pA (with a 95% CI of -7.29; 155.3) following the treatment of Pip6f-PMO. This increase in average amplitude of *mdx*-Pip6f-PMO Purkinje cells reached similar levels to the WT (88.32% of the WT level) (83.08 pA, with a 95% CI of 19.38; 146.4) while the untreated *mdx* is only 70.84% of WT level. The possible reason for the failure to observe any significant difference in the average frequency and amplitude of mIPSCs across the groups may be due to the small *n* number of slices

available in the current study. This was because only a limited number (5-6 slices) of cerebellar slices from each *mdx* mouse was obtained and survived throughout the culturing process, therefore priority was given to the immunofluorescence staining experiment to confirm the re-expression of dystrophin in *mdx* cultures following Pip6f-PMO treatment. Nevertheless, this result with limited cell numbers showed promising improvement with the treatment of Pip6f-PMO not only correcting the ultrastructural modification caused by dystrophin deficit at the GABAergic synapses but more importantly ameliorated the functional deficits associated with this ultrastructural change. Further experiments are required with larger cell numbers to provide greater insight into the advantages of Pip6f-PMO treatment in rescuing dystrophin.

4.5 Conclusion

Overall, the findings in this chapter demonstrated that treatment with Pip6f-PMO successfully rescued dystrophin expression in the *mdx*-Pip6f-PMO cultures, supporting the potential therapeutic use of AOs in restoring brain dystrophin. The recovery of this truncated protein was found on the Purkinje cell soma and proximal dendrites. The co-localisation of this partially rescued protein with $GABA_AR$ α1 subunit normalised the reduced size of $GABA_AR$ clusters linked to dystrophin loss, supporting the notion that dystrophin has an important role in stabilising the $GABA_AR$ clustering at synapses. Furthermore, current preliminary electrophysiological results suggests that the altered GABAergic synaptic function may be reversed following Pip6f-PMO treatment. While several exon skipping strategies using AOs in muscle dystrophin restoration have proceeded to clinical trials, with Eteplirsen and Golodirsen being recently approved by the US Food and Drug Administration for DMD treatment, little progress has been made to date in rescuing the brain dystrophin (Aartsma-Rus & Corey, 2020; Aartsma-Rus & Krieg, 2017; Komaki *et al.*, 2020). Thus, the positive findings in this chapter are encouraging as it provides further proof of concept that AOs may be used as a therapeutic

approach to rescue dystrophin and potentially ameliorate any dystrophin-dependent cognitive impairment.

Chapter 5. Imaging calcium in brain and muscle: Optimisation of different methods of loading cells with calcium indicators dye

5.1 Introduction

Duchenne muscular dystrophy is a severe muscle-wasting disease caused by the absence of muscle dystrophin. In muscle, dystrophin plays an important role in stabilizing the cell membrane during contraction. Its absence has been implicated in calcium dyshomeostasis in dystrophic muscle, a common manifestation in DMD pathology. Indeed, many studies have shown that the absence of cytoskeletal dystrophin is often accompanied by elevated $[Ca^{2+}]_i$. Several groups have reported an elevation in resting $[Ca^{2+}]_i$ in cultures of dystrophic human and *mdx* mouse muscle fibres (Fong *et al.*, 1990; Head, 1993; Mongini *et al.*, 1988; Turner *et al.*, 1988; Williams *et al.*, 1990).

This rise in $[Ca^{2+}]_i$ is an important triggering event in dystrophic muscle pathogenesis (Whitehead *et al.*, 2006). It is widely accepted that dystrophin deficiency increases the fragility of the sarcolemma (Petrof *et al.*, 1993) or disrupts the normal ion channel function (Alderton & Steinhardt, 2000; Vandebrouck *et al.*, 2007), which eventually causes an increased calcium influx and accumulation in the dystrophic muscle fibre. This in turn leads to an activation of Ca^{2+}-activated protease, such as calpain, which results in the branched fibre phenotype and subsequently myonecrosis (Head, 2010; Tidball & Spencer, 2000).

The contribution of increased $[Ca^{2+}]_i$ in the dystrophic muscle pathology has led to question if the dystrophic neurons shared a similar pathogenesis. Particularly, I was interested in the $[Ca^{2+}]_i$ in *mdx* cerebellar Purkinje cells.

This study focused on mice older than 12 months old as older *mdx* mice have been shown to display dystrophic phenotype that more closely resembles that of human DMD. In muscle pathology, young *mdx* mice (<3 months old) showed slow muscle disease progression due to the regeneration processes (Gillis, 1999). However, muscle fibres in aged *mdx* mice were more susceptible to membrane injury from lengthening contraction when compared to age-matched LC (Brooks, 1998; Head *et al.*, 1992; Moens *et al.*, 1993; Petrof *et al.*, 1993). Furthermore, the behavioural alteration and biochemical abnormalities in the brain are more evident in *mdx* mice that are older than 6 months old (Rae, Griffin, *et al.*, 2002).

To measure the level of cytosolic free calcium in dystrophic cells, the calcium indicator dye, Fura-2 was used. Fura-2 is a ratiometric (dual-wavelength) fluorescent indicator that is widely used for monitoring the dynamic changes in $[Ca^{2+}]_i$ in living cells (Roe *et al.*, 1990). A change in $[Ca^{2+}]_i$ will result in an alteration of 340/380 nm ratio. When cytosolic free calcium binds to Fura-2, the optimum excitation wavelength changes from 380 to 340 nm. Therefore, the ratio of fluorescence signal obtained from 340/380 nm excitation pairs is a good measure of $[Ca^{2+}]_i$ (Tsien, 1989). The key advantages of using a ratiometric dye over single wavelength indicators is that the ratio signal is unperturbed by variable dye concentration, cell thickness, optical path length, and illumination intensity allowing accurate $[Ca^{2+}]_i$ to be determined without the disturbance of these parameters (Grynkiewicz *et al.*, 1985).

This chapter presents the results of different ways calcium-sensitive fluorescence dye are introduced into Purkinje cells in acute cerebellar slice and dissociated flexor digitorum brevis (FDB) fibres. The efficacy of Fura-2 in the form of a pentapotassium salt (Fura-2 free acid) was compared with the acetoxymethyl (AM) ester form of Fura-2. Fura-2 free acid is a cell-impermeant probe that can be introduced into the cells via ionophoresis due to its negatively

charged carboxylate groups while Fura-2 AM is membrane permeant, allowing it to passively diffuse across the cell membrane. Fura-2 AM enables a less invasive method for loading. Once Fura-2 AM is inside the cells, the ester bonds of AM groups are cleaved by nonspecific cytosolic esterases leaving the highly charged Fura-2 molecule trapped inside the cytosol (Roe *et al.*, 1990; Tsien, 1981, 1989).

5.2 Method and materials

5.2.1 Animals, muscle, and brain slice preparations

All experiments were carried out with approval from Western Sydney University Animal Care and Ethics Committee, in accordance with the Australian code for the care and use of animals for scientific purposes and the New South Wales Animal Research Act. Littermate control and *mdx* mice (average age ~12 months for Purkinje neurons and ~21 months for FDB muscle fibres) were anesthetized with isoflurane and killed by decapitation. Cerebellum and FDB muscle were collected.

5.2.1.1 Cerebellar brain slice preparation

The details for cerebellar brain slice preparation are described in Chapter 2, section 2.3. Briefly, the cerebellum was rapidly removed and cut into 250µm thin slices using a vibroslicer (Leica VT1200S, Leica Microsystems) and immediately transferred into a holding chamber containing HEPES buffered aCSF, continuously bubbled with carbogen (95% O_2 and 5% CO_2) until used for experiment.

5.2.1.2 Muscle dissection

FDB muscles were dissected from the hind limbs. The muscle was placed in a bath containing Krebs solution (with the following composition (in mM): 4.75 KCl, 118 NaCl, 1.18 KH_2PO_4,

1.18 $MgSO_4$, 24.8 $NaHCO_3$, 2.5$CaCl_2$, and 10 glucose) with 0.1% fetal calf serum, and continuously bubbled with 95% O_2 and 5% CO_2 to maintain the pH at 7.4.

5.2.1.3 Single muscle fibre digestion

Muscles were digested in Krebs solution (without fetal calf serum) containing 3mg/ml collagenase type IV (Sigma Aldrich, MO, USA) with gentle aeration using carbogen at 37°C for 25 minutes. Following digestion, the muscle was washed twice with normal Krebs solution containing fetal calf serum to stop the digestion, and then gently agitated using a pipette to release individual fibres from the muscle mass.

5.2.2 Loading cells with Fura-2 free acid

The details of loading Fura-2 free acid in cerebellar slices and FBD fibres are described in Chapter 2, section 2.5.2. Briefly, 1 mM of Fura-2 was introduced into the cell via ionophoresis with a sharp electrode. Negative current was applied to repel the negatively charged dyes from the recording electrode. The cell was rested for at least 10 minutes before any recording was started to allow for the complete distribution of the dye in the cytoplasm.

5.2.3 Loading cells with Fura-2 AM

The details of loading Fura-2 AM in cerebellar slices are described in Chapter 2, section 2.5.1. The loading of Fura-2 AM in muscle fibres was similar to that in brain slices except Krebs solution (aerated with carbogen to maintain pH at 7.4) and a glass test tube was used in place of aCSF and a 6-well plate in the procedure. Prior to imaging, individual fibres were released from Fura-2 AM loaded FDB muscle mass using gentle agitation.

5.2.4 Stimulation protocols

5.2.4.1 Purkinje cells

The preparation of the stimulating electrode is described in Chapter 2, section 2.4.3. For Purkinje cell stimulation, a theta electrode was placed 100-200 µm away from the cell body in the molecular layer (where the PF were located), and stimuli with voltages in the range of 1-100 volts at 1 ms and at 30 Hz were delivered.

5.2.4.2 FDB fibres

Using a pipette, 0.5 ml (10-50 fibres) of enzymatically liberated single FDB fibres was transferred and placed on a cleaned glass coverslip located on the recording chamber of the upright microscope. These fibres were attached firmly on the glass coverslip and were continually superfused with Krebs bubbled with carbogen at a rate of around 0.5 ml per minute. For FDB stimulation, voltages above the threshold was delivered to the fibre using a bipolar stimulating electrode placed close to the neuromuscular junction, which can be easily visualised as a corrugated oval on the fibre under a light microscope, at 1 ms and at different frequencies (2, 5, 10, 15, 20, 25, and 30 Hz).

5.2.5 Calcium imaging and fluorescent measurement

The details for calcium imaging and fluorescent measurement are described in Chapter 2, section 2.5.4. Briefly, Purkinje cells were excited at 340 and 380 nm and changes in fluorescence were measured using Image J Fiji. Fura-2 is a dual-excitation ratiometric Ca^{2+} indicator. It changes its peak excitation wavelength from 380 nm to 340 nm upon binding to Ca^{2+}. An elevation in Ca^{2+} concentration is reflected by an increase in Fura-2 emission when the indicator is excited at 340 nm, with a corresponding decrease in emission at 380 nm. The 340/380 ratio is therefore a good reference for monitoring the $[Ca^{2+}]_i$ level when the dye was

excited in quick succession at 340 and 380 nm (Bootman *et al.*, 2013; Tsien, 1989; Tsien *et al.*, 1985). Fura-2 fluorescence was recorded at an interval of 50 ms (or 20 frames per second) for a desired length of time (20-60 seconds).

5.3 Results

5.3.1 Loading Purkinje cells with membrane impermeable Fura-2 using sharp electrode ionophoresis and permeable Fura-2 AM with bath incubation

To measure $[Ca^{2+}]_i$ in Purkinje cells, the Purkinje cell was filled with Fura-2 free acid using a sharp electrode (ionophoresis) and Fura-2 AM using bath loading method. Both loading methods successfully showed the big fluorescent cell soma (~20 µm in diameter) but not the dendritic trees when Purkinje cells were exposed to 340 nm and 380 nm UV light (Figure 5.1). The 340/380 ratio was lower in the cells loaded with Fura-2 when compared to cells loaded with Fura-2 AM (Figure 5.1). In addition, with the bath loading method, the granule cells (~5 µm in diameter), located in the granular layer also took up Fura 2-AM. The mean resting calcium ratio at 340/380 nm in Fura-2 loaded *mdx* Purkinje cells (0.8340 ± 0.07537, n=12 cells) was significantly higher than LC (0.6107 ± 0.02980, n=10 cells; p=0.0187) but showed no difference in Fura-2 AM loaded cells (LC 0.7437 ± 0.009768, n=57 cells, *mdx* 0.7496 ± 0.005483, n=102 cells; p=0.5692, student unpaired t-test) (Figure 5.2). Note that the ratio in Fura-2 AM loaded LC was higher than that in Fura-2 loaded LC, which was inconsistent to the 340/380 ratio image results shown in Figure 5.1. Next, I tried to record the calcium transient by stimulating the PF (where the dendritic arborisations were located) using a theta electrode placed in the molecular layer. However, I was not able to record any change in calcium with the stimulation protocol.

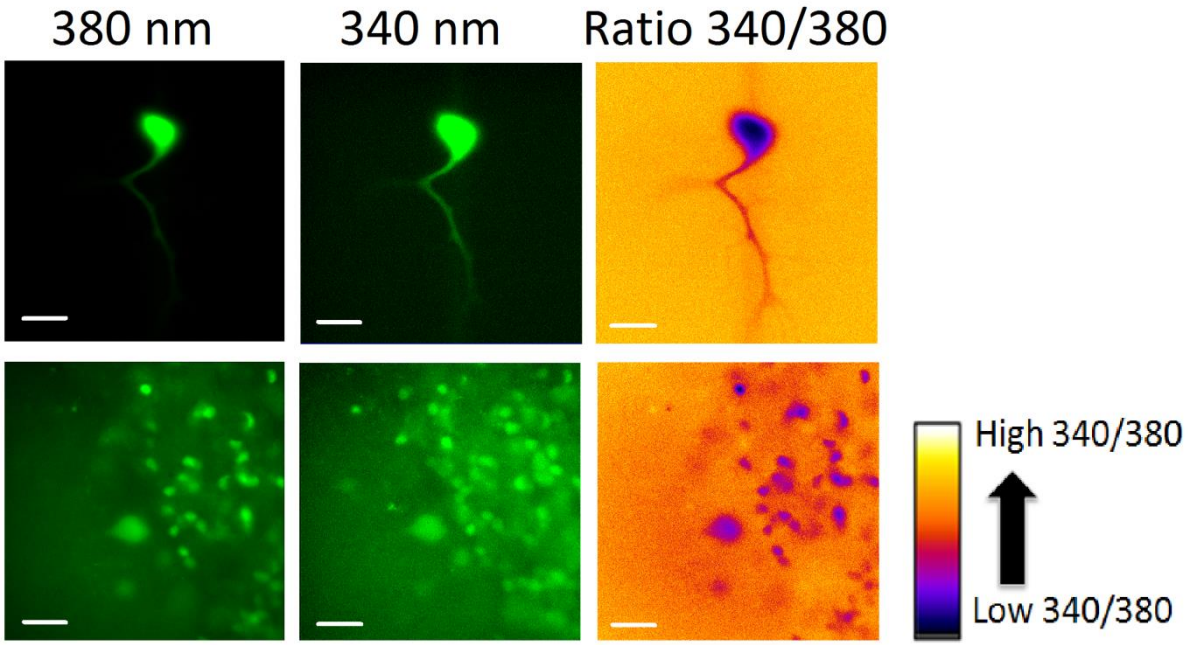

Figure 5.1 Baseline $[Ca^{2+}]_i$ in mdx Purkinje cells using Fura-2 calcium indicator.

Top: A Fura-2 free acid filled Purkinje cell using ionophoresis (-1 nA pulse-250 ms duration at 1 Hz s for 1 minute). *Bottom*: Purkinje cells and granule cells were filled with Fura-2 AM, bath loading, 1-hour incubation. Both top and bottom images were generated by exposing cells to 340 nm and 380 nm wavelength (10 ms exposure time, 50 ms interval or 20 frames per second, gain 2). All 340/380 ratio images were generated using Image J Fiji. Note that, Purkinje cell body filled with Fura-2 showed a lower ratio (340/380) than Purkinje cells that were loaded with Fura-2 AM. Each scale bar represents 20 µM at 60X magnification. Pseudocolour column shows the fluorescence change from dark to brighter colours to indicate an increase in 340/380 ratio.

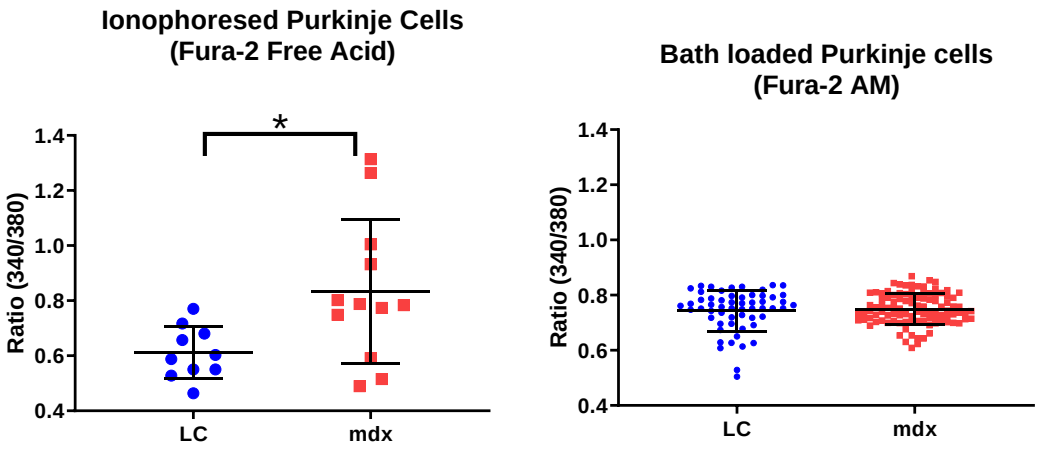

Figure 5.2 Baseline $[Ca^{2+}]_i$ ratios (340/380) of Fura-2 free acid ionophoresed and Fura-2 AM bath loaded Purkinje cells in ~12 months old *mdx* and LC mice.

Left: Purkinje cells were filled with 1 mM Fura-2 free acid via ionophoresis. Resting calcium was recorded after cells were rested for 10 minutes to allow the dye to diffuse across the dendritic arborisations. There was a significant increase in *mdx* (0.8340 ± 0.07537) resting calcium ratio (340/380) when compared to LC (0.6107 ± 0.02980, p=0.0187, student unpaired t-test). *Right*: Purkinje cells were loaded with 10 µM Fura 2-AM for an hour via the bath loading method (37°C). Resting calcium in Purkinje cell body was recorded after the cells were rested for an hour for de-esterification. There was no significant difference in 340/380 ratio between LC and *mdx* groups (LC 0.7437 ± 0.009768; *mdx* 0.7496 ± 0.005483, p=0.5692, student unpaired t-test). All data are presented as mean ± SEM.

5.3.2 Loading FDB fibres with membrane impermeable Fura-2 using sharp electrode ionophoresis and permeable Fura-2 AM with bath incubation

To further investigate if the failure to measure any changes in $[Ca^{2+}]_i$ in current recordings was a consequence of our detection system , the $[Ca^{2+}]_i$ in single dissociated FDB fibres was measured. Muscle fibres were loaded with either Fura-2 free acid or Fura-2 AM. As a single muscle fibre is significantly larger than Purkinje neurons, Fura-2 free acid was ionophoresed at stronger pulses than in Purkinje cell; -9 nA pulses-250 ms duration at 1 Hz for 2 minutes. The bath loading method used for muscle fibres was similar to that used for Purkinje cells. Similarly, the morphologies of these Fura-2 loaded muscle fibres was visualised when they were excited at 340 nm and 380 nm wavelengths (Figure 5.3). The recorded LC fibre was ~35 µm in width which is similar to the measurement made in Woods *et al.* (2004) and the presence of peripheral nuclei indicates that the fibre was in healthy condition (see white arrows in Figure 5.3). Consistent with results in Purkinje cells, the ionophoresed fibre also showed a lower 340/380 ratio compared to bath loaded fibre. Unlike LC fibre, central nuclei were seen in *mdx* mice (Figure 5.4).

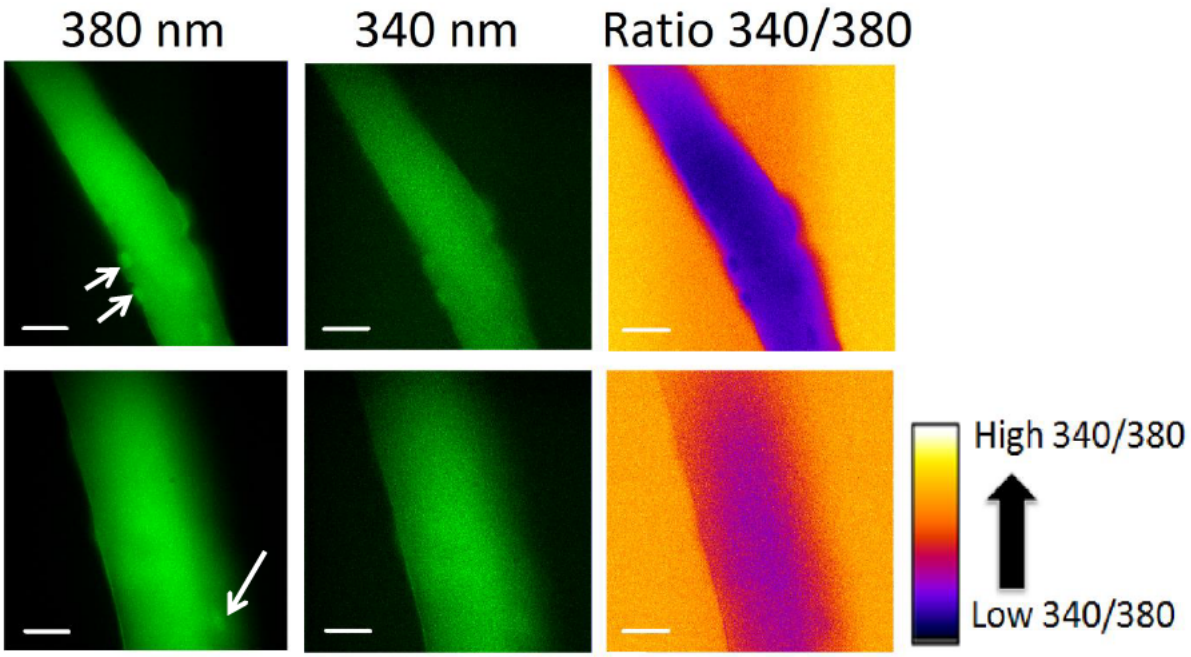

Figure 5.3 Representative Fura-2 filled FDB fibre from LC using both ionophoresis and bath loading methods.

Top: FDB fibre was filled with Fura-2 free acid by ionophoresis (-9 nA pulses-250 ms duration at 1 Hz for 2 minutes). *Bottom*: A FDB fibre was filled with Fura-2 AM using the bath loading method for 1 hr at 37°C. Images of both cells were generated by exposing cells to 340 nm and 380 nm wavelength (5 ms exposure time, 50 ms interval or 20 frames per second, gain 20). All the 340/380 ratio images were generated using Image J Fiji. Note that the ionophoresed fibre showed a lower 340/380 ratio than the fibre that was loaded with Fura-2 AM. White arrows show the peripheral nuclei. Each scale bar represents 20 µM at 60X magnification. Pseudocolour column shows the fluorescence change from dark to brighter colour in indicate an increase in 340/380 ratio.

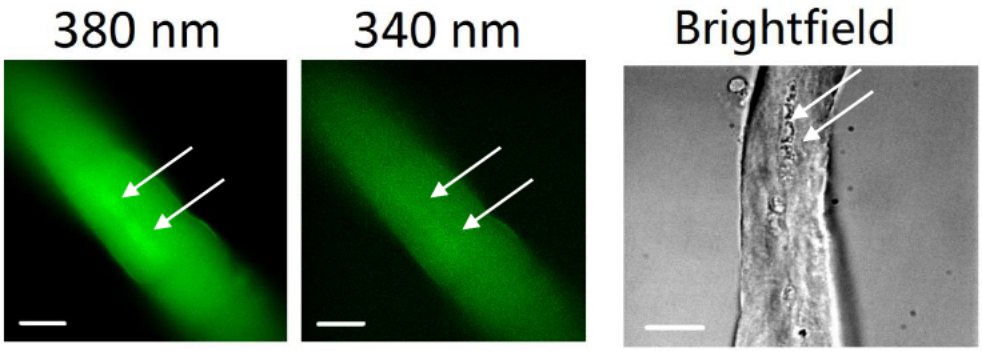

Figure 5.4 Morphologies of *mdx* FDB fibres.

Representative morphologies of *mdx* FDB fibres filled with Fura-2 using ionophoresis (-9 nA pulses-250 ms duration at 1 Hz for 2 minutes) when excited with 340 nm and 380 nm wavelength, and brightfield. The presence of central nuclei which is one of the hallmarks of *mdx* fibre pathology, is shown with white arrows when viewed at 380 nm wavelength and brightfield. Each scale bar represents 20 μm at 60X magnification.

In contrast to a Purkinje cell, changes in calcium intensity (calcium transient) were observed when the muscle fibre was stimulated using a bipolar stimulating electrode placed close to the neuromuscular junction. Once the stimulus threshold was reached, a sharp increase in fluorescence was observed immediately during the FDB fibre contraction. The increase in fluorescence was enhanced when the frequency of the stimulus was increased (Figure 5.5 A). This is also clearly depicted in the average calcium transient-frequency graphs (Figure 5.5 B). When observing the calcium transients in Fura-2 AM bath loaded fibres from *mdx* and LC, I first recorded the increasing then decreasing (after 25 Hz stimulation) trends in the change of 340/380 ratio in response to increasing stimulus frequencies (Figure 5.5 B). Note that the peak of calcium transients throughout the different stimulation frequencies tends to be slightly depressed in *mdx* fibres when compared to LC.

In addition to the individual calcium transient produced from a single stimulation at different frequency, I also recorded the repetitive calcium waves generated from continuous maximal fatiguing stimulation (Figure 5.6 A). A LC fibre was repeatedly stimulated for 0.5 seconds on and 0.5 seconds off at 30 Hz. Throughout the fatiguing protocol, $[Ca^{2+}]_i$ transient first increased then decreased (Figure 5.6 B), showing the typical pattern for intracellular calcium during fatigue in vertebrate skeletal muscle fibre (Allen *et al.*, 2008). This was also accompanied with an increase in resting $[Ca^{2+}]_i$ (Figure 5.6 C), which has generally been credited to metabolic fluctuations affecting the capability of the sarcoplasmic reticulum (SR) to reuptake $[Ca^{2+}]_i$.

A)

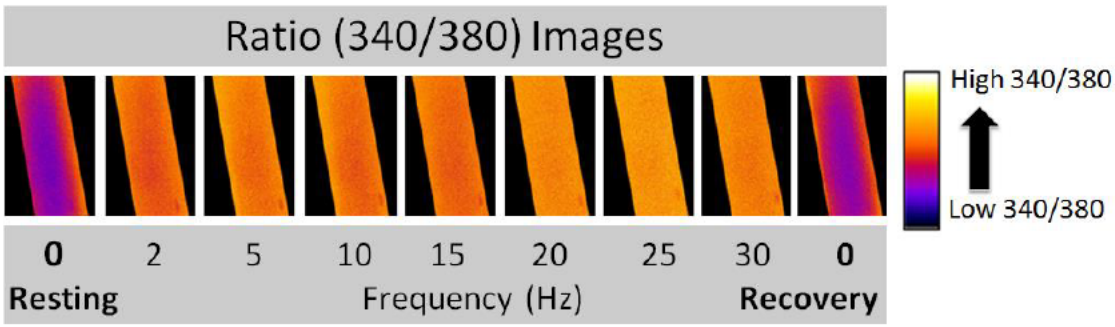

B)

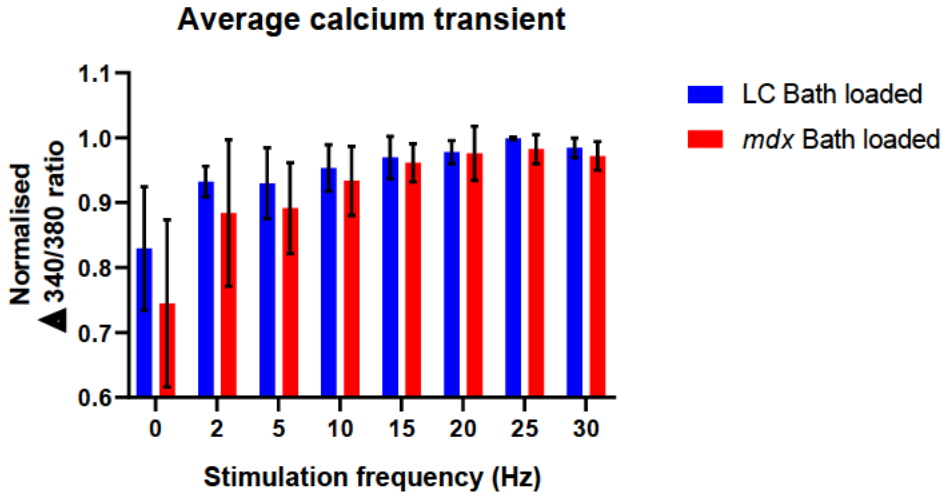

Figure 5.5 Calcium fluorescence/ frequency images of a stimulated FDB fibre (Fura-2 AM bath loaded).

(A) The change of Fura-2 fluorescence (340/380 ratio) in the central portion of this fibre was observed clearly when it was stimulated with different stimulus frequencies at 30 seconds intervals using a bipolar stimulating electrode. Pseudocolour column shows the fluorescence change from dark to brighter colour in indicate an increase in 340/380 ratio. B) Average calcium transient (Δ 340/380 Ratio) in bath loaded FDB fibres from two LC (n=3 cells) and *mdx* mice (n=3 cells). When the fibres were stimulated at different frequencies, the increase of Δ 340/380 Ratio in LC fibres overall were slightly higher than in *mdx* fibres. The maximum change in calcium transient for both genotypes was found at 25 Hz. Both calcium transients increased gradually when the stimulation frequency increased, reaching the maximum at 25 Hz and followed by a decrease at 30 Hz. All data are presented as mean ± SEM.

A)

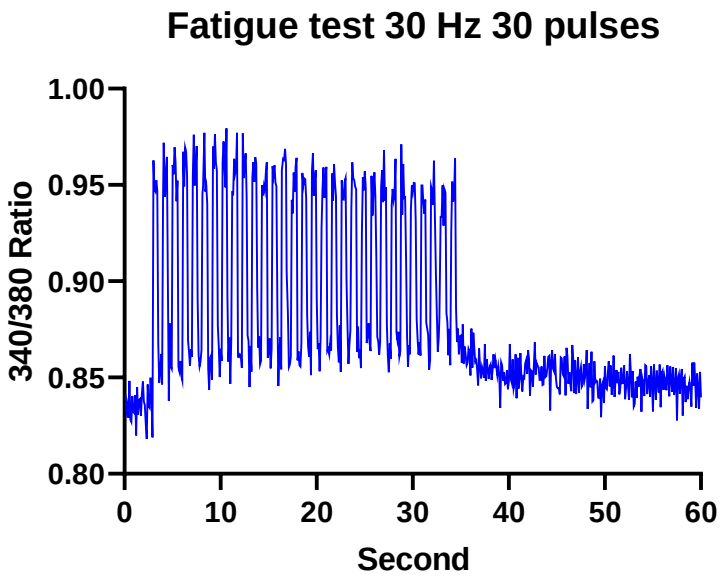

B)

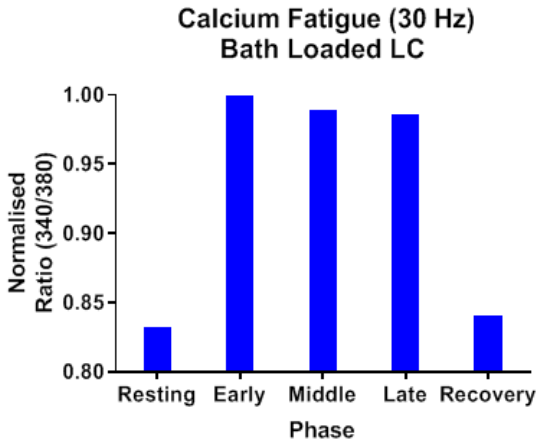

C)

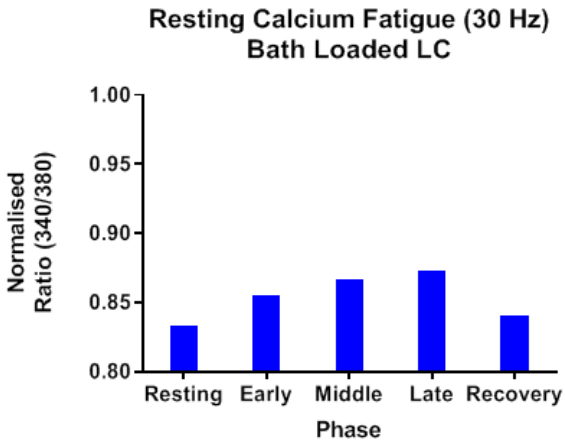

Figure 5.6 Calcium transients in a fatiguing FDB fibre.

A) Time course of calcium (340/380 ratio) in response to fatiguing stimulation in a single FDB fibre. Fibre was stimulated at 30 Hz for 0.5 seconds and then rested for another 0.5 seconds; this protocol was repeated for the duration of the stimulation. (B) The calcium wave shows a classical profile in LC fibres, with an initial increase in the height of the transient followed by a decrease. (C) There is an increase in resting Ca^{2+} ratio due to metabolic changes in the fatigued fibre.

5.4 Discussion

5.4.1 Calcium imaging in Purkinje cells

This chapter showed that Purkinje cells can be filled with a calcium indicator by means of ionophoresis (Fura-2 free acid) or bath loading (Fura-2 AM) methods. Using the same imaging setting, when comparing the fluorescence intensity from the two different loaded dyes in LC, the average 340/380 ratio in Purkinje cell body was generally higher in Fura-2 AM bath loaded cells when compared to Fura-2 free acid ionophoresed cells, implying a higher resting $[Ca^{2+}]_i$. A possible explanation for this phenomenon is the accumulation of Fura-2, not only in the cytoplasm, but also in the subcellular compartments (Malgaroli *et al.*, 1987). Unlike Fura-2 free acid which is a membrane-impermeant dye, the ester form of Fura-2 (Fura-2 AM) is a lipophilic and membrane-permeant indicator that can diffuse through both the cell membrane and the membranes of intracellular organelles during the 1-hour incubation at 37°C. This membrane-permeant property allowed Fura-2 AM to be present in both the cytosol and possibly also in intracellular compartments of Purkinje cells. Once the AM linkage of the Fura-2 AM is hydrolysed by the cytoplasmic esterases, Fura-2 is released and trapped within these compartments to bind with the free Ca^{2+} in the intracellular compartments, contributing to the measured fluorescent intensity.

The ability of Fura-2 AM to diffuse across the subcellular membrane and be compartmentalised within these organelles was demonstrated in an elegant study by Almers and Neher (1985). The authors reported a loss of 40-60% of the fluorescent signal during mast cell degranulation, suggesting ester loaded Fura-2 was present in the secretory granules and lost from the cell during exocytosis. In contrast, there was no issue when the cell was filled with membrane-

impermeant Fura-2 free acid. Instead, large changes in fluorescence signal was observed when the cell was stimulated to degranulate (Almers & Neher, 1985).

When comparing the resting 340/380 ratio between *mdx* and LC animals, only *mdx* cells that were loaded with Fura-2 free acid by ionophoresis showed a significant increase in average ratio whereas in cells loaded with Fura-2 AM (bath loading), the average 340/380 ratio at rest was similar in cells from both genotypes. The finding of a significant increase in resting $[Ca^{2+}]_i$ in *mdx* Purkinje neurons parallels the findings in a study on 6 month old *mdx* pyramidal cortical and hippocampal neurons (Lopez *et al.*, 2016). Using the double-barreled Ca^{2+}-selective microelectrodes, the authors showed that the $[Ca^{2+}]_i$ in 6-month *mdx* cortical neurons and hippocampal pyramidal neurons were significantly increased by 149% and 214%, respectively, when compared to WT. However, whether there was indeed a higher resting $[Ca^{2+}]_i$ in *mdx* compared to LC Purkinje cells remains unclear. In the current study, cell resting membrane potential was not measured when Fura-2 was introduced into the cell with a sharp electrode. Without measuring the cell membrane potential, cells that are potentially unhealthy or dying (high membrane potential) and therefore may have already had elevated $[Ca^{2+}]_i$ at the start of the experiment was not able to be excluded. Nevertheless, under the same experimental setting, higher 340/380 ratio was found in *mdx* mice compared to LC mice when loading Purkinje cells with Fura-2 free acid using a sharp electrode. This then led to an overall increase in the average resting $[Ca^{2+}]_i$ in *mdx* mice.

A common limitation found when using these two dyes loading methods was that while cells were successfully loaded, both methods failed to show any calcium changes in the cell body or local calcium transients when the PF were stimulated with a theta electrode that was positioned approximately 100-200 µm away from the cell body. The PF was stimulated for Purkinje cells

excitation because under physiological conditions, Purkinje cells receive excitatory inputs from mossy fibres. The mossy fibre activates the granule cell, whose axons give rise to the PF, which then form high synaptic contacts at the spines of the distal branch of the Purkinje dendritic tree (Cheron *et al.*, 2008). Harvey and Napper (1991) reported that one Purkinje cell has at least 150,000 PF-Purkinje cell synaptic contacts. The failure to detect calcium changes in the Purkinje cell body has also been reported in other studies (Konnerth *et al.*, 1992; Tank *et al.*, 1988). The authors reported that the change in $[Ca^{2+}]_i$ in the cell body was not detectable or the rise in $[Ca^{2+}]_i$ was very small during PF simulation. This is because the distribution of voltage-dependent Ca^{2+} channels is not prominent in the somatic membranes of cerebellar Purkinje neurons (Llinas & Sugimori, 1980a, 1980b). Furthermore, the failure to detect the local calcium transient is not surprising since the highly arborised Purkinje cell dendritic trees were not homogenously loaded with Fura-2 in both dye loading methods. This indicates that either Fura-2 free acid ionophoresis or Fura-2 AM bath loading methods did not allow Fura-2 to be homogenously distributed in Purkinje cell dendritic trees except in the cell body in the current study. Therefore, the Fura-2 loading method requires further improvement for the detection of dendritic calcium changes.

Given the limitation of the two calcium indicators, at this stage the preferred calcium indicator is the membrane impermeant Fura-2 free acid due to several reasons. Firstly, dye ionophoresis using recording electrode prevent loading large numbers of cells, thus allowing the characteristic morphology of a single Purkinje cell to be identified and analysed within a clean background. In contrast, when Fura-2 AM was used the level of background fluorescence that might arise from the indicator trapped in non-specific targets (surrounding tissues and cells) is unknown (Kirischuk & Verkhratsky, 1996). Secondly, the filling of Fura-2 free acid into a cell using the ionophoresis technique allows real time monitoring, thus allows better control than

when filling cells with Fura-2 AM using bath loading. In addition, while the bath loading of Fura-2 AM may appear to be simpler, there are many factors including the incubation time and temperature that needs to be considered when using this method. Loading of Fura-2 AM involves very strict incubation time and time for deesterification so that optimum fluorescence and accurate $[Ca^{2+}]_i$ estimation can be obtained. Also, the fluorescent signal intensity of Fura-2 AM loaded cells was lower compared to Fura-2 free acid loaded neurons which led to poorer signal-to noise ratio. This lower signal intensity in Fura-2 AM loaded cells may be due to the mature animals used. Yuste and Katz (1991) reported a striking age dependency in the capability of Fura-2 AM to load into neocortical neurons. The authors suggested that the ineffective loading of most mature neurons was due to the structure of these older cells in intact slices that prevented the access of the dye to the cell membrane.

Thirdly, Fura-2 free acid does not involve a deesterification process and therefore avoids the limitations arise associated when loading cells with Fura-2 AM. The accumulation of Fura-2 with the bath loading method relies heavily on the cleavage of the AM ester linkage by the nonspecific cytoplasmic enzyme, esterase (Bush & Jones, 1990; Williams *et al.*, 1985). The hydrolysis of the ester bond in AM may generate by-products such as formaldehyde which is toxic to cells (Bush & Jones, 1990; MacLean & Yuste, 2009). Moreover, the hydrolysis of AM is not always efficient as the presence of incomplete deesterified Fura-2 was shown in cells such as neuroblastoma cells, HPAE cells, and rat hepatocytes (Oakes *et al.*, 1988). Oakes *et al.* (1988) reported that there were more than 30 potential partly deesterified forms of Fura-2 AM when the five ester groups were randomly cleaved. The successful application of this method requires that Fura-2 is the main cellular fluorescent metabolite of Fura-2 AM. These incomplete deesterified fluorescent Fura-2 AM metabolites are Ca^{2+}-insensitive and together with the unhydrolysed Fura-2 AM will lead to high background fluorescence and complicate

the quantification of $[Ca^{2+}]_i$. The measurement of $[Ca^{2+}]_i$ can also be difficult if cells lack the necessary esterases to cleave the AM linkage, or the concentration of the AM form is reduced by extracellular esterases before it can accumulate within the cell (Bush & Jones, 1990). It is known that aging contributes to the deterioration of many physiological parameters (Bloom *et al.*, 1990). A study in old mice showed that aging contributed to a reduction in esterase activity and that this decline decreased the activation of cytotoxic T lymphocyte lysis (Bloom *et al.*, 1990). A similar reduction of esterase activity may also be present in the current aged mice, making the measurement of $[Ca^{2+}]_i$ with Fura 2- AM more challenging.

Additionally, as a consequence of low levels of cytosolic esterase activity, the cleaving of the ester bonds may be delayed, thus allowing Fura-2 AM to cross the membranes of cytosolic organelles (which also contain esterase activity) and accumulate in these organelles (Gunter *et al.*, 1988). In other words, dye sequestration is strongly correlated with the level of cytoplasmic esterase activity (Quintana & Hoth, 2004). The compartmentalisation of Fura-2 AM in non-cytoplasmic compartments have been demonstrated in the mitochondria, microsomes, nucleus, and other intracellular compartments (Blatter & Wier, 1990; Lee *et al.*, 2015; Roe *et al.*, 1990; Steinberg, Bilezikian, *et al.*, 1987). It has been shown that Fura-2 AM can be sequestered by liver and cardiacmyocyte mitochondria and fully hydrolysed by the mitochondrial esterases into the Ca^{2+} sensitive form (Gunter *et al.*, 1988; Lee *et al.*, 2015). Serious compartmentalisation of dye was found to be as high as 30-40% in the mitochondria of neonatal myocytes (Lemasters *et al.*, 1988; Roe *et al.*, 1990). Furthermore, Roe *et al.* (1990) also revealed that 16% of Fura-2 fluorescence was distributed in non-cytosolic compartments in rat hepatocytes. If a non-uniform distribution of fluorescence also occurred in Purkinje neurons derived from the old mice used in this study, the actual cytosolic free Ca^{2+} level might not be determined. Fura-2, if sequestered is not sensitive to changes in $[Ca^{2+}]_i$ in the cytosol. To

avoid Fura-2 sequestration following loading with Fura-2 AM, several techniques have been employed (Barber *et al.*, 1996; Bright *et al.*, 1996; Okada & Rechsteiner, 1982; Steinberg, Newman, *et al.*, 1987). For example, a study in T-lymphocytes demonstrated that the cytosolic calcium gradients produced from the mitochondrial Fura-2 sequestration due to AM loading can be eliminated by loading the cells with membrane-impermeant Fura-2 salt (Quintana & Hoth, 2004). While loading cells with membrane impermeant dye was the preferred method to bulk loading with Fura-2 AM, this method also has its own difficulties and limitation.

Firstly, the dyes did not diffuse through the dendrites so measurements of any local calcium transient during stimulation was not possible. Second, whether the stimulation protocol used in this study was effective in triggering a cell response was not clear. Electrical activity was not recorded as the sharp electrode was removed immediately after the dye loading process had been completed. The electrode was not left *in situ* due to the sensitivity of the impaled cell to any movement which may be introduced to the recording chamber when the filters were switched and perfusion flow that may tear or damage the cell resulting in cell death. In order to test if the current calcium detection system and stimulating protocol were effective for cells stimulation and measurement of calcium change, FDB muscle with simpler morphology were used, where calcium changes have been successfully measured in the current laboratory.

5.4.2 Morphology of *mdx* FDB fibres

In contrast to Purkinje cells, Fura-2 was well distributed in each individual FDB fibre, as indicated by the green fluorescence signal when excited at 340 and 380 nm in both ionophoresed and bath loaded cells. The peripheral nuclei in healthy fibre were also visible under 380 nm excitation. Unlike the healthy fibre, the presence of central nuclei was found in the *mdx* fibre. It has been reported in many studies that the presence of central nuclei is

sometimes also accompanied by fibre branching, both gross morphological abnormalities are commonly seen in *mdx* muscle but are absent in age-matched LC mice (Blake *et al.*, 2002; Chan *et al.*, 2007b; Head *et al.*, 1992). Head *et al.* (1992) reported that the appearance of malformed fibre can be observed in *mdx* mice aged as early as 3-15 weeks old. This was followed by a steady increase in the percentage of malformed fibres within the muscle after age 16-84 weeks. The presence of central nuclei is proof that *mdx* fibre had undergone regeneration (Chan & Head, 2011; Head *et al.*, 1992; Ontell *et al.*, 1982; Schmalbruch, 1976). These regenerated fibres are more susceptible to injury when stimulated within the muscle fibre. Head (2010) demonstrated that the branched *mdx* fibre is damaged by fatiguing activation, causing a breakdown of Ca^{2+} homeostasis, and break at branch points when submaximally activated in skinned fibre experiments. Similar malformed muscle morphology such as branched fibres are also found in muscle from boys with DMD. If DMD patients and *mdx* mice shared similar pathogenesis in muscle degeneration, the gradual loss of muscle function in DMD patients, which is the common fate of these patients, is unavoidable (Bell & Conen, 1968; Schmalbruch, 1984).

5.4.3 Calcium transient in FDB fibres

To induce calcium transient, a bipolar stimulating electrode was used to deliver voltage above the threshold for 1 ms at different frequencies for triggering fibre contraction. Upon stimulation, in contrast to the stimulation on brain slices, a sharp increase in fluorescent signal was observed immediately during the contraction or shortening of the fibre. This changing calcium was successfully detected using our imaging system and its fluorescence intensity was measured from the central portion of fibres using Image J. In the current optimisation study, the trend of amplitude of calcium transient follows the classical profile of those that was reported in Head (2010). It first showed a gradual increment with increasing stimulation frequency,

reaching its maximum at 25 Hz, after which it declines at the maximum stimulation frequency of 30 Hz. Similarly, these patterns of change in myoplasmic Ca^{2+} level were also observed when the fibre was stimulated to fatigue. Head (2010) reported that these alterations are generally due to the metabolic activities affecting the calcium regulation in the SR.

In short, the calcium transients in FDB fibres were detected successfully using the current experimental setting. This indicates that the stimulating protocol and imaging tools were sensitive enough to measure changes in $[Ca^{2+}]_i$.

5.5 Conclusion

In summary, due to the limitations of Fura-2 AM as discussed in section 5.4.1, the preferred calcium indicator for further experiment is Fura-2 free acid. By using a different cell type (FDB fibres), it was confirmed that the stimulating protocol and imaging system are in optimum condition to capture the calcium changes. Whether there was a missed recording of calcium change in the brain slice due to the setup of current stimulation equipment and imaging system (i.e., slow image acquisition rate) was also being clarified using the muscle study. Indeed, calcium change in skeletal muscle is at least 10 times quicker than Purkinje neurons, with a duration range in milliseconds compared to seconds in Purkinje neurons (Head, 1993; Hollingworth *et al.*, 2008; Inoue *et al.*, 2001; Konnerth *et al.*, 1992). Hence, to capture the clear calcium change in cerebellar Purkinje neurons, a better Fura-2 loading method is required for the homogenous distribution of dye not only in the cell body but also in the highly branched dendritic tree where it is going to be stimulated by the stimulating electrode. Alternatively, the details of Fura-2 diffusion with whole-cell patch-clamp electrode and more importantly the resting calcium level in Purkinje neurons will be presented in the next chapter.

Chapter 6. Electrophysiological properties and calcium signalling of cerebellar Purkinje cells in mature *mdx* mice

6.1 Introduction

A cognitive involvement has been reported in the *mdx* mice, a commonly used animal model for DMD (Anderson *et al.*, 2002). As discussed in Chapter 1, (section 1.6.2), Vaillend and colleagues reported an impaired recognition memory and long-term spatial memory in the *mdx* mouse following training in a water maze (Vaillend *et al.*, 2004). The authors suggested that the deficit in consolidation of long-term memory in dystrophic mice is due to altered synaptic plasticity, which is characterised by the abnormal enhancement of *mdx* hippocampal LTP. Similarly, an altered synaptic plasticity was also reported in the *mdx* cerebellum (Anderson *et al.*, 2003; Kueh *et al.*, 2011; Kueh *et al.*, 2008). Dystrophin is normally expressed in the cerebellar Purkinje cell of normal WT mice but absent in the *mdx* mouse. The mechanisms underlying the alterations in cerebellar synaptic function are unclear.

Brain dystrophins are mainly localised at the postsynaptic density of cortical and hippocampal pyramidal cells and cerebellar Purkinje cells (Knuesel *et al.*, 1999; Lidov *et al.*, 1990). Brain dystrophins together with the DAPC are thought to be associated with the maintenance and stabilisation of ion channels and receptors, which are essential to synaptogenesis and synaptic transmission (Perronnet & Vaillend, 2010). Immunocytochemical studies showed that dystrophin is co-localised with $GABA_AR$ clusters in the cerebral cortex, hippocampus, and cerebellum (Brunig, Suter, *et al.*, 2002; Knuesel *et al.*, 1999; Levi *et al.*, 2002). The loss of dystrophin has been associated with a reduction in the number and size of $GABA_AR$ clusters containing α1 and α2 subunits in cerebellar and hippocampal neurons of the *mdx* mouse (Knuesel *et al.*, 1999). This suggests that dystrophin is important in the regulation or

stabilisation of $GABA_AR$ clusters at inhibitory synapses. A study supporting this showed that, $GABA_AR$ clustering is restored in the hippocampus of the *mdx* mouse following dystrophin rescue with exon-skipping (Vaillend *et al.*, 2010).

In the cerebellum, full-length dystrophin is predominantly expressed at the postsynaptic density of Purkinje cells (Lidov *et al.*, 1990). The cerebellar Purkinje cell, which projects inhibitory signals to the vestibular and deep cerebellar nuclei, is the sole output from the cerebellar cortex impacting cerebellar-dependent behaviours (Kim *et al.*, 2012; Massey & Bashir, 2007). Long term depression is the main form of synaptic plasticity in Purkinje cells. In *mdx* mice, the loss of dystrophin in the cerebellum results in altered synaptic functions. Earlier studies from our group have shown a decreased heterosynaptic LTD but enhanced homosynaptic LTD of synaptic transmissions in cerebellar Purkinje neurons (Anderson *et al.*, 2004; Anderson *et al.*, 2010). In addition, other defects in neuronal activity have also been reported. Snow *et al.* (2014) demonstrated that the intrinsic electrophysiological properties of Purkinje cells in dissociated neurons from *mdx* mice were more hyperpolarised and fired more irregularly than those from WT mice. The firing frequency of these cells were also reduced. The altered intrinsic electrophysiological properties were found in dissociated neurons, however whether these changes were also happening in the *in vitro* cerebellar slice remains to be determined. Therefore, the first aim of this study is to investigate if the electrophysiological membrane properties and firing properties of *mdx* Purkinje cells were different from that of its LC in an acute cerebellar slice. The acute brain slice method is a powerful *in vitro* tool for the study of structural and functional characteristics of synapses, while maintaining functional connectivity and its relative homology to the intact brain.

In addition, another aim in this study is to measure the cytoplasmic calcium level and investigate the calcium handling properties in *mdx* Purkinje cells. It is known that in addition to the stabilising and structural roles played by dystrophin, another key role of dystrophin is the regulation of intracellular calcium homeostasis. The loss of dystrophin has been linked to a dysregulated $[Ca^{2+}]_i$ level in muscles. An earlier report showed an elevation of $[Ca^{2+}]_i$ by a factor of 2.4 in muscle biopsies taken from DMD patients when compared to control (Bodensteiner & Engel, 1978). Similarly, elevated resting cytoplasmic calcium level was also reported in *mdx* muscle fibre and in cultured dystrophic mouse and human muscle (Fong *et al.*, 1990; Mongini *et al.*, 1988; Turner *et al.*, 1988). The persistently high cytoplasmic calcium level is believed to be a consequence of dysregulated calcium release and calcium uptake by the SR, resulting in a reduced amplitude of AP-evoked calcium transient in the dystrophic cells (Bellinger *et al.*, 2009; Hollingworth *et al.*, 2008; Kargacin & Kargacin, 1996; Lovering *et al.*, 2009; Turner *et al.*, 1988; Woods *et al.*, 2004). This dysregulated calcium homeostasis impairs muscle function, subsequently results in progressive muscle weakness and eventual cell necrosis, which are the hallmarks of DMD muscle pathophysiology.

The altered calcium homeostasis in DMD is not restricted to muscle cells and is also evident in the CNS. An early study in cultured *mdx* mouse cerebellar granule cell demonstrated an increase in resting $[Ca^{2+}]_i$ (Hopf & Steinhardt, 1992). While the cerebellar granule cell does not normally express dystrophin, the cause of this increase in resting $[Ca^{2+}]_i$ remains unknown. Moreover, neurons in other brain regions such as cortical and hippocampal neurons also showed a significant increase in resting $[Ca^{2+}]_i$ in 3 and 6 months old *mdx* mice. This calcium elevation was shown to increase with age (Lopez *et al.*, 2016). Remarkably, the cognitive functions of these mice improved after the high $[Ca^{2+}]_i$ level was reversed using drugs which blocked the signalling molecules responsible for the increase in $[Ca^{2+}]_i$ level. This indicates that

a tightly regulated $[Ca^{2+}]_i$ level is necessary for normal cognitive function and further suggests that the cognitive impairment in *mdx* mice could be reversible when perturbed neuronal calcium ion levels are corrected (Lopez *et al.*, 2016).

Although $[Ca^{2+}]_i$ levels have been reported in some *mdx* brain regions, to date, there is no study addressing the $[Ca^{2+}]_i$ levels in cerebellar Purkinje cells. The level of $[Ca^{2+}]_i$ in Purkinje cells is very important as the synaptic signalling and the direction of synaptic plasticity are largely dependent on calcium ion level (Coesmans *et al.*, 2004) (refer Chapter 1 section 1.6.3.2 for more details). As calcium ion plays an essential role in LTD induction (Konnerth *et al.*, 1992; Wang *et al.*, 2000), and the fact that LTD is altered in dystrophic mice (Anderson *et al.*, 2004; Anderson *et al.*, 2010), the study on the impacts of dystrophin deficiency on Purkinje cells calcium handlings properties is a major interest in this study.

This chapter presents the results investigating the electrophysiological properties and $[Ca^{2+}]_i$ level in Purkinje cells from mature *mdx* mice using a simultaneous whole-cell patch-clamp recording and ratiometric calcium imaging with the low affinity calcium indicator, Fura-FF.

6.2 Method and materials

6.2.1 Animals and brain slice preparations

All experiments were carried out with approval from Western Sydney University Animal Ethics Committee and in compliance with the international guidelines on the care and use of experimental animals. Littermate control and *mdx* mice (average age 11-12 months old) were used.

6.2.1.1 Cerebellum brain slice preparation

A detailed description on cerebellar brain slice preparation is provided in Chapter 2, section 2.3. Briefly, mice were anesthetised with isoflurane and sacrificed by decapitation. The cerebellum was rapidly removed and transferred to ice-cold cutting aCSF. Cerebellar slices (250 µm) were made using a vibroslicer (Leica VT1200S, Leica Microsystems) and immediately transferred into a holding chamber containing HEPES buffered aCSF, continuously bubbled with carbogen (95% O_2 and 5% CO_2) until used for experiment.

6.2.2 Electrophysiological recording and data measurements

The detailed method for whole-cell patch-clamp recording on Purkinje cells is described in Chapter 2, section 2.4. Briefly, only Purkinje cells with a seal resistance of at least 1 GΩ were proceeded to obtain a whole cell mode. Prior to recordings and if needed, upon achieving whole cell configuration, neurons were held at -70 mV to improve the quality of the seal. Neurons with holding current greater than -200 pA were excluded from the recording. Electrophysiological recordings commenced approximately 5 minutes after obtaining whole-cell configuration to allow the cell to stabilise. Under current-clamp mode and without any holding current, both passive (i.e. resting membrane potential, input resistance) and active membrane properties [i.e. rheobase current, action potential (AP) amplitude, time at half-width of the AP, 10-90% rise time (ms) and slope (mV/ms), 90-10% decay time (ms) and slope (mV/ms)] were recorded. To calculate the *input resistance*, cells were subjected to hyperpolarising and depolarising currents (-50 pA to 50 pA for 500 ms, in 10 pA steps). The linear fitting of the membrane voltage changes in response to current injections (i.e. the slope of *V-I* curve) was used to calculate the input resistance of the cell. To determine the *rheobase current*, the minimum current magnitude required to elicit the first full AP, cells were injected with depolarising current steps in 30 pA (50 ms) increments. The AP amplitude produced at

rheobase current was measured as the difference between the threshold voltage and the peak. The amplitude of fast AP afterhyperpolarisation (AHP) was measured as the difference between the AP threshold and the negative peak of the AP. Action potential firing properties of Purkinje cells were measured by injecting depolarising currents from 100 pA to 1000 pA with increments of 100 pA of 500 ms duration with a step interval of 4 s. The membrane properties and AP firing patterns between *mdx* and LC mice were compared.

6.2.3 Calcium imaging

6.2.3.1 Loading cells with Fura-FF (Diffusion via patch electrode)

The details for Fura-FF pentapotassium salt loading in Purkinje cells are described in detail in Chapter 2, section 2.5.3. Briefly, microelectrodes were fabricated from borosilicate glass (Warner's instrument) and fire polished to give a resistance between 3 and 5 MΩ when filled with an internal solution containing in mM: 130 K-gluconate, 10 Na-gluconate, 4 NaCl, 2 Mg-ATP, 0.3 Na-GTP (290-300 mOsm; pH 7.2) and 0.3 mM Fura-FF (AAT Bioquest, Carlifornia, USA). Whole-cell patch was achieved, and Fura-FF was allowed to diffuse from a patch-electrode into the cell for 20-30 minutes. The low affinity Fura-FF calcium indicator was used instead of high affinity Fura-2 (refer to Chapter 5) because the low affinity dye has higher calcium dissociation constant than Fura-2 [K_d(calcium) = 6 and 0.14 µM, respectively] and is favoured for studying calcium changes in the dendrites and spines which have relatively low calcium buffering capacities (Aponte *et al.*, 2008; Canepari *et al.*, 2008; Grynkiewicz *et al.*, 1985; Hyrc *et al.*, 2000). Moreover, the low affinity Fura-FF shows immediate Ca^{2+} transient after the onset of PF stimulation whereas the high affinity dye shows a delay onset of Ca^{2+} increase after the onset of PF stimulation (Kuruma *et al.*, 2003).

6.2.3.2 Calcium signal imaging and fluorescent measurement

The details for calcium imaging and fluorescent measurement have been described in Chapter 2, section 2.5.4. Briefly, Purkinje cells filled with Fura-FF were excited at 340 and 380 nm. High-speed fluorescence measurements were made using a EMCCD camera (Andor iXon, Molecular Devices, California, USA). Changes in fluorescence were analysed using Image J/ Fiji software (http://fiji.sc/Fiji) (Schindelin *et al.*, 2012). To determine calcium changes during synaptic activation of Purkinje cells, depolarisation of Purkinje cell distal dendrites was evoked by stimulation of PF input. Local stimulation of presynaptic fibres was carried out with a theta electrode filled with extracellular solution (i.e. aCSF) positioned in the PF layer that showed clear fluorescence signal. Stimulation at threshold voltage, at 50 Hz, 0.5 second was delivered using an isolated pulse stimulator model 2100 (A-M Systems, Washington, USA). For Ca^{2+} measurements, the 340/380 pair images were acquired at 10 frames per second for 10 seconds. Resting 340/380 ratio were estimated using the average 340/380 ratio from the first 20 frames. The background fluorescence was subtracted for the measurement done in the distal dendrites for both resting calcium level and calcium change during the stimulation.

6.2.4 Data analysis

Statistical analysis on group data was performed with Prism 8 (GraphPad Software, SanDiego California USA). All data are presented as mean ± SEM unless otherwise stated. All statistical significance was taken as $p<0.05$ using two-tailed student unpaired *t*-test and one way-ANOVA.

6.3 Results

6.3.1 Membrane properties of Purkinje cells

Upon achieving whole-cell mode and establishment of a stable baseline (within the first 10 to 60 seconds in whole-cell mode), the passive membrane properties (i.e. resting membrane potential and input resistance) of Purkinje cells were recorded (Figure 6.1). The average resting membrane potential of *mdx* Purkinje cells (-55.12 ± 1.03 mV, n=19 cells) was not significantly different (p=0.3800, student unpaired t-test) from LC Purkinje cells (-57.29 ± 1.49 mV, n=14 cells) (Figure 6.1 A). Note that, the banded in appearance of the resting membrane potential in Figure 6.1A was not resulted from the ingroup variability in the resting membrane potential related to the different slices. Each band in both LC and *mdx* groups constituted resting membrane potentials from different brain slices. About one to three resting membrane potentials were recorded per animal. Resting membrane potentials in LC mice ranged between -52 mV to -67mV whereas it was ranged between -48 mV to -69 mV in *mdx* mice. Similar to the resting membrane potential, there was no difference in the input resistance (a combination of pipette resistance (3-6 MΩ) and membrane resistance) between these two genotypes (*mdx*=121.10 ± 15.87 MΩ; LC= 132.1 ± 21.2 MΩ, p=0.6715, student unpaired t-test) (Figure 6.1 B). The input resistance of each cell was calculated using the slope of *V-I* curves, in which the membrane potentials was plotted against the injected current steps (-50 to + 50 pA for 500 ms, in 10 pA steps) (Figure 6.2).

A) B)

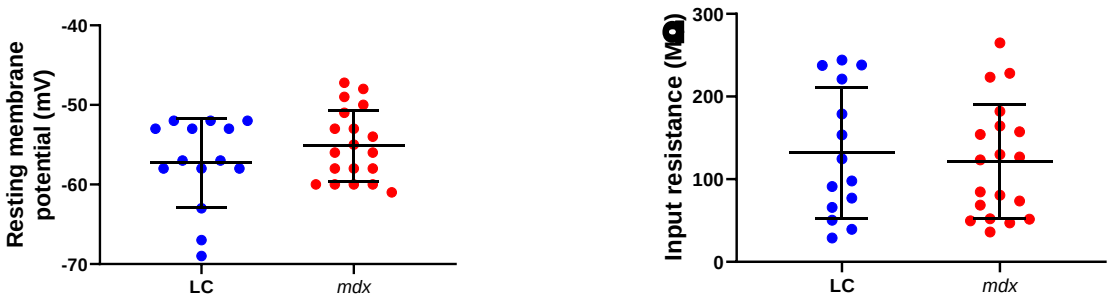

Figure 6.1 Passive membrane properties of *mdx* Purkinje cells were unaltered compared to LC Purkinje cells.

The passive membrane properties of *mdx* cells were similar to those in LC cells. (A) Resting membrane potential of LC cells was on average -57.29 ± 1.49mV while *mdx* cell was -55.12 ± 1.03 mV, p=0.3800, student unpaired t-test. (B) Input resistance of LC cells was on average 132.1 ± 21.2 MΩ while *mdx* cells was 121.0 ± 15.87 MΩ, p=0.6715, student unpaired t-test. Error bars are mean ± SEM.

A)

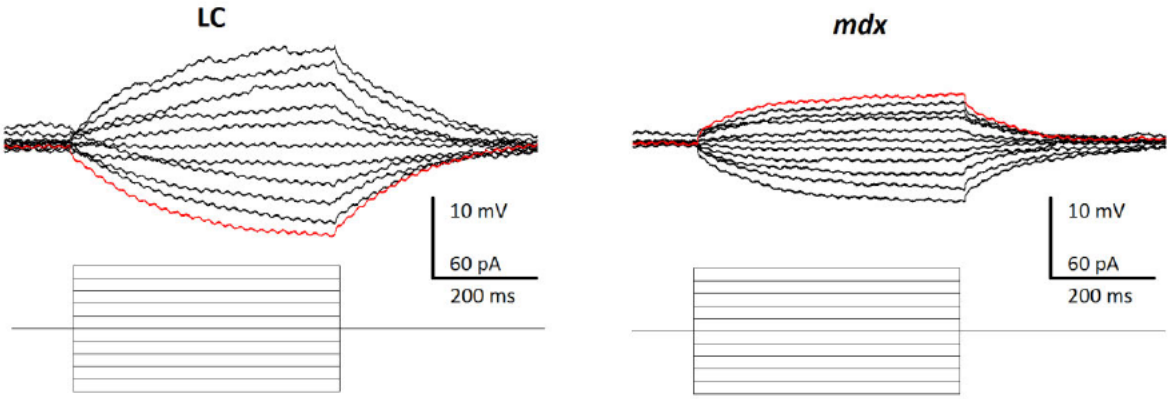

B)

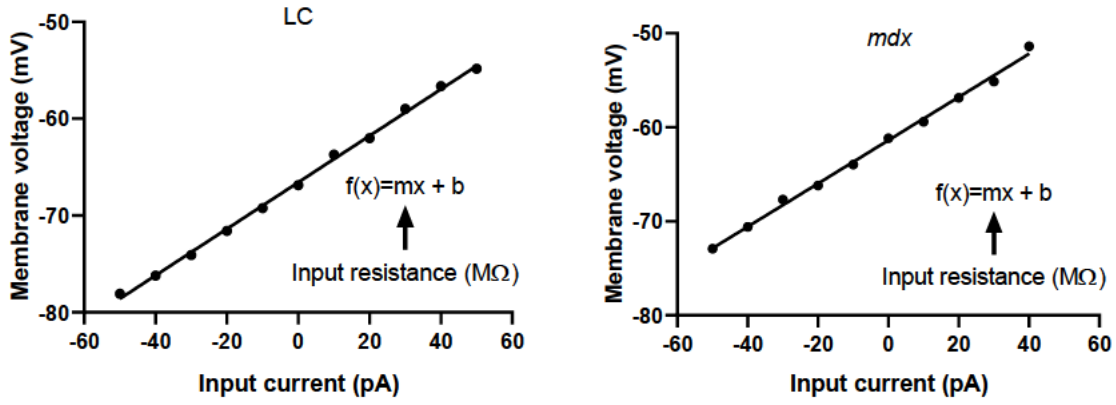

Figure 6.2 Input resistance measurements in Purkinje cells.

A) Depolarising and hyperpolarising current steps (-50 to + 50 pA for 500ms, in 10 pA steps; bottom traces) were used to determine the passive membrane properties shown as voltage changes in the membrane potential (top traces) of a representative LC (left) and *mdx* (right) Purkinje cell. (B) Input resistance was calculated using the linear fitting of the membrane voltage change in response to current injections.

Next, to measure the active membrane properties of Purkinje cells, an action potential was triggered with the rheobase current. Rheobase current, the minimal current required for eliciting the first full AP, was determined by injecting depolarising currents of 30 pA steps for 50 ms (Figure 6.3 A). The detailed analyses of the active membrane properties of AP triggered at rheobase current were also depicted in Figure 6.3 B. The average rheobase current of *mdx* cells was 252.90 ± 52.00 pA and was not significantly different from LC cells (231.5 ± 44.36 pA) (Figure 6.4 A). However, the average AP amplitude of *mdx* cells (39.48 ± 2.15 mV) was significantly reduced compared to LC cells (47.43 ± 3.13 mV), $p< 0.05$ (Figure 6.4 B). In addition, the average 10-90% rise time and slope were significantly longer and less steep in *mdx* mice (0.61 ± 0.06 ms, 61.05 ± 7.38 mV/ms, respectively) when compared to LC (0.44 ± 0.02 ms, 90.99 ± 9.00 mV/ms, respectively), $p< 0.05$ (Figure 6.4 C &D). The half width, 90-10% decay time and slope of AP were also measured and there were no significant difference between the two genotypes (Figure 6.4 E-G). A summary for both passive and active membrane properties of the recorded Purkinje cells is shown in Table 6.1.

A)

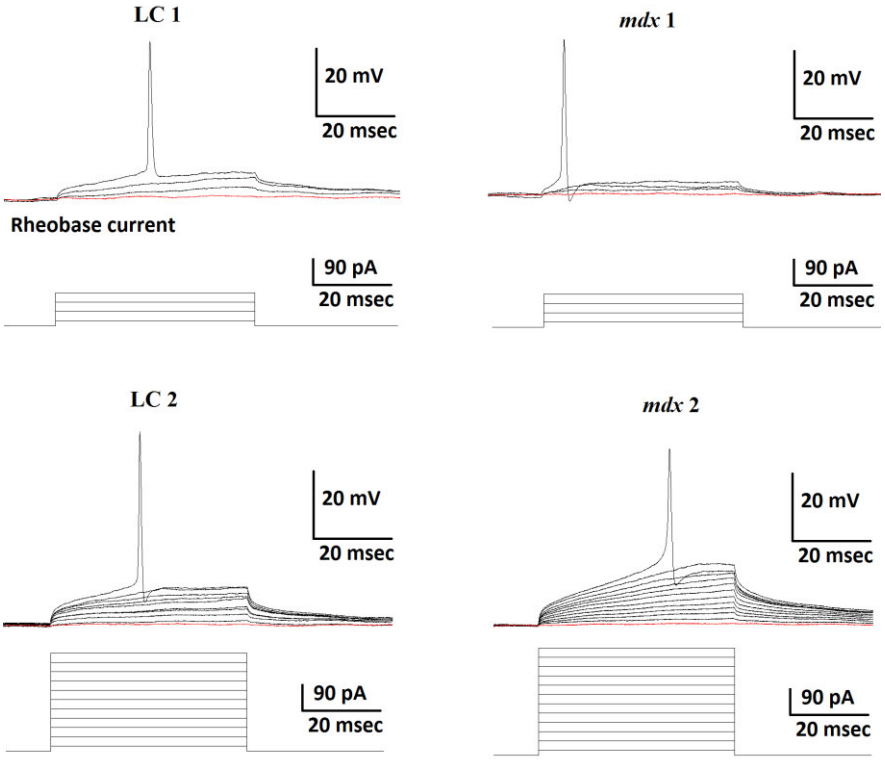

B)

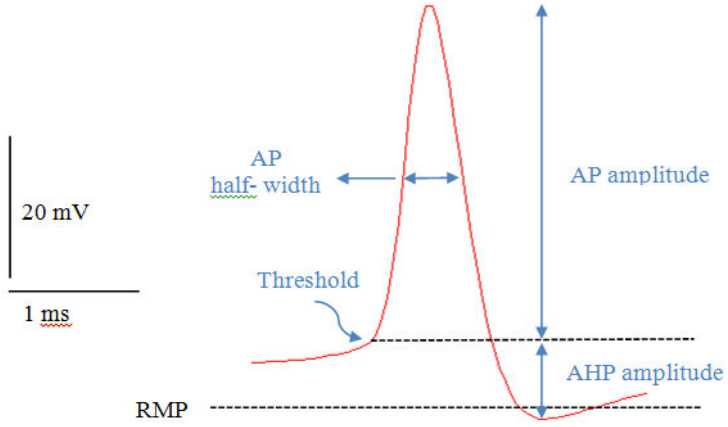

Figure 6.3 An action potential triggered by the rheobase current.

(A) *Top trace*: Action potential triggered by rheobase current in a Purkinje cell (left, LC; right, *mdx*). *Bottom traces* correspond to current command patterns. (B) Trace of an AP. The AP amplitude is measured as the voltage difference between the threshold voltage and the peak. AP half-width is measured as the AP duration at half-maximal spike amplitude. Fast AHP amplitude was measured as the difference between the peak hyperpolarization and the spike threshold voltage.

A)

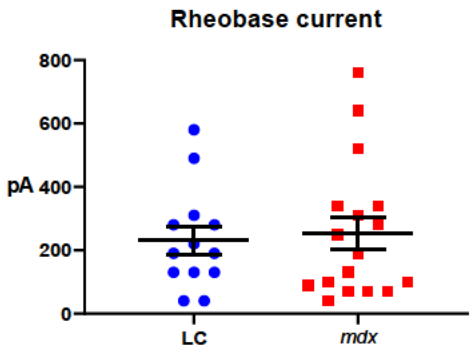
Rheobase current
800
600
pA 400
200
0
LC
mdx

B)

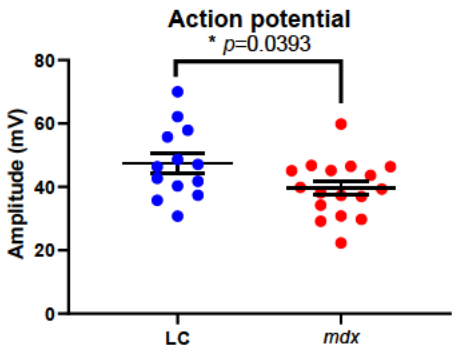
Action potential
* p=0.0393
80
60
40
20
0
Amplitude (mV)
LC
mdx

C)

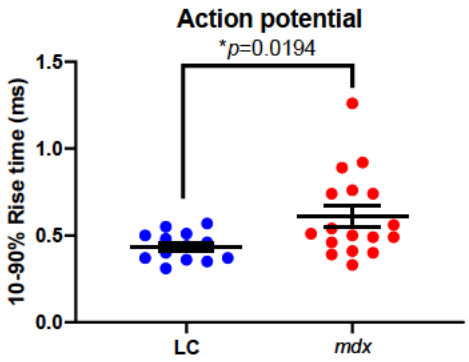
Action potential
*p=0.0194
1.5
1.0
0.5
0.0
10-90% Rise time (ms)
LC
mdx

D)

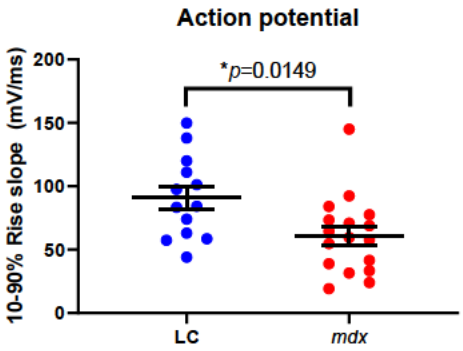
Action potential
*p=0.0149
200
150
100
50
0
10-90% Rise slope (mV/ms)
LC
mdx

E)

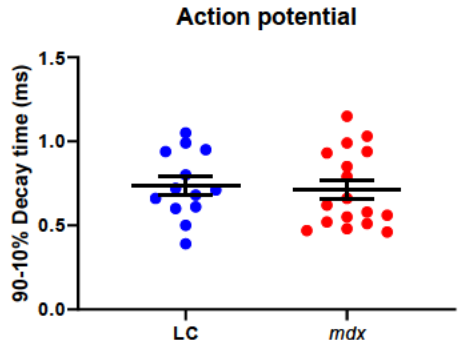
Action potential
1.5
1.0
0.5
0.0
90-10% Decay time (ms)
LC
mdx

F)

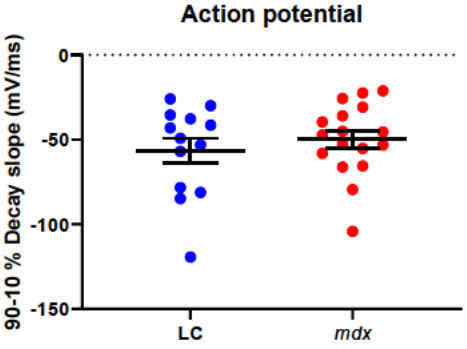
Action potential
0
-50
-100
-150
90-10 % Decay slope (mV/ms)
LC
mdx

(G)

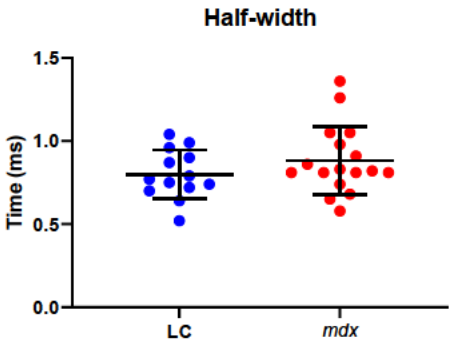
Half-width
1.5
1.0
0.5
0.0
Time (ms)
LC
mdx

Figure 6.4 Alterations of active membrane properties in *mdx* Purkinje cells.

(A) Rheobase current of *mdx* cells was not significantly different from LC cells (LC 231.5 ± 44.36 pA; *mdx* 252.90 ± 52.00 pA). (B) Action potential amplitude of *mdx* cells (39.48 ± 2.15 mV) was on average significantly lower than LC cells (47.43 ± 3.13mV), *p<0.05. (C) 10-90% rise time and (D) 10-90% rise slope of AP in *mdx* cells were significantly different from LC cells (10-90% rise time: LC 0.44 ± 0.02 ms; *mdx* 0.61 ± 0.06 ms, *p<0.05; 10-90% rise slope: LC 90.99 ± 9.00 mV/ms; *mdx* 61.05 ± 7.38 mV/ms, *p< 0.05). (E) 90-10% decay time and (F) 90-10% decay slope of AP in *mdx* cells were not significantly different from LC cells (90-10% decay time: LC 0.74 ± 0.06 ms; *mdx* 0.71 ± 0.06 ms; 90-10% decay slope: LC -56.63 ± 7.49 mV/ms; *mdx* -49.85 ± 5.19 mV/ms). Error bars were mean ± SEM.

Table 6.1 Membrane properties of Purkinje cells in LC and *mdx* mice.

Membrane properties		LC (8 animals) (13 cells)	*mdx* (8 animals) (17 cells)	*p* value
Passive membrane properties	Resting membrane potential (mV)	-57.29 ± 1.49	-55.12 ± 1.03	*p*=0.2244
	Input resistance (MΩ)	132.10 ± 21.20	121.10 ± 15.87	*p*=0.6715
Active membrane properties	Rheobase current (pA)	231.50 ± 44.36	252.90 ± 52.00	*p*=0.7656
	Amplitude (mV)	47.43 ± 3.13	39.48 ± 2.15	***p*=0.0393***
	10-90% rise time (ms)	0.44 ± 0.02	0.61 ± 0.06	***p*=0.0194***
	90-10% decay time (ms)	0.74 ± 0.06	0.71 ± 0.06	*p*=0.7337
	10-90% rise slope (mV/ms)	90.99 ± 9.00	61.05 ± 7.38	***p*=0.0149***
	90-10% decay slope (mV/ms)	-56.63 ± 7.49	-49.85 ± 5.19	*p*=0.4492
	Half-width (ms)	0.08 ± 0.04	0.88 ± 0.05	*p*=0.2237

Data are shown as as mean ± SEM. * indicates statistical significance, student unpaired *t*-test.

Representative sample traces of AP in *mdx* and LC Purkinje cells are depicted in Figure 6.5. These traces show a reduced amplitude and longer rise time in *mdx* APs (red traces) when compared to LC APs (blue traces). The AP fast AHP average amplitude, measured as the inward potential from AP threshold level to the negative peak of AHP, were larger in *mdx* (5.43 ± 1.17 mV) compared to LC (2.88 ± 1.00 mV), p=0.1668 (Figure 6.6 A), however it was not statistically significant. Similarly, the time to AHP and half height recovery time of AHP was on average longer in *mdx* cells (0.68 ± 0.06 ms, 2.69 ± 0.43 ms, respectively) but not significantly different compared to LC (0.47 ± 0.08 ms, 1.42 ± 0.34, respectively) (p=0.0567, p=0.0655, respectively, Figure 6.6 B & C).

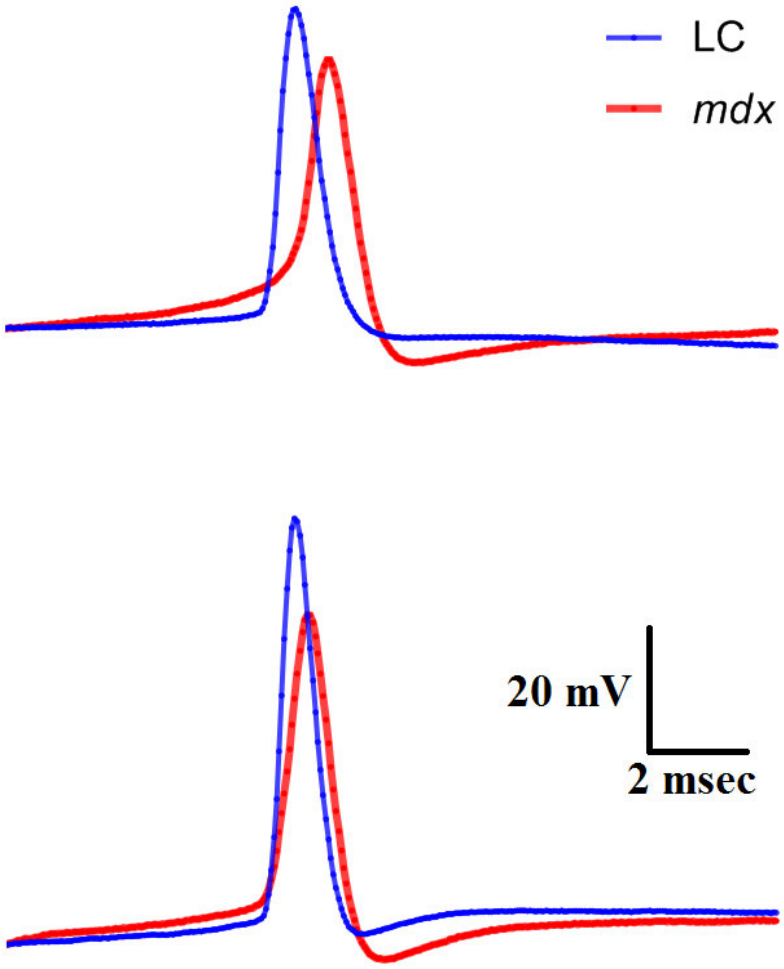

Figure 6.5 Sample traces of action potentials in Purkinje cells from *mdx* and LC mice.

Two pairs of AP recordings showed lower AP peaks and longer rise time in *mdx* Purkinje cells compared to LC cells. The AP AHP amplitudes in *mdx* cells, on average, were not significantly different from LC cells. In these examples, note that the AP AHP amplitudes in *mdx* cells were larger than LC cells.

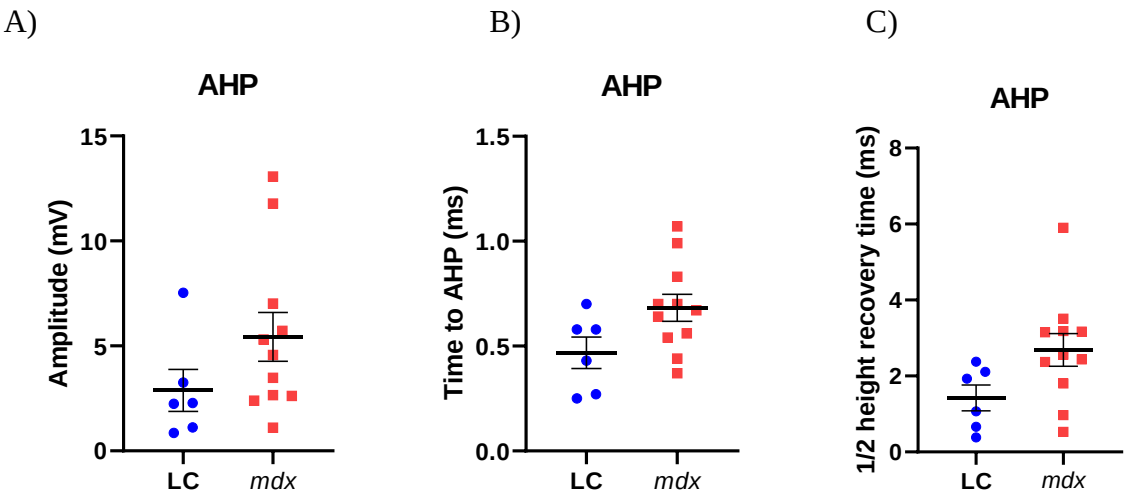

Figure 6.6 Properties of AHP triggered at rheobase current in Purkinje cells of *mdx* and LC mice.

(A) Amplitude of fast AHP in *mdx* mice (5.43 ± 1.16 mV) was not significantly different compared to LC mice (2.88 ± 1.00 mV), p=0.1668. (B) Time to fast AHP in *mdx* mice (0.68 ± 0.07ms) was not significantly different compared to LC mice (0.47 ± 0.08 ms), p=0.0567. (C) Half-height recovery time of fast AHP in *mdx* mice (2.69 ± 0.43ms) was not significantly different compared to LC mice (1.42 ± 0.34 ms), p=0.0655. Each point represents the value for a cell, and the bars represent the mean ± SEM. Significant level was set at p<0.05 with student unpaired *t-test*. Note scales of Y-axes were differ in each graph.

6.3.2 Action potential firing patterns

Next, the AP firing patterns induced by depolarising current pulses was recorded. Depolarising pulses (500 ms, 100 pA to 1000 pA) were delivered to Purkinje cells using the patch electrode. Following this stimulation protocol, two types of firing patterns were identified in Purkinje cells for both genotypes. For tonic firing neurons, the firing rate of AP in both *mdx and* LC mice increased initially with increased current but started to decrease after a current injection of 400 pA (Figure 6.7 A). These phenomena were observed in 27.27% LC cells (3 out of 11 cells), and 33.33% *mdx* cells (3 out of 9 cells) (see Table 6.2). On the other hand, 72.73% LC cells (8 out of 11 cells) and 66.67% *mdx* cells (3 out of 9 cells) were identified as the initial bursting neurons. These neurons only increased from 1 to 5 spikes when stimulated with depolarising pulses that were above the threshold and remained the same until the last stimulation of 1000 pA (Figure 6.7 B & Table 6.3). The average spike count for the two firing patterns (tonic and initial bursting) in both genotypes are shown in Figure 6.8 A and Figure 6.8 B respectively.

A)

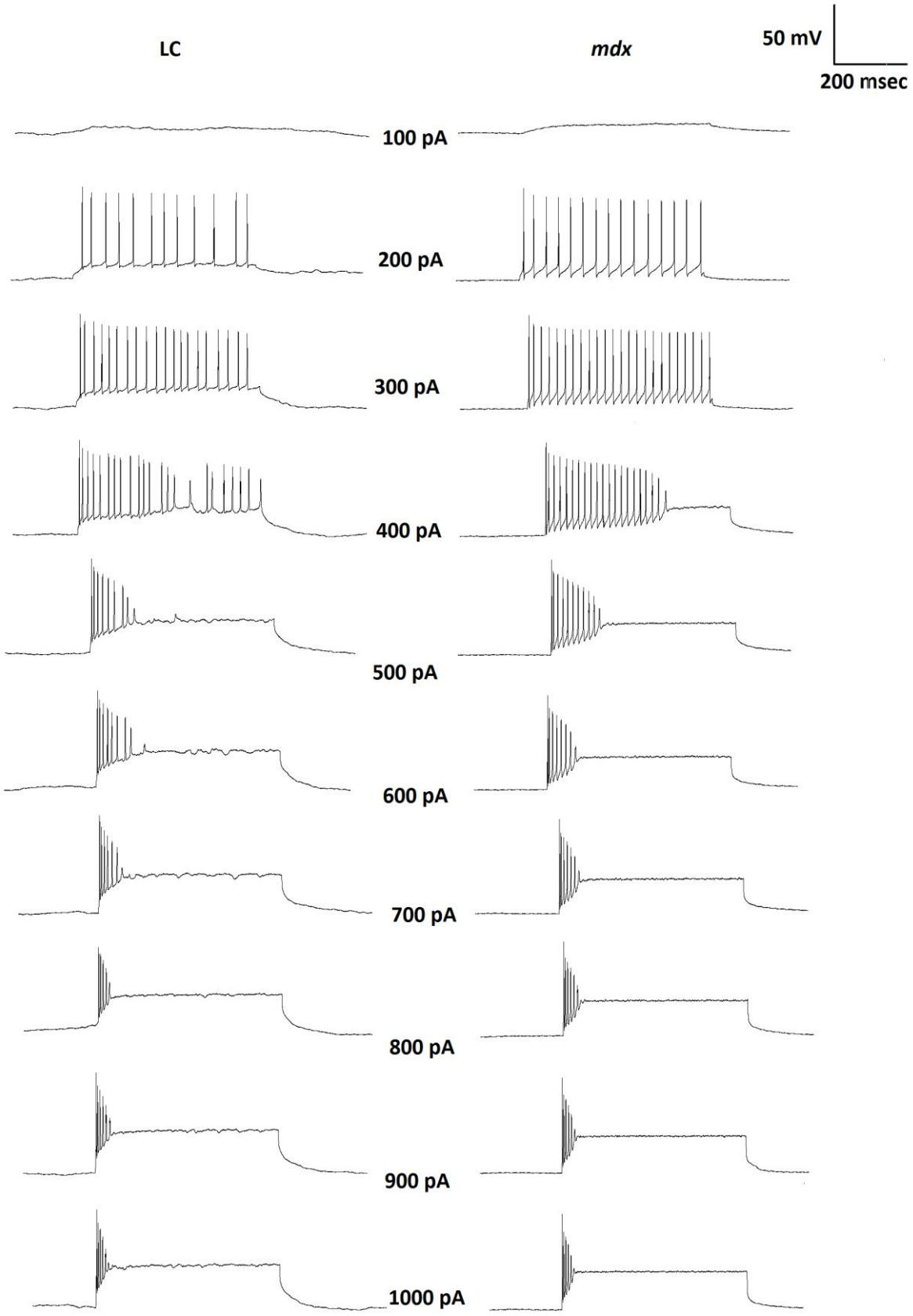
LC
mdx
50 mV
200 msec
100 pA
200 pA
300 pA
400 pA
500 pA
600 pA
700 pA
800 pA
900 pA
1000 pA

B)

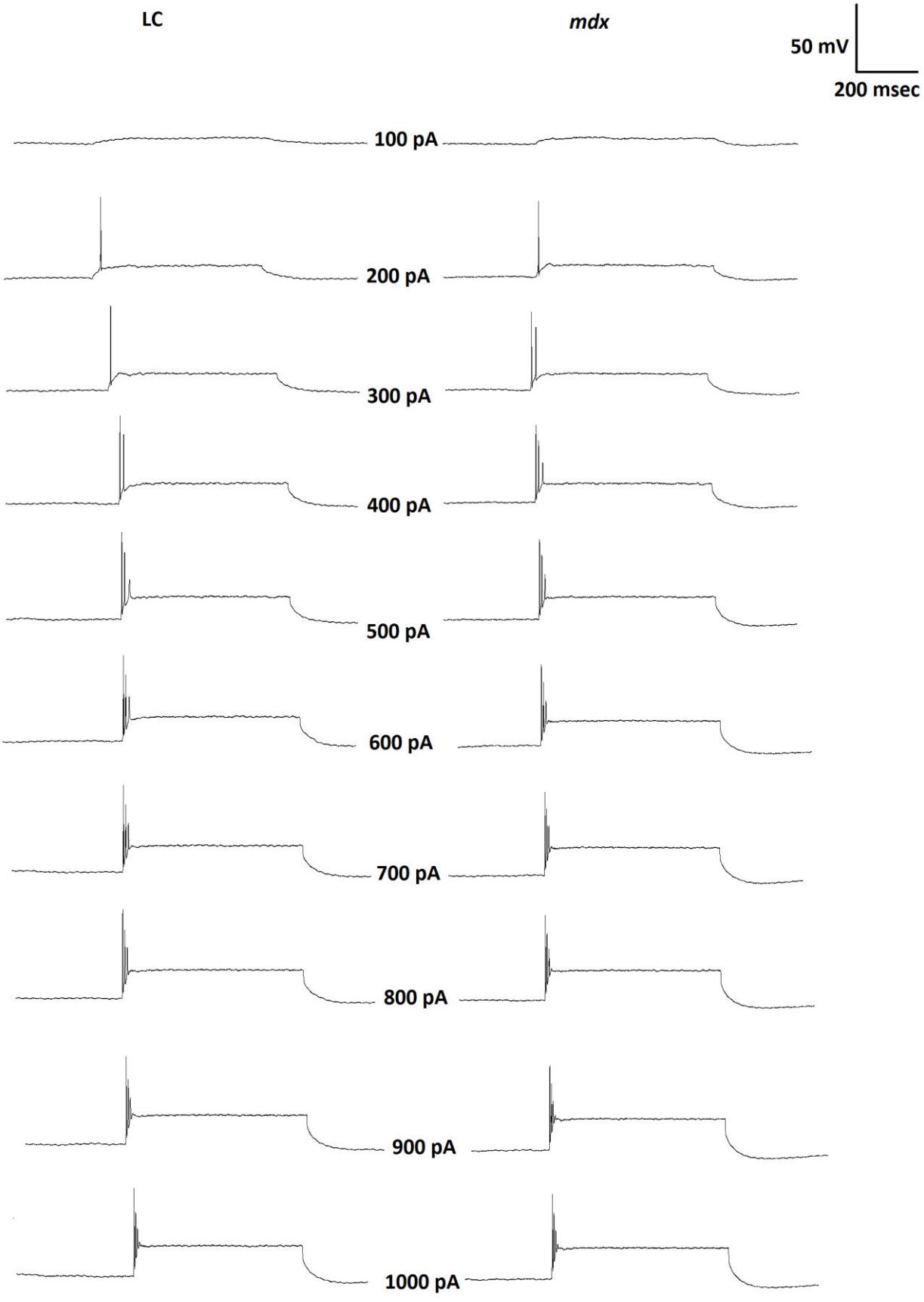
LC
mdx
50 mV
200 msec
100 pA
200 pA
300 pA
400 pA
500 pA
600 pA
700 pA
800 pA
900 pA
1000 pA

Figure 6.7 Action potential firing patterns induced by depolarising current pulse in *mdx* and LC Purkinje cells.

A) Tonic firing neurons first showed an increase rate (from 12 to 24 spikes with progressively increased stimulus strength from 200 pA to 400 pA in LC; from 15 to 24 spikes with progressively increased stimulus strength from 200 pA to 300 pA in *mdx*) follow by a decrease rate with increased stimulus strength in both animal groups. (B) Initial bursting pattern was observed in most of the recorded cells in both animal groups.

Table 6.2 Number of spikes of tonic firing Purkinje cells in *mdx* and LC mice.

	Littermate control			*mdx*		
Stimulus intensity (pA)	LC 1	LC 2	LC 3	*mdx* 1	*mdx* 2	*mdx* 3
100	0	0	0	0	1	0
200	0	12	0	15	8	0
300	0	20	0	24	9	0
400	0	24	0	21	8	0
500	16	9	1	11	6	1
600	18	9	7	8	7	2
700	26	7	22	7	6	5
800	9	5	36	6	6	12
900	4	6	36	6	6	13
1000	4	6	2	5	6	11

Table 6.3 Number of spikes of initial bursting Purkinje cells in *mdx* and LC mice.

	Littermate control								*mdx*					
Stimulus intensity (pA)	LC 1	LC 2	LC 3	LC 4	LC 5	LC 6	LC 7	LC 8	*mdx* 1	*mdx* 2	*mdx* 3	*mdx* 4	*mdx* 5	*mdx* 6
100	0	0	0	0	0	1	1	0	0	0	0	0	0	0
200	1	0	1	1	0	3	1	0	1	0	1	0	1	1
300	2	0	2	2	0	4	2	2	2	0	3	0	2	2
400	2	1	3	3	1	4	3	2	3	1	5	0	2	3
500	3	2	3	3	1	4	3	2	3	2	5	1	2	3
600	3	2	3	4	3	4	3	2	4	2	5	1	2	3
700	3	3	3	4	4	4	3	2	4	3	5	2	2	3
800	3	3	3	4	5	3	3	3	4	3	5	2	2	3
900	3	3	3	4	5	3	3	3	4	4	5	2	2	3
1000	3	3	3	4	5	3	3	3	4	4	5	2	2	3

A)

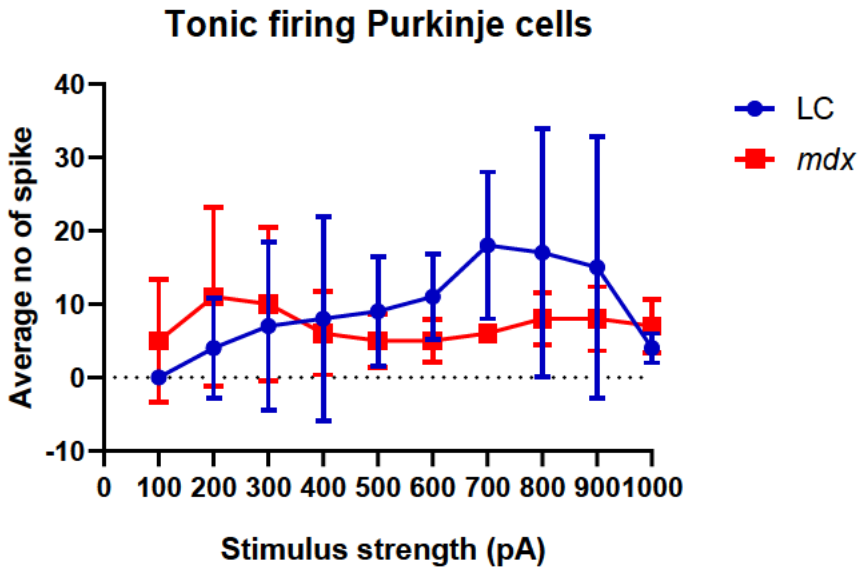

B)

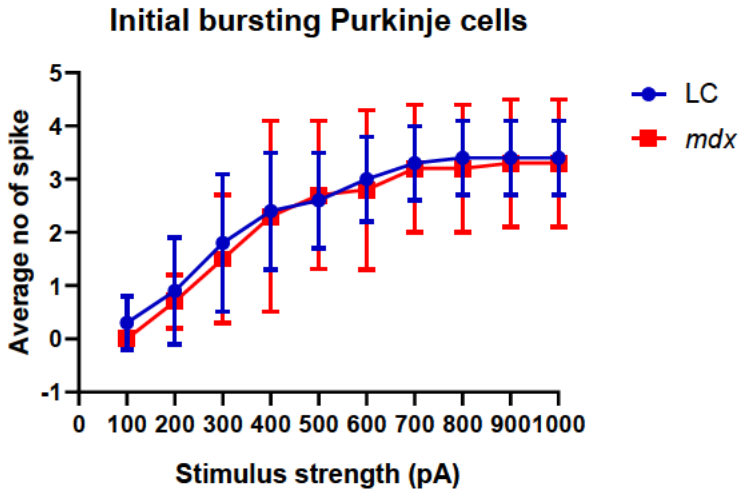

Figure 6.8 The average number of spikes in Purkinje cells of LC and *mdx* mice.

(A) The average of number of spikes in tonic firing neurons in *mdx* (n=3 animals) and LC (n=3 animals) mice. (B) The average of number of spikes in initial bursting neurons in *mdx* (n=6 animals) and LC (n=8 animals). Each point represents the average spike number plotted against stimulus strength of stimulus with the error bars showing SEM.

Next, several membrane properties of Purkinje cells with different types of AP firing patterns were compared between *mdx* and LC cells to see if the membrane properties were affected by the absence of dystrophin. Figure 6.9 showed that all the membrane properties including the input resistance (Figure 6.9 A & B), rheobase current (Figure 6.9 C & D), AP amplitude (Figure 6.9 E & F), 10-90% rise time (Figure 6.9 G & H), 10-90% rise slope (Figure 6.9 I & J), 90-10% decay time (Figure 6.9 K & L), 90-10% decay slope (Figure 6.9 M & N), and AHP amplitude (Figure 6.9 O & P) in *mdx* Purkinje cells with both types of firing patterns were not significantly different from the LC Purkinje cells. A detailed summary of the membrane properties for both tonic firing and initial bursting Purkinje cells of *mdx* and LC animals is shown in Table 6.4 and Table 6.5, respectively

(A)

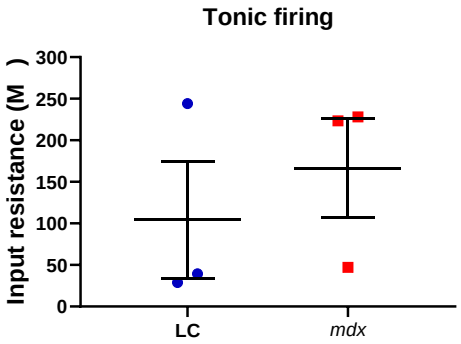
Tonic firing
Input resistance (M)
300
250
200
150
100
50
0
LC
mdx

(B)

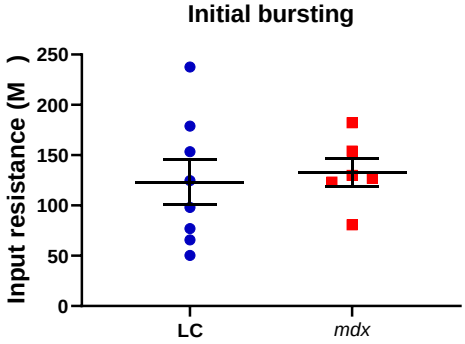
Initial bursting
Input resistance (M)
250
200
150
100
50
0
LC
mdx

(C)

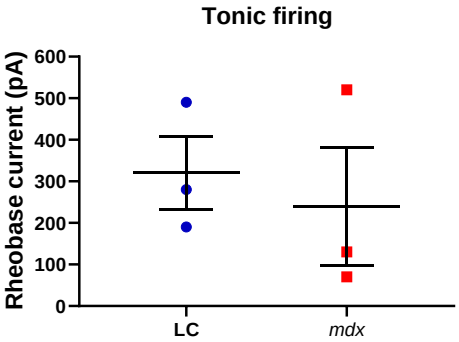
Tonic firing
Rheobase current (pA)
600
500
400
300
200
100
0
LC
mdx

(D)

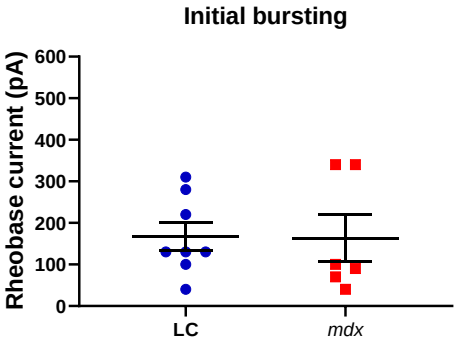
Initial bursting
Rheobase current (pA)
600
500
400
300
200
100
0
LC
mdx

(E)

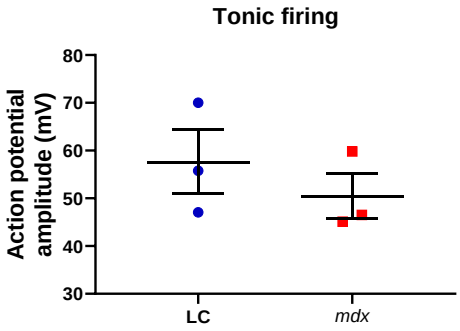
Tonic firing
Action potential amplitude (mV)
80
70
60
50
40
30
LC
mdx

(F)

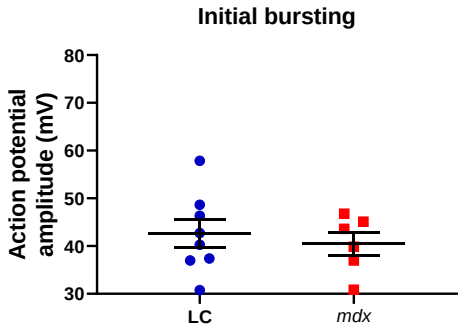
Initial bursting
Action potential amplitude (mV)
80
70
60
50
40
30
LC
mdx

(G)

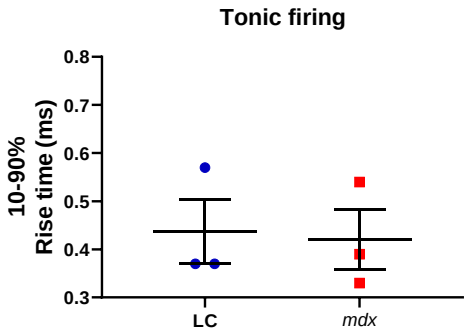
Tonic firing
10-90% Rise time (ms)
0.8
0.7
0.6
0.5
0.4
0.3
LC
mdx

(H)

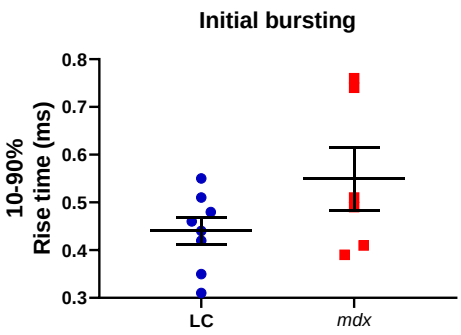
Initial bursting
10-90% Rise time (ms)
0.8
0.7
0.6
0.5
0.4
0.3
LC
mdx

(I)

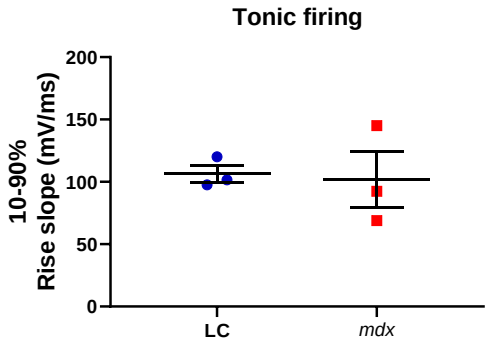
Tonic firing
10-90% Rise slope (mV/ms)
200
150
100
50
0
LC
mdx

(J)

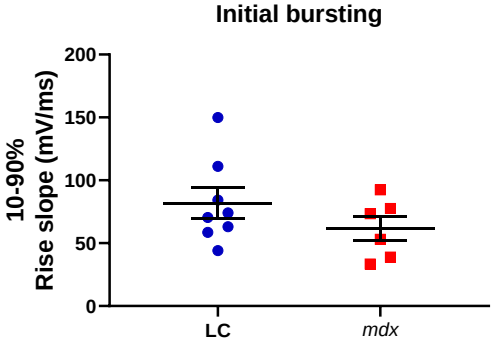
Initial bursting
10-90% Rise slope (mV/ms)
200
150
100
50
0
LC
mdx

(K)

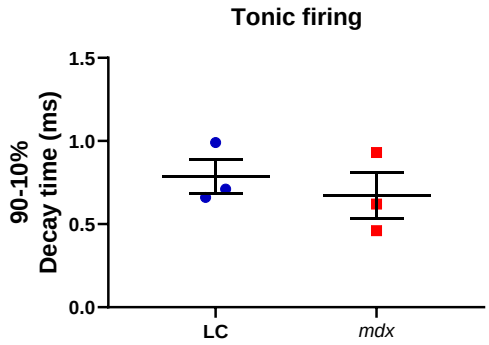
Tonic firing
90-10% Decay time (ms)
1.5
1.0
0.5
0.0
LC
mdx

(L)

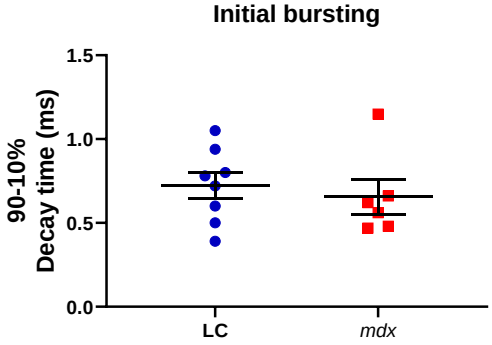
Initial bursting
90-10% Decay time (ms)
1.5
1.0
0.5
0.0
LC
mdx

(M)

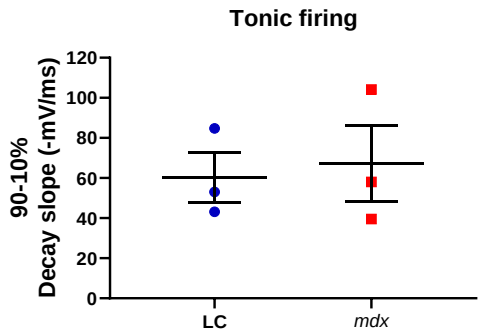
Tonic firing
90-10% Decay slope (-mV/ms)
120
100
80
60
40
20
0
LC
mdx

(N)

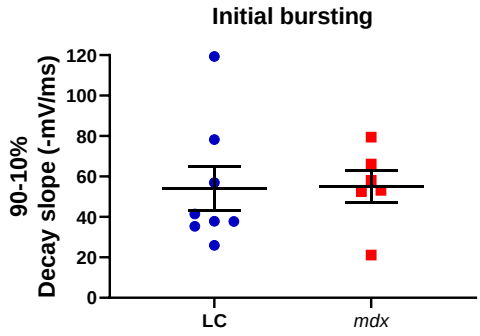
Initial bursting
90-10% Decay slope (-mV/ms)
120
100
80
60
40
20
0
LC
mdx

(O)

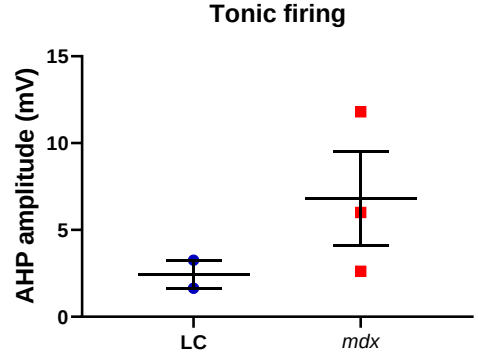
Tonic firing
AHP amplitude (mV)
15
10
5
0
LC
mdx

(P)

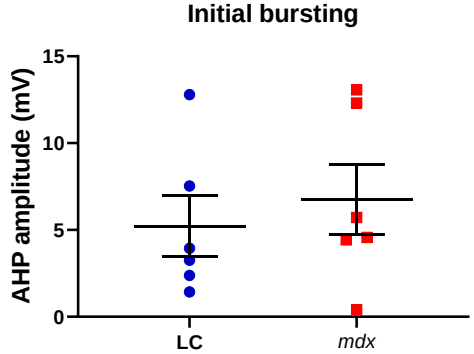
Initial bursting
AHP amplitude (mV)
15
10
5
0
LC
mdx

Figure 6.9 Passive and active membrane properties of tonic firing and initial bursting in the *mdx* Purkinje cells were not significantly different from the LC Purkinje cells.

There was no significant difference in passive (A-B Input resistance) and active membrane properties (C-D Rheobase current; E-F Action potential amplitude; G-H 10-90% rise time; I-J 10-90% rise slope; K-L 90-10% decay time; M-N 90-10% decay slope; O-P Fast AHP amplitude) between *mdx* and LC animals for both tonic firing and initial bursting Purkinje cell types. Each point represents the data from an individual cell. The mean and SEM are displayed in each graph.

Table 6.4 Membrane properties of tonic firing Purkinje cells in LC and *mdx* mice.

Tonic firing Purkinje cells			
Membrane properties	LC	*mdx*	*p* value
Input resistance (MΩ)	104.10 ± 70.04	166.20 ± 59.55	*p*=0.54
Rheobase current (pA)	320 ± 88.88	240 ± 141.1	*p*=0.66
Amplitude (mV)	57.62 ± 6.69	50.48 ± 4.68	*p*=0.43
10-90% rise time (ms)	0.44 ± 0.07	0.42 ± 0.06	*p*=0.86
90-10% decay time (ms)	0.79 ± 0.10	0.67 ± 0.14	*p*=0.54
10-90% rise slope (mV/ms)	106.40 ± 6.90	102.10 ± 22.49	*p*=0.86
90-10% decay slope (mV/ms)	60.32 ± 12.56	67.26 ± 19.20	*p*=0.78
AHP amplitude (mV)	2.445 ± 0.8050	6.813 ± 2.683	*p*=0.30

Data are indicated as mean ± SEM.

Table 6.5 Membrane properties of initial bursting Purkinje cells in LC and *mdx* mice.

Initial bursting Purkinje cells			
Membrane properties	LC	*mdx*	*p* value
Input resistance (MΩ)	123.20 ± 22.55	132.80 ± 13.84	*p*=0.75
Rheobase current (pA)	167.50 ± 32.94	163.30 ± 56.49	*p*=0.76
Amplitude (mV)	42.62 ± 2.95	40.53 ± 2.43	*p*=0.61
10-90% rise time (ms)	0.44 ± 0.03	0.55 ± 0.07	*p*=0.12
90-10% decay time (ms)	0.72± 0.08	0.66 ± 0.10	*p*=0.61
10-90% rise slope (mV/ms)	81.92 ± 11.96	61.50 ± 9.53	*p*=0.23
90-10% decay slope (mV/ms)	54.10 ± 10.93	55.09 ± 7.93	*p*=0.95
AHP amplitude (mV)	5.22 ± 1.74	6.75 ± 2.02	*p*=0.58

Data are indicated as mean ± SEM.

6.3.3 Calcium imaging in *mdx* and LC Purkinje cells

To determine $[Ca^{2+}]_i$ level in Purkinje cell, cells were filled with a ratiometric fluorescent calcium indicator, Fura-FF using a patch electrode. The increase or decrease in the fluorescent intensity of the signal reveals alteration in $[Ca^{2+}]_i$ level. The optimum excitation wavelength changes after the binding of Ca^{2+} to this ratiometric indicator. When $[Ca^{2+}]_i$ level is low, the Ca^{2+}-free form of Fura-FF has a peak excitation wavelength at 380 nm whereas when $[Ca^{2+}]_i$ level is high, the peak excitation wavelength for Ca^{2+}-bound Fura-FF is at 340 nm. In this experiment, when the Purkinje cell was at rest, it showed the brightest fluorescent signal when excited at 380 nm and a low 340/380 ratio image. This indicates a low $[Ca^{2+}]_i$ level (Figure 6.10). The morphology of the Purkinje cell can be seen clearly in the 340/380 ratio image, i.e. Purkinje cell body with a diameter of ~20 µm and an elaborate dendritic arborizations.

Next, in order to determine the $[Ca^{2+}]_i$ level in various parts of the Purkinje cell, regions of interest were drawn on the fluorescent cells using Image J/Fiji software. Fluorescent intensity was measured, and the data was plotted and analysed using GraphPad PRISM 8. A total of 17 *mdx* cells and 13 LC cells were analysed. In these cells, the soma of *mdx* mice (0.20 ± 0.01) showed a significantly higher average resting ratio (340/380) compared to LC (0.17 ± 0.01), p= 0.0295 (mean ± SEM, student unpaired *t*-test), indicating a higher resting $[Ca^{2+}]_i$ in *mdx* Purkinje soma (Figure 6.11 A). However, the average ratio (340/380) in the distal dendrites was not significantly different between both genotypes (*mdx* (0.19 ± 0.01; LC 0.22 ± 0.02, p=0.1978) (Figure 6.11 B). Overall, the loss of dystrophin has led to an altered calcium homeostasis in *mdx* Purkinje cell, in particular the resting $[Ca^{2+}]_i$ in the *mdx* mouse was significantly elevated in the cell soma.

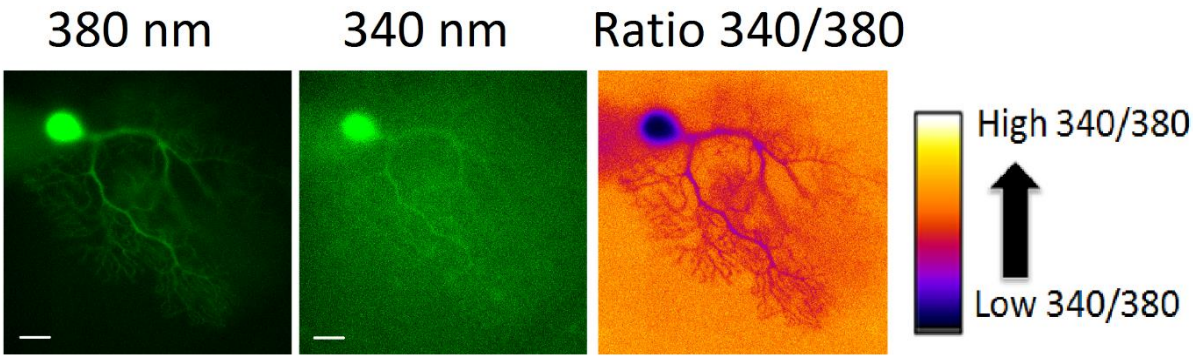

Figure 6.10 Fluorescent and ratio images of Fura-FF loaded LC Purkinje cell at rest, excited at 340 and 380 nm.

Fura-FF (300µM) was added in the internal solution and loaded into the cell using a patch clamp pipette. When at rest, the fluorescent intensity is brightest at (left) 380 nm but dimmer at (middle) 340 nm, giving a (right) low ratio (340/380) image. Colour bar indicates the scale of pseudocolour images (warmer colours for greater changes in fluorescence). Scale bar represents 20 µM at 40X magnification.

A) B)

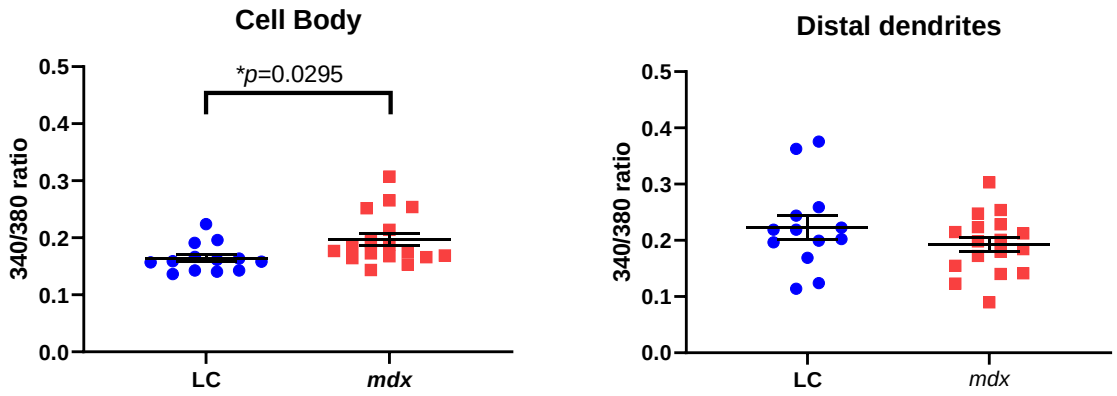

Figure 6.11 Intracellular resting calcium levels in *mdx* Purkinje cell were significantly altered compared to LC cells.

Resting $[Ca^{2+}]_i$ level was measured at various regions in Purkinje cells of *mdx* (n= 17 cells) and LC (n=13 cells). (A) The mean resting calcium ratio of Purkinje cell body in *mdx* (0.20 ± 0.01) was significantly increased when compared to LC (0.17 ± 0.01) (p= 0.0295, student unpaired *t*-test). However, (B) the distal dendritic $[Ca^{2+}]_i$ levels were not significantly different between the two groups (LC, 0.22 ± 0.02; *mdx* 0.19 ± 0.01, p=0.1978 student unpaired *t*-test). The points represent the value (340/380 ratio) for each cell, and bars indicate mean ± SEM. Significance level was set at $p<0.05$ with student unpaired *t-test*.

It is known that normal Purkinje cells receive more than 100,000 PF connections on their extensive dendritic arbors in the molecular layer (Braitenberg & Atwood, 1958; Palay & Chan-Palay, 2012). When Purkinje cells PF are stimulated, it results in the accumulation of calcium in Purkinje cells through Ca^{2+} influx via VGCCs or Ca^{2+} release from intracellular stores regulated by the activation of $InsP_3$ receptors (Finch & Augustine, 1998; Hartell, 1996; Takechi *et al.*, 1998). While the resting calcium in *mdx* Purkinje cell soma was significantly increased, whether there was also a change in calcium handling properties in *mdx* Purkinje cells dendrites remained unclear. To examine this, a stimulating electrode was positioned over the Fura-FF filled distal dendrites where they are highly synapsed with PF in the molecular layer. Using a theta electrode, small voltage stimulations (50 Hz for 0.5 second) were delivered to the PF until threshold was reached, i.e. the first fluorescence signal change or the first calcium change was captured by the EMCCD camera. In Figure 6.12, the regions of interest on the 340/380 ratio images of the Purkinje cells in LC (Figure 6.12 A) and in *mdx* mice (Figure 6.12 B) are indicated by the dark circle, where the theta electrode was placed nearby. The dendritic calcium change in response to stimulation during stimulation is depicted in Figure 6.13. Upon stimulation, the average ratio (340/380) in dendrites of *mdx* mice was increased significantly compared to the baseline ratio (prior to stimulation ratio 0.14 ± 0.02; during stimulation ratio 0.18 ± 0.052, p= 0.0128). Following stimulation, the $[Ca^{2+}]_i$ returned to near baseline level (post stimulation ratio 0.13 ± 0.02) (Figure 6.13 A). Similar trends in dendritic calcium changes were also seen in LC, however, compared to baseline levels (prior to stimulation ratio 0.15 ± 0.02; during stimulation ratio 0.20 ± 0.04, p= 0.0522) increase in $[Ca^{2+}]_i$ was not significant (Figure 6.13 B).

A)

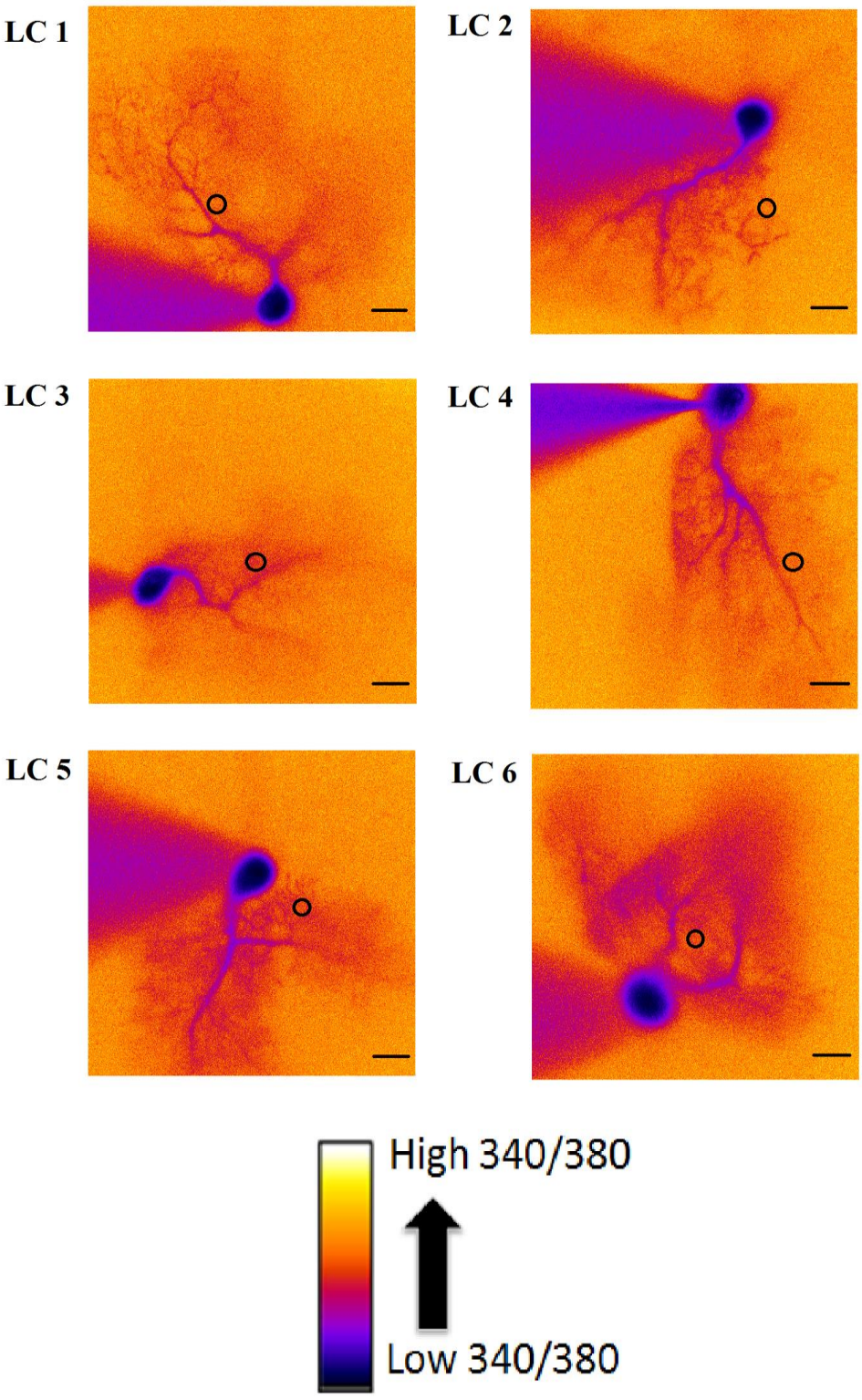

B)

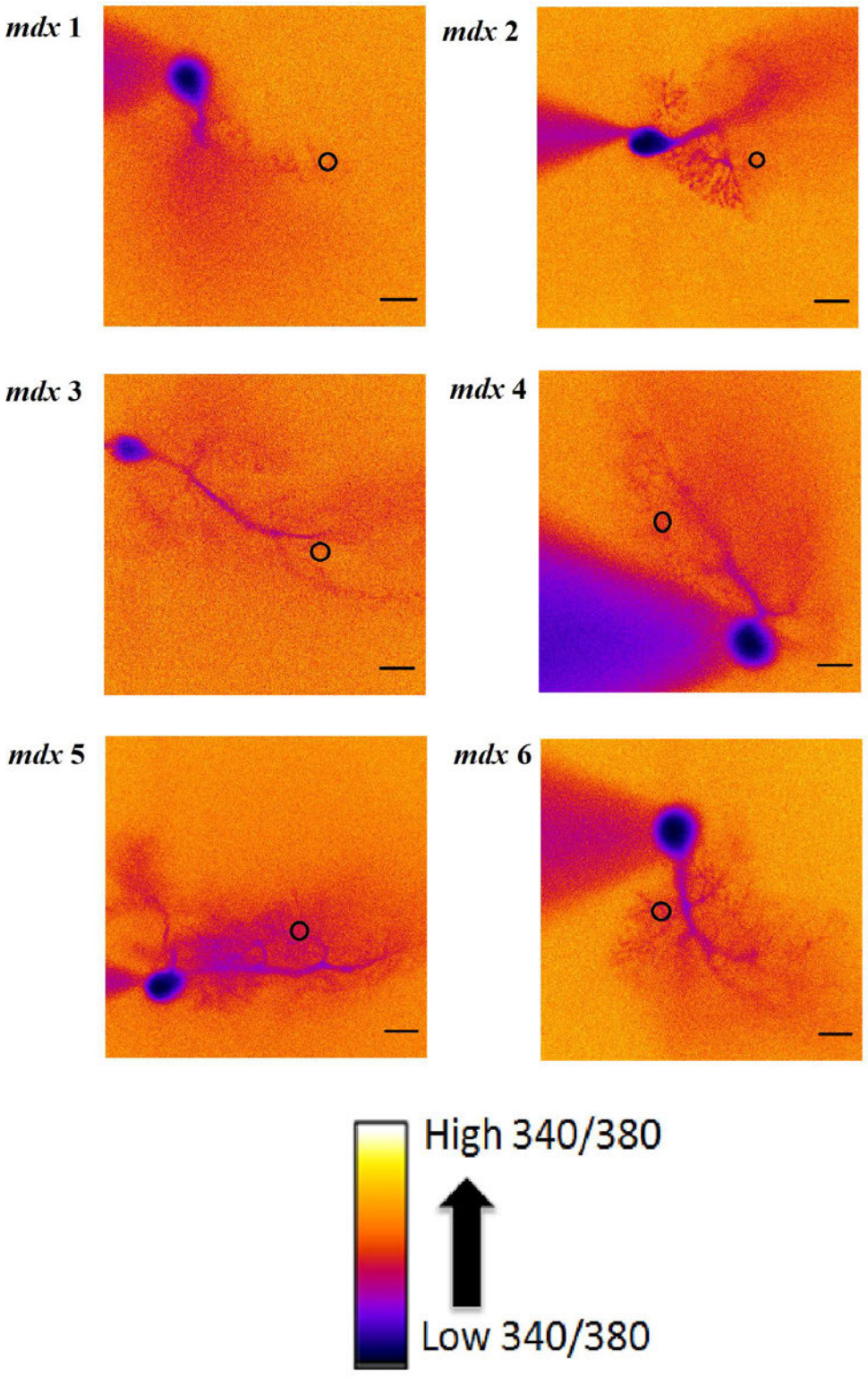

Figure 6.12 Regions of interest for the measurements of dendritic calcium change in Fura-FF filled Purkinje cells of LC and *mdx* mice.

Purkinje cells from (A) LC and (B) *mdx* mice (n=6 animals for each genotype) were filled with 0.3 mM Fura-FF using a patch electrode. Threshold voltage (50 Hz for 0.5 second) was delivered via a theta electrode to stimulate the parallel fibres. Calcium change in the regions of interest (i.e. the black circle on each cell) upon stimulation was determined by a change in the fluorescence intensity (340/380 ratio). Colour bar indicates the scale of pseudocolour images (warmer colours for greater changes in fluorescence). Scale bar represents 20 µM at 40X magnification.

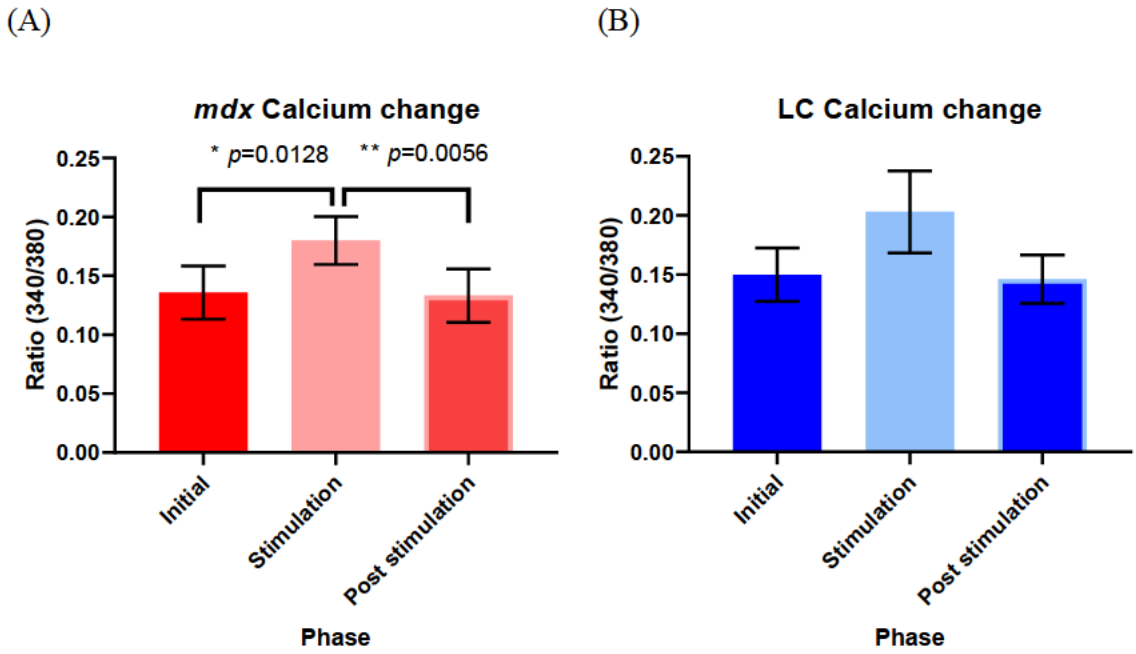

Figure 6.13 Significant calcium change in *mdx* Purkinje cell dendrites upon parallel fibres stimulation compared to LC cells.

The average increase in calcium level (340/380 ratio) in *mdx* (A) Purkinje cells (n=6 cells) during the stimulation (0.18 ± 0.052) differed significantly compared to resting levels (initial 0.14 ± 0.02, p=0.0128; post stimulation 0.13 ± 0.02, p=0.0056). On the other hand, the average increase in calcium (340/380 ratio) in (B) LC Purkinje cells (n=6 cells) during stimulation (0.20 ± 0.04) was not significantly different compared to baseline levels before and following stimulation (initial 0.15 ± 0.02, p=0.0522; post stimulation 0.15 ± 0.02, p=0.0769). Note that calcium levels post stimulation were similar to that at the initial states for both genotypes, indicating the recovery of resting calcium levels in these recorded cells. Bars indicate SEM. Significance level was set at p<0.05 with one way-ANOVA and corrected for multiple comparisons using Bonferroni test.

Next, to determine if the PF-evoked Ca^{2+} accumulation in dendrites was impacted by dystrophin deficiency, the calcium change in fluorescence intensity relative to the resting fluorescence intensity (ΔF/F (340/380)) in *mdx* Purkinje cells was compared with the ΔF/F (340/380) in LC Purkinje cells (Figure 6.14). No significant difference was found in the mean ΔF/F (340/380) between the two groups (LC, 0.052 ± 0.015; *mdx*, 0.045 ± 0.008; p=0.6948, student unpaired *t*-test). This indicates that the PF-evoked Ca^{2+} accumulation of *mdx* mice was similar to that in LC mice. It is important to point out that the current calcium changes were related to the threshold voltage stimulation used. Greater calcium change such as mean ΔF/F (340/380) of 0.10 could sometimes be observed when the cells were stimulated with a stronger stimulus (i.e. voltages that passed the threshold) or repeated stimuli. Although there was no significant difference in the level of PF-evoked calcium change between *mdx* and LC dendrites when using threshold voltage, LC cells could tolerate ΔF/F (340/380) of between 0.03-0.12 whereas *mdx* cells could only tolerate between 0.03-0.08, when stronger stimuli were given. When the calcium changes had exceeded these range, the cells were usually highly depolarised, and the recovery from high calcium levels to resting calcium levels was not possible, leading to the termination of the experiment/data collection. Overall, these results indicate that there was no significance difference in the PF-evoked Ca^{2+} accumulations in the dendrites of Purkinje cells between *mdx* and LC mice when using the threshold voltage stimulation. Nevertheless, *mdx* cells tended to have a smaller range of calcium change when compared to LC cells, following the application of stronger stimuli.

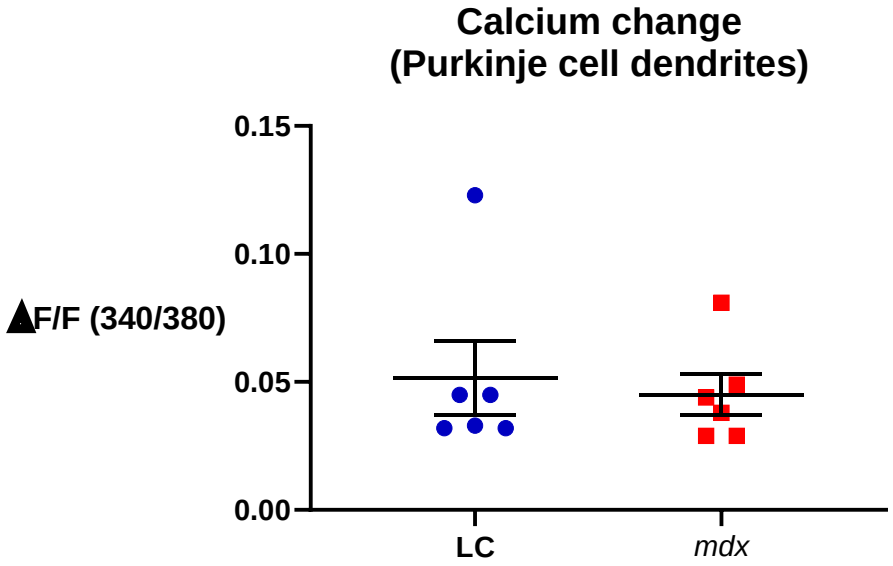

Figure 6.14 The change in calcium level (ΔF/F) at Purkinje dendrites of LC (n=6 cells) and *mdx* (6 cells).

The change in intensity is denoted as ΔF/F, which is the change in fluorescence intensity relative to the resting fluorescence intensity. ΔF/F (340/380 ratio) was calculated based on the equation (Maximum 340/380 ratio-Average baseline)/(Average baseline). There was no significant difference between the mean ΔF/F (340/380 ratio) in both animal groups (LC, 0.052 ± 0.015; *mdx*, 0.045 ± 0.008) (p=0.6948, student unpaired t-test).

6.4 Discussion

6.4.1 Electrophysiological properties of *mdx* Purkinje cell

This study investigated the impact of the absence of dystrophin on the intrinsic electrophysiological properties of neurons, in particular the membrane properties of cerebellar Purkinje cells in mature *mdx* mice (11-12 months old). This age group was selected as there was evidence of significant behavioural alterations and biochemical aberrations in older *mdx* mice (>6 months), matching the findings in the cerebellum of boys with DMD, where brain biochemistry was significantly altered in older DMD boys (Rae *et al.*, 1998).

The passive membrane properties (resting membrane potential and input resistance) of *mdx* Purkinje cells were similar to that of its age-matched LC. Excitable membrane behaves like a simple electrical circuit, in which the ion channels are the resistors and the membrane is the capacitor. Input resistance of a neuron may indicate its overall conductance across the membrane, and it fluctuates in response to neuronal size, shape and resting membrane conductance (Kim *et al.*, 2012). McKay and Turner (2005) showed that the input resistance of Purkinje cells decreased dramatically from 1400 ± 200 MΩ to 250 ±24 MΩ (~ 6-fold drop) over the first 9 postnatal days, when the somatic and dendritic tree sizes progressively increased over the developmental period. The current study showed that the input resistance in *mdx* mice was not significantly different from the LC mice. This indicates that the neuronal size and shape, or resting conductance in *mdx* mice may be similar to that in LC, implying that dystrophin deficiency may not have significant impacts on Purkinje somatic and dendritic sizes and shapes, as well as the functions of ion channels during resting state. In line with the input resistance result, the resting membrane potentials in *mdx* mice (-55.12 ± 1.03 mV) were also very similar to that in LC (-57.29 ± 1.49 mV). This result is consistent with the findings in

several earlier studies. Anderson and colleagues found no significant difference in resting membrane potential between *mdx* and WT Purkinje cells (3-month old) while another group also reported similar resting membrane potential in *mdx* and WT hippocampal CA1 pyramidal neurons (30-45 days) (Anderson *et al.*, 2003; Anderson *et al.*, 2010; Graciotti *et al.*, 2008).

Next, to understand how dystrophin deficiency affects Purkinje cell excitability, several parameters of the neuronal response to current injection (i.e. active membrane properties) in *mdx* Purkinje cells were analysed. Firstly, the membrane excitability can be calculated using the formula of 1/rhoebase (Fleshman *et al.*, 1981). Rheobase is an index of excitability, which is defined as the minimum current needed for triggering at least one AP (Jack *et al.*, 1975). Increasing current steps in 30 pA increments (500 ms square wave) are injected into Purkinje cells and the current responsible for the first voltage response was used to estimate the rheobase. The results showed that the current thresholds for eliciting an AP in Purkinje cell were similar between *mdx* and LC mice, indicating that the membrane excitability of *mdx* Purkinje cells is preserved and was not impacted by dystrophin deficiency. This finding is different from the findings in *mdx* muscle, where the absence of dystrophin led to a significant reduction in muscle excitability which in turn increased the susceptibility to contraction-induced muscle injury in these mice (Roy *et al.*, 2016). The authors reported that the voltage required to elicit 50% of maximal force was significantly increased in response to direct muscle stimulation in the tibialis anterior muscle of *mdx* mice. They suggested that the increased threshold for AP generation is an indication of reduced muscle excitability.

Despite the unchanged rheobase, the amplitude of the first spike elicited by rheobasic stimulation in *mdx* Purkinje cells was significantly lower than LC cells. The magnitude of the AP amplitude is regulated by sodium channel. During membrane depolarisation, the voltage-

gated sodium channels open, allowing the entry of sodium ions into the cell, further raising the cell membrane potential (depolarisation). Repolarisation, which happens immediately after depolarisation, is due to the inactivation of voltage-gated sodium channels. During the inactivation, sodium ion channel closes and the permeability to sodium ions decreases, returning the membrane potential to its resting state. The importance of sodium channels in the AP amplitude is well demonstrated by Ogiwara *et al.* (2007), in which mice with impaired sodium channel function as a result of *Scn1a* (sodium channel gene encoding Nav1.1) mutations had a reduced spike amplitude in the trains of evoked APs in the parvalbumin-positive interneurons located at the neocortex. More importantly, the loss of sodium channel function followed by a reduced sodium current resulted in a significant decrease in AP amplitude in cardiomyocytes of 4-6 months old dystrophic mice (Koenig *et al.*, 2011). Taken together, the reduced AP amplitudes in *mdx* Purkinje cell may reflect a change in normal sodium channel function as a consequence of dystrophin deficiency.

In addition, a significant increase in the 10-90% rise time and a significant decrease in the 10-90% rise slope (mV/ms) of AP in *mdx* mice were found. This result is consistent with earlier findings from our group, which also showed a trend towards an increase in the 10-90% rise time of evoked EPSP in the 3- month old *mdx* Purkinje cells when compared to wildtype cells, although this was not statistically significant (Anderson *et al.*, 2004; Anderson *et al.*, 2010). A similar study in malformed *mdx* myofibers also showed a 158.3% increase in AP time to peak (Hernandez-Ochoa *et al.*, 2015). The 10-90% rise time of an AP represents the time it takes to transition from 10% to 90% of the peak amplitude. This represents how quickly the activated receptors go from low to high ionic permeability while the rise slope describes the rate of voltage change. The decreased rise slope might reflect a difference in density of sodium channel expression or level of regulation of sodium channel activity by second-messenger-

regulated protein phosphorylation (Cantrell & Catterall, 2001; Kim *et al.*, 2012). Khaliq and Raman (2006) reported a decreased rise slope of Purkinje cells AP when the availability of perisomatic sodium channel was reduced by focal application of subsaturating concentration of TTX, a sodium channel blocker. These findings of a reduced amplitude and rise slope of AP in *mdx* Purkinje cells suggest that dystrophin deficiency might be associated with an altered sodium channel availability or function.

Afterhyperpolarisation occurs after the AP and it is generated by the voltage dependent potassium conductance activated during the spike, which rapidly hyperpolarises the membrane then deactivates slowly over 10 ms (Bean, 2007). Interestingly, using peak hyperpolarisation relative to spike threshold as an index for AHP amplitude, the amplitude of AHP following the first spike elicited by rheobasic stimulation in *mdx* Purkinje cells was found on average 88.5% higher than its LC. However, this increased in AHP amplitude was not significantly different from that of its LC. This increment in AHP was also accompanied by a tendency for an increase in both the time to AHP and half-height recovery time. It has been well established that the duration and actual depth of AHP could be regulated by the calcium-activated potassium channels (Han *et al.*, 2015). Several studies have shown that potassium channels including large conductance calcium-activated potassium channels (BK channels), small conductance calcium-activated potassium channels (SK channels), and voltage-gated potassium channels 7 (Kv 7) underlie AHP activation (Bond *et al.*, 2004; Edgerton & Reinhart, 2003; Lawrence *et al.*, 2006; Storm, 1987). In particular, the BK channels in Purkinje cells are coupled with P/Q type calcium channels and are activated by depolarisation and calcium influx during APs, playing an important role in AP repolarisation and AHP (Bock & Stuart, 2016; Edgerton & Reinhart, 2003; Raman & Bean, 1999; Sausbier *et al.*, 2004). Blocking of the BK channel using iberiotoxin in rat Purkinje neurons showed significantly reduced AHP amplitude

without having any impact on the spike width at half amplitude. This demonstrated the involvement of BK channels in shaping the AHP waveform (Edgerton & Reinhart, 2003). Interestingly, it was also suggested that the BK channel activity could affect the induction of LTD at parallel fibre-Purkinje cell synapse possibly through its role in regulating the amount of Ca^{2+} influx that accompanies each climbing fibre-evoked spike (Edgerton & Reinhart, 2003; Ito, 1989). Taken together, given the fact that the reduced LTD was found in 3-month-old *mdx* Purkinje cells when compared to its WT controls (Anderson *et al.*, 2004), and potentially altered BK channel function in dystrophic Purkinje cells due to the trend of an increase amplitude in *mdx* AHP as seen here (although no significant difference was found), further study on channel function in dystrophic animals is essential to clarify if they are associated with the altered synaptic depression (LTD) in *mdx* mice.

6.4.2 Action potential firing patterns of *mdx* Purkinje cell

Earlier studies have identified four types of AP firing patterns in Purkinje cells from acute brain slices, reflecting differences in the input-output functions of these cells. Firing patterns include tonic firing, complex bursting, initial bursting and gap firing (Edgerton & Reinhart, 2003; Kalume *et al.*, 2007; Kim *et al.*, 2012; Nelson *et al.*, 2003). The current study identified two populations of Purkinje cells with distinct firing patterns when 500 ms depolarising current injections were given in both *mdx* and LC cerebellar slices. The tonic firing Purkinje cells, which is depicted by continued discharge of APs in response to depolarising current injections is shown in Figure 6.7 A. It was reported that tonic firing cells were able to fire at low firing rate in response to mild depolarisation and linearly increasing this response with greater stimulus intensity and eventually cease firing in response to stronger stimulation (Prescott & De Koninck, 2002). This firing pattern was also reported in a study with P21-P23 Sprague-Dawley rats by Kim and colleagues (2012). The authors, showed that tonic firing cells

displayed greater firing frequency in response to growing current intensity until Na^+ spike failure occurred (Kim *et al.*, 2012).

In the current study, the membrane properties of tonic firing Purkinje cells in the *mdx* mice were not significantly different from LC cells (Table 6.4). The average AP amplitude and AP AHP amplitude in *mdx* group tended to be lower and higher respectively, when compared to the LC group. However, these differences were not statistically significant. This may be due the small number of cells displaying tonic firing for both genotypes. Only 3 out of 9 recorded *mdx* cells and 3 out of 11 recorded LC cells were identified as tonic firing neurons. In these tonic firing neurons, the numbers of spikes varied within the same animal group when they were stimulated using the same stimulus strength (Table 6.2). This was because cells with higher input resistance (LC2: 244 MΩ; *mdx*1: 228 MΩ, *mdx* 2: 233 MΩ) were able to start firing at depolarising current injection as low as 100 pA, whereas cells with lower input resistance (LC1: 40 MΩ, LC3: 28 MΩ; *mdx*3: 47 MΩ) only started to fire at 500 pA.

Input resistance of a cell is affected by the cell size and the number of open ion channels (Chang *et al.*, 2005). Increase cell size and the number of open ion channels will result in a lower input resistance and require more current injection to induce voltage changes according to Ohm's law (V=IR). Taken together, the current finding of different input resistances in the tonic firing neurons may imply that the recorded Purkinje cells varied in size. This is possible as current recording from Purkinje cells were performed randomly on different folia in the cerebellar vermis. Indeed, regional differences in the diameter of Purkinje cell axons and in the morphology of the dendritic trees had been reported in Purkinje cells located in the base compared with the apex of a folium (Cerminara *et al.*, 2015; Nedelescu & Abdelhack, 2013). Remarkably, a significant higher input resistance was reported in tonic firing Purkinje cells

located in cerebellar vermis lobule III-V as compared to those in lobule X (Kim *et al.*, 2012). In short, no significant difference was found in the membrane properties of tonic firing cells between the *mdx* and LC groups and this may be attributed to the small *n* numbers found in tonic firing neurons. The differences in the spike numbers seen in the tonic firing neurons may be due to the different input resistance of each cell and the differences in input resistance may be explained by the regional variations in Purkinje cell size and morphology.

The second type of discharge patterns found in this study was the initial bursting firing pattern. This type of firing pattern was also demonstrated in both *mdx* and LC mice (Figure 6.7 B). When compared with the first spike, the successive spikes of initial bursting neurons were found to have lower AP amplitude and higher AP threshold. Similar to the tonic firing Purkinje cells, no significant difference was found in the membrane properties of the initial bursting cells between *mdx* (n=6 cells) and LC (n=8 cells) groups (Table 6.5) although a tendency towards a longer 10-90% rise time or smaller 10-90% rise slope was found in the *mdx* group when compared to the LC group. Together with the tonic firing group, the significant differences reported for the membrane properties (AP amplitude, 10-90% rise time and rise slope) in all Purkinje cells in section 6.3.1 were not seen in the initial bursting cells between *mdx* and LC. This could be due to a smaller *n* number that was generated for each group when the cells were further categorised into the tonic firing and initial bursting groups.

Studies in Purkinje cells from acute slice preparation as well as from organotypic cerebellar slice culture showed that the initial bursting neurons are characterised as those that fired once or only a few spikes at the start of the depolarising current and then stayed silent during the rest of the current pulse stimulus (Cavelier *et al.*, 2002; Kim *et al.*, 2012; Pouille *et al.*, 2000). These neurons were incapable of firing at steady state, discharging only transient AP followed

by a long plateau potential. An unstable equilibrium state had been proposed as the mechanism that underlies this long plateau potential. Llinas and Sugimori (1980b) suggested that at least three simultaneously occurring voltage-dependence conductance were involved in this state, namely, a non-inactivating Na^+ conductance, a non-inactivating K^+ conductance and a dominant Ca^{2+}-dependent component. In addition to Llinas and Sugimori (1980b), Kim *et al.* (2012) showed that A-type K^+ currents (I_A) exert an effect on the formation of the initial bursting pattern in Purkinje cells. This is evident by the recovery of repetitive firing of rat Purkinje cell induced by depolarising current injection when the potassium channel blocker 4-aminopyridine was added to the bath. Additionally, rapid inactivation of fast Na^+ current may account for the generation of the initial bursting pattern as evidence of decreasing spike height and increasing spike threshold in the succeeding spike of the initial burst. The relevance of Na^+ current inactivation in this firing pattern was also demonstrated by several other studies which showed that Purkinje cells exhibiting the initial bursting pattern and could not maintain firing during current injections in sodium channel (Nav1.6) knockout mice, in which the transient Na^+ current was inactivated more rapidly than the WT mice (Kohrman *et al.*, 1996; Raman & Bean, 1997).

There was concern if the initial bursting Purkinje cells in the current study represented an unhealthy or damaged Purkinje cell population, given that damaged cells may cease repetitive firing. An early study suggested that the ceased repetitive firing of damaged cells was correlated to the low input resistance in the damaged cells (Alger *et al.*, 1984) . There are some explanations to suggest that the initial bursting Purkinje cells in the current study constituted a genuine group and are not damaged cells. Firstly, the discharging patterns of current Purkinje cell do not correlate with the input resistance. If initial bursting was a form of damaged cells discharging pattern, then it should correlate to a particular group, such as the low input

resistance group. However, it was found that cells with near 100 MΩ or above 200 MΩ could display tonic firing or initial bursting patterns in both groups, indicating that firing patterns of these cells in the current study were not dependent on the input resistance. Therefore, it is not surprising that a mixture of firing patterns was exhibited in both *mdx* and LC groups since the statistical analysis also showed no significant differences in input resistance between groups. Secondly, a similar resting membrane potential and spike overshot 0 mV were seen in all recorded cells before the depolarising protocol were given, demonstrating that they were all healthy cells.

The presentation of these two firing patterns in *mdx* and LC mice in the current study demonstrated that Purkinje cells in both groups exhibited similar spike firing patterns. Overall, no significant difference in membrane properties was found in *mdx* Purkinje cells when compared to LC cells, and this may be limited by the small *n* number in each firing pattern group. Nevertheless, a trend of changes in AP amplitude, AP AHP amplitude, 10-90% rise time and 10-90% rise slope were observed in *mdx* neurons. Supporting the potential changes in the Purkinje cells intrinsic properties in the *mdx* animal, an *in vitro* experiment by Snow *et al.* (2014) showed that the loss of dystrophin resulted in an irregular AP firing activity and lower AP firing rate in dissociated *mdx* Purkinje cells as compared to those in WT mice. The authors also reported that the membrane potential of *mdx* Purkinje cells was more hyperpolarised than WT Purkinje cells. Interestingly, a significant lower Purkinje cells simple spike firing rate and an increased complexed spike regularity were also reported in the awake and anesthetized female *mdx* mice when compared to its controls (Stay *et al.*, 2019). Taken together, dystrophin is important for normal Purkinje cell function and the absence of this protein may result in altered Purkinje cell firing properties.

6.4.3 Calcium signalling of *mdx* Purkinje cell

Calcium is a major intracellular signalling molecule that plays a fundamental role in controlling and modulating a variety of physiological functions in neurons (Berridge, 1998; Ghosh & Greenberg, 1995). These functions include neuronal excitability, firing patterns, neurotransmitter release, synaptic plasticity and circuit formation (Kitamura & Kano, 2013). Since calcium has a substantial role in many physiological activities and the fact that altered calcium homeostasis has been described in several cells that lack dystrophin, the calcium handling properties of mature *mdx* Purkinje cells was investigated by measuring the baseline $[Ca^{2+}]_i$ for the cell soma and distal dendrites as well as the dendritic calcium changes evoked by electrode stimulation applied at the PFs.

6.4.3.1 Resting $[Ca^{2+}]_i$ of *mdx* Purkinje cell soma and distal dendritic branches

In the current study, the average baseline $[Ca^{2+}]_i$ levels of Purkinje cells measured in both the cell soma and distal dendritic regions in *mdx* and LC mice were found within a range of 0.17-0.22 (340/380 ratio). These low ratios parallel the findings of Tank *et al.* (1988), where the authors showed that resting $[Ca^{2+}]_i$ levels were low throughout the cell (<60 nM), with a slightly lower level in the dendritic branches than in the soma of Purkinje cell in the guinea pig. Similarly, Konnerth *et al.* (1992) reported low resting $[Ca^{2+}]_i$ levels in the Purkinje cell soma and dendrites, which were all below 100 nM.

In the Purkinje cell soma, the average 340/380 ratio of resting $[Ca^{2+}]_i$ levels in the *mdx* population were significantly higher when compared to its LC population. However, no significant difference in resting $[Ca^{2+}]_i$ levels was observed in the distal dendrites between the two genotypes. The significant increase in resting $[Ca^{2+}]_i$ in *mdx* Purkinje cell soma is similar to findings of previous reports in various dystrophic cells including skeletal muscle fibres (Turner

et al., 1988; Williams *et al.*, 1990), cardiomyocytes (Tsurumi *et al.*, 2019), cortical and hippocampal neurons (Lopez *et al.*, 2016) and cerebellar granule cells (Hopf & Steinhardt, 1992).

The elevation of $[Ca^{2+}]_i$ is one of the major hallmarks in DMD. It is thought to serve as one of the major candidates for the initiation of muscle weakness that is commonly seen in *mdx* mice and in patients with DMD (Allen *et al.*, 2010; Allen *et al.*, 2016; Bodensteiner & Engel, 1978). More recently, an increase in calcium loading was also found in cardiomyocytes differentiated from human induced pluripotent stem cells derived from a DMD patient (Tsurumi *et al.*, 2019). An increase in calcium loading may result in cardiac damage leading to cardiomyopathy, the major cause of death among DMD patients (Tsurumi *et al.*, 2019). In view of the damages resulting from elevated $[Ca^{2+}]_i$ in different cell types, the altered resting $[Ca^{2+}]_i$ in Purkinje cells may impair the cell function in *mdx* mice, since Ca^{2+} is a key regulator of cell signalling/synaptic plasticity. If similar calcium perturbation is also found in the brain of DMD patients, a therapeutic approach targeting calcium dyshomeostasis may be useful in ameliorating any behavioural/cognitive dysfunctions seen in these patients.

Interestingly, a recent study showed that an increase of calcium deposits in 12-week-old *mdx* muscles was linked to reduced mitochondrial respiration, suggesting that the normal mitochondria function could be altered as a result of dystrophin deficiency (Gaglianone *et al.*, 2019). In neurons, mitochondria, the ATP supplier, are one of the important candidates in ATP-dependent calcium buffering or clearance mechanisms, to produce energy and act as calcium storage (Fierro *et al.*, 1998; Inoue, 2003; Ivannikov *et al.*, 2010). Calcium clearance demands very high ATP consumption, and it has been estimated that this process consumes more than 70% of all neuronal ATP (Attwell & Laughlin, 2001; Erecinska & Dagani, 1990;

Matsumura & Clark, 1982). Hence, it is expected that altered mitochondria function could impact on calcium homeostasis. Fierro *et al.* (1998) demonstrated that the resting $[Ca^{2+}]_i$ in Purkinje cell soma was increased when calcium uptake by mitochondria was blocked with addition of protonophores. Similarly, a more recent study showed that mitochondrial inhibitors cause a delay in $[Ca^{2+}]_i$ clearance in Purkinje spines, followed by the dendrites and the soma (Ivannikov *et al.*, 2010). This in turn led to a gradual increase in $[Ca^{2+}]_i$ in Purkinje cell soma, followed by the dendrites and the spines. The authors suggested that the gradual delay of $[Ca^{2+}]_i$ clearance in the different neuronal compartments is directly correlated with the normal mitochondrial distribution in neurons. In fact, the density of mitochondria in the dendrites is typically lower than in the soma (Ivannikov *et al.*, 2010). Most of the spines are devoid of mitochondria whereas the soma and proximal dendrites have more mitochondria (Li *et al.*, 2004; Muller *et al.*, 2005; Shepherd & Harris, 1998; Wu *et al.*, 1997). Taken together, the increased resting $[Ca^{2+}]_i$ in *mdx* Purkinje cell soma but not in the distal dendrites in the current study may be linked to altered mitochondrial respiration. Supporting this argument, the distribution of mitochondria is highly dynamic in different neuronal regions typically with a higher density in the cell soma but a much lower density in the dendritic regions. This may also explain that the current finding of unaltered calcium level in *mdx* distal dendrites is not unanticipated as altered mitochondrial respiration may not happened in dendritic regions which normally have limited expression levels of mitochondria in comparison to the somatic region.

6.4.3.2 Dendritic calcium change evoked by parallel fibre input

The Purkinje cell is the only output of the cerebellar cortex. It has highly branched dendrites and receive two types of excitatory inputs from a single CF and more than 100,000 PFs. These excitatory inputs lead to a wide range of dendritic Ca^{2+} signals in the postsynaptic Purkinje cell. The increase of postsynaptic $[Ca^{2+}]_i$ is very important in long-term synaptic plasticity including

LTP and LTD at PF synapse (Ekerot & Kano, 1985; Ito & Kano, 1982; Kakizawa *et al.*, 2012; Konnerth *et al.*, 1992; Lev-Ram *et al.*, 1992; Sakurai, 1987), and LTD at CF synapse (Hansel & Linden, 2000; Shen *et al.*, 2002; Weber *et al.*, 2003). The distinct synaptic plasticity in Purkinje cells is governed by the complex calcium signalling that arise from different Ca^{2+} sources including Ca^{2+} influx via the VGCCs and Ca^{2+} release from intracellular stores mediated by the mGluRs signalling pathways (Finch & Augustine, 1998; Inoue *et al.*, 1998; Konnerth *et al.*, 1992; Takechi *et al.*, 1998). It is well documented that the level of postsynaptic Ca^{2+} elevation is the critical factor determining the direction of plasticity. For instance, a higher elevated $[Ca^{2+}]_i$ level is required for PF-LTD induction than in PF-LTP induction, with the former contributed by CF inputs (Coesmans *et al.*, 2004; Wang *et al.*, 2000).

It is interesting that the absence of dystrophin in Purkinje cells has severe impact on both heterosynaptic and homosynaptic LTD at the PF-Purkinje cell synapse in the *mdx* mouse (Anderson *et al.*, 2004; Anderson *et al.*, 2010). The heterosynaptic LTD, which required simultaneous and repetitive activation of PF and CF, is reduced in 3-months old dystrophic mice (Anderson *et al.*, 2004). On the other hand, the homosynaptic LTD, which required only strong monosynaptic input from PF (Hartell, 1996), was enhanced in the same age group of *mdx* mice (Anderson *et al.*, 2010). As postsynaptic calcium level is very important in determining the direction of plasticity at PF synapse, the perturbation of both types of LTD in the *mdx* mouse Purkinje cells is likely a result of abnormal Ca^{2+} homeostasis. To investigate if the absence of dystrophin was affecting calcium signalling in Purkinje cells, the dendritic calcium changes evoked by distal dendritic stimulation in mature *mdx* mice was measured. Consistent with findings in the earlier studies, the current result illustrated that the dendritic Ca^{2+} change signals evoked by distal dendritic stimulation are highly confined to the stimulation site (Hartell, 1996; Rancz & Hausser, 2006; Schreurs *et al.*, 1996; Wang *et al.*,

2000). However, in line with previous findings, the change of somatic Ca^{2+} was barely detectable, due to an absence of VGCCs at the soma (Inoue *et al.*, 2001; Konnerth *et al.*, 1992; Kuruma *et al.*, 2003; Lev-Ram *et al.*, 1992). Indeed, the distribution of VGCCs are non-uniform in Purkinje cells, where a much higher Ca^{2+} channel density is found in the dendritic region than in the somatic region (Llinas & Sugimori, 1980a, 1980b).

When comparing the calcium changes in LC and *mdx* mice, the magnitude changes in $[Ca^{2+}]_i$ induced by PF stimulation in *mdx* dendrites was not significantly different from LC mice. This indicated that the absence of dystrophin may not exert an effect on calcium handling in *mdx* mice. Consistent with current findings, a recent study showed that electrically evoked Ca^{2+} transient peaks in *mdx* cardiomyocytes were similar to that in the WT mice (≥ 1 year of age) (Rubi *et al.*, 2018). In contrast, the findings in *mdx* FDB muscle fibres show that the amplitude of AP evoked Ca^{2+} transient was significantly decreased as a result of dystrophin deficiency (Hollingworth *et al.*, 2008; Woods *et al.*, 2004). Studies suggest that the reduced AP evoked Ca^{2+} transient and the increase in basal $[Ca^{2+}]_i$ level in the dystrophin-deficient muscle fibre are resulted from the impaired structure and function of RyRs, the Ca^{2+}-induced Ca^{2+} release channels that are located on the SR (Bellinger *et al.*, 2009; Kuwajima *et al.*, 1992; Llano *et al.*, 1994). A recent study showed that after a 4 weeks treatment of S48168, an RyR calcium release channel stabiliser that inhibits SR Ca^{2+} leaks, the pathologic Ca^{2+} leakage in the *mdx* myofibres was reduced compared to *mdx* vehicle-treated myofibres (Capogrosso *et al.*, 2018). Interestingly, the types of RyRs that are expressed in the skeletal muscle are also found in the endoplasmic reticulum of Purkinje cells, making Purkinje cells unique compared to other CNS neurons (Fierro *et al.*, 1998; Kuwajima *et al.*, 1992). Given the similarity of the type of RyRs expressed in both *mdx* myofibres and in Purkinje neurons, the normal function of RyRs in *mdx* Purkinje cells may also be impaired, resulting in increased Ca^{2+} release by RyRs. However, in

the current study, the calcium handling of *mdx* Purkinje cells was comparable to its LCs as the calcium changes in *mdx* during distal dendritic stimulation was not significantly altered when compared to its LC.

It is known that the rising phase of Ca^{2+} transient is determined by Ca^{2+} influx from extracellular space via plasma-membrane-bound cation channels and Ca^{2+} release from intra-cellular Ca^{2+} stores (Finch & Augustine, 1998; Takechi *et al.*, 1998) while the falling phase, that particularly affects the amplitude and decay time course of Ca^{2+} transient, is determined by Ca^{2+}-binding proteins and Ca^{2+} pumps (Fierro *et al.*, 1998). The potential effect of a chronic Ca^{2+} rise by RyRs dysfunction may be compensated for by highly concentrated endogenous Ca^{2+}-binding proteins including calbindin D_{28k}, calmodulin and parvalbumin in Purkinje cells (Bastianelli, 2003; De Talamoni *et al.*, 1993). Several studies have shown that the parvalbumin-positive and calbindin-positive interneuron were significantly increased in different parts of *mdx* brain region including the somatosensory and motor cortices, and proximal radiatum of hippocampal field CA1 (Carretta *et al.*, 2004; Carretta *et al.*, 2003; Del Tongo *et al.*, 2009). The authors speculated that the increase of Ca^{2+}-binding proteins in *mdx* mice may function as a compensatory mechanism to counteract the increased $[Ca^{2+}]_i$ as a result of the absence of dystrophin. Taken together, this suggests that if the leaky RyRs were accompanied by an increase in Ca^{2+}-binding proteins in Purkinje cells of *mdx* mice, the increase in $[Ca^{2+}]_i$ may be attenuated by the counteracting process of the binding of free Ca^{2+} to Ca^{2+}-binding proteins. This may explain the finding that there was no difference seen in the calcium handling ability in *mdx* Purkinje cells as compared to its LC. Additional experiments focusing on the mechanism of Ca^{2+} release or Ca^{2+} buffering may be useful in further characterising the calcium handling properties in *mdx* mice.

6.5 Conclusion

In summary, using the simultaneous whole-cell patch clamp and ratiometric calcium imaging in Purkinje cells, the current study showed some alterations in the active membrane properties of mature *mdx* Purkinje cell and this was accompanied by an increase in resting $[Ca^{2+}]_i$. Several parameters of AP elicited at rheobase were also significantly altered in the *mdx* mouse. These include the reduced amplitude, increased 10-90% rise time, and decreased 10-90% rise slope. Interestingly, the AP AHP in *mdx* population also had an overall increasing trend in its amplitude, time to AHP (ms), and half-height recovery time (ms). The AP firing patterns in both LC and *mdx* Purkinje cells displayed the tonic firing and initial bursting characteristics. Although the resting $[Ca^{2+}]_i$ was increased in *mdx* cell soma, the synaptically activated $[Ca^{2+}]_i$ changes in *mdx* Purkinje dendrites are similar to those in LC Purkinje dendrites. The results from this chapter suggest that dystrophin is necessary for normal Purkinje cell activity and its loss may also lead to impaired calcium homeostasis in the Purkinje cell soma.

Chapter 7. General discussion and conclusion

Duchenne muscular dystrophy is a monogenic disease, caused by the absence of dystrophin or expression of a non-functional truncated dystrophin protein. Dystrophin is a key protein of the DAPC, located at the inner surface membrane in both muscle and non-muscle tissues. Evidence suggest that dystrophin regulates the interactions between the cytoskeleton, cell membrane and extracellular matrix (Perronnet & Vaillend, 2010; Pilgram *et al.*, 2010). In muscle, dystrophin is important for the regulation of intracellular calcium homeostasis (Bakker *et al.*, 1993; Bellinger *et al.*, 2009; Franco & Lansman, 1990; Lovering *et al.*, 2009). Brain dystrophins together with the DAPC are associated with the maintenance and stabilisation of ion channels and receptors, which are essential to synaptogenesis and synaptic transmissions (Anderson *et al.*, 2003; Knuesel *et al.*, 1999; Vaillend *et al.*, 2010). Boys born without this protein suffer from progressive muscle degeneration and usually have a premature death, in their early 20s due to cardiac and respiratory complications. In addition to muscle impairment, about 1/3 of these patients also suffer from mild to severe non-progressive cognitive deficits. The mean IQ score of these boys is about one standard deviation lower than those of the general population (Ogasawara, 1989). The common clinical presentations of cognitive dysfunctions in these boys includes a delay in speech, poor verbal fluency and reading skills. Suzuki *et al.* (2017) reported that while the executive functions (i.e. strategic planning, organised searching, utilisation of environmental feedback to shift cognitive sets, behavioural direction toward achieving goal, and modulation of impulsive responses) of DMD patients deteriorate with age, their verbal IQ remains weak in both children and adults with DMD (Ueda *et al.*, 2017). In contrast, a meta-analysis of 1224 children with DMD showed that the deficits in verbal and language skills were less evident in older DMD patients, suggesting that these specific intellectual function change with age (Cotton *et al.*, 2005).

It has been argued that DMD is a cerebellar disorder because of the similarities in the type of cognitive deficits present in both DMD and cerebellar lesions. The verbal and language impairments (e.g., limited verbal span, difficulty with phonological processing and reading) in DMD are also seen in patients with cerebellar disease (i.e. injury, tumour, etc). It is believed that these cognitive impairments are caused by the absence of dystrophin in the cerebellar Purkinje cells of DMD patients. Dystrophin, typically expressed at the postsynaptic density of these neurons is thought to be involved in $GABA_AR$ clustering during synaptogenesis (Knuesel *et al.*, 1999). The loss of dystrophin in central synapses impairs both the postsynaptic membrane receptor clustering and synaptic transmission in *mdx* mice, a dystrophin-deficient mouse model widely used in DMD studies (Anderson *et al.*, 2003; Bulfield *et al.*, 1984; Knuesel *et al.*, 1999). These central perturbations may help explain the cognitive deficits and mental dysfunction associated with DMD. Whether the synaptic functioning is altered with aging remains unclear, as most studies were performed in young animals (about 3 months old) with only limited studies reporting the pathophysiology of DMD in old *mdx* mice. The findings from the old *mdx* mouse are highly regarded, because it has been shown that the disease progression in muscle, brain biochemistry, and behavioural disturbances in aged *mdx* better resembles that of the human DMD pathophysiology.

Moreover, with the improvement in multidisciplinary care and careful symptomatic treatment, including cardiopulmonary and nutritional intervention, it is no longer rare to finds patients with DMD surviving past the age of 40 (Doorenweerd *et al.*, 2017; Saito *et al.*, 2017; Villanova & Kazibwe, 2017). The mean age of DMD patients have increased from 23.6 to 30.1 years from 1999 to 2012 (Saito *et al.*, 2014). With the increase lifespan of DMD patients, it is becoming more important to understand the brain pathophysiology in DMD and to develop intervention which ameliorates the cognitive dysfunction and improves the quality of life in

adult DMD patients. This dissertation aims to provide insight into the role of dystrophin in the cerebellum extending previous finding in *mdx* mice, to include aged 11-12 months old and 23-26 months old *mdx* mice.

7.1 The role of dystrophin in Purkinje cells synaptic functions of old *mdx* mice

The major findings in this thesis confirmed and extended the findings from Kueh *et al.* (2011), in which the alteration in inhibitory input (GABAergic synapse transmission) in 3 months old Purkinje cells was also seen in the old *mdx* mouse (Chapter 3). Although the mIPSCs amplitude and frequency were significantly reduced in the *mdx* mice when compared to its LC, the magnitude of these changes remained similar comparing the young and old animal groups. This suggests that the impaired mIPSCs function in *mdx* mice did not progress with age. This finding supports the notion that the cerebellar involvement in DMD is non-progressive, consistent with the non-progressive and persistent poor verbal IQ reported in human DMD (Ueda *et al.*, 2017).

The reduced mIPSCs amplitude in the aged *mdx* mice resembles the finding in young *mdx* population. As mIPSCs amplitude is determined by the postsynaptic receptor number and conductance (Graziane & Dong, 2016; Nusser *et al.*, 1997), the reduced mIPSCs amplitude in the current study strongly suggest a similar alteration in the postsynaptic receptor number in the old and young *mdx* mouse. The current findings extend previous observations and electrophysiological evidence in young *mdx* to include aged animals, supporting the importance of dystrophin in postsynaptic receptor clustering throughout the lifespan of *mdx* mice (Knuesel *et al.*, 1999). In addition, current findings of similar mIPSCs amplitudes between the young and aged animals of both phenotypes may suggest that GABA signalling in the cerebellum is well preserved during aging. Evidence supporting this notion comes from a previous study in which

it was found that despite a significant decrease in the $GABA_AR$ α1 subunit mRNA expression in the cerebellum of aged rat (24-month-old), the expression of $GABA_AR$ α1 protein in aged rat was similar to those in young (2-month-old) rat (Gutiérrez *et al.*, 1997). Similarly, a recent human study did not find any significant difference in the expressions of $GABA_AR$ (α1, α2, α5, β3, and γ2 subunits) in pathologically normal cerebellum comparing the older (76 years ± 1.3 years) and younger (51.7 years ± 5.1 years) groups (Pandya *et al.*, 2019). Taken together, these reports and the findings in this study may suggest that there are no age-related changes in the expression of $GABA_AR$ α1 protein in the cerebellum of LC and *mdx* mice and that the altered mIPSCs amplitude seen in *mdx* animals is solely dependent on dystrophin loss.

Interestingly, this reduced mIPSCs amplitude was accompanied by a reduction in mIPSCs frequency. Altered mIPSCs frequency may imply a change in the presynaptic release probability (Graciotti *et al.*, 2008). Evidence supporting this notion comes from a recent study in which it was found that there were significant changes in the release and uptake of GABA in the cerebellum of *mdx* mice (Pereira da Silva *et al.*, 2018). Using synaptosomes isolated from the *mdx* and LC mice, the authors demonstrated a significant decrease (47%) in nicotine-induced GABA release, and an increased rate (44%) of GABA uptake in the synaptosomes of *mdx* cerebellum. As nicotinic acetylcholine receptors are calcium permeable ion channels that are involved in enhancing neurotransmitter release (McGehee *et al.*, 1995), the decrease in nicotine-induce GABA release may reflect a change in presynaptic calcium level. Whether there was a change in presynaptic calcium that resulted in reduced mIPSCs frequency associated with dystrophin loss remains unclear and requires further examination.

Reductions in both mIPSCs amplitude and frequency indicate a total reduction in synaptic strength (or net decrease in inhibition). This net decrease in inhibition in *mdx* Purkinje cells,

may over time disrupt the normal synaptic transmission in the brain and if they are not compensated for by homeostatic mechanisms, may underlie the cognitive impairment found in *mdx* mice. Indeed, elevated brain excitatory activity was suggested in *mdx* mice when compared to control mice (Rae, Griffin, *et al.*, 2002). By measuring glucose metabolism in *mdx* brain using MRS, the authors found that an increased flux of glucose (^{13}C) into brain metabolites associated with a decreased level of free glucose in the *mdx* brain. Their findings implicate that more glucose was needed for oxidation in *mdx* mice than in controls, suggesting a decrease inhibition in *mdx* brain as normally, excitatory stimulation results in increased glucose metabolism while inhibitory activation results in decreased glucose metabolism (Dienel, 2019; Ito *et al.*, 1994; Rae *et al.*, 2000).

The total reduction in inhibitory synaptic transmission may imply that, neuronal homeostasis in the CNS is severely perturbed with the loss of dystrophin. Homeostasis is the central concept in physiology describing a complex set of mechanisms that regulate the constancy of the internal environment (Turrigiano & Nelson, 2004). It is regulated by the constancy of temperature, pH, and electrolyte concentration. To maintain cellular homeostasis, the presynaptic compensatory effect in response to postsynaptic modification has been well described in several studies (Davis *et al.*, 1998; Paradis *et al.*, 2001). In mouse neuromuscular junction, a reduction in postsynaptic clustering of acetylcholine receptors (resulting from a knockdown of neuregulin) induces a compensatory presynaptic elevation in transmitter release (Sandrock *et al.*, 1997). Unfortunately, this compensatory mechanism was not seen in the Purkinje cell synapses of *mdx* mice (i.e. the reduced mIPSCs amplitude was accompanied by a reduced mIPSCs frequency). The findings reported in this thesis may imply that the perturbation in *mdx* postsynaptic site (mIPSCs amplitude), that is usually rich with dystrophin expression in control mice, may be extended to the presynaptic site (mIPSCs frequency).

A possible explanation for these differences is the involvement of a more complex homeostatic response in brain synapse in comparison to the simpler response in skeletal muscle. At excitatory brain synapses, the presynaptic release probability (frequency) remains the same when there is an increase in postsynaptic receptor clustering (increase amplitude of α-amino-3-hydroxy-5-methyl-4-isoxazole propionic acid (AMPA) miniature excitatory postsynaptic current or mEPSCs) in postnatal cortical and spinal cord culture during the inhibition of excitatory synaptic transmission with AMPA receptor blockade (chronic inhibition through incubation with 300 µM APV and 10 µM CNQX) (O'Brien *et al.*, 1998). To complicate things further, both the frequency and amplitude of mEPSCs were increased when a similar experiment was performed in hippocampal cultures (Thiagarajan *et al.*, 2002). These different presynaptic responses to postsynaptic modifications indicate that the homeostatic mechanisms regulating the synaptic strength in central neurons can be very complex.

Synaptic connections in central neurons are highly plastic due in part to the numerous synaptic inputs (hundreds or even thousands) received by neurons (Turrigiano & Nelson, 2004). The number and strength of these synapses can be modified significantly during development in response to many factors impinging on the neuron and local neural network. Evidence shows that the nervous system has a remarkable ability to adjust or compensate for synaptic perturbation. However, this is not the case in *mdx* mice. The loss of dystrophin resulted in impaired homeostasis at the Purkinje cell synapses through the synergistic effects, of both a reduction in mIPSCs amplitude and frequency. This consequently results in a reduction of inhibitory transmission in *mdx* mice. This dyshomeostasis between pre- and postsynaptic GABAergic synapses in dystrophic Purkinje cells may ultimately contribute to the learning and memory impairments as well as the behavioural abnormalities seen in *mdx* mice, and possibly in human DMD if humans and mice share a similar neuropathophysiology.

7.2 The dystrophin rescued by exon skipping reversed the altered GABAergic transmission in organotypic cerebellar culture derived from *mdx* mice

Since dystrophin plays an important role in normal synaptic transmission in the CNS, the second part of this thesis (Chapter 4) was to examine if dystrophin expression can be rescued with an exon skipping strategy using AOs. Pip6f-PMO, one of the AOs conjugated with cell penetrating peptides, has been shown to have high efficacy in modulating dystrophin pre-mRNA to restore dystrophin reading frame and in producing a truncated but semi-functional protein (Betts *et al.*, 2012). While effective dystrophin correction using Pip6f-PMO has been reported in both skeletal muscle and non-skeletal muscle tissue, including the heart in *mdx* mice, there is currently no studies to my knowledge that investigate its potential in restoring dystrophin expression in the CNS.

It has been well illustrated in the literature as well as in Chapter 3, that dystrophin loss results in altered inhibitory inputs which was likely due to the reduction in the number and size of $GABA_AR$ clusters in the *mdx* mice. In the current study using cerebellar organotypic cultures prepared from young *mdx* pups (P8-P11), the treatment with 1 µM of Pip6f-PMO can successfully restore dystrophin expression in Purkinje cells. More importantly, the re-expression of dystrophin can correct both the altered ultrastructure and function of GABAergic synapses in the *mdx* culture. Ultrastructurally, Pip6f-PMO corrected the reduced size of $GABA_AR$ clusters to near WT level, while functionally it showed an increased peak amplitude of mIPSCs in the Pip6f-PMO treated Purkinje cells. These finding suggest that Pip6f-PMO is a potential therapeutic candidate in reversing the ultrastructural and functional changes linked to dystrophin loss in the cerebellum.

Dystrophin dependent behavioural deficits such as enhanced fear and anxiety are apparent in the *mdx* mouse. It is widely accepted that this is primarily due to dystrophin loss in the *mdx* amygdala, which is a brain region involved in fear and anxiety-related behaviours (Manning *et al.*, 2014; Sekiguchi *et al.*, 2009). Interestingly, the enhanced freezing seen in *mdx* mice in response to restraint was compensated with the intracerebral microinjection of morpholino oligonucleotide (Sekiguchi *et al.*, 2009). At the neural level and similar current findings of altered GABAergic synapses in *mdx* cultures, Sekiguchi *et al.* (2009) also demonstrated a reduction in the number of $GABA_AR$ α2 subunit clusters as well as a reduced frequency of norepinephrine-induced GABAergic inhibitory synaptic currents in the basolateral nucleus of the *mdx* amygdala. These findings suggest an involvement of GABAergic alteration underlying the dystrophin dependent fear and anxiety behaviour in the *mdx* mice.

In addition to the amygdala, there are also evidences supporting the cerebellum as an important brain region that is involved in the anxiety-related behaviours and disorders, such as consolidation and prediction of fear memory (Ke *et al.*, 2016; Lorivel *et al.*, 2014; Moreno-Rius, 2018; Sacchetti *et al.*, 2004). Numerous human neuroimaging studies on patients with post-traumatic stress disorder, a condition triggered by a traumatic episode(s) causing severe anxiety, showed an increase in cerebellar activity when they were either at resting condition or when presented with trauma-related pictures and, interestingly, symptom improvement in these patients was associated with a reduction in cerebellar activity (Bing *et al.*, 2013; Ke *et al.*, 2016). A study in VPA rats, an animal model for autism generated by prenatal application of valproic acid (VPA), reported that the increased anxiety-like behaviours in VPA rats were associated with a lower level of GABA expression, not only in the amygdala but also in the cerebellum (Olexova *et al.*, 2016). This study supports the associative relationship between amygdala and cerebellum as underlying the anxiety-like behaviours, and the involvement of the

GABAergic system. Interestingly, several animal and human studies have shown that drugs improving GABA transmission are effective in reducing abnormal fear and anxiety-related behaviours (Ballenger *et al.*, 1988; Rickels & Rynn, 2002; Toth *et al.*, 2012). Since the cerebellum is involved in these emotive functions, and it is likely that the GABAergic system is involved in the mechanisms underlying fear and anxiety, the ability of Pip6f-PMO seen in the current study to enhance the clustering and function of $GABA_AR$ in Purkinje cells may provide a useful avenue of investigation to ameliorate the abnormal fear and anxiety-behaviour exhibited in the *mdx* mice. As 24% to 69% of boys with DMD were found with anxiety, these findings may provide new insight into the management of neurobehavioral concerns in these patients (Banihani *et al.*, 2015; Latimer *et al.*, 2017; Lee *et al.*, 2018; Pangalila *et al.*, 2015).

Both findings from Chapter 3 and Chapter 4 strongly support a role for dystrophin in normal GABAergic function, and that the loss of dystrophin led to the reduced GABAergic transmission in *mdx* mice Purkinje cells. The working hypothesis is that the re-expression of dystrophin can ameliorate the reduction of $GABA_AR$ clustering and transmission in *mdx* mice. Insight into this hypothesis may be obtained by ascertaining if altered GABAergic synapses can be corrected by exon skipping-mediated dystrophin rescue. While findings on organotypic cerebellar cultures have provided some evidence towards proving the concept, the application of this therapeutic strategy to the whole animal in reversing the CNS deficits associated with dystrophin loss is still in its early infancy. This is because the molecular weight of cell-penetrating peptide-oligonucleotide conjugates is usually larger than 450 Da, which makes it almost impossible to cross the BBB if it is being delivered systemically (Abbott *et al.*, 2010). To overcome the BBB, several authors have attempted to deliver AOs to the brain of *mdx* animals using intracerebral microinjections (Dallerac *et al.*, 2011; Sekiguchi *et al.*, 2009; Vaillend *et al.*, 2010), with findings to date promising in *mdx* mice.

Both findings from Chapter 3 and Chapter 4 strongly support a role for dystrophin in normal GABAergic function, and that the loss of dystrophin led to the reduced GABAergic transmission in *mdx* mice Purkinje cells. The working hypothesis is that the re-expression of dystrophin can ameliorate the reduction of $GABA_AR$ clustering and transmission in *mdx* mice. Insight into this hypothesis may be obtained by ascertaining if altered GABAergic synapses can be corrected by exon skipping-mediated dystrophin rescue. While findings on organotypic cerebellar cultures have provided some evidence towards proving the concept, the application of this therapeutic strategy to the whole animal in reversing the CNS deficits associated with dystrophin loss is still in its early infancy. This is because the molecular weight of cell-penetrating peptide-oligonucleotide conjugates is usually larger than 450 Da, which makes it almost impossible to cross the BBB if it is being delivered systemically (Abbott *et al.*, 2010). To overcome the BBB, several authors have attempted to deliver AOs to the brain of *mdx* animals using intracerebral microinjections (Dallerac *et al.*, 2011; Sekiguchi *et al.*, 2009; Vaillend *et al.*, 2010), with findings to date promising in *mdx* mice.

To translate the potential therapeutic benefits of Pip6f-PMO to patients with DMD, low invasiveness and relative simplicity and safety of a route of administration is preferred. While more research is needed for the development of peripherally administered AOs crossing the BBB for DMD, remarkably, intrathecal administration, which is a less invasive and more effective avenue of delivering AOs into the CNS, has been shown to be feasible in transporting the AOs to the CNS in animal models of other diseases (Chen *et al.*, 2019; Kordasiewicz *et al.*, 2012; Rigo *et al.*, 2014). More importantly, this method also has been implemented in human clinical trials for amyotrophic lateral sclerosis and SMA treatments (Chiriboga *et al.*, 2016; Miller *et al.*, 2013). In addition to intrathecal administration, a novel and non-invasive intranasal delivery of AOs for the CNS has been demonstrated by Lee *et al.* (2012). These

authors reported that the drug administrated using the intranasal route had reached the brain and subsequently normalised the brain-derived neurotrophic factor levels and memory function in mice with Alzheimer disease. Moreover, a very interesting report was recently published by Zeniya *et al.* (2018), in which they showed that the concept for systemic delivery of AOs to the CNS via intravenous administration is possible when Angubindin-1, a novel binder to angulin-1 which increases the permeability of the mouse BBB, is intravenously injected prior to AOs administration. More importantly, a recent human study also shows that the BBB of four amyotrophic lateral sclerosis patients could be transiently opened by the transcranial magnetic resonance-guided focused ultrasound and resulted in gadolinium leakage in the primary motor cortex immediately after sonication, which normalised after 24 hours later (Abrahao *et al.*, 2019).

Taken together, there are a number of possible therapeutic approaches that may aid in the delivery of AOs to the CNS, and based on these concepts, new delivery methods can be developed for the treatment in *mdx* animals as well as in DMD patients. Although there is still a long journey for the development of drugs targeting the brain in DMD, current findings are encouraging as it is the first evidence that dystrophin is essential in normal cerebellar GABAergic transmission in organotypic *mdx* cultures and that the altered GABAergic synapses associated with this protein loss can be reversed by exon skipping using Pip6f-PMO. This proof-of-concept study can be the foundation for the future development of safe and effective therapeutic approaches that target the cognitive impairments in DMD patients.

7.3 The role of dystrophin in voltage-dependent ion channels (sodium and potassium channels)

In addition to the importance of dystrophin in normal inhibitory synaptic functioning, electrophysiological results also showed that dystrophin is essential for maintaining normal intrinsic electrical membrane properties of Purkinje cells (Chapter 6). The loss of dystrophin caused significant alterations in the amplitude and kinetics (10-90% rise time (ms), 10-90% (mV/ms) rise slope) of the first AP triggered with a minimum current injection. As discussed in Chapter 6, the reduced amplitude with increased 10-90% rise time, and subsequently a decrease in 10-90% rise slope, potentially resulted from a dysfunction in sodium channels. These ion channels are responsible for the entry of sodium ions into the cell to raise the membrane potential.

The importance of dystrophin in voltage-dependent ions channel function has been described in the cardiomyocyte, a non-neuronal cell that also expresses dystrophin. In adult ventricular cardiomyocytes, the principle channel isoform expressed is Na_v 1.5, a voltage-dependent sodium channel responsible for the rapid depolarisation during the upstroke phase of an AP (Gellens *et al.*, 1992). It was suggested that aberrant Na_v 1.5 channel expression and function can result in cardiomyopathy (Wan *et al.*, 2016). Cardiomyopathy, resulting from dystrophin deficiency is the primary cause of death in DMD patients (Chenard *et al.*, 1993; Koenig *et al.*, 2018). Notably, a recent study using human cells showed that abnormal AP parameters were found in induced pluripotent stem cells derived cardiomyocytes from a 32-year old male DMD patient (Eisen *et al.*, 2019). The authors reported a low spontaneous firing rate, arrhythmias and prolonged AP duration in these cells. Similarly, Koenig *et al.* (2011) reported a significant decrease in AP velocity and amplitude in 4-6 month old dystrophic cardiomyocytes. The findings here in Purkinje cells are consistent with those of Koenig *et al.* (2011). Together with

other groups, these authors concluded that the altered AP properties were due to a significant reduction in Na^+ currents (i.e. Na^+ current densities) in dystrophic cardiomyocytes when compared to the WT controls (Albesa *et al.*, 2011; Gavillet *et al.*, 2006; Koenig *et al.*, 2011; Rougier *et al.*, 2013). The reduced Na^+ currents were due to a down regulation of Na_v 1.5 protein expression and loss of Na^+ channel function (Albesa *et al.*, 2011; Colussi *et al.*, 2010; Koenig *et al.*, 2011). Therefore, if dystrophin deficiency impacted the Purkinje cell function in a similar way as in cardiomyocytes, it is conceivable that the sodium channel properties in dystrophic Purkinje cells may be altered and malfunctions, and consequently lead to the altered AP properties seen in the current study.

Furthermore, the possible change in other AP parameters (i.e. the tendency of increased peak AHP amplitude) in *mdx* neurons may be associated with altered BK channel function. Sausbier *et al.* (2004) showed that BK channels are important for normal cerebellar functions as several cerebellar learning deficits (i.e. deficiency in conditioned eye-blink reflex, locomotion, and motor coordination) were found in mice lacking BK channels. While the involvement of BK channels in the AHP of dystrophin-deficient Purkinje cells is yet to be elucidated, several studies in *C. elegans* have beautifully described the impacts of dystrophin deficiency on BK channel functions.

There is accumulating evidence showing BK channel deficits in the neuromuscular junction of the *C. elegans* that carries DAPC gene mutations (Carre-Pierrat *et al.*, 2006; Kim *et al.*, 2009; Sancar *et al.*, 2011). The nematode *C. elegans* is recognised to be a good model system for the investigation of neuromuscular development and function (Sancar *et al.*, 2011). The straited muscles of *C. elegans* show remarkable resemblance to vertebrate muscles and contains conserved DAPC components including dystrophin, dystroglycan, dystrobrevin, syntrophin,

δ/γ-sarcoglycan, and the C-terminal PDZ-domain ligand of nNOS (Sancar *et al.*, 2011). The mutations in DAPC result in the unusual behavioural phenotypes such as exaggerated head bending and hypercontraction in *C. elegans* when they are moving forward (Bessou *et al.*, 1998; Carre-Pierrat *et al.*, 2006; Gieseler *et al.*, 1999; Kim *et al.*, 2004). The altered locomotor phenotypes may be attributed to BK channel dysfunction. Under the normal physiological conditions, BK channels regulate muscle excitability (i.e. muscle inactivation) through conduction of the major outward rectifying current in muscle (Kim *et al.*, 2009). Indeed, Carre-Pierrat *et al.* (2006) show that the inactivation of dystrophin homologue *dys-1* in *C. elegans* caused a down-regulation of *slo-1* that encodes for the SLO-1 channel, which is a large conductance voltage- and calcium-gated potassium channel belonging to the family of BK channels. SLO-1 channel is normally localised near the L-type calcium channels in muscle, where $[Ca^{2+}]_i$ level is considerably higher than other regions during a calcium influx (Kim *et al.*, 2009). Follow up studies by Kim *et al.* (2009) and Sancar *et al.* (2011) showed that compromises in *C. elegans* dystrophin complex abrogates the normal SLO-1 channel localisation to calcium-rich regions of *C. elegans* muscle resulting in muscle hyperexcitability during periods of prolonged synaptic stimulation. The normal SLO-1 channel localisation to calcium-rich regions is very important as high calcium concentration (>10 μM) is required for the full activation of SLO-1 channels in mammals and *C. elegans* to prevent muscle over excitation (Brenner *et al.*, 2000; Marty, 1981; Wang *et al.*, 2001). More importantly, the SLO-1 channel mislocalisation may impair the repolarisation of membrane and disinhibit muscle AP generation, which eventually leads to enhanced Ca^{2+} influx through VGCCs (Sancar *et al.*, 2011). This may be one of the mechanisms that underlies the increase in $[Ca^{2+}]_i$ level, which has been well-demonstrated in the dystrophic muscles of both DMD patients and *mdx* mice.

Taken together, current findings suggest a potential role for dystrophin in sodium and BK channel localisation and function, which are crucial in governing the normal AP waveforms of Purkinje cells. The predominant sodium channel isoforms expressed in cerebellar Purkinje cells are $Na_v1.1$ and $Na_v1.6$ channels (Kalume *et al.*, 2007; Ransdell & Nerbonne, 2018; Schaller & Caldwell, 2003). These channels are important in shaping the waveforms of APs and control the rate of repetitive firing in Purkinje cells (Kalume *et al.*, 2007; Levin *et al.*, 2006; Meisler *et al.*, 2004; Raman *et al.*, 1997). The deletion or mutation in genes and disruption in ion channel clustering will impair normal Purkinje cell function. However, whether $Na_v1.1$, $Na_v1.6$ or both channels are impacted by dystrophin deficiency remains unclear. Further experiments are required to investigate the contribution of dystrophin to the function of these channels, and if involved they may serve as a potential therapeutic target in DMD.

Similarly, further experiments investigating the function of BK channel in dystrophin-deficient cells is necessary. The loss- or gain-of-functional BK channel and missense mutations in $Na_v1.1$ channel have been linked to epilepsy, that is also presented in DMD patients (Du *et al.*, 2005; Escayg *et al.*, 2001; Hu *et al.*, 2003; Knuesel *et al.*, 2001; Lorenz *et al.*, 2007; Medici *et al.*, 2011; Pane *et al.*, 2013; Wallace *et al.*, 2001; Yu *et al.*, 2006). Since sodium and BK channels are crucial in regulating the AP waveforms, and the deficit in channel function may result in epilepsy, future studies (i.e. immunohistochemistry and whole-cell voltage-clamp recording studies) in sodium and BK currents may provide further insight into the role of dystrophin in ion channel modulation and function. A solid understanding of the impacts of dystrophin deficiency on channel function will help us to identify potential targets for the development of new therapeutic approaches to improve the neuronal function in DMD patients.

7.4 The role of dystrophin in Purkinje cell calcium handling

While previous studies in *mdx* mice have shown unimpaired calcium homeostasis with normal resting $[Ca^{2+}]_i$ levels reported in both the skeletal and smooth muscle fibres (Boland *et al.*, 1993; Gailly *et al.*, 1993), to date, numerous studies have frequently described an impaired calcium homeostasis in DMD (Bodensteiner & Engel, 1978; Fong *et al.*, 1990; Mongini *et al.*, 1988; Tsurumi *et al.*, 2019). It has been hypothesised that the absence of dystrophin in skeletal muscle causes structural instability in muscle fibres rendering the fibres leakier to the extracellular environment and excessive influx of calcium (for review, see Vallejo-Illarramendi *et al.* (2014)). Accumulation of calcium and of hypercontracted fibres in muscle biopsies of DMD patients and other animal models that lack dystrophin are well documented (Cullen & Fulthorpe, 1975; Duncan, 1978; Mongini *et al.*, 1988; Sancar *et al.*, 2011; Turner *et al.*, 1988; Williams *et al.*, 1990). A recent study in cardiac muscle showed an increase in L-type Ca^{2+} current, the major depolarising current during early repolarisation in cardiomyocytes (Grant, 2009), as well as in DMD induced pluripotent stem cells derived cardiomyocytes and adult cardiomyocytes of *mdx* mice (Koenig *et al.*, 2014). The increase Ca^{2+} influx or dysfunction in calcium handling in dystrophic cells may lead to the activation of proteases and/or lipases that result in Ca^{2+} overload within cellular mitochondria and subsequent muscle degeneration (Timpani *et al.*, 2015).

Notably, this impaired calcium homeostasis is not only well described in dystrophic muscles but is also mirrored in neural tissues (Lopez *et al.*, 2016). Indeed, consistent with the elevated levels of $[Ca^{2+}]_i$ in dystrophic muscles, an earlier study in hippocampal pyramidal neurons from *mdx* mice showed a 123% and 214% increase in resting levels of $[Ca^{2+}]_i$ in 3- and 6-month *mdx* neurons when compared to age matched WT (Lopez *et al.*, 2016). The same authors also reported an increase in resting levels of $[Ca^{2+}]_i$ in the cortical neurons of *mdx* mice, although the

magnitude of the elevation in $[Ca^{2+}]_i$ was smaller than that in hippocampal neurons. This increase in $[Ca^{2+}]_i$ was significantly reduced by intraperitoneal injection of GsMTx-4, a blocker of stretch-activated cation channels, resulting in an improved spatial learning in *mdx* mice (Lopez *et al.*, 2016).

A major finding in this thesis also supports dystrophin as an essential candidate for maintaining the intracellular Ca^{2+} homeostasis in the Purkinje cell (Chapter 6). The results showed that a lack of dystrophin caused a significant increase in the resting level of $[Ca^{2+}]_i$ in the Purkinje cell body of *mdx* mice in comparison to LC mice. This finding is important, as calcium homeostasis is critical to many aspects of cell signalling and functions. Alterations in neuronal calcium regulation may have profound implications for proper cellular function, including associativity, excitability, neurotransmitter release, gene transcription, synaptic plasticity and graded regulation of neuronal firing patters (Finkbeiner & Greenberg, 1998; Ghosh & Greenberg, 1995; Mehler, 2000). Consequently, dysregulated cellular functions due to altered Ca^{2+} homeostasis may result in many pathological conditions and subsequent cell necrosis and death (Carafoli & Molinari, 1998; Deconinck & Dan, 2007; Raymackers *et al.*, 2003).

Dystrophin deficiency may impact calcium homeostasis in a number of ways (Allen *et al.*, 2016). VGCCs gain-of-function including enhanced Ca^{2+} current densities and reduced channel inactivation were reported in *mdx* cardiomyocytes (Koenig *et al.*, 2011; Koenig *et al.*, 2014; Li *et al.*, 2014; Sadeghi *et al.*, 2002; Viola *et al.*, 2014; Woolf *et al.*, 2006). These altered channel functions may contribute to cellular Ca^{2+} overload, as seen in the finding of increased *in vivo* left ventricular Ca^{2+} influx in the *mdx* mice identified by manganese-enhanced cardiovascular magnetic resonance imaging (Greally *et al.*, 2013; Mijares *et al.*, 2014; Williams & Allen, 2007; Zhou *et al.*, 1998). Similarly, the physiological properties and/ or membrane localisation

of VGCCs subtypes at CF-Purkinje cell proximal dendritic synapses could be altered if dystrophin deficiency impacts neuronal Ca^{2+} channel functions in a comparable fashion to that found in cardiomyocytes. Moreover, Ca^{2+} homeostasis in dystrophic cells may be altered by a deficit in the RyRs, the Ca^{2+}- induced Ca^{2+} release channels located on the SR. It was reported that the altered structure and function of RyRs result in Ca^{2+} leakage into the cytosol and subsequent Ca^{2+} overload in *mdx* muscle fibres (Allen *et al.*, 2016; Bellinger *et al.*, 2009; Fauconnier *et al.*, 2010). It is interesting to note that this increase in $[Ca^{2+}]_i$ can be reversed by the RyRs calcium release stabiliser that inhibits SR Ca^{2+} leak (Capogrosso *et al.*, 2018). Since the SR of skeletal muscle and the endoplasmic reticulum of Purkinje cells expresses the same type of RyRs (Fierro *et al.*, 1998; Kuwajima *et al.*, 1992), it is conceivable that the RyRs in Purkinje cells may have similar defects to those detected in the *mdx* muscle. Further research on the functions of VGCCs and RyRs in *mdx* Purkinje cells may provide new insights into the role that dystrophin plays in calcium homeostasis in the CNS.

7.5 Conclusion

The life expectancy of DMD patients has been improving due to increased understanding of the pathophysiology of the disease and as a result of improved care. However, there remains no effective treatment to restore brain dystrophin expression levels and ameliorate the cognitive deficits associated with the absence of dystrophin in the CNS. Thus, to improve the quality of life of DMD patients, there is an urgent need to fully understand the pathophysiology underlying the cognitive dysfunction resulting from dystrophin loss so that more effective therapeutic treatments can be developed for DMD. Using a dystrophin deficient animal model, the *mdx* mouse, the possible roles that dystrophin may play in the cerebellum was investigated. The results presented in this dissertation suggest that dystrophin is essential in maintaining the normal function of the inhibitory synapses, the intrinsic electrophysiological properties, and

calcium handling of the mature cerebellar Purkinje neurons. Remarkably, the findings shown in the organotypic cerebellar culture suggest that the altered GABAergic synaptic transmission may be reversable in *mdx* cultures treated with Pip6f-PMO. This showed that exon skipping using AOs is a potential way to re-express dystrophin in the CNS, and to restore GABAergic function. While the results from this dissertation shed light on the role of dystrophin in the cerebellum and a potential way to restore its expression in Purkinje cells, the cognitive deficits in DMD associated with brain dystrophin loss is complex and remains to be fully elucidated. Nevertheless, if the molecular perturbations resulting from dystrophin loss in *mdx* brains were also shared in patients with DMD, this current work would provide a foundation for the development of effective therapeutic strategies in alleviating the cognitive deficits in DMD. Future work building upon these findings can be focused on investigating the role that dystrophin plays in the functioning of ion channels (i.e. sodium and BK channels) that shape the AP properties and the VGCCs and RyRs that regulate calcium homeostasis in Purkinje neurons. This increased understanding may provide greater insight into the role that dystrophin plays in the function of the cerebellum.

References

Aartsma-Rus, A., & Corey, D. R. (2020). The 10th Oligonucleotide Therapy Approved: Golodirsen for Duchenne Muscular Dystrophy. *Nucleic Acid Ther, 30*(2), 67-70. doi:10.1089/nat.2020.0845

Aartsma-Rus, A., Fokkema, I., Verschuuren, J., Ginjaar, I., van Deutekom, J., van Ommen, G. J., & den Dunnen, J. T. (2009). Theoretic applicability of antisense-mediated exon skipping for Duchenne muscular dystrophy mutations. *Hum Mutat, 30*(3), 293-299. doi:10.1002/humu.20918

Aartsma-Rus, A., Janson, A. A., Kaman, W. E., Bremmer-Bout, M., den Dunnen, J. T., Baas, F., . . . van Deutekom, J. C. (2003). Therapeutic antisense-induced exon skipping in cultured muscle cells from six different DMD patients. *Hum Mol Genet, 12*(8), 907-914. doi:10.1093/hmg/ddg100

Aartsma-Rus, A., Janson, A. A., Kaman, W. E., Bremmer-Bout, M., van Ommen, G. J., den Dunnen, J. T., & van Deutekom, J. C. (2004). Antisense-induced multiexon skipping for Duchenne muscular dystrophy makes more sense. *Am J Hum Genet, 74*(1), 83-92. doi:10.1086/381039

Aartsma-Rus, A., & Krieg, A. M. (2017). FDA Approves Eteplirsen for Duchenne Muscular Dystrophy: The Next Chapter in the Eteplirsen Saga. *Nucleic Acid Ther, 27*(1), 1-3. doi:10.1089/nat.2016.0657

Abbott, N. J., Patabendige, A. A., Dolman, D. E., Yusof, S. R., & Begley, D. J. (2010). Structure and function of the blood-brain barrier. *Neurobiol Dis, 37*(1), 13-25. doi:10.1016/j.nbd.2009.07.030

Abrahao, A., Meng, Y., Llinas, M., Huang, Y., Hamani, C., Mainprize, T., . . . Zinman, L. (2019). First-in-human trial of blood-brain barrier opening in amyotrophic lateral sclerosis using MR-guided focused ultrasound. *Nat Commun, 10*(1), 4373. doi:10.1038/s41467-019-12426-9

Adams, A. M., & Gathercole, S. E. (2000). Limitations in working memory: implications for language development. *Int J Lang Commun Disord, 35*(1), 95-116.

Aiba, A., Kano, M., Chen, C., Stanton, M. E., Fox, G. D., Herrup, K., . . . Tonegawa, S. (1994). Deficient cerebellar long-term depression and impaired motor learning in mGluR1 mutant mice. *Cell, 79*(2), 377-388.

al-Qudah, A. A., Kobayashi, J., Chuang, S., Dennis, M., & Ray, P. (1990). Etiology of intellectual impairment in Duchenne muscular dystrophy. *Pediatr Neurol, 6*(1), 57-59.

Albesa, M., Ogrodnik, J., Rougier, J. S., & Abriel, H. (2011). Regulation of the cardiac sodium channel Nav1.5 by utrophin in dystrophin-deficient mice. *Cardiovasc Res, 89*(2), 320-328. doi:10.1093/cvr/cvq326

Alderton, J. M., & Steinhardt, R. A. (2000). Calcium influx through calcium leak channels is responsible for the elevated levels of calcium-dependent proteolysis in dystrophic myotubes. *J Biol Chem, 275*(13), 9452-9460. doi:10.1074/jbc.275.13.9452

Alger, B. E., Dhanjal, S. S., Dingledine, R., Grathwaite, J., Henderson, G., King, G. L., . . . Williams, J. (1984). Brain slice methods. In R. Dingledine (Ed.), *Brain Slices* (pp. 381-437). New York: Plenum Press.

Allen, D. G., Gervasio, O. L., Yeung, E. W., & Whitehead, N. P. (2010). Calcium and the damage pathways in muscular dystrophy. *Can J Physiol Pharmacol, 88*(2), 83-91. doi:10.1139/Y09-058

Allen, D. G., Lamb, G. D., & Westerblad, H. (2008). Impaired calcium release during fatigue. *J Appl Physiol (1985), 104*(1), 296-305. doi:10.1152/japplphysiol.00908.2007

Allen, D. G., Whitehead, N. P., & Froehner, S. C. (2016). Absence of Dystrophin Disrupts Skeletal Muscle Signaling: Roles of Ca2+, Reactive Oxygen Species, and Nitric Oxide in the Development of Muscular Dystrophy. *Physiol Rev, 96*(1), 253-305. doi:10.1152/physrev.00007.2015

Almers, W., & Neher, E. (1985). The Ca signal from fura-2 loaded mast cells depends strongly on the method of dye-loading. *FEBS Lett, 192*(1), 13-18. doi:10.1016/0014-5793(85)80033-8

Alter, J., Lou, F., Rabinowitz, A., Yin, H., Rosenfeld, J., Wilton, S. D., . . . Lu, Q. L. (2006). Systemic delivery of morpholino oligonucleotide restores dystrophin expression bodywide and improves dystrophic pathology. *Nat Med, 12*(2), 175-177. doi:10.1038/nm1345

Anderson, J., Morley, J., & Head, S. (2012). *Duchenne muscular dystrophy and brain function*: INTECH Open Access Publisher.

Anderson, J. L., Head, S. I., & Morley, J. W. (2003). Altered inhibitory input to Purkinje cells of dystrophin-deficient mice. *Brain Res, 982*(2), 280-283.

Anderson, J. L., Head, S. I., & Morley, J. W. (2004). Long-term depression is reduced in cerebellar Purkinje cells of dystrophin-deficient mdx mice. *Brain Res, 1019*(1-2), 289-292. doi:10.1016/j.brainres.2004.06.011

Anderson, J. L., Head, S. I., Rae, C., & Morley, J. W. (2002). Brain function in Duchenne muscular dystrophy. *Brain, 125*(Pt 1), 4-13.

Anderson, J. L., Morley, J. W., & Head, S. I. (2010). Enhanced homosynaptic LTD in cerebellar Purkinje cells of the dystrophic mdx mouse. *Muscle Nerve, 41*(3), 329-334.

Aponte, Y., Bischofberger, J., & Jonas, P. (2008). Efficient Ca2+ buffering in fast-spiking basket cells of rat hippocampus. *J Physiol, 586*(8), 2061-2075. doi:10.1113/jphysiol.2007.147298

Araki, E., Nakamura, K., Nakao, K., Kameya, S., Kobayashi, O., Nonaka, I., . . . Katsuki, M. (1997). Targeted disruption of exon 52 in the mouse dystrophin gene induced muscle

degeneration similar to that observed in Duchenne muscular dystrophy. *Biochem Biophys Res Commun, 238*(2), 492-497. doi:10.1006/bbrc.1997.7328

Assaf, Y., & Pasternak, O. (2008). Diffusion tensor imaging (DTI)-based white matter mapping in brain research: a review. *J Mol Neurosci, 34*(1), 51-61. doi:10.1007/s12031-007-0029-0

Attwell, D., & Laughlin, S. B. (2001). An energy budget for signaling in the grey matter of the brain. *J Cereb Blood Flow Metab, 21*(10), 1133-1145. doi:10.1097/00004647-200110000-00001

Avner, P., Amar, L., Arnaud, D., Hanauer, A., & Cambrou, J. (1987). Detailed ordering of markers localizing to the Xq26-Xqter region of the human X chromosome by the use of an interspecific Mus spretus mouse cross. *Proc Natl Acad Sci U S A, 84*(6), 1629-1633.

Baer, K., Essrich, C., Benson, J. A., Benke, D., Bluethmann, H., Fritschy, J. M., & Luscher, B. (1999). Postsynaptic clustering of gamma-aminobutyric acid type A receptors by the gamma3 subunit in vivo. *Proc Natl Acad Sci U S A, 96*(22), 12860-12865.

Bakker, A. J., Head, S. I., Williams, D. A., & Stephenson, D. G. (1993). Ca2+ levels in myotubes grown from the skeletal muscle of dystrophic (mdx) and normal mice. *J Physiol, 460*, 1-13.

Ballenger, J. C., Burrows, G. D., DuPont, R. L., Jr., Lesser, I. M., Noyes, R., Jr., Pecknold, J. C., . . . Swinson, R. P. (1988). Alprazolam in panic disorder and agoraphobia: results from a multicenter trial. I. Efficacy in short-term treatment. *Arch Gen Psychiatry, 45*(5), 413-422. doi:10.1001/archpsyc.1988.01800290027004

Banihani, R., Smile, S., Yoon, G., Dupuis, A., Mosleh, M., Snider, A., & McAdam, L. (2015). Cognitive and Neurobehavioral Profile in Boys With Duchenne Muscular Dystrophy. *J Child Neurol, 30*(11), 1472-1482. doi:10.1177/0883073815570154

Banks, W. A., Farr, S. A., Butt, W., Kumar, V. B., Franko, M. W., & Morley, J. E. (2001). Delivery across the blood-brain barrier of antisense directed against amyloid beta: reversal of learning and memory deficits in mice overexpressing amyloid precursor protein. *J Pharmacol Exp Ther, 297*(3), 1113-1121.

Barber, K., Mala, R. R., Lambert, M. P., Qiu, R., MacDonald, R. C., & Klein, W. L. (1996). Delivery of membrane-impermeant fluorescent probes into living neural cell populations by lipotransfer. *Neurosci Lett, 207*(1), 17-20. doi:10.1016/0304-3940(96)12497-6

Barbiroli, B., Montagna, P., Martinelli, P., Lodi, R., Iotti, S., Cortelli, P., . . . Zaniol, P. (1993). Defective brain energy metabolism shown by in vivo 31P MR spectroscopy in 28 patients with mitochondrial cytopathies. *J Cereb Blood Flow Metab, 13*(3), 469-474. doi:10.1038/jcbfm.1993.61

Barreto-Chang, O. L., & Dolmetsch, R. E. (2009). Calcium imaging of cortical neurons using Fura-2 AM. *J Vis Exp*(23). doi:10.3791/1067

Bassett, D., & Currie, P. D. (2004). Identification of a zebrafish model of muscular dystrophy. *Clin Exp Pharmacol Physiol, 31*(8), 537-540. doi:10.1111/j.1440-1681.2004.04030.x

Bastianelli, E. (2003). Distribution of calcium-binding proteins in the cerebellum. *Cerebellum, 2*(4), 242-262. doi:10.1080/14734220310022289

Bean, B. P. (2007). The action potential in mammalian central neurons. *Nat Rev Neurosci, 8*(6), 451-465. doi:10.1038/nrn2148

Belelli, D., & Lambert, J. J. (2005). Neurosteroids: endogenous regulators of the GABA(A) receptor. *Nat Rev Neurosci, 6*(7), 565-575. doi:10.1038/nrn1703

Bell, C. D., & Conen, P. E. (1968). Histopathological changes in Duchenne muscular dystrophy. *J Neurol Sci, 7*(3), 529-544.

Bellinger, A. M., Reiken, S., Carlson, C., Mongillo, M., Liu, X., Rothman, L., . . . Marks, A. R. (2009). Hypernitrosylated ryanodine receptor calcium release channels are leaky in dystrophic muscle. *Nat Med, 15*(3), 325-330. doi:10.1038/nm.1916

Belzung, C. (1992). Hippocampal mossy fibres: implication in novelty reactions or in anxiety behaviours? *Behavioural brain research, 51*(2), 149-155.

Bennett, C. F., Baker, B. F., Pham, N., Swayze, E., & Geary, R. S. (2017). Pharmacology of Antisense Drugs. *Annu Rev Pharmacol Toxicol, 57*, 81-105. doi:10.1146/annurev-pharmtox-010716-104846

Berridge, M. J. (1998). Neuronal calcium signaling. *Neuron, 21*(1), 13-26. doi:10.1016/s0896-6273(00)80510-3

Berridge, M. J. (2009). Inositol trisphosphate and calcium signalling mechanisms. *Biochim Biophys Acta, 1793*(6), 933-940. doi:10.1016/j.bbamcr.2008.10.005

Bessou, C., Giugia, J. B., Franks, C. J., Holden-Dye, L., & Segalat, L. (1998). Mutations in the Caenorhabditis elegans dystrophin-like gene dys-1 lead to hyperactivity and suggest a link with cholinergic transmission. *Neurogenetics, 2*(1), 61-72. doi:10.1007/s100480050053

Betts, C., Saleh, A. F., Arzumanov, A. A., Hammond, S. M., Godfrey, C., Coursindel, T., . . . Wood, M. J. (2012). Pip6-PMO, A New Generation of Peptide-oligonucleotide Conjugates With Improved Cardiac Exon Skipping Activity for DMD Treatment. *Mol Ther Nucleic Acids, 1*, e38. doi:10.1038/mtna.2012.30

Bies, R. D., Friedman, D., Roberts, R., Perryman, M. B., & Caskey, C. T. (1992). Expression and localization of dystrophin in human cardiac Purkinje fibers. *Circulation, 86*(1), 147-153.

Bies, R. D., Phelps, S. F., Cortez, M. D., Roberts, R., Caskey, C. T., & Chamberlain, J. S. (1992). Human and murine dystrophin mRNA transcripts are differentially expressed during skeletal muscle, heart, and brain development. *Nucleic Acids Res, 20*(7), 1725-1731.

Billard, C., Gillet, P., Barthez, M., Hommet, C., & Bertrand, P. (1998). Reading ability and processing in Duchenne muscular dystrophy and spinal muscular atrophy. *Dev Med Child Neurol, 40*(1), 12-20.

Billard, C., Gillet, P., Signoret, J. L., Uicaut, E., Bertrand, P., Fardeau, M., . . . Santini, J. J. (1992). Cognitive functions in Duchenne muscular dystrophy: a reappraisal and comparison with spinal muscular atrophy. *Neuromuscul Disord, 2*(5-6), 371-378.

Binder, M. D., Hirokawa, N., & Windhorst, U. (2009). *Encyclopedia of neuroscience* (Vol. 3166): Springer Berlin, Heidelberg.

Bing, X., Ming-Guo, Q., Ye, Z., Jing-Na, Z., Min, L., Han, C., . . . Shao-Xiang, Z. (2013). Alterations in the cortical thickness and the amplitude of low-frequency fluctuation in patients with post-traumatic stress disorder. *Brain Res, 1490*, 225-232. doi:10.1016/j.brainres.2012.10.048

Bishop, D. V. (2002). Cerebellar abnormalities in developmental dyslexia: cause, correlate or consequence? *Cortex, 38*(4), 491-498.

Bishop, D. V., & Snowling, M. J. (2004). Developmental dyslexia and specific language impairment: same or different? *Psychol Bull, 130*(6), 858-886. doi:10.1037/0033-2909.130.6.858

Blake, D. J., & Kroger, S. (2000). The neurobiology of duchenne muscular dystrophy: learning lessons from muscle? *Trends Neurosci, 23*(3), 92-99.

Blake, D. J., Weir, A., Newey, S. E., & Davies, K. E. (2002). Function and genetics of dystrophin and dystrophin-related proteins in muscle. *Physiol Rev, 82*(2), 291-329. doi:10.1152/physrev.00028.2001

Blatter, L. A., & Wier, W. G. (1990). Intracellular diffusion, binding, and compartmentalization of the fluorescent calcium indicators indo-1 and fura-2. *Biophys J, 58*(6), 1491-1499. doi:10.1016/S0006-3495(90)82494-2

Bliss, T. V., & Collingridge, G. L. (1993). A synaptic model of memory: long-term potentiation in the hippocampus. *Nature, 361*(6407), 31-39. doi:10.1038/361031a0

Bloom, E. T., Umehara, H., Bleackley, R. C., Okumura, K., Mostowski, H., & Babbitt, J. T. (1990). Age-related decrement in cytotoxic T lymphocyte (CTL) activity is associated with decreased levels of mRNA encoded by two CTL-associated serine esterase genes and the perforin gene in mice. *Eur J Immunol, 20*(10), 2309-2316. doi:10.1002/eji.1830201021

Bock, T., & Stuart, G. J. (2016). Impact of calcium-activated potassium channels on NMDA spikes in cortical layer 5 pyramidal neurons. *J Neurophysiol, 115*(3), 1740-1748. doi:10.1152/jn.01047.2015

Bodensteiner, J. B., & Engel, A. G. (1978). Intracellular Calcium Accumulation in Duchenne Dystrophy and Other Myopathies - Study of 567,000 Muscle-Fibers in 114 Biopsies. *Neurology, 28*(5), 439-446. doi:Doi 10.1212/Wnl.28.5.439

Boland, B., Himpens, B., Casteels, R., & Gillis, J.-M. (1993). Lack of dystrophin but normal calcium homeostasis in smooth muscle from dystrophic mdx mice. *Journal of Muscle Research & Cell Motility, 14*(1), 133-139.

Bond, C. T., Herson, P. S., Strassmaier, T., Hammond, R., Stackman, R., Maylie, J., & Adelman, J. P. (2004). Small conductance Ca2+-activated K+ channel knock-out mice reveal the identity of calcium-dependent afterhyperpolarization currents. *J Neurosci, 24*(23), 5301-5306. doi:10.1523/JNEUROSCI.0182-04.2004

Bootman, M. D., Rietdorf, K., Collins, T., Walker, S., & Sanderson, M. (2013). Ca2+-sensitive fluorescent dyes and intracellular Ca2+ imaging. *Cold Spring Harb Protoc, 2013*(2), 83-99. doi:10.1101/pdb.top066050

Braitenberg, V., & Atwood, R. P. (1958). Morphological observations on the cerebellar cortex. *J Comp Neurol, 109*(1), 1-33. doi:10.1002/cne.901090102

Brenner, R., Jegla, T. J., Wickenden, A., Liu, Y., & Aldrich, R. W. (2000). Cloning and functional characterization of novel large conductance calcium-activated potassium channel beta subunits, hKCNMB3 and hKCNMB4. *J Biol Chem, 275*(9), 6453-6461. doi:10.1074/jbc.275.9.6453

Bresolin, N., Castelli, E., Comi, G. P., Felisari, G., Bardoni, A., Perani, D., . . . et al. (1994). Cognitive impairment in Duchenne muscular dystrophy. *Neuromuscul Disord, 4*(4), 359-369.

Briatore, F., Pregno, G., Di Angelantonio, S., Frola, E., De Stefano, M. E., Vaillend, C., . . . Patrizi, A. (2020). Dystroglycan Mediates Clustering of Essential GABAergic Components in Cerebellar Purkinje Cells. *Front Mol Neurosci, 13*, 164. doi:10.3389/fnmol.2020.00164

Bright, G. R., Kuo, N. T., Chow, D., Burden, S., Dowe, C., & Przybylski, R. J. (1996). Delivery of macromolecules into adherent cells via electroporation for use in fluorescence spectroscopic imaging and metabolic studies. *Cytometry, 24*(3), 226-233. doi:10.1002/(SICI)1097-0320(19960701)24:3<226::AID-CYTO5>3.0.CO;2-F

Brooks, S. V. (1998). Rapid recovery following contraction-induced injury to in situ skeletal muscles in mdx mice. *J Muscle Res Cell Motil, 19*(2), 179-187.

Brunig, I., Penschuck, S., Berninger, B., Benson, J., & Fritschy, J. M. (2001). BDNF reduces miniature inhibitory postsynaptic currents by rapid downregulation of GABA(A) receptor surface expression. *Eur J Neurosci, 13*(7), 1320-1328.

Brunig, I., Scotti, E., Sidler, C., & Fritschy, J. M. (2002). Intact sorting, targeting, and clustering of gamma-aminobutyric acid A receptor subtypes in hippocampal neurons in vitro. *J Comp Neurol, 443*(1), 43-55.

Brunig, I., Suter, A., Knuesel, I., Luscher, B., & Fritschy, J. M. (2002). GABAergic terminals are required for postsynaptic clustering of dystrophin but not of GABA(A) receptors and gephyrin. *J Neurosci, 22*(12), 4805-4813.

Bulfield, G., Siller, W. G., Wight, P. A., & Moore, K. J. (1984). X chromosome-linked muscular dystrophy (mdx) in the mouse. *Proc Natl Acad Sci U S A, 81*(4), 1189-1192. doi:10.1073/pnas.81.4.1189

Bush, D. S., & Jones, R. L. (1990). Measuring intracellular ca levels in plant cells using the fluorescent probes, indo-1 and fura-2 : progress and prospects. *Plant Physiol, 93*(3), 841-845. doi:10.1104/pp.93.3.841

Buskila, Y., Breen, P. P., Tapson, J., Van Schaik, A., Barton, M., & Morley, J. W. (2014). Extending the viability of acute brain slices. *Scientific reports, 4*.

Buzin, C. H., Feng, J., Yan, J., Scaringe, W., Liu, Q., den Dunnen, J., . . . Sommer, S. S. (2005). Mutation rates in the dystrophin gene: a hotspot of mutation at a CpG dinucleotide. *Hum Mutat, 25*(2), 177-188. doi:10.1002/humu.20132

Cabeza, R., & Nyberg, L. (2000). Imaging cognition II: An empirical review of 275 PET and fMRI studies. *J Cogn Neurosci, 12*(1), 1-47. doi:10.1162/08989290051137585

Cameron, M., Kekesi, O., Morley, J. W., Tapson, J., Breen, P. P., van Schaik, A., & Buskila, Y. (2016). Calcium Imaging of AM Dyes Following Prolonged Incubation in Acute Neuronal Tissue. *PloS one, 11*(5), e0155468. doi:10.1371/journal.pone.0155468

Cameron, M. A., Kekesi, O., Morley, J. W., Bellot-Saez, A., Kueh, S., Breen, P., . . . Buskila, Y. (2017). Prolonged Incubation of Acute Neuronal Tissue for Electrophysiology and Calcium-imaging. *J Vis Exp*(120). doi:10.3791/55396

Canepari, M., Vogt, K., & Zecevic, D. (2008). Combining voltage and calcium imaging from neuronal dendrites. *Cell Mol Neurobiol, 28*(8), 1079-1093. doi:10.1007/s10571-008-9285-y

Cantrell, A. R., & Catterall, W. A. (2001). Neuromodulation of Na+ channels: an unexpected form of cellular plasticity. *Nat Rev Neurosci, 2*(6), 397-407. doi:10.1038/35077553

Capogrosso, R. F., Mantuano, P., Uaesoontrachoon, K., Cozzoli, A., Giustino, A., Dow, T., . . . De Luca, A. (2018). Ryanodine channel complex stabilizer compound S48168/ARM210 as a disease modifier in dystrophin-deficient mdx mice: proof-of-concept study and independent validation of efficacy. *FASEB J, 32*(2), 1025-1043. doi:10.1096/fj.201700182RRR

Carafoli, E., & Molinari, M. (1998). Calpain: a protease in search of a function? *Biochem Biophys Res Commun, 247*(2), 193-203. doi:10.1006/bbrc.1998.8378

Carlson, C. G. (1998). The dystrophinopathies: an alternative to the structural hypothesis. *Neurobiol Dis, 5*(1), 3-15. doi:10.1006/nbdi.1998.0188

Carre-Pierrat, M., Grisoni, K., Gieseler, K., Mariol, M. C., Martin, E., Jospin, M., . . . Segalat, L. (2006). The SLO-1 BK channel of Caenorhabditis elegans is critical for muscle function and is involved in dystrophin-dependent muscle dystrophy. *J Mol Biol, 358*(2), 387-395. doi:10.1016/j.jmb.2006.02.037

Carretta, D., Santarelli, M., Sbriccoli, A., Pinto, F., Catini, C., & Minciacchi, D. (2004). Spatial analysis reveals alterations of parvalbumin- and calbindin-positive local circuit neurons in the cerebral cortex of mutant mdx mice. *Brain Res, 1016*(1), 1-11. doi:10.1016/j.brainres.2004.04.021

Carretta, D., Santarelli, M., Vanni, D., Carrai, R., Sbriccoli, A., Pinto, F., & Minciacchi, D. (2001). The organisation of spinal projecting brainstem neurons in an animal model of muscular dystrophy. A retrograde tracing study on mdx mutant mice. *Brain Res, 895*(1-2), 213-222.

Carretta, D., Santarelli, M., Vanni, D., Ciabatti, S., Sbriccoli, A., Pinto, F., & Minciacchi, D. (2003). Cortical and brainstem neurons containing calcium-binding proteins in a murine model of Duchenne's muscular dystrophy: selective changes in the sensorimotor cortex. *J Comp Neurol, 456*(1), 48-59. doi:10.1002/cne.10506

Cavelier, P., Beekenkamp, H., Shin, H. S., Jun, K., & Bossu, J. L. (2002). Cerebellar slice cultures from mice lacking the P/Q calcium channel: electroresponsiveness of Purkinje cells. *Neurosci Lett, 333*(1), 64-68. doi:10.1016/s0304-3940(02)00962-x

Cepeda, C., Lee, N., Buchwald, N. A., Radisavljevic, Z., & Levine, M. S. (1992). Age-induced changes in electrophysiological responses of neostriatal neurons recorded in vitro. *Neuroscience, 51*(2), 411-423. doi:10.1016/0306-4522(92)90325-v

Cerminara, N. L., Lang, E. J., Sillitoe, R. V., & Apps, R. (2015). Redefining the cerebellar cortex as an assembly of non-uniform Purkinje cell microcircuits. *Nat Rev Neurosci, 16*(2), 79-93. doi:10.1038/nrn3886

Chae, H. G., Ahn, S. J., Hong, Y. H., Chang, W. S., Kim, J., & Kim, S. J. (2012). Transient receptor potential canonical channels regulate the induction of cerebellar long-term depression. *J Neurosci, 32*(37), 12909-12914. doi:10.1523/JNEUROSCI.0073-12.2012

Chan, S., Head, S., & Morley, J. (2007a). Branched fibers in dystrophic mdx muscle are associated with a loss of force following lengthening contractions. *American Journal of Physiology-Cell Physiology, 293*(3), C985-C992.

Chan, S., & Head, S. I. (2011). The role of branched fibres in the pathogenesis of Duchenne muscular dystrophy. *Exp Physiol, 96*(6), 564-571. doi:10.1113/expphysiol.2010.056713

Chan, S., Head, S. I., & Morley, J. W. (2007b). Branched fibers in dystrophic mdx muscle are associated with a loss of force following lengthening contractions. *Am J Physiol Cell Physiol, 293*(3), C985-992. doi:10.1152/ajpcell.00128.2007

Chang, Y. M., Rosene, D. L., Killiany, R. J., Mangiamele, L. A., & Luebke, J. I. (2005). Increased action potential firing rates of layer 2/3 pyramidal cells in the prefrontal cortex are significantly related to cognitive performance in aged monkeys. *Cereb Cortex, 15*(4), 409-418. doi:10.1093/cercor/bhh144

Chapman, V. M., Miller, D. R., Armstrong, D., & Caskey, C. T. (1989). Recovery of induced mutations for X chromosome-linked muscular dystrophy in mice. *Proc Natl Acad Sci U S A, 86*(4), 1292-1296.

Chelly, J., Hamard, G., Koulakoff, A., Kaplan, J. C., Kahn, A., & Berwald-Netter, Y. (1990). Dystrophin gene transcribed from different promoters in neuronal and glial cells. *Nature, 344*(6261), 64-65. doi:10.1038/344064a0

Chen, Y., Mazur, C., Luo, Y., Sun, L., Zhang, M., McCampbell, A., & Tomassy, G. S. (2019). Intrathecal Delivery of Antisense Oligonucleotides in the Rat Central Nervous System. *J Vis Exp*(152). doi:10.3791/60274

Chenard, A. A., Becane, H. M., Tertrain, F., de Kermadec, J. M., & Weiss, Y. A. (1993). Ventricular arrhythmia in Duchenne muscular dystrophy: prevalence, significance and prognosis. *Neuromuscul Disord, 3*(3), 201-206. doi:10.1016/0960-8966(93)90060-w

Cheron, G., Servais, L., & Dan, B. (2008). Cerebellar network plasticity: from genes to fast oscillation. *Neuroscience, 153*(1), 1-19. doi:10.1016/j.neuroscience.2008.01.074

Chiriboga, C. A., Swoboda, K. J., Darras, B. T., Iannaccone, S. T., Montes, J., De Vivo, D. C., . . . Bishop, K. M. (2016). Results from a phase 1 study of nusinersen (ISIS-SMN(Rx)) in children with spinal muscular atrophy. *Neurology, 86*(10), 890-897. doi:10.1212/WNL.0000000000002445

Cirak, S., Feng, L., Anthony, K., Arechavala-Gomeza, V., Torelli, S., Sewry, C., . . . Muntoni, F. (2012). Restoration of the dystrophin-associated glycoprotein complex after exon skipping therapy in Duchenne muscular dystrophy. *Mol Ther, 20*(2), 462-467. doi:10.1038/mt.2011.248

Coesmans, M., Weber, J. T., De Zeeuw, C. I., & Hansel, C. (2004). Bidirectional parallel fiber plasticity in the cerebellum under climbing fiber control. *Neuron, 44*(4), 691-700. doi:10.1016/j.neuron.2004.10.031

Collingridge, G. L., Peineau, S., Howland, J. G., & Wang, Y. T. (2010). Long-term depression in the CNS. *Nat Rev Neurosci, 11*(7), 459-473. doi:10.1038/nrn2867

Collins, C. A., & Morgan, J. E. (2003). Duchenne's muscular dystrophy: animal models used to investigate pathogenesis and develop therapeutic strategies. *Int J Exp Pathol, 84*(4), 165-172.

Colussi, C., Berni, R., Rosati, J., Straino, S., Vitale, S., Spallotta, F., . . . Capogrossi, M. C. (2010). The histone deacetylase inhibitor suberoylanilide hydroxamic acid reduces cardiac arrhythmias in dystrophic mice. *Cardiovasc Res, 87*(1), 73-82. doi:10.1093/cvr/cvq035

Cotton, S., Voudouris, N. J., & Greenwood, K. M. (2001). Intelligence and Duchenne muscular dystrophy: full-scale, verbal, and performance intelligence quotients. *Dev Med Child Neurol, **43***(7), 497-501.

Cotton, S. M., Voudouris, N. J., & Greenwood, K. M. (2005). Association between intellectual functioning and age in children and young adults with Duchenne muscular dystrophy: further results from a meta-analysis. *Developmental Medicine & Child Neurology, 47*(04), 257-265.

Cox, G. A., Phelps, S. F., Chapman, V. M., & Chamberlain, J. S. (1993). New mdx mutation disrupts expression of muscle and nonmuscle isoforms of dystrophin. *Nat Genet, 4*(1), 87-93. doi:10.1038/ng0593-87

Creager, R., Dunwiddie, T., & Lynch, G. (1980). Paired-pulse and frequency facilitation in the CA1 region of the in vitro rat hippocampus. *J Physiol, 299*, 409-424.

Cullen, M. J., & Fulthorpe, J. J. (1975). Stages in fibre breakdown in Duchenne muscular dystrophy. An electron-microscopic study. *J Neurol Sci, 24*(2), 179-200. doi:10.1016/0022-510x(75)90232-4

Cyrulnik, S. E., & Hinton, V. J. (2008). Duchenne muscular dystrophy: a cerebellar disorder? *Neuroscience & Biobehavioral Reviews, 32*(3), 486-496.

Dallerac, G., Perronnet, C., Chagneau, C., Leblanc-Veyrac, P., Samson-Desvignes, N., Peltekian, E., . . . Vaillend, C. (2011). Rescue of a dystrophin-like protein by exon skipping normalizes synaptic plasticity in the hippocampus of the mdx mouse. *Neurobiol Dis, 43*(3), 635-641. doi:10.1016/j.nbd.2011.05.012

Dangain, J., & Vrbova, G. (1984). Muscle development in mdx mutant mice. *Muscle Nerve, 7*(9), 700-704. doi:10.1002/mus.880070903

Daoud, F., Angeard, N., Demerre, B., Martie, I., Benyaou, R., Leturcq, F., . . . Tuffery, S. (2009). Analysis of Dp71 contribution in the severity of mental retardation through comparison of Duchenne and Becker patients differing by mutation consequences on Dp71 expression. *Human Molecular Genetics, 18*(20), 3779-3794.

Darian-Smith, I., Galea, M. P., & Darian-Smith, C. (1996). Manual dexterity: how does the cerebral cortex contribute? *Clin Exp Pharmacol Physiol, 23*(10-11), 948-956.

Davis, G. W., DiAntonio, A., Petersen, S. A., & Goodman, C. S. (1998). Postsynaptic PKA controls quantal size and reveals a retrograde signal that regulates presynaptic transmitter release in Drosophila. *Neuron, 20*(2), 305-315.

de Brabander, J. M., Kramers, R. J., & Uylings, H. B. (1998). Layer-specific dendritic regression of pyramidal cells with ageing in the human prefrontal cortex. *Eur J Neurosci, 10*(4), 1261-1269. doi:10.1046/j.1460-9568.1998.00137.x

De Luca, A., Pierno, S., Camerino, C., Cocchi, D., & Camerino, D. C. (1999). Higher content of insulin-like growth factor-I in dystrophic mdx mouse: potential role in the spontaneous regeneration through an electrophysiological investigation of muscle function. *Neuromuscular disorders, 9*(1), 11-18.

De Luca, A., Pierno, S., & Camerino, D. C. (1995). Changes of membrane electrical properties in extensor digitorum longus muscle from dystrophic (mdx) mice. *Muscle & Nerve: Official Journal of the American Association of Electrodiagnostic Medicine, 18*(10), 1196-1198.

De Luca, A., Pierno, S., & Camerino, D. C. (1997). Electrical properties of diaphragm and EDL muscles during the life of dystrophic mice. *American Journal of Physiology-Cell Physiology, 272*(1), C333-C340.

De Talamoni, N., Smith, C., Wasserman, R., Beltramino, C., Fullmer, C., & Penniston, J. (1993). Immunocytochemical localization of the plasma membrane calcium pump, calbindin-D28k, and parvalbumin in Purkinje cells of avian and mammalian cerebellum. *Proceedings of the National Academy of Sciences, 90*(24), 11949-11953.

Deconinck, N., & Dan, B. (2007). Pathophysiology of duchenne muscular dystrophy: current hypotheses. *Pediatr Neurol, 36*(1), 1-7. doi:10.1016/j.pediatrneurol.2006.09.016

Del Carlo Giannini, G., & Marcheschi, M. (1959). Sui disturbi psichici nella distrofia muscolare primitiva. *Sis Nerv, 6*, 461-480.

Del Tongo, C., Carretta, D., Fulgenzi, G., Catini, C., & Minciacchi, D. (2009). Parvalbumin-positive GABAergic interneurons are increased in the dorsal hippocampus of the dystrophic mdx mouse. *Acta Neuropathol, 118*(6), 803-812. doi:10.1007/s00401-009-0567-3

Denetclaw, W. F., Jr., Hopf, F. W., Cox, G. A., Chamberlain, J. S., & Steinhardt, R. A. (1994). Myotubes from transgenic mdx mice expressing full-length dystrophin show normal calcium regulation. *Mol Biol Cell, 5*(10), 1159-1167.

Desguerre, I., Christov, C., Mayer, M., Zeller, R., Becane, H.-M., Bastuji-Garin, S., . . . Gherardi, R. K. (2009). Clinical heterogeneity of duchenne muscular dystrophy (DMD): definition of sub-phenotypes and predictive criteria by long-term follow-up. *PloS one, 4*(2), e4347.

Devinsky, O., & Bear, D. (1984). Varieties of aggressive behavior in temporal lobe epilepsy. *Am J Psychiatry, 141*(5), 651-656. doi:10.1176/ajp.141.5.651

Di Lazzaro, V., Restuccia, D., Servidei, S., Nardone, R., Oliviero, A., Profice, P., . . . Rothwell, J. C. (1998). Functional involvement of cerebral cortex in Duchenne muscular dystrophy. *Muscle Nerve, 21*(5), 662-664.

Dickson, G., Hill, V., & Graham, I. R. (2002). Screening for antisense modulation of dystrophin pre-mRNA splicing. *Neuromuscul Disord, 12 Suppl 1*, S67-70. doi:10.1016/s0960-8966(02)00085-8

Dienel, G. A. (2019). Brain Glucose Metabolism: Integration of Energetics with Function. *Physiol Rev, 99*(1), 949-1045. doi:10.1152/physrev.00062.2017

Dingledine, R., Hynes, M. A., & King, G. L. (1986). Involvement of N-methyl-D-aspartate receptors in epileptiform bursting in the rat hippocampal slice. *J Physiol, 380*, 175-189.

Doorenweerd, N., Dumas, E. M., Ghariq, E., Schmid, S., Straathof, C. S., Roest, A. A., . . . Kan, H. E. (2017). Decreased cerebral perfusion in Duchenne muscular dystrophy patients. *Neuromuscul Disord, 27*(1), 29-37. doi:10.1016/j.nmd.2016.10.005

Doorenweerd, N., Straathof, C. S., Dumas, E. M., Spitali, P., Ginjaar, I. B., Wokke, B. H., . . . Kan, H. E. (2014). Reduced cerebral gray matter and altered white matter in boys with Duchenne muscular dystrophy. *Ann Neurol, 76*(3), 403-411. doi:10.1002/ana.24222

Dorman, C., Hurley, A. D., & D'Avignon, J. (1988). Language and learning disorders of older boys with Duchenne muscular dystrophy. *Dev Med Child Neurol, 30*(3), 316-327.

Draguhn, A., Axmacher, N., & Kolbaev, S. (2008). Presynaptic ionotropic GABA receptors. *Results Probl Cell Differ, 44*, 69-85. doi:10.1007/400_2007_040

Du, L., Kayali, R., Bertoni, C., Fike, F., Hu, H., Iversen, P. L., & Gatti, R. A. (2011). Arginine-rich cell-penetrating peptide dramatically enhances AMO-mediated ATM aberrant splicing correction and enables delivery to brain and cerebellum. *Hum Mol Genet, 20*(16), 3151-3160. doi:10.1093/hmg/ddr217

Du, W., Bautista, J. F., Yang, H., Diez-Sampedro, A., You, S. A., Wang, L., . . . Wang, Q. K. (2005). Calcium-sensitive potassium channelopathy in human epilepsy and paroxysmal movement disorder. *Nat Genet, 37*(7), 733-738. doi:10.1038/ng1585

Duan, H., Wearne, S. L., Rocher, A. B., Macedo, A., Morrison, J. H., & Hof, P. R. (2003). Age-related dendritic and spine changes in corticocortically projecting neurons in macaque monkeys. *Cereb Cortex, 13*(9), 950-961. doi:10.1093/cercor/13.9.950

Dubowitz, V. (1965). Intellectual impairment in muscular dystrophy. *Archives of disease in childhood, 40*(211), 296.

Dubowitz, V., & Crome, L. (1969). The central nervous system in Duchenne muscular dystrophy. *Brain, 92*(4), 805-808.

Duchenne, G. B. A. (1868). Recherches sur la paralysie musculaire pseudo-hypertrophique ou paralysie myosclerosique. *Archives of General Medicine, 11*(5), 25.

Duncan, C. J. (1978). Role of Intracellular Calcium in Promoting Muscle Damage - a Strategy for Controlling Dystrophic Condition. *Experientia, 34*(12), 1531-1535. doi:Doi 10.1007/Bf02034655

Dunckley, M. G., Manoharan, M., Villiet, P., Eperon, I. C., & Dickson, G. (1998). Modification of splicing in the dystrophin gene in cultured Mdx muscle cells by antisense oligoribonucleotides. *Human Molecular Genetics, 7*(7), 1083-1090. doi:10.1093/hmg/7.7.1083

Dunn, J. F., & Zaim-Wadghiri, Y. (1999). Quantitative magnetic resonance imaging of the mdx mouse model of Duchenne muscular dystrophy. *Muscle Nerve, 22*(10), 1367-1371.

Eagle, M., Baudouin, S. V., Chandler, C., Giddings, D. R., Bullock, R., & Bushby, K. (2002). Survival in Duchenne muscular dystrophy: improvements in life expectancy since 1967 and the impact of home nocturnal ventilation. *Neuromuscul Disord, 12*(10), 926-929. doi:10.1016/s0960-8966(02)00140-2

Eccles, J. C., Llinas, R., & Sasaki, K. (1966a). The excitatory synaptic action of climbing fibres on the Purkinje cells of the cerebellum. *J Physiol, 182*(2), 268-296.

Eccles, J. C., Llinas, R., & Sasaki, K. (1966b). The inhibitory interneurones within the cerebellar cortex. *Exp Brain Res, 1*(1), 1-16.

Eccles, J. C., Sasaki, K., & Strata, P. (1967). A comparison of the inhibitory actions of Golgi cells and of basket cells. *Exp Brain Res, 3*(1), 81-94.

Eckert, M. A., Leonard, C. M., Richards, T. L., Aylward, E. H., Thomson, J., & Berninger, V. W. (2003). Anatomical correlates of dyslexia: frontal and cerebellar findings. *Brain, 126*(Pt 2), 482-494. doi:10.1093/brain/awg026

Edgerton, J. R., & Reinhart, P. H. (2003). Distinct contributions of small and large conductance Ca2+-activated K+ channels to rat Purkinje neuron function. *J Physiol, 548*(Pt 1), 53-69. doi:10.1113/jphysiol.2002.027854

Eichenbaum, H. (2000). A cortical-hippocampal system for declarative memory. *Nat Rev Neurosci, 1*(1), 41-50. doi:10.1038/35036213

Eisen, B., Ben Jehuda, R., Cuttitta, A. J., Mekies, L. N., Shemer, Y., Baskin, P., . . . Binah, O. (2019). Electrophysiological abnormalities in induced pluripotent stem cell-derived cardiomyocytes generated from Duchenne muscular dystrophy patients. *J Cell Mol Med, 23*(3), 2125-2135. doi:10.1111/jcmm.14124

Ekerot, C. F., & Kano, M. (1985). Long-term depression of parallel fibre synapses following stimulation of climbing fibres. *Brain Res, 342*(2), 357-360. doi:10.1016/0006-8993(85)91136-9

Emery, A., & Emery, M. (1993). Edward Meryon (1809-1880) and muscular dystrophy. *Journal of medical genetics, 30*(6), 506-511.

Erb, W. (1891). Dystrophia muscularis progressiva. *Journal of Neurology, 1*(3), 173-261.

Erecinska, M., & Dagani, F. (1990). Relationships between the neuronal sodium/potassium pump and energy metabolism. Effects of K+, Na+, and adenosine triphosphate in isolated brain synaptosomes. *J Gen Physiol, 95*(4), 591-616. doi:10.1085/jgp.95.4.591

Ervasti, J. M., & Campbell, K. P. (1993). A role for the dystrophin-glycoprotein complex as a transmembrane linker between laminin and actin. *J Cell Biol, 122*(4), 809-823. doi:10.1083/jcb.122.4.809

Escayg, A., Heils, A., MacDonald, B. T., Haug, K., Sander, T., & Meisler, M. H. (2001). A novel SCN1A mutation associated with generalized epilepsy with febrile seizures plus--and prevalence of variants in patients with epilepsy. *Am J Hum Genet, 68*(4), 866-873. doi:10.1086/319524

Essex, C., & Roper, H. (2001). Lesson of the week: late diagnosis of Duchenne's muscular dystrophy presenting as global developmental delay. *BMJ, 323*(7303), 37-38.

Essrich, C., Lorez, M., Benson, J. A., Fritschy, J. M., & Luscher, B. (1998). Postsynaptic clustering of major GABAA receptor subtypes requires the gamma 2 subunit and gephyrin. *Nat Neurosci, 1*(7), 563-571. doi:10.1038/2798

Faber, D. S. (1998). *Central Synapses: Quantal Mechanisms and Plasticity: Workshop IV*: Human Frontier Science Program.

Farkhani, S. M., Valizadeh, A., Karami, H., Mohammadi, S., Sohrabi, N., & Badrzadeh, F. (2014). Cell penetrating peptides: efficient vectors for delivery of nanoparticles, nanocarriers, therapeutic and diagnostic molecules. *Peptides, 57*, 78-94. doi:10.1016/j.peptides.2014.04.015

Farr, S. A., Erickson, M. A., Niehoff, M. L., Banks, W. A., & Morley, J. E. (2014). Central and peripheral administration of antisense oligonucleotide targeting amyloid-beta protein precursor improves learning and memory and reduces neuroinflammatory cytokines in Tg2576 (AbetaPPswe) mice. *J Alzheimers Dis, 40*(4), 1005-1016. doi:10.3233/JAD-131883

Fatt, P., & Katz, B. (1952). Spontaneous subthreshold activity at motor nerve endings. *J Physiol, 117*(1), 109-128.

Fauconnier, J., Thireau, J., Reiken, S., Cassan, C., Richard, S., Matecki, S., . . . Lacampagne, A. (2010). Leaky RyR2 trigger ventricular arrhythmias in Duchenne muscular dystrophy. *Proc Natl Acad Sci U S A, 107*(4), 1559-1564. doi:10.1073/pnas.0908540107

Feener, C. A., Koenig, M., & Kunkel, L. M. (1989). Alternative splicing of human dystrophin mRNA generates isoforms at the carboxy terminus. *Nature, 338*(6215), 509-511. doi:10.1038/338509a0

Felisari, G., Martinelli Boneschi, F., Bardoni, A., Sironi, M., Comi, G. P., Robotti, M., . . . Bresolin, N. (2000). Loss of Dp140 dystrophin isoform and intellectual impairment in Duchenne dystrophy. *Neurology, 55*(4), 559-564.

Fierro, L., DiPolo, R., & Llano, I. (1998). Intracellular calcium clearance in Purkinje cell somata from rat cerebellar slices. *J Physiol, 510 (Pt 2)*, 499-512. doi:10.1111/j.1469-7793.1998.499bk.x

Fiez, J. A., Petersen, S. E., Cheney, M. K., & Raichle, M. E. (1992). Impaired non-motor learning and error detection associated with cerebellar damage. A single case study. *Brain, 115 Pt 1*, 155-178.

Finch, E. A., & Augustine, G. J. (1998). Local calcium signalling by inositol-1,4,5-trisphosphate in Purkinje cell dendrites. *Nature, 396*(6713), 753-756. doi:10.1038/25541

Finkbeiner, S., & Greenberg, M. E. (1998). Ca2+ channel-regulated neuronal gene expression. *J Neurobiol, 37*(1), 171-189.

Fisher, S. A., Fischer, T. M., & Carew, T. J. (1997). Multiple overlapping processes underlying short-term synaptic enhancement. *Trends Neurosci, 20*(4), 170-177.

Fleshman, J. W., Munson, J. B., Sypert, G. W., & Friedman, W. A. (1981). Rheobase, input resistance, and motor-unit type in medial gastrocnemius motoneurons in the cat. *J Neurophysiol, 46*(6), 1326-1338. doi:10.1152/jn.1981.46.6.1326

Fong, P. Y., Turner, P. R., Denetclaw, W. F., & Steinhardt, R. A. (1990). Increased activity of calcium leak channels in myotubes of Duchenne human and mdx mouse origin. *Science, 250*(4981), 673-676.

Franco, A., Jr., & Lansman, J. B. (1990). Calcium entry through stretch-inactivated ion channels in mdx myotubes. *Nature, 344*(6267), 670-673. doi:10.1038/344670a0

Fritschy, J. M., Johnson, D. K., Mohler, H., & Rudolph, U. (1998). Independent assembly and subcellular targeting of GABA(A)-receptor subtypes demonstrated in mouse hippocampal and olfactory neurons in vivo. *Neurosci Lett, 249*(2-3), 99-102.

Fritschy, J. M., Schweizer, C., Brunig, I., & Luscher, B. (2003). Pre- and post-synaptic mechanisms regulating the clustering of type A gamma-aminobutyric acid receptors (GABAA receptors). *Biochem Soc Trans, 31*(Pt 4), 889-892. doi:10.1042/

Fuenzalida, M., Espinoza, C., Perez, M. A., Tapia-Rojas, C., Cuitino, L., Brandan, E., & Inestrosa, N. C. (2016). Wnt signaling pathway improves central inhibitory synaptic transmission in a mouse model of Duchenne muscular dystrophy. *Neurobiol Dis, 86*, 109-120. doi:10.1016/j.nbd.2015.11.018

Gaglianone, R. B., Santos, A. T., Bloise, F. F., Ortiga-Carvalho, T. M., Costa, M. L., Quirico-Santos, T., . . . Mermelstein, C. (2019). Reduced mitochondrial respiration and increased calcium deposits in the EDL muscle, but not in soleus, from 12-week-old dystrophic mdx mice. *Sci Rep, 9*(1), 1986. doi:10.1038/s41598-019-38609-4

Gailly, P., Boland, B., Himpens, B., Casteels, R., & Gillis, J. M. (1993). Critical-Evaluation of Cytosolic Calcium Determination in Resting Muscle-Fibers from Normal and Dystrophic (Mdx) Mice. *Cell Calcium, 14*(6), 473-483. doi:Doi 10.1016/0143-4160(93)90006-R

Gavillet, B., Rougier, J. S., Domenighetti, A. A., Behar, R., Boixel, C., Ruchat, P., . . . Abriel, H. (2006). Cardiac sodium channel Nav1.5 is regulated by a multiprotein complex composed of syntrophins and dystrophin. *Circ Res, 99*(4), 407-414. doi:10.1161/01.RES.0000237466.13252.5e

Gellens, M. E., George, A. L., Jr., Chen, L. Q., Chahine, M., Horn, R., Barchi, R. L., & Kallen, R. G. (1992). Primary structure and functional expression of the human cardiac tetrodotoxin-insensitive voltage-dependent sodium channel. *Proc Natl Acad Sci U S A, 89*(2), 554-558. doi:10.1073/pnas.89.2.554

Ghosh, A., & Greenberg, M. E. (1995). Calcium signaling in neurons: molecular mechanisms and cellular consequences. *Science, 268*(5208), 239-247. doi:10.1126/science.7716515

Gieseler, K., Bessou, C., & Segalat, L. (1999). Dystrobrevin- and dystrophin-like mutants display similar phenotypes in the nematode Caenorhabditis elegans. *Neurogenetics, 2*(2), 87-90. doi:10.1007/s100480050057

Gillis, J. M. (1999). Understanding dystrophinopathies: an inventory of the structural and functional consequences of the absence of dystrophin in muscles of the mdx mouse. *J Muscle Res Cell Motil, 20*(7), 605-625.

Goddard, G. V., McIntyre, D. C., & Leech, C. K. (1969). A permanent change in brain function resulting from daily electrical stimulation. *Exp Neurol, 25*(3), 295-330. doi:10.1016/0014-4886(69)90128-9

Gorecki, D. C., Monaco, A. P., Derry, J. M., Walker, A. P., Barnard, E. A., & Barnard, P. J. (1992). Expression of four alternative dystrophin transcripts in brain regions regulated by different promoters. *Hum Mol Genet, 1*(7), 505-510.

Gowers, W. R. (1879). *Pseudo-hypertrophic muscular paralysis: a clinical lecture*: J. & A. Churchill.

Goyenvalle, A., Griffith, G., Babbs, A., El Andaloussi, S., Ezzat, K., Avril, A., . . . Garcia, L. (2015). Functional correction in mouse models of muscular dystrophy using exon-skipping tricyclo-DNA oligomers. *Nat Med, 21*(3), 270-275. doi:10.1038/nm.3765

Graciotti, L., Minelli, A., Minciacchi, D., Procopio, A., & Fulgenzi, G. (2008). GABAergic miniature spontaneous activity is increased in the CA1 hippocampal region of dystrophic mdx mice. *Neuromuscul Disord, 18*(3), 220-226. doi:10.1016/j.nmd.2007.11.009

Graham, I. R., Hill, V. J., Manoharan, M., Inamati, G. B., & Dickson, G. (2004). Towards a therapeutic inhibition of dystrophin exon 23 splicing in mdx mouse muscle induced by antisense oligoribonucleotides (splicomers): target sequence optimisation using oligonucleotide arrays. *J Gene Med, 6*(10), 1149-1158. doi:10.1002/jgm.603

Grant, A. O. (2009). Cardiac ion channels. *Circ Arrhythm Electrophysiol, 2*(2), 185-194. doi:10.1161/CIRCEP.108.789081

Graziane, N., & Dong, Y. (2016). *Electrophysiological Analysis of Synaptic Transmission* (1st ed 2016. ed.). New York, NY: Springer New York : Imprint: Humana Press.

Greally, E., Davison, B. J., Blain, A., Laval, S., Blamire, A., Straub, V., & MacGowan, G. A. (2013). Heterogeneous abnormalities of in-vivo left ventricular calcium influx and function in mouse models of muscular dystrophy cardiomyopathy. *J Cardiovasc Magn Reson, 15*, 4. doi:10.1186/1532-429X-15-4

Grounds, M. D., Radley, H. G., Lynch, G. S., Nagaraju, K., & De Luca, A. (2008). Towards developing standard operating procedures for pre-clinical testing in the mdx mouse model of Duchenne muscular dystrophy. *Neurobiology of disease, 31*(1), 1-19.

Grynkiewicz, G., Poenie, M., & Tsien, R. Y. (1985). A new generation of Ca2+ indicators with greatly improved fluorescence properties. *Journal of Biological Chemistry, 260*(6), 3440-3450.

Gunter, T. E., Restrepo, D., & Gunter, K. K. (1988). Conversion of esterified fura-2 and indo-1 to Ca2+-sensitive forms by mitochondria. *Am J Physiol, 255*(3 Pt 1), C304-310. doi:10.1152/ajpcell.1988.255.3.C304

Gutiérrez, A., Khan, Z. U., Miralles, C. P., Mehta, A. K., Ruano, D., Araujo, F., . . . De Blas, A. L. (1997). GABAA receptor subunit expression changes in the rat cerebellum and cerebral cortex during aging. *Molecular Brain Research, 45*(1), 59-70. doi:https://doi.org/10.1016/S0169-328X(96)00237-9

Hammond, S. M., Hazell, G., Shabanpoor, F., Saleh, A. F., Bowerman, M., Sleigh, J. N., . . . Wood, M. J. (2016). Systemic peptide-mediated oligonucleotide therapy improves long-term survival in spinal muscular atrophy. *Proc Natl Acad Sci U S A, 113*(39), 10962-10967. doi:10.1073/pnas.1605731113

Hammond, S. M., & Wood, M. J. (2011). Genetic therapies for RNA mis-splicing diseases. *Trends Genet, 27*(5), 196-205. doi:10.1016/j.tig.2011.02.004

Han, P., Trinidad, B. J., & Shi, J. (2015). Hypocalcemia-induced seizure: demystifying the calcium paradox. *ASN Neuro, 7*(2). doi:10.1177/1759091415578050

Hanse, E., & Gustafsson, B. (1994). Onset and stabilization of NMDA receptor-dependent hippocampal long-term potentiation. *Neurosci Res, 20*(1), 15-25.

Hansel, C., & Linden, D. J. (2000). Long-term depression of the cerebellar climbing fiber--Purkinje neuron synapse. *Neuron, 26*(2), 473-482. doi:10.1016/s0896-6273(00)81179-4

Hartell, N. A. (1996). Strong activation of parallel fibers produces localized calcium transients and a form of LTD that spreads to distant synapses. *Neuron, 16*(3), 601-610.

Harvey, R. J., & Napper, R. M. (1991). Quantitative studies on the mammalian cerebellum. *Prog Neurobiol, 36*(6), 437-463.

Haws, C. M., & Lansman, J. B. (1991). Calcium-permeable ion channels in cerebellar neurons from mdx mice. *Proc Biol Sci, 244*(1311), 185-189. doi:10.1098/rspb.1991.0068

Head, S. I. (1993). Membrane potential, resting calcium and calcium transients in isolated muscle fibres from normal and dystrophic mice. *J Physiol, 469*, 11-19. doi:10.1113/jphysiol.1993.sp019801

Head, S. I. (2010). Branched fibres in old dystrophic mdx muscle are associated with mechanical weakening of the sarcolemma, abnormal Ca2+ transients and a breakdown of Ca2+ homeostasis during fatigue. *Exp Physiol, 95*(5), 641-656. doi:10.1113/expphysiol.2009.052019

Head, S. I., Williams, D. A., & Stephenson, D. G. (1992). Abnormalities in structure and function of limb skeletal muscle fibres of dystrophic mdx mice. *Proc Biol Sci, 248*(1322), 163-169. doi:10.1098/rspb.1992.0058

Hendriksen, J. G., & Vles, J. S. (2006). Are males with Duchenne muscular dystrophy at risk for reading disabilities? *Pediatric neurology, 34*(4), 296-300.

Hendriksen, R. G., Hoogland, G., Schipper, S., Hendriksen, J. G., Vles, J. S., & Aalbers, M. W. (2015). A possible role of dystrophin in neuronal excitability: a review of the current literature. *Neurosci Biobehav Rev, 51*, 255-262. doi:10.1016/j.neubiorev.2015.01.023

Hernandez-Ochoa, E. O., Pratt, S. J. P., Garcia-Pelagio, K. P., Schneider, M. F., & Lovering, R. M. (2015). Disruption of action potential and calcium signaling properties in malformed myofibers from dystrophin-deficient mice. *Physiol Rep, 3*(4). doi:10.14814/phy2.12366

Hinton, V., De Vivo, D., Fee, R., Goldstein, E., & Stern, Y. (2004). Investigation of poor academic achievement in children with Duchenne muscular dystrophy. *Learning Disabilities Research & Practice, 19*(3), 146-154.

Hinton, V. J., De Vivo, D. C., Nereo, N. E., Goldstein, E., & Stern, Y. (2001). Selective deficits in verbal working memory associated with a known genetic etiology: the neuropsychological profile of duchenne muscular dystrophy. *J Int Neuropsychol Soc, 7*(1), 45-54.

Hinton, V. J., Fee, R. J., Goldstein, E. M., & De Vivo, D. C. (2007). Verbal and memory skills in males with Duchenne muscular dystrophy. *Dev Med Child Neurol, 49*(2), 123-128. doi:10.1111/j.1469-8749.2007.00123.x

Hirano, T. (2013). Long-term depression and other synaptic plasticity in the cerebellum. *Proc Jpn Acad Ser B Phys Biol Sci, 89*(5), 183-195.

Hoffman, E. P., Brown, R. H., & Kunkel, L. M. (1987). Dystrophin: the protein product of the Duchenne muscular dystrophy locus. *Cell, 51*(6), 919-928.

Hoffman, E. P., & Dressman, D. (2001). Molecular pathophysiology and targeted therapeutics for muscular dystrophy. *Trends Pharmacol Sci, 22*(9), 465-470. doi:10.1016/s0165-6147(00)01770-3

Hoffman, E. P., & Gorospe, J. R. M. (1991). Chapter 8 The Animal Models of Duchenne Muscular Dystrophy: Windows on the Pathophysiological Consequences of Dystrophin Deficiency. In M. S. Mooseker & J. S. Morrow (Eds.), *Current Topics in Membranes* (Vol. 38, pp. 113-154): Academic Press.

Hoffman, E. P., Knudson, C. M., Campbell, K. P., & Kunkel, L. M. (1987). Subcellular fractionation of dystrophin to the triads of skeletal muscle. *Nature, 330*(6150), 754-758.

Hollingworth, S., Zeiger, U., & Baylor, S. M. (2008). Comparison of the myoplasmic calcium transient elicited by an action potential in intact fibres of mdx and normal mice. *J Physiol, 586*(21), 5063-5075. doi:10.1113/jphysiol.2008.160507

Hopf, F. W., & Steinhardt, R. A. (1992). Regulation of intracellular free calcium in normal and dystrophic mouse cerebellar neurons. *Brain Res, 578*(1-2), 49-54.

Hu, S., Labuda, M. Z., Pandolfo, M., Goss, G. G., McDermid, H. E., & Ali, D. W. (2003). Variants of the KCNMB3 regulatory subunit of maxi BK channels affect channel inactivation. *Physiol Genomics, 15*(3), 191-198. doi:10.1152/physiolgenomics.00110.2003

Hudziak, R. M., Barofsky, E., Barofsky, D. F., Weller, D. L., Huang, S. B., & Weller, D. D. (1996). Resistance of morpholino phosphorodiamidate oligomers to enzymatic degradation. *Antisense Nucleic Acid Drug Dev, 6*(4), 267-272. doi:10.1089/oli.1.1996.6.267

Humpel, C. (2015). Organotypic brain slice cultures: A review. *Neuroscience, 305*, 86-98. doi:10.1016/j.neuroscience.2015.07.086

Hyrc, K. L., Bownik, J. M., & Goldberg, M. P. (2000). Ionic selectivity of low-affinity ratiometric calcium indicators: mag-Fura-2, Fura-2FF and BTC. *Cell Calcium, 27*(2), 75-86. doi:10.1054/ceca.1999.0092

Inoue, T. (2003). Dynamics of calcium and its roles in the dendrite of the cerebellar Purkinje cell. *Keio J Med, 52*(4), 244-249. doi:10.2302/kjm.52.244

Inoue, T., Kato, K., Kohda, K., & Mikoshiba, K. (1998). Type 1 inositol 1,4,5-trisphosphate receptor is required for induction of long-term depression in cerebellar Purkinje neurons. *J Neurosci, 18*(14), 5366-5373.

Inoue, T., Lin, X., Kohlmeier, K. A., Orr, H. T., Zoghbi, H. Y., & Ross, W. N. (2001). Calcium dynamics and electrophysiological properties of cerebellar Purkinje cells in SCA1 transgenic mice. *J Neurophysiol, 85*(4), 1750-1760. doi:10.1152/jn.2001.85.4.1750

Ito, K., Sawada, Y., Sugiyama, Y., Suzuki, H., Hanano, M., & Iga, T. (1994). Linear relationship between GABAA receptor occupancy of muscimol and glucose metabolic response in the conscious mouse brain. Clinical implication based on comparison with benzodiazepine receptor agonist. *Drug Metabolism and Disposition, 22*(1), 50.

Ito, M. (1989). Long-term depression. *Annu Rev Neurosci, 12*, 85-102. doi:10.1146/annurev.ne.12.030189.000505

Ito, M. (2001). Cerebellar long-term depression: characterization, signal transduction, and functional roles. *Physiol Rev, 81*(3), 1143-1195.

Ito, M., & Kano, M. (1982). Long-lasting depression of parallel fiber-Purkinje cell transmission induced by conjunctive stimulation of parallel fibers and climbing fibers in the cerebellar cortex. *Neurosci Lett, 33*(3), 253-258. doi:10.1016/0304-3940(82)90380-9

Ito, M., & Yoshida, M. (1964). The cerebellar-evoked monosynaptic inhibition of Deiters' neurones. *Experientia, 20*(9), 515-516.

Ito, M., & Yoshida, M. (1966). The origin of cerebral-induced inhibition of Deiters neurones. I. Monosynaptic initiation of the inhibitory postsynaptic potentials. *Exp Brain Res, 2*(4), 330-349.

Ito, M., Yoshida, M., & Obata, K. (1964). Monosynaptic inhibition of the intracerebellar nuclei induced rom the cerebellar cortex. *Experientia, 20*(10), 575-576.

Ivannikov, M. V., Sugimori, M., & Llinas, R. R. (2010). Calcium clearance and its energy requirements in cerebellar neurons. *Cell Calcium, 47*(6), 507-513. doi:10.1016/j.ceca.2010.04.004

Ivanova, G. D., Arzumanov, A., Abes, R., Yin, H., Wood, M. J., Lebleu, B., & Gait, M. J. (2008). Improved cell-penetrating peptide-PNA conjugates for splicing redirection in HeLa cells and exon skipping in mdx mouse muscle. *Nucleic Acids Res, 36*(20), 6418-6428. doi:10.1093/nar/gkn671

Iversen, P. L., Aird, K. M., Wu, R., Morse, M. M., & Devi, G. R. (2009). Cellular uptake of neutral phosphorodiamidate morpholino oligomers. *Curr Pharm Biotechnol, 10*(6), 579-588.

Jack, J. J. B., Noble, D., & Tsien, R. W. (1975). *Electric current flow in excitable cells*. Oxford, UK: Clarendon Press.

Jacob, T. C., Moss, S. J., & Jurd, R. (2008). GABA(A) receptor trafficking and its role in the dynamic modulation of neuronal inhibition. *Nat Rev Neurosci, 9*(5), 331-343. doi:10.1038/nrn2370

Jagadha, V., & Becker, L. E. (1988). Brain morphology in Duchenne muscular dystrophy: a Golgi study. *Pediatr Neurol, 4*(2), 87-92.

Jarrard, L. E. (1995). What does the hippocampus really do? *Behav Brain Res, 71*(1-2), 1-10.

Jay, V., & Vajsar, J. (2001). The dystrophy of Duchenne. *The Lancet, 357*(9255), 550-552.

Kakizawa, S., Yamazawa, T., Chen, Y., Ito, A., Murayama, T., Oyamada, H., . . . Iino, M. (2012). Nitric oxide-induced calcium release via ryanodine receptors regulates neuronal function. *EMBO J, 31*(2), 417-428. doi:10.1038/emboj.2011.386

Kalume, F., Yu, F. H., Westenbroek, R. E., Scheuer, T., & Catterall, W. A. (2007). Reduced sodium current in Purkinje neurons from Nav1.1 mutant mice: implications for ataxia in severe myoclonic epilepsy in infancy. *J Neurosci, 27*(41), 11065-11074. doi:10.1523/JNEUROSCI.2162-07.2007

Kandel, E., Schwartz, J., & Jessell, T. (2012). *Principles of Neural Science, Fifth Edition*: McGraw-Hill Professional.

Kandel, E., Schwartz, J., Jessell, T., Siegelbaum, S., & Hudspeth, A. J. (2012). *Principles of Neural Science, Fifth Edition*. Blacklick, United States: McGraw-Hill Publishing.

Kang, T., Gao, X., & Chen, J. (2014). Harnessing the capacity of cell-penetrating peptides for drug delivery to the central nervous system. *Curr Pharm Biotechnol, 15*(3), 220-230. doi:10.2174/1389201015666140617094952

Kaplan, L. C., Osborne, P., & Elias, E. (1986). The diagnosis of muscular dystrophy in patients referred for language delay. *J Child Psychol Psychiatry, 27*(4), 545-549.

Kargacin, M. E., & Kargacin, G. J. (1996). The sarcoplasmic reticulum calcium pump is functionally altered in dystrophic muscle. *Biochim Biophys Acta, 1290*(1), 4-8. doi:10.1016/0304-4165(95)00180-8

Ke, J., Zhang, L., Qi, R., Li, W., Hou, C., Zhong, Y., . . . Lu, G. (2016). A longitudinal fMRI investigation in acute post-traumatic stress disorder (PTSD). *Acta Radiol, 57*(11), 1387-1395. doi:10.1177/0284185115585848

Ke, J. B., Chen, W., Yang, X. L., & Wang, Z. (2010). Characterization of spontaneous inhibitory postsynaptic currents in cultured rat retinal amacrine cells. *Neuroscience, 165*(2), 395-407. doi:10.1016/j.neuroscience.2009.10.010

Kelm, M. K., Criswell, H. E., & Breese, G. R. (2007). Calcium release from presynaptic internal stores is required for ethanol to increase spontaneous gamma-aminobutyric acid release onto cerebellum Purkinje neurons. *J Pharmacol Exp Ther, 323*(1), 356-364. doi:10.1124/jpet.107.126144

Khaliq, Z. M., & Raman, I. M. (2006). Relative contributions of axonal and somatic Na channels to action potential initiation in cerebellar Purkinje neurons. *J Neurosci, 26*(7), 1935-1944. doi:10.1523/JNEUROSCI.4664-05.2006

Khorkova, O., & Wahlestedt, C. (2017). Oligonucleotide therapies for disorders of the nervous system. *Nat Biotechnol, 35*(3), 249-263. doi:10.1038/nbt.3784

Kim, C. H., Oh, S. H., Lee, J. H., Chang, S. O., Kim, J., & Kim, S. J. (2012). Lobule-specific membrane excitability of cerebellar Purkinje cells. *J Physiol, 590*(2), 273-288. doi:10.1113/jphysiol.2011.221846

Kim, H., Pierce-Shimomura, J. T., Oh, H. J., Johnson, B. E., Goodman, M. B., & McIntire, S. L. (2009). The dystrophin complex controls bk channel localization and muscle activity in Caenorhabditis elegans. *PLoS Genet, 5*(12), e1000780. doi:10.1371/journal.pgen.1000780

Kim, H., Rogers, M. J., Richmond, J. E., & McIntire, S. L. (2004). SNF-6 is an acetylcholine transporter interacting with the dystrophin complex in Caenorhabditis elegans. *Nature, 430*(7002), 891-896. doi:10.1038/nature02798

Kimura, T., Sugimori, M., & Llinas, R. R. (2005). Purkinje cell long-term depression is prevented by T-588, a neuroprotective compound that reduces cytosolic calcium release from intracellular stores. *Proc Natl Acad Sci U S A, 102*(47), 17160-17165. doi:10.1073/pnas.0508190102

Kinali, M., Arechavala-Gomeza, V., Feng, L., Cirak, S., Hunt, D., Adkin, C., . . . Muntoni, F. (2009). Local restoration of dystrophin expression with the morpholino oligomer AVI-4658 in Duchenne muscular dystrophy: a single-blind, placebo-controlled, dose-escalation, proof-of-concept study. *Lancet Neurol, 8*(10), 918-928. doi:10.1016/S1474-4422(09)70211-X

Kingston, H. M., Thomas, N. S., Pearson, P. L., Sarfarazi, M., & Harper, P. S. (1983). Genetic linkage between Becker muscular dystrophy and a polymorphic DNA sequence on the short arm of the X chromosome. *J Med Genet, 20*(4), 255-258.

Kirischuk, S., & Verkhratsky, A. (1996). [Ca2+]i recordings from neural cells in acutely isolated cerebellar slices employing differential loading of the membrane-permeant form of the calcium indicator fura-2. *Pflugers Arch, 431*(6), 977-983.

Kitamura, K., & Kano, M. (2013). Dendritic calcium signaling in cerebellar Purkinje cell. *Neural Netw, 47*, 11-17. doi:10.1016/j.neunet.2012.08.001

Knuesel, I., Mastrocola, M., Zuellig, R. A., Bornhauser, B., Schaub, M. C., & Fritschy, J. M. (1999). Short communication: altered synaptic clustering of GABAA receptors in mice lacking dystrophin (mdx mice). *Eur J Neurosci, 11*(12), 4457-4462.

Knuesel, I., Zuellig, R. A., Schaub, M. C., & Fritschy, J. M. (2001). Alterations in dystrophin and utrophin expression parallel the reorganization of GABAergic synapses in a mouse model of temporal lobe epilepsy. *Eur J Neurosci, 13*(6), 1113-1124.

Koenig, M., Hoffman, E. P., Bertelson, C. J., Monaco, A. P., Feener, C., & Kunkel, L. M. (1987). Complete cloning of the Duchenne muscular dystrophy (DMD) cDNA and preliminary genomic organization of the DMD gene in normal and affected individuals. *Cell, 50*(3), 509-517.

Koenig, M., Monaco, A. P., & Kunkel, L. M. (1988). The complete sequence of dystrophin predicts a rod-shaped cytoskeletal protein. *Cell, 53*(2), 219-228.

Koenig, X., Dysek, S., Kimbacher, S., Mike, A. K., Cervenka, R., Lukacs, P., . . . Hilber, K. (2011). Voltage-gated ion channel dysfunction precedes cardiomyopathy development in the dystrophic heart. *PloS one, 6*(5), e20300. doi:10.1371/journal.pone.0020300

Koenig, X., Ebner, J., & Hilber, K. (2018). Voltage-Dependent Sarcolemmal Ion Channel Abnormalities in the Dystrophin-Deficient Heart. *Int J Mol Sci, 19*(11). doi:10.3390/ijms19113296

Koenig, X., Rubi, L., Obermair, G. J., Cervenka, R., Dang, X. B., Lukacs, P., . . . Hilber, K. (2014). Enhanced currents through L-type calcium channels in cardiomyocytes disturb the electrophysiology of the dystrophic heart. *American Journal of Physiology-Heart and Circulatory Physiology, 306*(4), H564-H573. doi:10.1152/ajpheart.00441.2013

Kohrman, D. C., Smith, M. R., Goldin, A. L., Harris, J., & Meisler, M. H. (1996). A missense mutation in the sodium channel Scn8a is responsible for cerebellar ataxia in the mouse mutant jolting. *J Neurosci, 16*(19), 5993-5999.

Komaki, H., Takeshima, Y., Matsumura, T., Ozasa, S., Funato, M., Takeshita, E., . . . Takeda, S. (2020). Viltolarsen in Japanese Duchenne muscular dystrophy patients: A phase 1/2 study. *Annals of Clinical and Translational Neurology, 7*(12), 2393-2408. doi:http://dx.doi.org/10.1002/acn3.51235

Kong, J., & Anderson, J. E. (1999). Dystrophin is required for organizing large acetylcholine receptor aggregates. *Brain Res, 839*(2), 298-304. doi:10.1016/s0006-8993(99)01737-0

Konnerth, A., Dreessen, J., & Augustine, G. J. (1992). Brief dendritic calcium signals initiate long-lasting synaptic depression in cerebellar Purkinje cells. *Proc Natl Acad Sci U S A, 89*(15), 7051-7055. doi:10.1073/pnas.89.15.7051

Koo, T., & Wood, M. J. (2013). Clinical trials using antisense oligonucleotides in duchenne muscular dystrophy. *Hum Gene Ther, 24*(5), 479-488. doi:10.1089/hum.2012.234

Kordasiewicz, H. B., Stanek, L. M., Wancewicz, E. V., Mazur, C., McAlonis, M. M., Pytel, K. A., . . . Cleveland, D. W. (2012). Sustained therapeutic reversal of Huntington's disease by transient repression of huntingtin synthesis. *Neuron, 74*(6), 1031-1044. doi:10.1016/j.neuron.2012.05.009

Kornegay, J. N., Bogan, J. R., Bogan, D. J., Childers, M. K., Li, J., Nghiem, P., . . . Hoffman, E. P. (2012). Canine models of Duchenne muscular dystrophy and their use in therapeutic strategies. *Mamm Genome, 23*(1-2), 85-108. doi:10.1007/s00335-011-9382-y

Kueh, S., Dempster, J., Head, S., & Morley, J. (2011). Reduced postsynaptic GABA A receptor number and enhanced gaboxadol induced change in holding currents in Purkinje cells of the dystrophin-deficient mdx mouse. *Neurobiology of disease, **43***(3), 558-564.

Kueh, S. L., Head, S. I., & Morley, J. W. (2008). GABA(A) receptor expression and inhibitory post-synaptic currents in cerebellar Purkinje cells in dystrophin-deficient mdx mice. *Clin Exp Pharmacol Physiol, **35***(2), 207-210. doi:10.1111/j.1440-1681.2007.04816.x

Kunkel, L. M., Beggs, A. H., & Hoffman, E. P. (1989). Molecular genetics of Duchenne and Becker muscular dystrophy: emphasis on improved diagnosis. *Clin Chem, 35*(7 Suppl), B21-24.

Kunkel, L. M., Monaco, A. P., Hoffman, E., Koenig, M., Feener, C., & Bertelson, C. (1987). Molecular studies of progressive muscular dystrophy (Duchenne). *Enzyme, 38*(1-4), 72-75.

Kuruma, A., Inoue, T., & Mikoshiba, K. (2003). Dynamics of Ca(2+) and Na(+) in the dendrites of mouse cerebellar Purkinje cells evoked by parallel fibre stimulation. *Eur J Neurosci, 18*(10), 2677-2689. doi:10.1111/j.1460-9568.2003.02977.x

Kuwajima, G., Futatsugi, A., Niinobe, M., Nakanishi, S., & Mikoshiba, K. (1992). Two types of ryanodine receptors in mouse brain: skeletal muscle type exclusively in Purkinje cells and cardiac muscle type in various neurons. *Neuron, 9*(6), 1133-1142. doi:10.1016/0896-6273(92)90071-k

Lambert, M., Chafey, P., Hugnot, J. P., Koulakoff, A., Berwald-Netter, Y., Billard, C., . . . Gilgenkrantz, H. (1993). Expression of the transcripts initiated in the 62nd intron of the dystrophin gene. *Neuromuscul Disord, 3*(5-6), 519-524.

Latimer, R., Street, N., Conway, K. C., James, K., Cunniff, C., Oleszek, J., . . . Research, N. (2017). Secondary Conditions Among Males With Duchenne or Becker Muscular Dystrophy. *J Child Neurol, 32*(7), 663-670. doi:10.1177/0883073817701368

Lawrence, J. J., Saraga, F., Churchill, J. F., Statland, J. M., Travis, K. E., Skinner, F. K., & McBain, C. J. (2006). Somatodendritic Kv7/KCNQ/M channels control interspike interval in hippocampal interneurons. *J Neurosci, 26*(47), 12325-12338. doi:10.1523/JNEUROSCI.3521-06.2006

Lee, A. J., Buckingham, E. T., Kauer, A. J., & Mathews, K. D. (2018). Descriptive Phenotype of Obsessive Compulsive Symptoms in Males With Duchenne Muscular Dystrophy. *J Child Neurol, 33*(9), 572-579. doi:10.1177/0883073818774439

Lee, J. H., Ha, J. M., & Leem, C. H. (2015). A Novel Nicotinamide Adenine Dinucleotide Correction Method for Mitochondrial Ca(2+) Measurement with FURA-2-FF in Single Permeabilized Ventricular Myocytes of Rat. *Korean J Physiol Pharmacol, 19*(4), 373-382. doi:10.4196/kjpp.2015.19.4.373

Lee, J. J., & Yokota, T. (2013). Antisense therapy in neurology. *J Pers Med, 3*(3), 144-176. doi:10.3390/jpm3030144

Lee, J. S., Pfund, Z., Juhasz, C., Behen, M. E., Muzik, O., Chugani, D. C., . . . Chugani, H. T. (2002). Altered regional brain glucose metabolism in Duchenne muscular dystrophy: a pet study. *Muscle Nerve, 26*(4), 506-512. doi:10.1002/mus.10238

Lee, S. T., Chu, K., Jung, K. H., Kim, J. H., Huh, J. Y., Yoon, H., . . . Roh, J. K. (2012). miR-206 regulates brain-derived neurotrophic factor in Alzheimer disease model. *Ann Neurol, 72*(2), 269-277. doi:10.1002/ana.23588

Lefaucheur, J. P., Pastoret, C., & Sebille, A. (1995). Phenotype of dystrophinopathy in old mdx mice. *Anat Rec, 242*(1), 70-76. doi:10.1002/ar.1092420109

Lefebvre, S., Burglen, L., Reboullet, S., Clermont, O., Burlet, P., Viollet, L., . . . et al. (1995). Identification and characterization of a spinal muscular atrophy-determining gene. *Cell, 80*(1), 155-165. doi:10.1016/0092-8674(95)90460-3

Leibowitz, D., & Dubowitz, V. (1981). Intellect and behaviour in Duchenne muscular dystrophy. *Dev Med Child Neurol, 23*(5), 577-590.

Lemaire, C., Heilig, R., & Mandel, J. L. (1988). The chicken dystrophin cDNA: striking conservation of the C-terminal coding and 3' untranslated regions between man and chicken. *EMBO J, 7*(13), 4157-4162.

Lemasters, J. J., Inman, R. T., Bond, J. M., Gores, G. J., & Herman, B. (1988). Free calcium transients in spontaneously beating rat neonatal myocytes measured by digitized video microscopy. *J Mol Cell Cardiol, 20* (Suppl. IV), 542.

Lenk, U., Hanke, R., Thiele, H., & Speer, A. (1993). Point mutations at the carboxy terminus of the human dystrophin gene: implications for an association with mental retardation in DMD patients. *Hum Mol Genet, 2*(11), 1877-1881. doi:10.1093/hmg/2.11.1877

Lev-Ram, V., Miyakawa, H., Lasser-Ross, N., & Ross, W. N. (1992). Calcium transients in cerebellar Purkinje neurons evoked by intracellular stimulation. *J Neurophysiol, 68*(4), 1167-1177. doi:10.1152/jn.1992.68.4.1167

Levi, S., Grady, R. M., Henry, M. D., Campbell, K. P., Sanes, J. R., & Craig, A. M. (2002). Dystroglycan is selectively associated with inhibitory GABAergic synapses but is dispensable for their differentiation. *J Neurosci, 22*(11), 4274-4285. doi:20026440

Levin, S. I., Khaliq, Z. M., Aman, T. K., Grieco, T. M., Kearney, J. A., Raman, I. M., & Meisler, M. H. (2006). Impaired motor function in mice with cell-specific knockout of sodium channel Scn8a (NaV1.6) in cerebellar purkinje neurons and granule cells. *J Neurophysiol, 96*(2), 785-793. doi:10.1152/jn.01193.2005

Li, Y., Zhang, S., Zhang, X., Li, J., Ai, X., Zhang, L., . . . Chen, X. (2014). Blunted cardiac beta-adrenergic response as an early indication of cardiac dysfunction in Duchenne muscular dystrophy. *Cardiovasc Res, 103*(1), 60-71. doi:10.1093/cvr/cvu119

Li, Z., Okamoto, K., Hayashi, Y., & Sheng, M. (2004). The importance of dendritic mitochondria in the morphogenesis and plasticity of spines and synapses. *Cell, 119*(6), 873-887. doi:10.1016/j.cell.2004.11.003

Lidov, H. G. (1996). Dystrophin in the nervous system. *Brain Pathol, 6*(1), 63-77.

Lidov, H. G., Byers, T. J., & Kunkel, L. M. (1993). The distribution of dystrophin in the murine central nervous system: an immunocytochemical study. *Neuroscience, 54*(1), 167-187.

Lidov, H. G., Byers, T. J., Watkins, S. C., & Kunkel, L. M. (1990). Localization of dystrophin to postsynaptic regions of central nervous system cortical neurons. *Nature, 348*(6303), 725-728. doi:10.1038/348725a0

Liu, Y., & Rouiller, E. M. (1999). Mechanisms of recovery of dexterity following unilateral lesion of the sensorimotor cortex in adult monkeys. *Exp Brain Res, 128*(1-2), 149-159.

Llano, I., DiPolo, R., & Marty, A. (1994). Calcium-induced calcium release in cerebellar Purkinje cells. *Neuron, 12*(3), 663-673. doi:10.1016/0896-6273(94)90221-6

Llano, I., & Gerschenfeld, H. M. (1993). Inhibitory synaptic currents in stellate cells of rat cerebellar slices. *J Physiol, 468*, 177-200.

Llano, I., Gonzalez, J., Caputo, C., Lai, F. A., Blayney, L. M., Tan, Y. P., & Marty, A. (2000). Presynaptic calcium stores underlie large-amplitude miniature IPSCs and spontaneous calcium transients. *Nat Neurosci, 3*(12), 1256-1265. doi:10.1038/81781

Llinas, R., & Sugimori, M. (1980a). Electrophysiological properties of in vitro Purkinje cell dendrites in mammalian cerebellar slices. *J Physiol, 305*, 197-213.

Llinas, R., & Sugimori, M. (1980b). Electrophysiological properties of in vitro Purkinje cell somata in mammalian cerebellar slices. *J Physiol, 305*, 171-195.

Llinas, R., & Sugimori, M. (1990). Intracellular calcium concentration changes during cell death (pp. 1-10): Raven Press, New York.

Lopez, J. R., Kolster, J., Uryash, A., Esteve, E., Altamirano, F., & Adams, J. A. (2016). Dysregulation of Intracellular Ca2+ in Dystrophic Cortical and Hippocampal Neurons. *Mol Neurobiol*. doi:10.1007/s12035-016-0311-7

Lorenz, S., Heils, A., Kasper, J. M., & Sander, T. (2007). Allelic association of a truncation mutation of the KCNMB3 gene with idiopathic generalized epilepsy. *Am J Med Genet B Neuropsychiatr Genet, 144B*(1), 10-13. doi:10.1002/ajmg.b.30369

Lorivel, T., Roy, V., & Hilber, P. (2014). Fear-related behaviors in Lurcher mutant mice exposed to a predator. *Genes Brain Behav, 13*(8), 794-801. doi:10.1111/gbb.12173

Lovering, R. M., Michaelson, L., & Ward, C. W. (2009). Malformed mdx myofibers have normal cytoskeletal architecture yet altered EC coupling and stress-induced Ca2+ signaling. *Am J Physiol Cell Physiol, 297*(3), C571-580. doi:10.1152/ajpcell.00087.2009

Lv, S. Y., Zou, Q. H., Cui, J. L., Zhao, N., Hu, J., Long, X. Y., . . . Zang, Y. F. (2011). Decreased gray matter concentration and local synchronization of spontaneous activity in the motor cortex in Duchenne muscular dystrophy. *AJNR Am J Neuroradiol, 32*(11), 2196-2200. doi:10.3174/ajnr.A2718

Lynch, G. S., Rafael, J. A., Hinkle, R. T., Cole, N. M., Chamberlain, J. S., & Faulkner, J. A. (1997). Contractile properties of diaphragm muscle segments from old mdx and old transgenic mdx mice. *Am J Physiol, 272*(6 Pt 1), C2063-2068.

MacLean, J. N., & Yuste, R. (2009). Imaging action potentials with calcium indicators. *Cold Spring Harb Protoc, 2009*(11), pdb prot5316. doi:10.1101/pdb.prot5316

Malenka, R. C., Kauer, J. A., Zucker, R. S., & Nicoll, R. A. (1988). Postsynaptic calcium is sufficient for potentiation of hippocampal synaptic transmission. *Science, 242*(4875), 81-84.

Malenka, R. C., & Nicoll, R. A. (1993). NMDA-receptor-dependent synaptic plasticity: multiple forms and mechanisms. *Trends Neurosci, 16*(12), 521-527.

Malgaroli, A., Milani, D., Meldolesi, J., & Pozzan, T. (1987). Fura-2 measurement of cytosolic free Ca2+ in monolayers and suspensions of various types of animal cells. *J Cell Biol, 105*(5), 2145-2155. doi:10.1083/jcb.105.5.2145

Mandel, J. L. (1989). Dystrophin. The gene and its product. *Nature, 339*(6226), 584-586. doi:10.1038/339584a0

Manning, J., Kulbida, R., Rai, P., Jensen, L., Bouma, J., Singh, S. P., . . . Yilmazer-Hanke, D. (2014). Amitriptyline is efficacious in ameliorating muscle inflammation and depressive symptoms in the mdx mouse model of Duchenne muscular dystrophy. *Exp Physiol, 99*(10), 1370-1386. doi:10.1113/expphysiol.2014.079475

Manole, E. (1995). The dystrophin gene and its product--a view. *Rom J Neurol Psychiatry, 33*(2), 109-119.

Manzur, A. Y., Kinali, M., & Muntoni, F. (2008). Update on the management of Duchenne muscular dystrophy. *Arch Dis Child, 93*(11), 986-990. doi:10.1136/adc.2007.118141

Marcu, R., Neeley, C. K., Karamanlidis, G., & Hawkins, B. J. (2012). Multi-parameter measurement of the permeability transition pore opening in isolated mouse heart mitochondria. *J Vis Exp*(67). doi:10.3791/4131

Maren, S., & Fanselow, M. S. (1995). Synaptic plasticity in the basolateral amygdala induced by hippocampal formation stimulation in vivo. *J Neurosci, 15*(11), 7548-7564.

Marsh, G. G., & Munsat, T. L. (1974). Evidence of early impairment of verbal intelligence in Duchenne muscular dystrophy. *Arch Dis Child, 49*(2), 118-122. doi:10.1136/adc.49.2.118

Marty, A. (1981). Ca-dependent K channels with large unitary conductance in chromaffin cell membranes. *Nature, 291*(5815), 497-500. doi:10.1038/291497a0

Maruyama, R., Echigoya, Y., Caluseriu, O., Aoki, Y., Takeda, S., & Yokota, T. (2017). Systemic Delivery of Morpholinos to Skip Multiple Exons in a Dog Model of Duchenne Muscular Dystrophy. *Methods Mol Biol, 1565*, 201-213. doi:10.1007/978-1-4939-6817-6_17

Massey, P. V., & Bashir, Z. I. (2007). Long-term depression: multiple forms and implications for brain function. *Trends Neurosci, 30*(4), 176-184. doi:10.1016/j.tins.2007.02.005

Matsumura, F., & Clark, J. M. (1982). ATP-utilizing systems in the squid axons: a review on the biochemical aspects of ion-transport. *Prog Neurobiol, 18*(4), 231-255. doi:10.1016/0301-0082(82)90011-9

McGehee, D. S., Heath, M. J., Gelber, S., Devay, P., & Role, L. W. (1995). Nicotine enhancement of fast excitatory synaptic transmission in CNS by presynaptic receptors. *Science, 269*(5231), 1692-1696.

McKay, B. E., & Turner, R. W. (2005). Physiological and morphological development of the rat cerebellar Purkinje cell. *J Physiol, 567*(Pt 3), 829-850. doi:10.1113/jphysiol.2005.089383

Medici, V., Frassoni, C., Tassi, L., Spreafico, R., & Garbelli, R. (2011). Aquaporin 4 expression in control and epileptic human cerebral cortex. *Brain Res, 1367*, 330-339. doi:10.1016/j.brainres.2010.10.005

Mehler, M. F. (2000). Brain dystrophin, neurogenetics and mental retardation. *Brain Res Brain Res Rev, 32*(1), 277-307.

Mehler, M. F., Haas, K. Z., Kessler, J. A., & Stanton, P. K. (1992). Enhanced sensitivity of hippocampal pyramidal neurons from mdx mice to hypoxia-induced loss of synaptic transmission. *Proc Natl Acad Sci U S A, 89*(6), 2461-2465.

Meisler, M. H., Plummer, N. W., Burgess, D. L., Buchner, D. A., & Sprunger, L. K. (2004). Allelic mutations of the sodium channel SCN8A reveal multiple cellular and physiological functions. *Genetica, 122*(1), 37-45. doi:10.1007/s10709-004-1441-9

Mendell, J. R., Rodino-Klapac, L. R., Sahenk, Z., Roush, K., Bird, L., Lowes, L. P., . . . Eteplirsen Study, G. (2013). Eteplirsen for the treatment of Duchenne muscular dystrophy. *Ann Neurol, 74*(5), 637-647. doi:10.1002/ana.23982

Menke, A., & Jockusch, H. (1991). Decreased osmotic stability of dystrophin-less muscle cells from the mdx mouse. *Nature, 349*(6304), 69-71. doi:10.1038/349069a0

Mijares, A., Altamirano, F., Kolster, J., Adams, J. A., & Lopez, J. R. (2014). Age-dependent changes in diastolic Ca(2+) and Na(+) concentrations in dystrophic cardiomyopathy: Role of Ca(2+) entry and IP3. *Biochem Biophys Res Commun, 452*(4), 1054-1059. doi:10.1016/j.bbrc.2014.09.045

Miller, T. M., Pestronk, A., David, W., Rothstein, J., Simpson, E., Appel, S. H., . . . Cudkowicz, M. E. (2013). An antisense oligonucleotide against SOD1 delivered intrathecally for patients with SOD1 familial amyotrophic lateral sclerosis: a phase 1, randomised, first-in-man study. *Lancet Neurol, 12*(5), 435-442. doi:10.1016/S1474-4422(13)70061-9

Minciacchi, D., Del Tongo, C., Carretta, D., Nosi, D., & Granato, A. (2010). Alterations of the Cortico-Cortical Network in Sensori-Motor Areas of Dystrophin Deficient Mice. *Neuroscience, 166*(4), 1129-1139. doi:10.1016/j.neuroscience.2010.01.040

Miranda, R., Laroche, S., & Vaillend, C. (2016). Reduced neuronal density in the CA1 anterodorsal hippocampus of the mdx mouse. *Neuromuscul Disord, 26*(11), 775-781. doi:10.1016/j.nmd.2016.08.006

Miranda, R., Nudel, U., Laroche, S., & Vaillend, C. (2011). Altered presynaptic ultrastructure in excitatory hippocampal synapses of mice lacking dystrophins Dp427 or Dp71. *Neurobiol Dis, 43*(1), 134-141. doi:10.1016/j.nbd.2011.02.017

Miranda, R., Sebrie, C., Degrouard, J., Gillet, B., Jaillard, D., Laroche, S., & Vaillend, C. (2009). Reorganization of inhibitory synapses and increased PSD length of perforated excitatory synapses in hippocampal area CA1 of dystrophin-deficient mdx mice. *Cereb Cortex, 19*(4), 876-888. doi:10.1093/cercor/bhn135

Mitchell, D. J., Kim, D. T., Steinman, L., Fathman, C. G., & Rothbard, J. B. (2000). Polyarginine enters cells more efficiently than other polycationic homopolymers. *J Pept Res, 56*(5), 318-325. doi:10.1034/j.1399-3011.2000.00723.x

Miyakawa, H., Lev-Ram, V., Lasser-Ross, N., & Ross, W. N. (1992). Calcium transients evoked by climbing fiber and parallel fiber synaptic inputs in guinea pig cerebellar Purkinje neurons. *J Neurophysiol, 68*(4), 1178-1189.

Moens, P., Baatsen, P. H., & Marechal, G. (1993). Increased susceptibility of EDL muscles from mdx mice to damage induced by contractions with stretch. *J Muscle Res Cell Motil, 14*(4), 446-451.

Moizard, M. P., Billard, C., Toutain, A., Berret, F., Marmin, N., & Moraine, C. (1998). Are Dp71 and Dp140 brain dystrophin isoforms related to cognitive impairment in Duchenne muscular dystrophy? *Am J Med Genet, 80*(1), 32-41.

Moizard, M. P., Toutain, A., Fournier, D., Berret, F., Raynaud, M., Billard, C., . . . Moraine, C. (2000). Severe cognitive impairment in DMD: obvious clinical indication for Dp71 isoform point mutation screening. *Eur J Hum Genet, 8*(7), 552-556. doi:10.1038/sj.ejhg.5200488

Monaco, A. P., Neve, R. L., Colletti-Feener, C., Bertelson, C. J., Kurnit, D. M., & Kunkel, L. M. (1986). Isolation of candidate cDNAs for portions of the Duchenne muscular dystrophy gene. *Nature, 323*(6089), 646-650. doi:10.1038/323646a0

Mongini, T., Ghigo, D., Doriguzzi, C., Bussolino, F., Pescarmona, G., Pollo, B., . . . Bosia, A. (1988). Free cytoplasmic Ca++ at rest and after cholinergic stimulus is increased in cultured muscle cells from Duchenne muscular dystrophy patients. *Neurology, 38*(3), 476-480. doi:10.1212/wnl.38.3.476

Moreno-Rius, J. (2018). The cerebellum in fear and anxiety-related disorders. *Prog Neuropsychopharmacol Biol Psychiatry, 85*, 23-32. doi:10.1016/j.pnpbp.2018.04.002

Moulton, J. (2016). Guide for morpholino users: toward therapeutics. *J Drug Discov Dev Deliv, 3*(2), 1023.

Moyer, J. R., Jr., & Brown, T. H. (1998). Methods for whole-cell recording from visually preselected neurons of perirhinal cortex in brain slices from young and aging rats. *J Neurosci Methods, 86*(1), 35-54.

Muller, M., Mironov, S. L., Ivannikov, M. V., Schmidt, J., & Richter, D. W. (2005). Mitochondrial organization and motility probed by two-photon microscopy in cultured mouse brainstem neurons. *Exp Cell Res, 303*(1), 114-127. doi:10.1016/j.yexcr.2004.09.025

Muntoni, F., Mateddu, A., & Serra, G. (1991). Passive avoidance behaviour deficit in the mdx mouse. *Neuromuscul Disord, 1*(2), 121-123.

Muntoni, F., Torelli, S., & Ferlini, A. (2003). Dystrophin and mutations: one gene, several proteins, multiple phenotypes. *Lancet Neurol, 2*(12), 731-740.

Murray, J., Davies, K., Harper, P., Meredith, L., Mueller, C., & Williamson, R. (1982). Linkage relationship of a cloned DNA sequence on the short arm of the X chromosome to Duchenne muscular dystrophy. *Nature, 300*, 69-71.

Nachman, M. W., & Crowell, S. L. (2000). Contrasting evolutionary histories of two introns of the duchenne muscular dystrophy gene, Dmd, in humans. *Genetics, 155*(4), 1855-1864.

Nedelescu, H., & Abdelhack, M. (2013). Comparative morphology of dendritic arbors in populations of Purkinje cells in mouse sulcus and apex. *Neural Plast, 2013*, 948587. doi:10.1155/2013/948587

Nelson, A. B., Krispel, C. M., Sekirnjak, C., & du Lac, S. (2003). Long-lasting increases in intrinsic excitability triggered by inhibition. *Neuron, 40*(3), 609-620. doi:10.1016/s0896-6273(03)00641-x

Nguyen, Q., & Yokota, T. (2019). Antisense oligonucleotides for the treatment of cardiomyopathy in Duchenne muscular dystrophy. *Am J Transl Res, 11*(3), 1202-1218.

Nicolson, R. I., Fawcett, A. J., & Dean, P. (2001). Developmental dyslexia: the cerebellar deficit hypothesis. *Trends Neurosci, 24*(9), 508-511. doi:10.1016/s0166-2236(00)01896-8

Nowak, K. J., & Davies, K. E. (2004). Duchenne muscular dystrophy and dystrophin: pathogenesis and opportunities for treatment. *EMBO Rep, 5*(9), 872-876. doi:10.1038/sj.embor.7400221

Nudel, U., Zuk, D., Einat, P., Zeelon, E., Levy, Z., Neuman, S., & Yaffe, D. (1989). Duchenne muscular dystrophy gene product is not identical in muscle and brain. *Nature, 337*(6202), 76-78. doi:10.1038/337076a0

Nusser, Z., Cull-Candy, S., & Farrant, M. (1997). Differences in synaptic GABA(A) receptor number underlie variation in GABA mini amplitude. *Neuron, 19*(3), 697-709.

O'Brien, K. F., & Kunkel, L. M. (2001). Dystrophin and muscular dystrophy: past, present, and future. *Mol Genet Metab, 74*(1-2), 75-88. doi:10.1006/mgme.2001.3220

O'Brien, R. J., Kamboj, S., Ehlers, M. D., Rosen, K. R., Fischbach, G. D., & Huganir, R. L. (1998). Activity-dependent modulation of synaptic AMPA receptor accumulation. *Neuron, 21*(5), 1067-1078.

O'Keefe, J., & Conway, D. H. (1978). Hippocampal place units in the freely moving rat: why they fire where they fire. *Exp Brain Res, 31*(4), 573-590.

Oakes, S. G., Martin, W. J., 2nd, Lisek, C. A., & Powis, G. (1988). Incomplete hydrolysis of the calcium indicator precursor fura-2 pentaacetoxymethyl ester (fura-2 AM) by cells. *Anal Biochem, 169*(1), 159-166. doi:10.1016/0003-2697(88)90267-9

Ogasawara, A. (1989). Downward shift in IQ in persons with Duchenne muscular dystrophy compared to those with spinal muscular atrophy. *American Journal on Mental Retardation*.

Ogiwara, I., Miyamoto, H., Morita, N., Atapour, N., Mazaki, E., Inoue, I., . . . Yamakawa, K. (2007). Nav1.1 localizes to axons of parvalbumin-positive inhibitory interneurons: a circuit basis for epileptic seizures in mice carrying an Scn1a gene mutation. *J Neurosci, 27*(22), 5903-5914. doi:10.1523/JNEUROSCI.5270-06.2007

Okada, C. Y., & Rechsteiner, M. (1982). Introduction of macromolecules into cultured mammalian cells by osmotic lysis of pinocytic vesicles. *Cell, 29*(1), 33-41. doi:10.1016/0092-8674(82)90087-3

Olexova, L., Stefanik, P., & Krskova, L. (2016). Increased anxiety-like behaviour and altered GABAergic system in the amygdala and cerebellum of VPA rats - An animal model of autism. *Neurosci Lett, 629*, 9-14. doi:10.1016/j.neulet.2016.06.035

Olton, D. S., Becker, J. T., & Handelmann, G. E. (1979). Hippocampus, space, and memory. *Behavioral and Brain Sciences, 2*(03), 313-322.

Ontell, M., Hughes, D., & Bourke, D. (1982). Secondary myogenesis of normal muscle produces abnormal myotubes. *Anat Rec, 204*(3), 199-207. doi:10.1002/ar.1092040304

Ouardouz, M., & Lacaille, J. C. (1997). Properties of unitary IPSCs in hippocampal pyramidal cells originating from different types of interneurons in young rats. *J Neurophysiol, 77*(4), 1939-1949.

Page, T. L., Einstein, M., Duan, H., He, Y., Flores, T., Rolshud, D., . . . Hof, P. R. (2002). Morphological alterations in neurons forming corticocortical projections in the neocortex of aged Patas monkeys. *Neurosci Lett, 317*(1), 37-41. doi:10.1016/s0304-3940(01)02428-4

Palay, S. L., & Chan-Palay, V. (2012). *Cerebellar cortex: cytology and organization*: Springer Science & Business Media.

Pandya, M., Palpagama, T. H., Turner, C., Waldvogel, H. J., Faull, R. L., & Kwakowsky, A. (2019). Sex- and age-related changes in GABA signaling components in the human cortex. *Biol Sex Differ, 10*(1), 5. doi:10.1186/s13293-018-0214-6

Pane, M., Messina, S., Bruno, C., D'Amico, A., Villanova, M., Brancalion, B., . . . Mercuri, E. (2013). Duchenne muscular dystrophy and epilepsy. *Neuromuscul Disord, 23*(4), 313-315. doi:10.1016/j.nmd.2013.01.011

Pangalila, R. F., van den Bos, G. A., Bartels, B., Bergen, M., Stam, H. J., & Roebroeck, M. E. (2015). Prevalence of fatigue, pain, and affective disorders in adults with duchenne muscular dystrophy and their associations with quality of life. *Arch Phys Med Rehabil, 96*(7), 1242-1247. doi:10.1016/j.apmr.2015.02.012

Paradis, S., Sweeney, S. T., & Davis, G. W. (2001). Homeostatic control of presynaptic release is triggered by postsynaptic membrane depolarization. *Neuron, 30*(3), 737-749.

Pardridge, W. M. (2012). Drug transport across the blood-brain barrier. *J Cereb Blood Flow Metab, 32*(11), 1959-1972. doi:10.1038/jcbfm.2012.126

Passamano, L., Taglia, A., Palladino, A., Viggiano, E., D'Ambrosio, P., Scutifero, M., . . . Politano, L. (2012). Improvement of survival in Duchenne Muscular Dystrophy: retrospective analysis of 835 patients. *Acta Myol, 31*(2), 121-125.

Pastoret, C., & Sebille, A. (1995). mdx mice show progressive weakness and muscle deterioration with age. *J Neurol Sci, 129*(2), 97-105.

Peng, H. B., Xie, H., Rossi, S. G., & Rotundo, R. L. (1999). Acetylcholinesterase clustering at the neuromuscular junction involves perlecan and dystroglycan. *J Cell Biol, 145*(4), 911-921. doi:10.1083/jcb.145.4.911

Pereira da Silva, J. D., Campos, D. V., Nogueira-Bechara, F. M., Stilhano, R. S., Han, S. W., Sinigaglia-Coimbra, R., . . . Souccar, C. (2018). Altered release and uptake of gamma-aminobutyric acid in the cerebellum of dystrophin-deficient mice. *Neurochem Int, 118*, 105-114. doi:10.1016/j.neuint.2018.06.001

Perkel, D. J., Hestrin, S., Sah, P., & Nicoll, R. A. (1990). Excitatory synaptic currents in Purkinje cells. *Proc Biol Sci, 241*(1301), 116-121. doi:10.1098/rspb.1990.0074

Perronnet, C., & Vaillend, C. (2010). Dystrophins, utrophins, and associated scaffolding complexes: role in mammalian brain and implications for therapeutic strategies. *J Biomed Biotechnol, 2010*, 849426. doi:10.1155/2010/849426

Petrof, B. J., Shrager, J. B., Stedman, H. H., Kelly, A. M., & Sweeney, H. L. (1993). Dystrophin protects the sarcolemma from stresses developed during muscle contraction. *Proc Natl Acad Sci U S A, 90*(8), 3710-3714.

Pilgram, G. S., Potikanond, S., Baines, R. A., Fradkin, L. G., & Noordermeer, J. N. (2010). The roles of the dystrophin-associated glycoprotein complex at the synapse. *Mol Neurobiol, 41*(1), 1-21. doi:10.1007/s12035-009-8089-5

Plotogea, A. V., Keresztes, A., & Moarcas, M. (2009). GUILLAUME-BENJAMIN-AMAND DUCHENNE-BETWEEN MEDICINE AND ART. *Bulletin of the Transilvania University of Brasov. Medical Sciences. Series VI, 6*(51), 185-188.

Poisbeau, P., Rene, F., Egles, C., Felix, J. M., Feltz, P., & Schlichter, R. (1996). Characterization of functional GABAergic synapses formed between rat hypothalamic neurons and pituitary intermediate lobe cells in coculture: Ca2+ dependence of spontaneous IPSCs. *J Neurosci, 16*(16), 4835-4845.

Pouille, F., Cavelier, P., Desplantez, T., Beekenkamp, H., Craig, P. J., Beattie, R. E., . . . Bossu, J. L. (2000). Dendro-somatic distribution of calcium-mediated electrogenesis in purkinje cells from rat cerebellar slice cultures. *J Physiol, 527 Pt 2*, 265-282. doi:10.1111/j.1469-7793.2000.00265.x

Prescott, S. A., & De Koninck, Y. (2002). Four cell types with distinctive membrane properties and morphologies in lamina I of the spinal dorsal horn of the adult rat. *J Physiol, 539*(Pt 3), 817-836. doi:10.1113/jphysiol.2001.013437

Prosser, E., Murphy, E., & Thompson, M. (1969). Intelligence and the gene for Duchenne muscular dystrophy. *Archives of disease in childhood, 44*(234), 221-230.

Puliti, A., Caridi, G., Ravazzolo, R., & Ghiggeri, G. M. (2007). Teaching molecular genetics: chapter 4—positional cloning of genetic disorders. *Pediatric Nephrology (Berlin, Germany), 22*(12), 2023-2029. doi:10.1007/s00467-007-0548-5

Quintana, A., & Hoth, M. (2004). Apparent cytosolic calcium gradients in T-lymphocytes due to fura-2 accumulation in mitochondria. *Cell Calcium, 36*(2), 99-109. doi:10.1016/j.ceca.2004.01.003

Racine, R. J. (1972). Modification of seizure activity by electrical stimulation. II. Motor seizure. *Electroencephalogr Clin Neurophysiol, 32*(3), 281-294. doi:10.1016/0013-4694(72)90177-0

Rae, C., Griffin, J. L., Blair, D. H., Bothwell, J. H., Bubb, W. A., Maitland, A., & Head, S. (2002). Abnormalities in brain biochemistry associated with lack of dystrophin: studies of the mdx mouse. *Neuromuscul Disord, 12*(2), 121-129.

Rae, C., Harasty, J. A., Dzendrowskyj, T. E., Talcott, J. B., Simpson, J. M., Blamire, A. M., . . . Stein, J. F. (2002). Cerebellar morphology in developmental dyslexia. *Neuropsychologia, 40*(8), 1285-1292. doi:10.1016/s0028-3932(01)00216-0

Rae, C., Lawrance, M. L., Dias, L. S., Provis, T., Bubb, W. A., & Balcar, V. J. (2000). Strategies for studies of neurotoxic mechanisms involving deficient transport of L-glutamate: antisense knockout in rat brain in vivo and changes in the neurotransmitter metabolism following inhibition of glutamate transport in guinea pig brain slices. *Brain Res Bull, 53*(4), 373-381. doi:10.1016/s0361-9230(00)00372-5

Rae, C., Scott, R. B., Thompson, C. H., Dixon, R. M., Dumughn, I., Kemp, G. J., . . . Radda, G. K. (1998). Brain biochemistry in Duchenne muscular dystrophy: a 1H magnetic resonance and neuropsychological study. *J Neurol Sci, 160*(2), 148-157.

Rae, M. G., & O'Malley, D. (2016). Cognitive dysfunction in Duchenne muscular dystrophy: a possible role for neuromodulatory immune molecules. *J Neurophysiol, 116*(3), 1304-1315. doi:10.1152/jn.00248.2016

Raman, I. M., & Bean, B. P. (1997). Resurgent sodium current and action potential formation in dissociated cerebellar Purkinje neurons. *J Neurosci, 17*(12), 4517-4526.

Raman, I. M., & Bean, B. P. (1999). Ionic currents underlying spontaneous action potentials in isolated cerebellar Purkinje neurons. *J Neurosci, 19*(5), 1663-1674.

Raman, I. M., Sprunger, L. K., Meisler, M. H., & Bean, B. P. (1997). Altered subthreshold sodium currents and disrupted firing patterns in Purkinje neurons of Scn8a mutant mice. *Neuron, 19*(4), 881-891. doi:10.1016/s0896-6273(00)80969-1

Rancz, E. A., & Hausser, M. (2006). Dendritic calcium spikes are tunable triggers of cannabinoid release and short-term synaptic plasticity in cerebellar Purkinje neurons. *J Neurosci, 26*(20), 5428-5437. doi:10.1523/JNEUROSCI.5284-05.2006

Ransdell, J. L., & Nerbonne, J. M. (2018). Voltage-gated sodium currents in cerebellar Purkinje neurons: functional and molecular diversity. *Cell Mol Life Sci, 75*(19), 3495-3505. doi:10.1007/s00018-018-2868-y

Rapaport, D., Passos-Bueno, M. R., Brandão, L., Love, D., Vainzof, M., & Zatz, M. (1991). Apparent association of mental retardation and specific patterns of deletions screened with probes cf56a and cf23a in Duchenne muscular dystrophy. *Am J Med Genet, 39*(437-441).

Rapaport, D., Passos-Bueno, M. R., Takata, R. I., Campiotto, S., Eggers, S., Vainzof, M., . . . Zatz, M. (1992). A deletion including the brain promoter of the Duchenne muscular dystrophy gene is not associated with mental retardation. *Neuromuscul Disord., 2*(2), 117-120.

Ravizza, S. M., McCormick, C. A., Schlerf, J. E., Justus, T., Ivry, R. B., & Fiez, J. A. (2006). Cerebellar damage produces selective deficits in verbal working memory. *Brain, 129*(Pt 2), 306-320. doi:10.1093/brain/awh685

Raymackers, J. M., Debaix, H., Colson-Van Schoor, M., De Backer, F., Tajeddine, N., Schwaller, B., . . . Gillis, J. M. (2003). Consequence of parvalbumin deficiency in the mdx mouse: histological, biochemical and mechanical phenotype of a new double mutant. *Neuromuscul Disord, 13*(5), 376-387. doi:10.1016/s0960-8966(03)00031-2

Rickels, K., & Rynn, M. (2002). Pharmacotherapy of generalized anxiety disorder. *J Clin Psychiatry, 63 Suppl 14*, 9-16.

Rigo, F., Chun, S. J., Norris, D. A., Hung, G., Lee, S., Matson, J., . . . Bennett, C. F. (2014). Pharmacology of a central nervous system delivered 2'-O-methoxyethyl-modified survival of motor neuron splicing oligonucleotide in mice and nonhuman primates. *J Pharmacol Exp Ther, 350*(1), 46-55. doi:10.1124/jpet.113.212407

Robert, R. G., Bobrow, M., & Bentley, D. R. (1992). Point mutations in the dystrophin gene. *Proc Natl Acad Sci USA, 89*, 2331-2335.

Roberts, R. G., Coffey, A. J., Bobrow, M., & Bentley, D. R. (1993). Exon structure of the human dystrophin gene. *Genomics, 16*(2), 536-538. doi:10.1006/geno.1993.1225

Roe, M. W., Lemasters, J. J., & Herman, B. (1990). Assessment of Fura-2 for measurements of cytosolic free calcium. *Cell Calcium, 11*(2-3), 63-73.

Rosman, N. P. (1970). The cerebral defect and myopathy in Duchenne muscular dystrophy. A comparative clinicopathological study. *Neurology, 20*(4), 329-335.

Rosman, N. P., & Kakulas, B. A. (1966). Mental deficiency associated with muscular dystrophy. A neuropathological study. *Brain, 89*(4), 769-788.

Rougier, J. S., Gavillet, B., & Abriel, H. (2013). Proteasome inhibitor (MG132) rescues Nav1.5 protein content and the cardiac sodium current in dystrophin-deficient mdx (5cv) mice. *Front Physiol, 4*, 51. doi:10.3389/fphys.2013.00051

Roy, P., Rau, F., Ochala, J., Messeant, J., Fraysse, B., Laine, J., . . . Ferry, A. (2016). Dystrophin restoration therapy improves both the reduced excitability and the force drop induced by lengthening contractions in dystrophic mdx skeletal muscle. *Skelet Muscle, 6*, 23. doi:10.1186/s13395-016-0096-4

Rubi, L., Todt, H., Kubista, H., Koenig, X., & Hilber, K. (2018). Calcium current properties in dystrophin‐deficient ventricular cardiomyocytes from aged mdx mice. *Physiol Rep, 6*(1), e13567.

Ruggiu, A. A., Bannwarth, M., & Johnsson, K. (2010). Fura-2FF-based calcium indicator for protein labeling. *Org Biomol Chem, 8*(15), 3398-3401. doi:10.1039/c000158a

Ryder-Cook, A. S., Sicinski, P., Thomas, K., Davies, K. E., Worton, R. G., Barnard, E. A., . . . Barnard, P. J. (1988). Localization of the mdx mutation within the mouse dystrophin gene. *EMBO J, 7*(10), 3017-3021.

Sacchetti, B., Scelfo, B., Tempia, F., & Strata, P. (2004). Long-term synaptic changes induced in the cerebellar cortex by fear conditioning. *Neuron, 42*(6), 973-982. doi:10.1016/j.neuron.2004.05.012

Sadeghi, A., Doyle, A. D., & Johnson, B. D. (2002). Regulation of the cardiac L-type Ca2+ channel by the actin-binding proteins alpha-actinin and dystrophin. *American Journal of Physiology-Cell Physiology, 282*(6), C1502-C1511. doi:10.1152/ajpcell.00435.2001

Sadoulet-Puccio, H. M., & Kunkel, L. M. (1996). Dystrophin and its isoforms. *Brain Pathol, 6*(1), 25-35.

Saito, T., Kawai, M., Kimura, E., Ogata, K., Takahashi, T., Kobayashi, M., . . . Matsumura, T. (2017). Study of Duchenne muscular dystrophy long-term survivors aged 40 years and older living in specialized institutions in Japan. *Neuromuscular disorders, 27*(2), 107-114.

Saito, T., Tatara, K., & Kawai, M. (2014). [Changes in clinical condition and causes of death of inpatients with Duchenne muscular dystrophy in Japan from 1999 to 2012]. *Rinsho Shinkeigaku, 54*(10), 783-790. doi:10.5692/clinicalneurol.54.783

Sakurai, M. (1987). Synaptic modification of parallel fibre-Purkinje cell transmission in in vitro guinea-pig cerebellar slices. *J Physiol, 394*, 463-480.

Sancar, F., Touroutine, D., Gao, S., Oh, H. J., Gendrel, M., Bessereau, J. L., . . . Richmond, J. E. (2011). The dystrophin-associated protein complex maintains muscle excitability by regulating Ca(2+)-dependent K(+) (BK) channel localization. *J Biol Chem, 286*(38), 33501-33510. doi:10.1074/jbc.M111.227678

Sandrock, A. W., Jr., Dryer, S. E., Rosen, K. M., Gozani, S. N., Kramer, R., Theill, L. E., & Fischbach, G. D. (1997). Maintenance of acetylcholine receptor number by neuregulins at the neuromuscular junction in vivo. *Science, 276*(5312), 599-603.

Sausbier, M., Hu, H., Arntz, C., Feil, S., Kamm, S., Adelsberger, H., . . . Ruth, P. (2004). Cerebellar ataxia and Purkinje cell dysfunction caused by Ca2+-activated K+ channel deficiency. *Proc Natl Acad Sci U S A, 101*(25), 9474-9478. doi:10.1073/pnas.0401702101

Sbriccoli, A., Santarelli, M., Carretta, D., Pinto, F., Granato, A., & Minciacchi, D. (1995). Architectural changes of the cortico-spinal system in the dystrophin defective mdx mouse. *Neurosci Lett, 200*(1), 53-56.

Scaglioni, D., Catapano, F., Ellis, M., Torelli, S., Chambers, D., Feng, L., . . . Muntoni, F. (2021). The administration of antisense oligonucleotide golodirsen reduces pathological regeneration in patients with Duchenne muscular dystrophy. *Acta Neuropathologica Communications, 9*(1), 7. doi:10.1186/s40478-020-01106-1

Schaller, K. L., & Caldwell, J. H. (2003). Expression and distribution of voltage-gated sodium channels in the cerebellum. *Cerebellum, 2*(1), 2-9. doi:10.1080/14734220309424

Schindelin, J., Arganda-Carreras, I., Frise, E., Kaynig, V., Longair, M., Pietzsch, T., . . . Cardona, A. (2012). Fiji: an open-source platform for biological-image analysis. *Nat Methods, 9*(7), 676-682. doi:10.1038/nmeth.2019

Schmahmann, J. D. (1991). An emerging concept. The cerebellar contribution to higher function. *Arch Neurol, 48*(11), 1178-1187.

Schmalbruch, H. (1976). The morphology of regeneration of skeletal muscles in the rat. *Tissue Cell, 8*(4), 673-692.

Schmalbruch, H. (1984). Regenerated muscle fibers in Duchenne muscular dystrophy: a serial section study. *Neurology, 34*(1), 60-65. doi:10.1212/wnl.34.1.60

Schreurs, B. G., Oh, M. M., & Alkon, D. L. (1996). Pairing-specific long-term depression of Purkinje cell excitatory postsynaptic potentials results from a classical conditioning procedure in the rabbit cerebellar slice. *J Neurophysiol, 75*(3), 1051-1060. doi:10.1152/jn.1996.75.3.1051

Sekiguchi, M., Zushida, K., Yoshida, M., Maekawa, M., Kamichi, S., Yoshida, M., . . . Wada, K. (2009). A deficit of brain dystrophin impairs specific amygdala GABAergic transmission and enhances defensive behaviour in mice. *Brain, 132*(Pt 1), 124-135. doi:10.1093/brain/awn253

Sesay, A. K., Errington, M. L., Levita, L., & Bliss, T. V. (1996). Spatial learning and hippocampal long-term potentiation are not impaired in mdx mice. *Neurosci Lett, 211*(3), 207-210.

Shen, Y., Hansel, C., & Linden, D. J. (2002). Glutamate release during LTD at cerebellar climbing fiber-Purkinje cell synapses. *Nat Neurosci, 5*(8), 725-726. doi:10.1038/nn895

Shepherd, G. M., & Harris, K. M. (1998). Three-dimensional structure and composition of CA3-->CA1 axons in rat hippocampal slices: implications for presynaptic connectivity and compartmentalization. *J Neurosci, 18*(20), 8300-8310.

Shi, S. R., Cote, R. J., & Taylor, C. R. (2001). Antigen retrieval techniques: current perspectives. *J Histochem Cytochem, 49*(8), 931-937. doi:10.1177/002215540104900801

Shi, S. R., Key, M. E., & Kalra, K. L. (1991). Antigen retrieval in formalin-fixed, paraffin-embedded tissues: an enhancement method for immunohistochemical staining based on microwave oven heating of tissue sections. *J Histochem Cytochem, 39*(6), 741-748. doi:10.1177/39.6.1709656

Shigemoto, R., Abe, T., Nomura, S., Nakanishi, S., & Hirano, T. (1994). Antibodies inactivating mGluR1 metabotropic glutamate receptor block long-term depression in cultured Purkinje cells. *Neuron, 12*(6), 1245-1255.

Sicinski, P., Geng, Y., Ryder-Cook, A. S., Barnard, E. A., Darlison, M. G., & Barnard, P. J. (1989). The molecular basis of muscular dystrophy in the mdx mouse: a point mutation. *Science, 244*(4912), 1578-1580.

Silva, A. J., Rosahl, T. W., Chapman, P. F., Marowitz, Z., Friedman, E., Frankland, P. W., . . . Bourtchuladze, R. (1996). Impaired learning in mice with abnormal short-lived plasticity. *Curr Biol, 6*(11), 1509-1518.

Sim, B., & Rae, C. (2011). The effect of Duchenne muscular dystrophy on Purkinje cell numbers in the mdx mouse. *Aust Med Student J, 2*, 52-55.

Simpson, A. W. M. (2006). Fluorescent measurement of [Ca2+]c: basic practical considerations. *Methods in molecular biology (Clifton, N.J.), 312*, 3-36.

Sironi, M., Bardoni, A., Felisari, G., Cagliani, R., Robotti, M., Comi, G. P., . . . Bresolin, N. (2001). Transcriptional activation of the non-muscle, full-length dystrophin isoforms in Duchenne muscular dystrophy skeletal muscle. *J Neurol Sci, 186*(1-2), 51-57.

Smith, R. A., Sibert, J. R., & Harper, P. S. (1990). Early development of boys with Duchenne muscular dystrophy. *Dev Med Child Neurol, 32*(6), 519-527.

Snow, W. M., Anderson, J. E., & Fry, M. (2014). Regional and genotypic differences in intrinsic electrophysiological properties of cerebellar Purkinje neurons from wild-type and dystrophin-deficient mdx mice. *Neurobiol Learn Mem, 107*, 19-31. doi:10.1016/j.nlm.2013.10.017

Snow, W. M., Anderson, J. E., & Jakobson, L. S. (2013). Neuropsychological and neurobehavioral functioning in Duchenne muscular dystrophy: a review. *Neurosci Biobehav Rev, 37*(5), 743-752. doi:10.1016/j.neubiorev.2013.03.016

Song, S. K., Yoshino, J., Le, T. Q., Lin, S. J., Sun, S. W., Cross, A. H., & Armstrong, R. C. (2005). Demyelination increases radial diffusivity in corpus callosum of mouse brain. *Neuroimage, 26*(1), 132-140. doi:10.1016/j.neuroimage.2005.01.028

Stanton, P. K., & Moskal, J. R. (1991). Diphenylhydantoin protects against hypoxia-induced impairment of hippocampal synaptic transmission. *Brain Res, 546*(2), 351-354.

Stay, T. L., Miterko, L. N., Arancillo, M., Lin, T., & Sillitoe, R. V. (2019). In vivo cerebellar circuit function is disrupted in an mdx mouse model of Duchenne muscular dystrophy. *Dis Model Mech, 13*(2). doi:10.1242/dmm.040840

Stedman, H. H., Sweeney, H. L., Shrager, J. B., Maguire, H. C., Panettieri, R. A., Petrof, B., . . . Kelly, A. M. (1991). The mdx mouse diaphragm reproduces the degenerative changes of Duchenne muscular dystrophy. *Nature, 352*(6335), 536-539. doi:10.1038/352536a0

Steinberg, S. F., Bilezikian, J. P., & Al-Awqati, Q. (1987). Fura-2 fluorescence is localized to mitochondria in endothelial cells. *Am J Physiol, 253*(5 Pt 1), C744-747. doi:10.1152/ajpcell.1987.253.5.C744

Steinberg, T. H., Newman, A. S., Swanson, J. A., & Silverstein, S. C. (1987). ATP4- permeabilizes the plasma membrane of mouse macrophages to fluorescent dyes. *J Biol Chem, 262*(18), 8884-8888.

Storm, J. F. (1987). Action potential repolarization and a fast after-hyperpolarization in rat hippocampal pyramidal cells. *J Physiol, 385*, 733-759. doi:10.1113/jphysiol.1987.sp016517

Summerton, J., Stein, D., Huang, S. B., Matthews, P., Weller, D., & Partridge, M. (1997). Morpholino and phosphorothioate antisense oligomers compared in cell-free and in-cell systems. *Antisense Nucleic Acid Drug Dev, 7*(2), 63-70. doi:10.1089/oli.1.1997.7.63

Sun, C., Shen, L., Zhang, Z., & Xie, X. (2020). Therapeutic strategies for duchenne muscular dystrophy: An update. *Genes, 11*(8), 837.

Sundstrom, L., Morrison, B., 3rd, Bradley, M., & Pringle, A. (2005). Organotypic cultures as tools for functional screening in the CNS. *Drug Discov Today, 10*(14), 993-1000. doi:10.1016/S1359-6446(05)03502-6

Suzuki, Y., Higuchi, S., Aida, I., Nakajima, T., & Nakada, T. (2017). Abnormal distribution of GABAA receptors in brain of duchenne muscular dystrophy patients. *Muscle Nerve, 55*(4), 591-595. doi:10.1002/mus.25383

Takechi, H., Eilers, J., & Konnerth, A. (1998). A new class of synaptic response involving calcium release in dendritic spines. *Nature, 396*(6713), 757-760. doi:10.1038/25547

Takeshima, Y., Yagi, M., Okizuka, Y., Awano, H., Zhang, Z., Yamauchi, Y., . . . Matsuo, M. (2010). Mutation spectrum of the dystrophin gene in 442 Duchenne/Becker muscular dystrophy cases from one Japanese referral center. *J Hum Genet, 55*(6), 379-388. doi:10.1038/jhg.2010.49

Tanaka, K., Khiroug, L., Santamaria, F., Doi, T., Ogasawara, H., Ellis-Davies, G. C., . . . Augustine, G. J. (2007). Ca2+ requirements for cerebellar long-term synaptic depression: role for a postsynaptic leaky integrator. *Neuron, 54*(5), 787-800. doi:10.1016/j.neuron.2007.05.014

Tank, D. W., Sugimori, M., Connor, J. A., & Llinas, R. R. (1988). Spatially resolved calcium dynamics of mammalian Purkinje cells in cerebellar slice. *Science, 242*(4879), 773-777. doi:10.1126/science.2847315

Taylor, P. J., Betts, G. A., Maroulis, S., Gilissen, C., Pedersen, R. L., Mowat, D. R., . . . Buckley, M. F. (2010). Dystrophin gene mutation location and the risk of cognitive impairment in Duchenne muscular dystrophy. *PloS one, 5*(1), e8803. doi:10.1371/journal.pone.0008803

Thiagarajan, T. C., Piedras-Renteria, E. S., & Tsien, R. W. (2002). alpha- and betaCaMKII. Inverse regulation by neuronal activity and opposing effects on synaptic strength. *Neuron, 36*(6), 1103-1114.

Tidball, J. G., & Spencer, M. J. (2000). Calpains and muscular dystrophies. *Int J Biochem Cell Biol, 32*(1), 1-5.

Timpani, C. A., Hayes, A., & Rybalka, E. (2015). Revisiting the dystrophin-ATP connection: How half a century of research still implicates mitochondrial dysfunction in Duchenne Muscular Dystrophy aetiology. *Med Hypotheses, 85*(6), 1021-1033. doi:10.1016/j.mehy.2015.08.015

Torelli, S., Ferlini, A., Obici, L., Sewry, C., & Muntoni, F. (1999). Expression, regulation and localisation of dystrophin isoforms in human foetal skeletal and cardiac muscle. *Neuromuscul Disord, 9*(8), 541-551.

Torres, L. F., & Duchen, L. W. (1987). The mutant mdx: inherited myopathy in the mouse. Morphological studies of nerves, muscles and end-plates. *Brain, 110 (Pt 2)*, 269-299.

Toth, I., Neumann, I. D., & Slattery, D. A. (2012). Social fear conditioning: a novel and specific animal model to study social anxiety disorder. *Neuropsychopharmacology, 37*(6), 1433-1443. doi:10.1038/npp.2011.329

Townsend, D., Yasuda, S., Li, S., Chamberlain, J. S., & Metzger, J. M. (2008). Emergent dilated cardiomyopathy caused by targeted repair of dystrophic skeletal muscle. *Mol Ther, 16*(5), 832-835. doi:10.1038/mt.2008.52

Tracey, I., Scott, R. B., Thompson, C. H., Dunn, J. F., Barnes, P. R., Styles, P., . . . Radda, G. K. (1995). Brain abnormalities in Duchenne muscular dystrophy: phosphorus-31 magnetic resonance spectroscopy and neuropsychological study. *Lancet, 345*(8960), 1260-1264.

Truitt, C. J. (1955). Personal and social adjustments of children with muscular dystrophy. *Am J Phys Med, 34*(1), 124-128.

Tsien, R. Y. (1981). A non-disruptive technique for loading calcium buffers and indicators into cells. *Nature, 290*(5806), 527-528. doi:10.1038/290527a0

Tsien, R. Y. (1989). Fluorescent probes of cell signaling. *Annu Rev Neurosci, 12*, 227-253. doi:10.1146/annurev.ne.12.030189.001303

Tsien, R. Y., Rink, T. J., & Poenie, M. (1985). Measurement of cytosolic free Ca2+ in individual small cells using fluorescence microscopy with dual excitation wavelengths. *Cell Calcium, 6*(1-2), 145-157. doi:10.1016/0143-4160(85)90041-7

Tsurumi, F., Baba, S., Yoshinaga, D., Umeda, K., Hirata, T., Takita, J., & Heike, T. (2019). The intracellular Ca2+ concentration is elevated in cardiomyocytes differentiated from hiPSCs derived from a Duchenne muscular dystrophy patient. *PloS one, 14*(3), e0213768. doi:10.1371/journal.pone.0213768

Tuckett, E., Gosetti, T., Hayes, A., Rybalka, E., & Verghese, E. (2015). Increased calcium in neurons in the cerebral cortex and cerebellum is not associated with cell loss in the mdx mouse model of Duchenne muscular dystrophy. *NeuroReport, 26*(13), 785-790.

Turner, P. R., Westwood, T., Regen, C. M., & Steinhardt, R. A. (1988). Increased protein degradation results from elevated free calcium levels found in muscle from mdx mice. *Nature, 335*(6192), 735-738. doi:10.1038/335735a0

Turrigiano, G. G., & Nelson, S. B. (2004). Homeostatic plasticity in the developing nervous system. *Nat Rev Neurosci, 5*(2), 97-107. doi:10.1038/nrn1327

Ueda, Y., Suwazono, S., Maedo, S., & Higuchi, I. (2017). Profile of cognitive function in adults with duchenne muscular dystrophy. *Brain Dev, 39*(3), 225-230. doi:10.1016/j.braindev.2016.10.005

US Food and Drug Administration. (2016). FDA grants accelerated approval to first drug for Duchenne muscular dystrophy. *US Food and Drug Administration*.

Vaillend, C., & Billard, J. M. (2002). Facilitated CA1 hippocampal synaptic plasticity in dystrophin-deficient mice: role for GABAA receptors? *Hippocampus, 12*(6), 713-717. doi:10.1002/hipo.10068

Vaillend, C., Billard, J. M., Claudepierre, T., Rendon, A., Dutar, P., & Ungerer, A. (1998). Spatial discrimination learning and CA1 hippocampal synaptic plasticity in mdx and mdx3cv mice lacking dystrophin gene products. *Neuroscience, 86*(1), 53-66.

Vaillend, C., Billard, J. M., & Laroche, S. (2004). Impaired long-term spatial and recognition memory and enhanced CA1 hippocampal LTP in the dystrophin-deficient Dmd(mdx) mouse. *Neurobiol Dis, 17*(1), 10-20. doi:10.1016/j.nbd.2004.05.004

Vaillend, C., & Chaussenot, R. (2017). Relationships linking emotional, motor, cognitive and GABAergic dysfunctions in dystrophin-deficient mdx mice. *Hum Mol Genet, 26*(6), 1041-1055. doi:10.1093/hmg/ddx013

Vaillend, C., Perronnet, C., Ros, C., Gruszczynski, C., Goyenvalle, A., Laroche, S., . . . Peltekian, E. (2010). Rescue of a dystrophin-like protein by exon skipping in vivo restores GABAA-receptor clustering in the hippocampus of the mdx mouse. *Mol Ther, 18*(9), 1683-1688. doi:10.1038/mt.2010.134

Vaillend, C., Rendon, A., Misslin, R., & Ungerer, A. (1995). Influence of dystrophin-gene mutation on mdx mouse behavior. I. Retention deficits at long delays in spontaneous alternation and bar-pressing tasks. *Behav Genet, 25*(6), 569-579.

Vaillend, C., & Ungerer, A. (1999). Behavioral characterization of mdx3cv mice deficient in C-terminal dystrophins. *Neuromuscul Disord, 9*(5), 296-304.

Vaillend, C., Ungerer, A., & Billard, J. M. (1999). Facilitated NMDA receptor-mediated synaptic plasticity in the hippocampal CA1 area of dystrophin-deficient mice. *Synapse, 33*(1), 59-70. doi:10.1002/(SICI)1098-2396(199907)33:1<59::AID-SYN6>3.0.CO;2-K

Vallejo-Illarramendi, A., Toral-Ojeda, I., Aldanondo, G., & Lopez de Munain, A. (2014). Dysregulation of calcium homeostasis in muscular dystrophies. *Expert Rev Mol Med, 16*, e16. doi:10.1017/erm.2014.17

van Deutekom, J. C., Bremmer-Bout, M., Janson, A. A., Ginjaar, I. B., Baas, F., den Dunnen, J. T., & van Ommen, G. J. (2001). Antisense-induced exon skipping restores dystrophin expression in DMD patient derived muscle cells. *Hum Mol Genet, 10*(15), 1547-1554.

van Deutekom, J. C., Janson, A. A., Ginjaar, I. B., Frankhuizen, W. S., Aartsma-Rus, A., Bremmer-Bout, M., . . . van Ommen, G. J. (2007). Local dystrophin restoration with antisense oligonucleotide PRO051. *N Engl J Med, 357*(26), 2677-2686. doi:10.1056/NEJMoa073108

van Deutekom, J. C., & van Ommen, G. J. (2003). Advances in Duchenne muscular dystrophy gene therapy. *Nat Rev Genet, 4*(10), 774-783. doi:10.1038/nrg1180

van Dongen, H. R., Catsman-Berrevoets, C. E., & van Mourik, M. (1994). The syndrome of'cerebellar'mutism and subsequent dysarthria. *Neurology, 44*(11), 2040-2040.

van Ommen, G. J., Bertelson, C., Ginjaar, H. B., den Dunnen, J. T., Bakker, E., Chelly, J., . . . et al. (1987). Long-range genomic map of the Duchenne muscular dystrophy (DMD) gene: isolation and use of J66 (DXS268), a distal intragenic marker. *Genomics, 1*(4), 329-336.

Vandebrouck, A., Sabourin, J., Rivet, J., Balghi, H., Sebille, S., Kitzis, A., . . . Constantin, B. (2007). Regulation of capacitative calcium entries by alpha1-syntrophin: association of TRPC1 with dystrophin complex and the PDZ domain of alpha1-syntrophin. *FASEB J, 21*(2), 608-617. doi:10.1096/fj.06-6683com

Vandermosten, M., Boets, B., Wouters, J., & Ghesquiere, P. (2012). A qualitative and quantitative review of diffusion tensor imaging studies in reading and dyslexia. *Neurosci Biobehav Rev, 36*(6), 1532-1552. doi:10.1016/j.neubiorev.2012.04.002

Villanova, M., & Kazibwe, S. (2017). New Survival Target for Duchenne Muscular Dystrophy. *Am J Phys Med Rehabil, 96*(2), e28-e30. doi:10.1097/PHM.0000000000000569

Vincent, P., & Marty, A. (1996). Fluctuations of inhibitory postsynaptic currents in Purkinje cells from rat cerebellar slices. *J Physiol, 494 (Pt 1)*, 183-199.

Viola, H. M., Adams, A. M., Davies, S. M., Fletcher, S., Filipovska, A., & Hool, L. C. (2014). Impaired functional communication between the L-type calcium channel and mitochondria contributes to metabolic inhibition in the mdx heart. *Proc Natl Acad Sci U S A, 111*(28), E2905-2914. doi:10.1073/pnas.1402544111

Voogd, J., & Glickstein, M. (1998). The anatomy of the cerebellum. *Trends Neurosci, 21*(9), 370-375.

Wahlsten, D., Metten, P., Phillips, T. J., Boehm, S. L., 2nd, Burkhart-Kasch, S., Dorow, J., . . . Crabbe, J. C. (2003). Different data from different labs: lessons from studies of gene-environment interaction. *J Neurobiol, 54*(1), 283-311. doi:10.1002/neu.10173

Wallace, R. H., Scheffer, I. E., Barnett, S., Richards, M., Dibbens, L., Desai, R. R., . . . Berkovic, S. F. (2001). Neuronal sodium-channel alpha1-subunit mutations in

generalized epilepsy with febrile seizures plus. *Am J Hum Genet, 68*(4), 859-865. doi:10.1086/319516

Wallis, T., Bubb, W. A., McQuillan, J. A., Balcar, V. J., & Rae, C. (2004). For want of a nail. Ramifications of a single gene deletion, dystrophin, in the brain of the mouse. *Frontiers in Bioscience, 9*, 74-84.

Walton, J. N., & Nattrass, F. J. (1954). On the classification, natural history and treatment of the myopathies. *Brain, 77*(2), 169-231.

Wan, E., Abrams, J., Weinberg, R. L., Katchman, A. N., Bayne, J., Zakharov, S. I., . . . Marx, S. O. (2016). Aberrant sodium influx causes cardiomyopathy and atrial fibrillation in mice. *J Clin Invest, 126*(1), 112-122. doi:10.1172/JCI84669

Wan, Q., Xiong, Z. G., Man, H. Y., Ackerley, C. A., Braunton, J., Lu, W. Y., . . . Wang, Y. T. (1997). Recruitment of functional GABA(A) receptors to postsynaptic domains by insulin. *Nature, 388*(6643), 686-690. doi:10.1038/41792

Wang, S. S., Denk, W., & Hausser, M. (2000). Coincidence detection in single dendritic spines mediated by calcium release. *Nat Neurosci, 3*(12), 1266-1273. doi:10.1038/81792

Wang, Z. W., Saifee, O., Nonet, M. L., & Salkoff, L. (2001). SLO-1 potassium channels control quantal content of neurotransmitter release at the C. elegans neuromuscular junction. *Neuron, 32*(5), 867-881. doi:10.1016/s0896-6273(01)00522-0

Warrier, A., Borges, S., Dalcino, D., Walters, C., & Wilson, M. (2005). Calcium from internal stores triggers GABA release from retinal amacrine cells. *J Neurophysiol, 94*(6), 4196-4208. doi:10.1152/jn.00604.2005

Weber, J. T., De Zeeuw, C. I., Linden, D. J., & Hansel, C. (2003). Long-term depression of climbing fiber-evoked calcium transients in Purkinje cell dendrites. *Proc Natl Acad Sci U S A, 100*(5), 2878-2883. doi:10.1073/pnas.0536420100

Wertz, K., & Fuchtbauer, E. (1998). Dmd (mdx-ß geo): a new allele for the mouse dystrophin gene. *Dev. Dyn, 212*, 229-241.

White, S., Kalf, M., Liu, Q., Villerius, M., Engelsma, D., Kriek, M., . . . den Dunnen, J. T. (2002). Comprehensive detection of genomic duplications and deletions in the DMD gene, by use of multiplex amplifiable probe hybridization. *Am J Hum Genet, 71*(2), 365-374. doi:10.1086/341942

Whitehead, N. P., Yeung, E. W., & Allen, D. G. (2006). Muscle damage in mdx (dystrophic) mice: role of calcium and reactive oxygen species. *Clin Exp Pharmacol Physiol, 33*(7), 657-662. doi:10.1111/j.1440-1681.2006.04394.x

Wicksell, R. K., Kihlgren, M., Melin, L., & Eeg-Olofsson, O. (2004). Specific cognitive deficits are common in children with Duchenne muscular dystrophy. *Dev Med Child Neurol, 46*(3), 154-159.

Wierenga, C. J., & Wadman, W. J. (1999). Miniature inhibitory postsynaptic currents in CA1 pyramidal neurons after kindling epileptogenesis. *J Neurophysiol, 82*(3), 1352-1362. doi:10.1152/jn.1999.82.3.1352

Williams, D. A., Fogarty, K. E., Tsien, R. Y., & Fay, F. S. (1985). Calcium gradients in single smooth muscle cells revealed by the digital imaging microscope using Fura-2. *Nature, 318*(6046), 558-561. doi:10.1038/318558a0

Williams, D. A., Head, S. I., Bakker, A. J., & Stephenson, D. G. (1990). Resting calcium concentrations in isolated skeletal muscle fibres of dystrophic mice. *J Physiol, 428*, 243-256. doi:10.1113/jphysiol.1990.sp018210

Williams, I. A., & Allen, D. G. (2007). Intracellular calcium handling in ventricular myocytes from mdx mice. *Am J Physiol Heart Circ Physiol, 292*(2), H846-855. doi:10.1152/ajpheart.00688.2006

Willmann, R., Possekel, S., Dubach-Powell, J., Meier, T., & Ruegg, M. A. (2009). Mammalian animal models for Duchenne muscular dystrophy. *Neuromuscular disorders, 19*(4), 241-249.

Wilton, S. D., Lloyd, F., Carville, K., Fletcher, S., Honeyman, K., Agrawal, S., & Kole, R. (1999). Specific removal of the nonsense mutation from the mdx dystrophin mRNA using antisense oligonucleotides. *Neuromuscul Disord, 9*(5), 330-338. doi:10.1016/s0960-8966(99)00010-3

Wirth, B. (2000). An update of the mutation spectrum of the survival motor neuron gene (SMN1) in autosomal recessive spinal muscular atrophy (SMA). *Hum Mutat, 15*(3), 228-237. doi:10.1002/(SICI)1098-1004(200003)15:3<228::AID-HUMU3>3.0.CO;2-9

Wong, T. P., Marchese, G., Casu, M. A., Ribeiro-da-Silva, A., Cuello, A. C., & De Koninck, Y. (2000). Loss of presynaptic and postsynaptic structures is accompanied by compensatory increase in action potential-dependent synaptic input to layer V neocortical pyramidal neurons in aged rats. *J Neurosci, 20*(22), 8596-8606.

Woods, C. E., Novo, D., DiFranco, M., & Vergara, J. L. (2004). The action potential-evoked sarcoplasmic reticulum calcium release is impaired in mdx mouse muscle fibres. *J Physiol, 557*(Pt 1), 59-75. doi:10.1113/jphysiol.2004.061291

Woolf, P. J., Lu, S., Cornford-Nairn, R., Watson, M., Xiao, X. H., Holroyd, S. M., . . . Hoey, A. J. (2006). Alterations in dihydropyridine receptors in dystrophin-deficient cardiac muscle. *Am J Physiol Heart Circ Physiol, 290*(6), H2439-2445. doi:10.1152/ajpheart.00844.2005

Worden, D. K., & Vignos, P. J., Jr. (1962). Intellectual function in childhood progressive muscular dystrophy. *Pediatrics, 29*, 968-977.

Wu, H., Lima, W. F., Zhang, H., Fan, A., Sun, H., & Crooke, S. T. (2004). Determination of the role of the human RNase H1 in the pharmacology of DNA-like antisense drugs. *J Biol Chem, 279*(17), 17181-17189. doi:10.1074/jbc.M311683200

Wu, K., Aoki, C., Elste, A., Rogalski-Wilk, A. A., & Siekevitz, P. (1997). The synthesis of ATP by glycolytic enzymes in the postsynaptic density and the effect of endogenously generated nitric oxide. *Proc Natl Acad Sci U S A, 94*(24), 13273-13278. doi:10.1073/pnas.94.24.13273

Wurster, C. D., & Ludolph, A. C. (2018). Antisense oligonucleotides in neurological disorders. *Ther Adv Neurol Disord, 11*, 1756286418776932. doi:10.1177/1756286418776932

Xu, S., Shi, D., Pratt, S. J., Zhu, W., Marshall, A., & Lovering, R. M. (2015). Abnormalities in brain structure and biochemistry associated with mdx mice measured by in vivo MRI and high resolution localized (1)H MRS. *Neuromuscul Disord, 25*(10), 764-772. doi:10.1016/j.nmd.2015.07.003

Yang, Y. H., Yang, Y., Chen, B. G., Zhang, Y. W., & Bi, H. Y. (2016). Anomalous Cerebellar Anatomy in Chinese Children with Dyslexia. *Front Psychol, 7*, 324. doi:10.3389/fpsyg.2016.00324

Yin, H., Saleh, A. F., Betts, C., Camelliti, P., Seow, Y., Ashraf, S., . . . Wood, M. J. (2011). Pip5 transduction peptides direct high efficiency oligonucleotide-mediated dystrophin exon skipping in heart and phenotypic correction in mdx mice. *Mol Ther, 19*(7), 1295-1303. doi:10.1038/mt.2011.79

Yokota, T., Lu, Q. L., Partridge, T., Kobayashi, M., Nakamura, A., Takeda, S., & Hoffman, E. (2009). Efficacy of systemic morpholino exon-skipping in Duchenne dystrophy dogs. *Ann Neurol, 65*(6), 667-676. doi:10.1002/ana.21627

Yokota, T., Pistilli, E., Duddy, W., & Nagaraju, K. (2007). Potential of oligonucleotide-mediated exon-skipping therapy for Duchenne muscular dystrophy. *Expert Opin Biol Ther, 7*(6), 831-842. doi:10.1517/14712598.7.6.831

Yoshihara, Y., Onodera, H., Iinuma, K., & itoyama, Y. (2003). Abnormal kainic acid receptor density and reduced seizure susceptibility in dystrophin-deficient mdx mice. *Neuroscience, 117*(2), 391-395.

Yoshioka, M., Okuno, T., Honda, Y., & Nakano, Y. (1980). Central nervous system involvement in progressive muscular dystrophy. *Arch Dis Child, 55*(8), 589-594.

Yu, F. H., Mantegazza, M., Westenbroek, R. E., Robbins, C. A., Kalume, F., Burton, K. A., . . . Catterall, W. A. (2006). Reduced sodium current in GABAergic interneurons in a mouse model of severe myoclonic epilepsy in infancy. *Nat Neurosci, 9*(9), 1142-1149. doi:10.1038/nn1754

Yuste, R., & Katz, L. C. (1991). Control of postsynaptic Ca2+ influx in developing neocortex by excitatory and inhibitory neurotransmitters. *Neuron, 6*(3), 333-344. doi:10.1016/0896-6273(91)90243-s

Zeniya, S., Kuwahara, H., Daizo, K., Watari, A., Kondoh, M., Yoshida-Tanaka, K., . . . Yokota, T. (2018). Angubindin-1 opens the blood-brain barrier in vivo for delivery of antisense oligonucleotide to the central nervous system. *J Control Release, 283*, 126-134. doi:10.1016/j.jconrel.2018.05.010

Zhou, Y. Y., Lakatta, E. G., & Xiao, R. P. (1998). Age-associated alterations in calcium current and its modulation in cardiac myocytes. *Drugs Aging, 13*(2), 159-171. doi:10.2165/00002512-199813020-00007